The Mechanical Behavior of Heavily Overconsolidated Resedimented Boston Blue Clay

by

Albalyra Geraldine Vargas Bustamante

Licenciatura en Gerencia Financiera, Bancaria y de Negocios Internacionales
Universidad Latina de Panamá, Panamá, 2009

Licenciatura en Ingeniería Civil
Universidad Tecnológica de Panamá, Panamá, 2010

Submitted to the Department of Civil and Environmental Engineering
in Partial Fulfillment of the Requirements for the Degree of

Master of Science in Civil and Environmental Engineering

at the

MASSACHUSETTS INSTITUTE OF TECHNOLOGY

June 2013

ARCHIVES

MASSACHUSETTS INSTITUTE OF TECHNOLOGY
JUL 08 2013
LIBRARIES

© 2013 Massachusetts Institute of Technology. All rights reserved.

Signature of Author.....
Department of Civil and Environmental Engineering
May 10, 2013

Certified by.....
John T. Germaine
Senior Research Associate of Civil and Environmental Engineering
Thesis Supervisor

Certified by.....
Herbert Einstein
Professor of Civil and Environmental Engineering
Thesis Supervisor

Accepted by.....
Heidi M. Nepf
Chair, Departmental Committee for Graduate Students

The Mechanical Behavior of Heavily Overconsolidated Resedimented Boston Blue Clay

by

Albalyra Geraldine Vargas Bustamante

Submitted to the Department of Civil and Environmental Engineering on
May 10th, 2013 in Partial Fulfillment of the Requirements for the Degree of
Master of Science in Civil and Environmental Engineering

ABSTRACT

Geotechnical engineers encounter some of the most challenging problems in heavily overconsolidated soils. Clays under this condition originated in nature or man-made construction. This thesis investigates the mechanical behavior heavily overconsolidated Resedimented Boston Blue Clay (RBBC), as an analog test material. The uniformity, reproducibility, and extensive knowledgebase on this clay permit the investigation of only the effect of overconsolidation.

A series of undrained triaxial compression shear tests have been performed on specimens that were K_0-consolidated and swelled to overconsolidation ratios (OCR) ranging from 5 to 62 on RBBC, as well as on Intact Presumpscot Maine Clay. Specimens were consolidated to maximum stress levels between 1.1 and 5.4 MPa.

The undrained shear behavior revealed an important relationship with overconsolidation ratio. The triaxial compression test results exhibit a significant increase in the undrained strength ratio (s_u/σ'_{vc}) when normalized to the minimum consolidation stress. It also shows an important increase in the stiffness, increase in the strain (ε_f) to mobilize the peak resistance and a significant increase of friction angle (φ') with overconsolidation. The applicability of the SHANSEP equation and impact on its equation parameters are also discussed in detail. A comprehensive comparison of the new results with prior normally consolidated and lightly overconsolidated data is presented, showing the distinct behavior of heavily overconsolidated specimens. The failure envelope displays a non-linear behavior and the undrained shear strength (s_u) is reduced up to about 80% from a normally consolidated clay to a heavily overconsolidated clay with an OCR = 50. These observations demonstrate the importance of selecting appropriate design values in the presence of overconsolidated soils.

Thesis Supervisor: John T. Germaine
Title: Senior Research Associate of Civil and Environmental Engineering

Thesis Supervisor: Herbert Einstein
Title: Professor of Civil and Environmental Engineering

ACKNOWLEDGEMENTS

There are not enough words to describe my gratitude to my thesis supervisor and research advisor Dr. G, the personification of patience, and who was always there to help me solve my issues. I want to thank him for his support and guidance through the development of my research, as well as for his sense of humor and kindness every time I had a concern and entered his office. His superior knowledge and problem solving skills were my inspiration.

I would like to express my deep appreciation to my academic and thesis supervisor Prof. Herbert Einstein, for all his support during my time at MIT. I am especially thankful for his encouragement and motivation during the most difficult times at the beginning of my studies at MIT. I gratefully acknowledge his careful review and input during my research, especially for improving my writing skills and weekly research delivery.

I extend special thanks to my other geotechnical teachers, Prof. Whittle and Dr. Jen, with whom I had the opportunity to take their classes and built up the basis for my future professional development. I also thank the staff at CEE Stephen Rudolph, Kris Kipp, Sheila Fay, Carolyn Jundzilo, Jeanette Marchocki and Mira Parsons.

I am indebted to the Fulbright-SENACYT Scholarship, which supported a great deal of my learning experience at MIT and made possible my desire to become a Geotechnical Engineer.

I feel blessed with the opportunity to meet so many bright individuals during my 2 years at MIT. I specially thank those who started this journey with me, Rob, Rachel and Vinnie Geotech. M.Engs '12, with whom I spent countless hours studying and playing. To those who continued with me a second year, in particular to Shehab Agaiby for helping when I was completely lost, for believing in group work and for being my true friend, to my dear girlfriend Alessandra Vecchiarelli for sharing so much time with me during lunch, dinners, and wine but most importantly for offering me your friendship and confidence, to Vasso Founta for taking the time to explain basic concepts and for always sharing a smile. To all the bright individuals at the third floor and office-mates in 1-341, those who got here before me and after me, thank you for always cheering up in the corridors.

Many thanks to my lab mates and research groups: Amy and Jana, the strong girls, for always being there when I needed help figuring out what was wrong to one of my tests, Aiden Horan, for explaining me in careful detail the procedures on the triaxial equipment once again after 1.37, and to Brendan Casey for all his instruction, answering all my lab questions without hesitation and lifting heavy equipment. I would like to acknowledge my colleagues in the rock mechanics group: Bruno, Steve, and Dr. Zenzi for your listening and guidance.

Living far away from home was bearable thanks to my roomates, Winnie and Alicia thank you for all your support during my first months at MIT and to our neighbors in Westgate: Marce, Carlos and Luz for offering your friendship. I have to mention all the amazing women I met at GWAMIT, specially Sunny and Wei for co-sharing the Orientations Women Welcome Lunch.

A special thanks must go to my family and friends in Panama, especially to those who listen to my failures and give me courage every day and to all the visits which I deeply appreciate. I owe everything I am to my family, thanks to my parents *Papi, Mami* and my little sis *Karla* for your constant encouragement without your advice and love this wouldn't have being possible.

I will be forever grateful to my lovely husband, *Jose Francisco*, thank you for your decision of living this unforgettable experience together. Without, your love, countless support and consolation I wouldn't have overcome the many obstacles I encountered during my time at MIT.

And finally, I need to thanks Dear God for keeping an eye on me during all this time.

Dedico esta tesis a mis queridos padres Carlos y Albalyra,
Gracias por enseñarme el valor de la educación y la importancia del esfuerzo.

TABLE OF CONTENTS

LIST OF TABLES

LIST OF FIGURES

LIST OF SYMBOLS

AC	Alternating Current
A/D	Analog-to-Digital Converter
BASIC	Beginner's All-purpose Symbolic Instruction Code
BBC	Boston Blue Clay
CK_0U	K_0-Consolidated Undrained Shear Test
CK_0UC	K_0-Consolidated Undrained Compression Test
CL	Low Plasticity Clay
CR	Virgin Compression Ratio
CRS	Constant Rate of Strain
CU	Consolidated Undrained Test
D/A	Digital-to-Analog Converter
DC	Direct Current
ESE	Effective Stress Envelope
ESP	Effective Stress Path
LIR	Load Increment Ratio
LVDT	Linear Variable Differential Transformer
MADC	Multi-Channel Analog to Digital Converter
MIT	Massachusetts Institute of Technology
NC	Normally Consolidated
NSP	Normalized Soil Parameter
OC	Overconsolidated
OCR	Overconsolidation Ratio
PC	Personal Computer
PID	Proportional-Integral-Derivative
PVC	Pressure-Volume Controller
RBBC	Resedimented Boston Blue Clay
SR	Swelling Ratio
TC	Triaxial Compression Shear Test
TX	Triaxial
USR	Undrained Strength Ratio (s_u/σ'_{vc})
SHANSEP	Stress History and Normalized Soil Engineering Properties
TSP	Total Stress Path
VCL	Virgin Compression Line

A (A_f)	Skempton's pore pressure parameter (at failure)
B	Skempton's pore pressure parameter
C_c	Compression index
C_s	Swelling index
C_α	Secondary compression index
$C_{\alpha\varepsilon}$	Secondary compression ratio
c_v	Coefficient of consolidation
c'	Cohesion intercept

E_u	Undrained secant Young's modulus
E_{uMAX}	Undrained secant Young's modulus (maximum)
e	Void ratio
e_0	Initial void ratio
G_s	Specific gravity
I_p	Plasticity index
K	Lateral coefficient of earth pressure
K_0	Coefficient of lateral earth pressure at rest
K_{0NC}	Coefficient of lateral earth pressure at rest for NC soil
K_c	Lateral coefficient of earth pressure at end of consolidation
m	OCR exponent in SHANSEP equation for undrained strength ratio
m_v	Coefficient of volume change
p, p'	Average effective stress, $(\sigma_1 + \sigma_3) / 2$, $(\sigma'_1 + \sigma'_3) / 2$
p_m	Mean effective stress, $(\sigma_1 + \sigma_2 + \sigma_3) / 3$
q	Shear stress, $(\sigma_1 - \sigma_3) / 2$
q_u	Unconfined compressive strength
r^2	Coefficient of determination
S	Undrained strength ratio for NC soil in SHANSEP equation
S_i	Initial Saturation
s_u	Undrained shear strength
t	Time
t_p	Time to end of primary
u, Δu	Pore pressure, change in pore pressure
u_e	Excess pore pressure
u_s	Shear induced pore pressure
u_0	Pore (back) pressure at start of shearing
V, ΔV	Current volume, change in volume
V_0	Initial volume
w	Water content
w_L	Liquid limit
w_p	Plastic limit

ε	Strain
ε_a	Axial strain
ε_f	Strain at peak shear stress
ε_v	Specimen volume strain
ε_r	Radial strain
$\dot{\varepsilon}$	Strain rate
$\dot{\varepsilon}_a$	Axial strain rate
φ, φ'	Friction angle, effective friction angle
φ'_p	Effective friction angle at peak
φ'_{mo}	Effective friction angle at maximum obliquity
ν	Poisson's ratio
ρ	Density
σ_v, σ'_v	Vertical stress, vertical effective stress

σ_h, σ'_h	Horizontal stress, horizontal effective stress
σ_r	Radial stress
σ_p	Preconsolidation pressure
σ'_v	Vertical effective stress
σ'_{vc}	Vertical consolidation effective stress
σ'_{vm}	Maximum vertical consolidation effective stress
σ_1, σ_2, σ_3	Principal stresses
σ_{oct}	Mean octahedral stress

1 INTRODUCTION

1.1 Problem Statement

Several of the most challenging problems in geotechnical engineering practice arise in heavily overconsolidated clays. Overconsolidated clays have been subjected to effective vertical pressures much larger than the current state of stress. These preconsolidation pressures can be generated by nature, or triggered by man-made construction. Geological deposition and erosion are examples of natural processes that can cause changes of stresses over time. For instance, London clay is a formation deposited under marine conditions during the Eocene, uplift and erosion removed between half and two thirds of the overlaying parts of London clay. On the other hand, the Boston Blue Clay (BBC) is a formation in which sediments were transported by streams of melted glaciers during the Pleistocene and deposited in the quiet marine waters of the Boston Basin. This clay was uplifted, submerged, and subjected to cementation by geological processes. Furthermore, there are several construction activities that result in a reduction of stress. For example, the excavation of the Panama Canal resulted in considerable unloading of the soil in the canal and immediately adjacent to it. This massive excavation, or unloading, resulted in a decrease in the strength of the shale and contributed to the slides that occurred along the canal, interrupting its operation for months. Other examples of overconsolidated clays are the Cucaracha formation in Panama, Mexico City Clay, Yorktown Formation, and Brazilian Residual Clay. (Lambe & Whitman, 1969)

There is an extensive knowledgebase in the mechanical behavior of normally consolidated and lightly overconsolidated soils. However, the complex and particular behavior of heavily overconsolidated clays is still not completely understood in the soil mechanics field. This study focuses on understanding of the mechanical behavior of heavily overconsolidated resedimented Boston Blue Clay (RBBC).

1.2 Thesis Scope and Objectives

The main objective of this research has been to gain a better understanding of the overconsolidation effects on the undrained shear behavior of soils. To isolate overconsolidation as the a single study parameter, the specific objective of this thesis is to characterize the one dimensional compression and triaxial compression undrained shear behavior of Resedimented Boston Blue Clay (RBBC) at very high overconsolidation ratios. RBBC is a soil resedimented in the MIT Geotechnical Laboratory that has been well studied by many researchers. This 'analog' material enables the author to focus on the effects of the overconsolidation and compare it to work by others such as Abdulhadi in 2009.

1.3 Organization of the Thesis

This thesis is organized into six chapters to provide the reader with a comprehensive picture of the conducted research. Following this introductory section (Chapter 1), Chapter 2 presents the background information. First, a review of overconsolidated clays and the digenetic process that can cause overconsolidation in nature is given, second an overview on the current state of

knowledge on ductile-brittle transition is presented, third the normalized undrained shear behavior theories that will be used in the analysis and finally the previous studies performed on soils under similar conditions are discussed.

An overview of the materials used for the thesis is presented in Chapter 3. In the first section, a general overview on Resedimented Boston Blue Clay is given. A summary on the resedimentation process and equipment, as well as the index properties and engineering behavior of RBBC is presented. In the following section, the author provides a description on Presumpscot Maine Clay, the natural material used in this testing program.

Chapter 4 presents a complete description of the experimental equipment used to conduct the tests presented in this thesis. This includes the lower pressure triaxial equipment, the control system and details on the instrumentation. This chapter also describes the data acquisition system.

Chapter 5 provides an overview of the general interpretation methods used in the analysis of all the tests. The one dimensional compression and undrained shear measurements and analysis of the behavior for both materials are presented in two separate sections. Lastly, this chapter compares the author's results with prior test results on RBBC with OCR up to 4 reported by Abdulhadi in 2009.

Finally, a summary of the results and main conclusions obtained from the analysis are presented in Chapter 6. Additionally, recommendations for future work are presented.

2 BACKGROUND

2.1 Introduction

In situ soils are commonly subjected to changes in stress over time. These changes can be caused by a geological deposition, erosion, or man-made construction. The change in the stress state of soils is known as the stress history. The stress history of a soil is measured by dividing the maximum vertical stress by the current state of stress, resulting in the expression known as overconsolidation ratio, or OCR. Soils currently experiencing the highest stress level are known as normally consolidated (OCR = 1). On the other hand, soils that were compressed by a greater overburden than at the present are considered to be overconsolidated (OCR >1). Several of the most challenging problems in geotechnical engineering take place in heavily overconsolidated clays. Stability analysis of natural and cut slopes in highly overconsolidated clays have proven to be difficult and generally unreliable because of its unique behavior.

The mechanical behavior of clays is of significant interest to the geotechnical engineering community. Although many research efforts have been directed toward the understanding of the effects of overconsolidation, or stress history, on the engineering properties of clays there is still much research to be done on the behavior of *heavily* overconsolidated clays (OCR > 8). This study focuses on understanding of the mechanical behavior of heavily overconsolidated resedimented Boston Blue Clay (RBBC).

Section 2.2 gives a general overview of overconsolidated clays with special attention to the diagenetic processes which is considered one of the natural causes of overconsolidation. The

ductile-brittle transition of materials will be discussed in section **Error! Reference source not found.**. This section will also provide the reader a better insight of the present knowledge on this behavior.

Section 2.3 describes a review of the normalized behavior concept used for the analysis of this thesis and the influence of high stress on the parameters of the SHANSEP equation technique. Finally, section 2.4 of this chapter gives a general overview of a number of previous studies on overconsolidated clays.

2.2 Overconsolidated Clay

Clays that have been consolidated under very high loads but now exists under substantially reduced pressures are considered to be overconsolidated. In order to understand the behavior of overconsolidated clays a general overview on geological and stress history is presented in this section.

Stress History

Figure 2-1 shows a simplified diagram of the process of deposition at the bottom of a lake. The deposition of more clay results in an increase in the vertical effective stress and a corresponding reduction in water content. A clay at point P_B is normally consolidated and a overconsolidated clay is represented by P_D. The drained shear strength of a normally consolidated clay is directly proportional to the vertical effective stress and the ratio between the horizontal and vertical stress, called K_o, is constant. However, the removal of vertical pressure

will cause the swelling of the clay increasing the water content. From Figure 2-1 it can be seen that point D (P_D) is at the same vertical stress as point B (P_B) but with a significant lower water content value. This condition leads to the conclusion that an overconsolidated soil is at a denser state than the normally consolidated soil. (Singh, 1971)

Micro and Macro-Features

Heavily overconsolidated clays in nature typically have fissure structures and macro discontinuities. These discontinuities are surfaces of weakness and can reduce the strength of the clay mass. Many studies (see Table 2-1) have attributed, in part-at-least, the difference in behavior between laboratory and field shear strengths to these features that cannot be reproduced in the laboratory.

K_o-Unloading

The unloading process has a significant impact in on the overconsolidation stress state. Figure 2-2 shows the relationship between the horizontal and vertical stress from laboratory data by Brooker and Ireland (1966). It can be observed from this picture that as the vertical stress is reduced the rate of decrease of the vertical stress is greater than that of the horizontal stress. The lateral stress ratio reaches unity at OCR of about 3.5 to. Then the horizontal stress becomes greater than the vertical stress, as this is further reduced reaching a limiting Ko value at OCR of about 22 when the passive failure envelope is reached. Figure 2-3 summarizes the behavior of Ko as a function of OCR. (Singh, 1971)

2.2.1 Diagenesis

The effect of digenetic processes on the engineering behavior of overconsolidated clays is complex. The purpose of this section is to give a better of understanding of this process which influences the formation of overconsolidated soils.

2.2.1.1 Definition

Diagenesis includes all the physical and chemical processes that affect the lithification of sediments into sedimentary rocks. The phases that may be affected by this process are the period of burial between deposition and weathering, as well as the stage between deposition and the onset metamorphism. Winker (1979) and Turner (1981) define metamorphism as the stage where a rock is completely recrystallized (~350°C - 375°C at 10 km). The preceding stage is called very-low grade metamorphism and incipient metamorphism. The limit between diagenesis and metamorphism is based on two criteria: mineralogy and temperature, which do not necessarily coincide. Regarding the mineralogy criteria, determining a boundary between diagenesis and metamorphism is highly subjective and temperature varies with the mineral used as indicator.

Table 2-2 shows the diagenesis process divided into early, middle, and late stages based on the smectite to illite ratio of the < 2μm fraction. The temperature at which these changes occur depends on the grain size of the mineral; therefore it is common to use the < 2μm fraction to standardize the boundaries between diagenesis, very-low-grade and low-grade metamorphism. Many authors have stated that the boundary between diagenesis and metamorphism is at ~200°C when recrystallization of clays occurs. However, recrystallization of clay starts at a temperature of <50°C and is not complete until temperatures of 350°C to 400°C. (Weaver, 1989)

2.2.1.2 Physical Processes

The physical processes during diagenesis occur mainly in the early stages of burial, prior to substantial lithifaction when grain rearrangement by bioturbation and compaction are almost accomplished. Effects of physical grain rearrangement of unconsolidated sediment on permeability and grain surface characteristics control the following path of chemical diagenesis. The major categories of physical processes in diagenesis are: bioturbation, elutriation, compaction and tectonic deformation.

Bioturbation is a process (in certain depositional environments) by which substantial grain rearrangement occurs, which can be due to the activity of living organisms. During this process primary depositional fabrics may be significantly rearranged and new fabrics are established. The permeability of sediments and the rock developed from them is significantly reduced if the fine and coarse detrital components, such as clay and sand, become mixed. Figure 2-4 shows the grades of bioturbation.

Elutriation refers to the infiltration of fine-grained particles through the pore spaces followed by deposition. Figure 2-5 shows the conceptualization of this process. This process may lead to rocks with reduced permeability. The path of diagenesis in the sediment can be profoundly altered through thick grain coating by clays. Such clay coatings are the product of elutriation and adhere tightly to grain surfaces via constant wetting and drying. This reduces the overall permeability, and creates a partial barrier to reaction between pore fluid and grain surfaces.

Compression/compaction is the process responsible for the reduction for intergranular space during burial and deformation. Figure 2-6 shows the mechanism of compression/compaction. In

contrast to cementation, compaction develops from the rearrangement of detrital grains. In well-sorted sand-size sediments the intergranular volume, known as IGV, or "minus-cement porosity" is the sum of primary intergranular pore space and intergranular cements. The volume loss by compaction was calculated by Landegard (1992), as follows:

$$Compactional\ porosity\ loss = P_i - \Big(\big((100 - P_I) * IGV\big)/(100 - IGV)\Big)$$

Where the initial porosity Pi , ranges from around 40% of sediment volume for sand-size materials, to much larger values (~80%) for sediments with abundant clay-size particles, and sediments containing grains with abundant primary intragranular pores. Compaction by simple grain rearrangement can reduce IGV to 26% (Graton & Fraser, 1935) but greater reductions are generally believed to require additional mechanisms of compaction such as ductile grain deformation, extreme brittle deformation (as in quartz-rich fault gouges), or pressure solution. (Lundgard, 1992)

Deformation is a fundamental element of diagenesis at different scales. Besides grain pressing during burial compaction, stress applied tectonically, especially while thc rock is still porous as shown in

Figure 2-7, may also crush grains. Deformation bands are planar zones of compressed and cemented grains that are obvious in some porous sandstones. In rocks that are highly lithified, deformation may be thoroughgoing, cutting across detrital and authigenic components. Significant variation of porosity results from deformation, where fracture porosity is one of the main categories of secondary porosity. Secondary porosity can be defined as a subsequent or separate porosity system in a rock, resulting from a chemical leaching of minerals or the generation of a fracture system, often enhancing overall porosity of a rock. This can replace the

primary porosity or coexist with it. Fracture porosity is associated with a fracture system or faulting.

2.2.1.3 Chemical Processes

The chemical processes that occur during diagenesis include the interaction between solids and fluids enclosed within the depositional environment that continue to develop until metamorphism occurs while diagenetic conditions remain. These reactions appear to occur at a slow rate in comparison to reactions at higher temperatures. These lethargic reactions influence the mineral assemblages and texture that begin in diagenesis.

It has being stated that chemical equilibrium between solid phases may not be completed during diagenesis. Even if a phase is in gross equilibrium (e.g. detrital albite in contact with albite-saturated water), the actual crystal lattice may still have trace element, isotopic, and structural disequilibrium with ambient conditions. Such a disequilibrium can lead to dissolution, even in the presence of fluids that are near equilibrium with the bulk mineral. Transient local, micro scale equilibrium between individual authigenic phase and pore fluids occurs in diagenesis, at least theoretically. This does not apply more generally to the bulk rock that contains a diversity of phases that are nor in equilibrium either with pore fluids or one another. The equilibrium between phases is an important factor during the analysis of the composition of fluids responsible for precipitation.

Smectite to Illite

The dominant diagenetic chemical change in shales is the progressive reaction of smectite to illite via a series of mixed-layer illite/smectite (I/S) intermediates (Hower, Eslinger, Hower, & Perry, 1976). Smectite comprises 25-50 percent of most shales, which have not been deeply buried, and since shales are the most abundant sedimentary rock type, this reaction plays a leading role in influencing rock and fluid chemistry in both shales and interbedded sandstone. The smectite-to-illite reaction may release large amounts of water, silica, and other ions during dehydration and by diffusion. (Eslinger & Pevear, 1988)

Examination of the type and distribution of clay minerals in shales of all ages reveals that smectite, ML clays, and kaolinite gradually decrease in abundance with increasing age, whereas illite and chlorite become more abundant. Discrete smectite is completely absent from most Paleozoic rocks. These data suggest that smectite and kaolinite, originally in older shales, have been diagenetically transformed to illite and chlorite. Assuming that the original smectite layers remain intact and that the change to illite involves substitution of aluminum (in tetrahedral sheets see Figure 2-8) and potassium the following reaction is reached:

$$4.5K^{+} + 8Al^{+3} + \text{Smectite} \rightarrow \text{Illite} + 3\ Si^{+4} + (\text{Cations \& Water})$$

K and Al are derived from the dissolution of K-feldspar. Silica, Mg, and Fe are released from the smectite to chlorite and quartz. The reaction of smectite to illite requires the uptake of potassium and aluminum, but the 2:1 silicate skeleton could remain more-or-less intact. The intermediate members of the smectite-illite series are the ML illite-smectites, and the reaction appears to take place either by successive transformation of smectite, or by the neoformation of thin illite "fundamental particles." In order to transform smectite to illite, the smectite must

absorb aluminum into the tetrahedrons, which increases layer charge and allows potassium to be fixed in the interlayer position. Neoformation requires dissolution of smectite and other phases and the precipitation of thin illite crystals, which have smectite-like swelling interfaces.

This reaction was first studied in burial sequences from Gulf Coast wells by Burst (1959), who suggested that the released interlayer water might play a role in hydrocarbon migration and over pressuring. The released waters may also carry silica, Mg, and Fe, which may form quartz, ankerite and chlorite in pores of associated sandstones. The degree of illitization (% of illite in I/S) is a fair indicator of paleotemperature and organic maturity level. Figure 2-9 shows the relationship of illite content of I/S with temperature found by Jennings and Thompson.

Controls of the reaction

The primary controls of the smectite-to-illite reaction in shales are temperature, time, and rock and fluid chemistry. It may seem surprising that pressure is not important, but it has been shown that pressures of the sort found in oil wells are not high enough to dehydrate the interlayer water from smectite; the water is driven out by the contraction of the layers due to an increase in layer charge resulting from the substitution of Al for Si in the tetrahedral sheets or by the dissolution of smectite and precipitation of illite. (Eslinger & Pevear, 1988)

The effect of time is controversial, but there is little doubt that reaction kinetics are important. When smectite is heated in the laboratory under hydrothermal conditions with sufficient potassium, no randomly interstratified phase forms; rather the structure goes directly to the ordered condition at the appropriate temperature. Similar observations have been made on K-rich bentonite, which was relatively rapidly heated by intrusive igneous rocks. These

observations suggest that the development of random interstratification is controlled by **reaction kinetics.**

Besides temperature and time, the other major influence on the illitization reaction is fluid and rock composition. Little is known about the composition of shale pore waters; due to the low permeability of shales, the pore waters must be strongly influenced by mineral dissolution and precipitation reactions within shale itself. Research has shown that in hydrothermal experiments large amounts of Ca ions greatly inhibit the illitization reaction.

Furthermore, there must be sufficient potassium in the shale to satisfy the requirements of the reaction. Typically, the initial potassium in shales is in the form of K-feldspar or discrete detrital mica; therefore, the reaction to illite is also influenced by the rate of dissolution or these minerals.

Fundamental particle theory suggests that the % illite in I/S will be influenced by factors, which control the thickness of the illite particles. This explains that sands interbedded with shales contain an I/S with more illite layers than the I/S in the enclosing shales. The sands have larger pores in which larger crystals might be expected to grow. Alternatively, the permeable sands may have been better able to supply potassium from an external source.

Temperature and Maturation

The previous sections established that shales with sufficient initial potassium have a direct relationship between the I% in I/S and burial temperature. However, the application of the I/S geothermomether must be made with some caution since clay minerals provide information on

the burial and thermal history of sedimentary rocks that is useful in the exploration, evaluation, and production of hydrocarbons. It is important to make several determinations from different samples that will give more reliable results. Additionally, the samples should be washed to remove smectite-rich drilling mud. Also it is important to consider that kinetic factors limit the applicability of a simple I/S geothermometer. However this factor is significant over the higher expandability range (<50% I). I/S geothermometers are more reliable for lower Tertiary and Mesozoic rocks.

In burial-diagenetic settings the reaction takes place over the same temperature interval as hydrocarbon maturation, and the release of interstitial water during I/S diagenesis may cause zones of overpressure and aid in petroleum migration . The conversion of smectite layers to illite layers has been proposed as a major source of cements (especially quartz) in associated sandstones (Hower et al., 1976), and the extent of the reaction has been applied as a geothermometer (summarized in Pollastro, 1993) . (Lynch, Mack, & Land, 1997)

The use of mixed-layer illite/smectite (I/S) as a geothermometer and indicator of thermal maturity in petroleum geology studies is based on concepts of shale diagenesis that were first described in detail on studies of the Gulf Coast (Hower et al., 1976). Quantitatively, the most important diagenetic clay reaction in shale is the progressive transformation of smectite into illite via mixed layer illite/smectite (I/S) because smectite plus I/S account for 30% of the total sediment/rock mass (Srodon, 1989). This reaction is also commonly referred to as *smectite diagenesis or smectite illitization.* The reaction is irreversible under progressive burial conditions.

Changes in the proportion of illite, smectite (also referred to as expandability), and ordering

of I/S, interpreted from X-ray powder diffraction (XRD) profiles, correlate with changes in temperature due to burial depth (Figure 2-9).

Models applying temperatures to clay minerals for their use as geothermometers in burial diagenetic or low-grade metamorphic settings were first proposed by and Weaver (1979). Similar empirical clay mineral-to-temperature relations have been demonstrated for hydrothermal fluid systems and contact metamorphic situations. However, temperatures initiating change in the illite/smectite ratio and ordering of I/S differ between relatively short-lived geothermal systems and long-term burial settings. These specific changes in I/S, therefore, indicate maximum temperatures provided that the proper temperature model is used. (Pollastro, 1993).

In summary, Pollastro (1993) prove that I/S geothermometry can greatly assist in evaluating the thermal and tectonic history of a sedimentary basin. Specific I/S geothermometers are approximately coincident with temperatures for hydrocarbon "windows" and, therefore, are useful in energy exploration for determining the hydrocarbon-generation potential and thermal maturity of petroleum source rocks. (Pollastro, 1993)

Quartz cementation

Cementation is a diagenetic process, where the particles that make up a sedimentary rock are cemented together by new minerals after deposition. Cements are precipitated from mineral rich water moving through any cavities or pore spaces between the grains of sediment. Figure 2-10 shows the mechanism of cementation. (University of Canterbury)

Some of the factors that control quartz cementation include temperature, pressure, time and pore water composition. Experiments showed that in hydrothermal reactors indicate that "pressure solution" resulted in "sutured" quartz grains along a surface of mutual quartz dissolution. Houseknecht (1984) stated "the volume of quartz cement present in Hartshorne sandstones was controlled by the amount of intergranular pressure solution that a sample experienced and by local geochemical and mineralogical factors. The volume of quartz cement generally increases with increasing grain size and decreasing thermal maturity because of the primary influence exerted by intergranular pressure solution. The maximum possible volume of quartz cement present in a sandstone can be predicted on the basis of grain size and thermal maturity, but absolute volumes of cement are impossible to predict"

An experiment conducted in a closed system where quartz grains were partially dissolved in some areas and quartz cement precipitated in others. They established relationships between grain size and quartz overgrowth. For instance, coarse-grained sands were cemented more rapidly than fine-grained sands were water flow was rapid. Conversely, were the influx rate was slow due to low permeability; the fine-grained sands were cemented more rapidly than coarse-grained sands.

In addition, as shown in Figure 2-11, Thomson (1959) discovered that clay coatings stimulate quartz cementation by providing microenvironments in which pH is elevated such that the parts of quartz grains can dissolve. This results in sutured quartz grains in high pH zones, and the precipitation of quartz overgrowths in low pH zones. Thyberg et. al (2009) stated that silica released from the dissolution of smectite, resulting in precipitation of illite during progressive burial has most likely been the source of the locally precipitated micro-quartz in mudstones in the northern North Sea (Eslinger & Pevear, 1988).

2.2.1.4 Overpressuring (Thomson, 1959)

Under normal conditions, in a pile of porous and permeable strata, the hydrostatic pressure is less than the rock pressure. Since the rock is more than twice dense as water, the lithostatic pressure exceeds the hydrostatic, assuming that the mineral grains are in contact and support the rock and that the water passively fills the interconnected pores.

In shale, the smectite to illite reaction produced water and may also be affected by the lithostatic pressure if the water produced by the process is allowed to drain from the system. This drainage condition would constitute normally pressured shale. But in the case of a water-rich mud that is rapidly buried such that it is too impermeable for the water to escape as it does during normal compaction, the water supports the weight of the overlying rock, and the water pressure rises from the hydrostatic value to approach that of lithostatic pressure. This condition is known as overpressuring and is fairly common in the subsurface.

The release of diagenetic water from the illitization of smectite could also be another cause of overpressuring. (Figure 2-12) During the transformation of smectite to illite, there is a maximum of 30% volume reduction of the solid phase and water is expelled out of the mineral into pores. If the mineral grains are no longer in supportive contact and the water cannot escape, the fluid pressure will rise above normal hydrostatic pressure causing overpressuring

2.3 Normalized Undrained Shear Behavior

Research on a wide range of clays, conducted at Imperial College and MIT, has shown results of laboratory tests on clay samples with the same overconsolidation ratio (OCR), but different consolidation stresses (σ'_{vc}) and different maximum pressures (σ'_{vm}), exhibit very

similar strength and stress-strain characteristics when normalized with respect to the consolidation stress. (Ladd & Foot, New Design Procedure for Stability of Soft Clays, 1974). Figure 2-14 shows an example of normalized behavior using idealized triaxial compression test data for homogenous clay. The normalized behavior concept is observed to apply to pore pressure data as well.

During the past 50 years, the normalized method has been used extensively by many researchers at MIT. Results exhibited small divergences on the normalized strength, and not exceeding 10% of the mean. The Normalized Soil Parameter (NSP) concept derives from these empirical observations and provides a useful framework for comparing and relating soil behavior. The development of the SHANSEP (Stress History and Normalized Soil Engineering Properties) design method from Ladd and Foot (1974) is based on the NSP concept. This concept is also the basis for frameworks such as the Critical State Soil Mechanics (Schofield & Wroth, 1968) and various analytical models such as Modified Cam Clay (Roscoe & Burland, 1968) and MIT-E3 (Whittle & Kavvadas, 1994).

The SHANSEP design method is applicable to overconsolidated uniform cohesive soils or truly normally consolidated. It is important to consider that this technique is not intended to be used in cemented, highly sensitive clays or in drying crust of a soil deposit. This method is oftend used to describe the undrained shear compression and extension in triaxial, plane strain or direct simple shear tests. The main premise of this method is that the in situ stress history can be replicated in the laboratory and provide accurate predictions of soil behavior at different OCRs. Figure 2-15 shows the how to reproduce the stress history in a specimen. The stress history is simulated in the laboratory by imposing stresses above the preconsolidation pressure to some new maximum stress (points A or B in Figure 2-15), σ'_{vm}, to the specimen in K_o-Consolidation.

(Ladd, Stability Evaluation during Staged Construction, 1991) Under the assumption that all overconsolidated soils behave the same way regardless the mechanisms that caused its condition, the soil is mechanically overconsolidated by Ko swelling (points C or D) to achieve an overconsolidation ratio above 1. Typical results of a SHANSEP test program conducted on AGS Plastic Marine Clay is exhibit in Figure 2-16 (Koutsofas & Ladd, 1985). These results can be related using the expression known as the SHANSEP equation:

$$\frac{s_u}{\sigma'_{vc}} = S \cdot (OCR)^m$$

Where S is the undrained strength ratio for the normally consolidated clay, and m is the slope of regression line (Abdulhadi, 2009). Previous researchers have stated that the SHANSEP method is ideal for resedimented samples as a reconsolidation technique prior shearing.

2.3.1 Effect of Stress Level on Normalized Strength

SHANSEP technique's premise is that normalized behavior is only dependent in OCR. Research conducted by Moniz (2009) and Ahmed (1990) on normally consolidated resedimented clay showed that the normalized strength decreases while increasing the stress level. Furthermore, Abdulhadi (2009) examined the effect of stress level on normalized strength of overconsolidated RBBC. Figure 2-17 exhibits the stress level influence on the normalized properties. It can be observed that the S parameter decreases from 0.314 at σ'_{vm} = 0.2 MPa to 0.281 at σ'_{vm} = 10 MPa. On the other hand, the m parameter varies slightly from previous reported values. However, for the range of stresses commonly encountered in geotechnical engineering the effect is not considered significant.

2.3.2 Normalized Behavior of Clay Shales

Clay shales consist on fine grained soft rocks with a clay fraction above 50%. The formation of these soft rocks occurs in sedimentary basins by diagenetic processes, which turn young clay sediments in cemented and lithified shales. Johnston and Novello (1994) stated that clay shales exhibit an intermediate behavior between soft clays and hard cemented rocks. The applicability of SHANSEP to clays shales have being studied by few researchers in the recent years, (e.g., Steiger & Leung, 1991; Gutierrez et al., 2008). Gutierrez et al (2009) compiled consolidated undrained triaxial results of 25 types of clay shales from different locations and various degrees of diagenesis and cementation. This study was conducted using the recompression technique by Bjerrum (1973), to reconsolidate the intact samples; however the normalization aspect of SHANSEP was applied in the analysis. Figure 2-18 shows the normalized shear stress-strain responses for intact samples of Kimmeridge Shale and Barents Sea Shale, with apparent preconsolidation stresses estimated of 22 MPa and 40 MPa respectively. The normalized undrained shear strength versus OCR presented by Gutierrez et al show that SHANSEP might be applicable to clay shales as shown in Figure 2-19. The correlation presented by Gutierrez et al yielded on SHANSEP parameter S = 0.37 and m = 0.87 with an $R^2 = 0.80$.

2.4 Previous Experimental and Field Studies on Overconsolidated Clays

Overconsolidated clays have been of interest for geotechnical engineers since the late 1930s. In 1936, Terzaghi was the first to spotlight the discrepancy between the average shear stress along a failure surface in a landslide and the shear strength measured in laboratory testing.

Table 2-1 summarizes some of the publications on overconsolidated clays. Regardless of the interest of many researchers about various aspects of heavily overconsolidated clay, the author found it challenging to find published data regarding the behavior of such clays at low effective stresses. Furthermore, limited field evidence shows that heavily overconsolidated clays undergo a distinct change in its behavior at small effective stress.

Subsequent studies by Skempton (1948), and Binger (1948) confirmed the softening of stiff, fissured clays with time as suggested by Terzagui (1936). Then, in 1954, Henkel and Skempton demonstrated that the effective stress analysis of stability for natural slopes using the drained angle of shearing resistance and zero "cohesion intercept" resulted on unreliable factors of safety. Furthermore, Henkel (1955) discussed the problem of earth pressures exerted by stiff clays such as London Clay, which is known as overconsolidated soil.

Later, in 1960, Gould concluded that the existence of previous slides or small deformations in slopes in California have a significant impact on the long-term stability of stiff clays. Afterwards, Wilson and Johnson (1964) pointed out the nature of instability of heavily overconsolidated clays in Seattle. The combination of "locked in" lateral stresses, susceptibility to fracture and layering resulted in progressive failure for the case study.

In 1979, Banerjee and Stipho suggested a model to predict the undrained behavior of heavily overconsolidated clays. This study compares undrained compression and extension test results with the theoretical predications performed by the model for heavily overconsolidated clays. By using a consistent set of characteristic material parameters satisfactory agreement between the theoretical and experimental results have been achieved. Figure 2-20 shows the normalized stress-strain responses of three samples in compression tests and two samples in extension tests.

The authors attributed the difference between the observed and the predicted behavior during the early stages to the assumption of elastic conditions up to the peak (Banerjee & Stipho, 1979).

In 1990, Atkinson et al. considered the effects of a change in the direction of the loading path on the stiffness of overconsolidated soil on reconstituted samples of London Clay and other soils with a variety of plasticity values. The authors reported that the response of overconsolidated soil is largely inelastic and highly nonlinear, and that the recent history has a major effect on the subsequent stiffness, particularly for relatively small changes of stress or strain. (Atkinson, Richardson, & Stallebrass, 1990)

In 1993, Brooker and Peck, investigated the occurrence of slides in overconsolidated, flat-bedded clays and clay shales giving special attention to the failure mechanism, evaluation and engineering design (Brooker & Peck, 1993)

In 2006, Smith et al looked at the technical and non-technical factors, affecting selection of design shear strength values for specific projects. The authors argued that for many long-term projects the decision often involves the consideration of residual strength, fully softened strength or some other value. This paper studied in detail the issue of slope stability of the Cretaceous-aged Potomac Formation in the Washington, DC area (Smith, Jahangir, & Rinker, 2006).

In 2011, B. Schädlich & H. F. Schweiger presented a novel approach to model the shear strength of highly overconsolidated, stiff clays in numerical analysis. The multilaminate framework of the model is explained, and details of the yield surfaces, plastic potential functions and hardening rules are given. Figure 2-21 shows a comparison between experimental and calculated undrained stress paths for the normally and overconsolidated samples (Schädlich & Schweiger, 2011).

In 2012, Budhu integrated bearing capacity–settlement approach to the design of shallow foundations on heavily overconsolidated clays by alterations of the "modified Cam clay" (MCC) model. The proposed method is limited to homogeneous, saturated, heavily overconsolidated clays. It cannot be used to determine the collapse load. Rather, it gives the load at the limiting stress condition in a soil mass and a suitable factor of safety (suggested value = 1.25) to prevent the soil mass from reaching this state. While the method can be extended to dense coarse-grained soils, the difficulty is in defining an overconsolidation ratio for these soils (Budhu, 2012).

Table 2-1 Overview of previous studies in overconsolidated soils

Year	Researcher	Topic
1936	Terzagui	Stability of Slopes of Natural Clays
1948	Skempton	The rate of softening in still fissured clays with special reference to London Clay
1948	Binger	Analytical Studies of the Panama Canal Slides
1954	Peterson	Studies of Bearpaw Shale at dam site in Sasketchewan
1955	Henkel and Skempton	A landslide at Jackfield, Shrosphire, in Heavily Overconsolidated Clay
1955	Henkel	Discussion on Earth Pressure on Stiff Fissured Clays
1957	Henkel	Investigation of two long-term Failures in London Clay Slopes at Wood Green and North-holt
1960	Gould	A Study of Shear Failure in certain Testiary Marine Sediments
1964	Skempton	Long-term Stability of Clay Slopes
1964	Ringheim	Experience with the Bearpaw Shale at the South Saskatchewan River Dam
1964	Wilson and Johnson	Slides in Overconsolidated Clays along the Seattle Freeway
1965	Fookes	Orientation of Fissures in Overconsolidated Clay of the Siwalki System
1966	Fookes and Wilson	The Geometry of Discontinuities and Slope Failure in the Siwalki Clay
1967	Bjerrum	Progressive Failure in Slopes in Overconsolidated Plastic Clay and Clay Shales
1967	Morhnstern and Tchalenko	Microstructural Observation on Shear Zones from Slips in Natural Clay
1969	Yudhbir	Engineering Behavior of Heavily Overconsolidated Clays and Clay Shales with Special Reference to Long-term Stability
1971	Singh	The behavior of normally consolidated and heavily overconsolidated clays at low effective stress
1979	Banerjee And Stipho	An Elasto-Plastic Model for Undrained Behaviour Of Heavily Overconsolidated Clays
1982	Gens	Stress-strain and Strength Characteristics of a Low Plasticity Clay
1990	Atikinson et al	Effect of Recent Stress History on the Stiffness of Overconsolidated Soil
1993	Brooker and Peck	Rational Design Treatment of Slides in Overconsolidated Clays and Clay Shales
1994	Whittle and Kavvadas	Formulation of MIT-E3 Constitutive Model for Overconsolidated Clays
2006	Smith et al	Selection of Design Strengths for Overconsolidated Clays and Clay Shales
2011	Schädlich & Schweiger	A Multilaminate Soil Model for Highly Overconsolidated Clays
2012	Muniram Budhu	Design of Shallow Footings on Heavily Overconsolidated Clays

Table 2-2 Stages of Diagenesis (adapted from Weaver 1989)

Stage	Description	Illite/Smectite Layers	Temperature
Early diagenesis	From the water-mud contact to regular mixed-layer I/S is present.	~60% Illite	~90 - 140°C
Middle diagenesis	From the first regular mixed-layer (~14 to 13 Å peak when glycolated) to the disappearance of a discrete glycolated peak.*	~90% Illite	~200°C
Late diagenesis	Stage from where the glycolated mixed-layer phase appears as an integral part of the 10 Å peak to the beginning of anchizone*.	<10% Smectite	~250 to 280°C

*Glycolation is an experimental treatment of clays by exposure in an open container of ethylene glycol at 80°C for 4 hours, used to study expansion of smectite clays during an XRD. An internal standard X-ray diffraction (XRD) analysis technique permits one to reproduce and accurately calculate the mineral contents of rocks, including the major clay mineral families

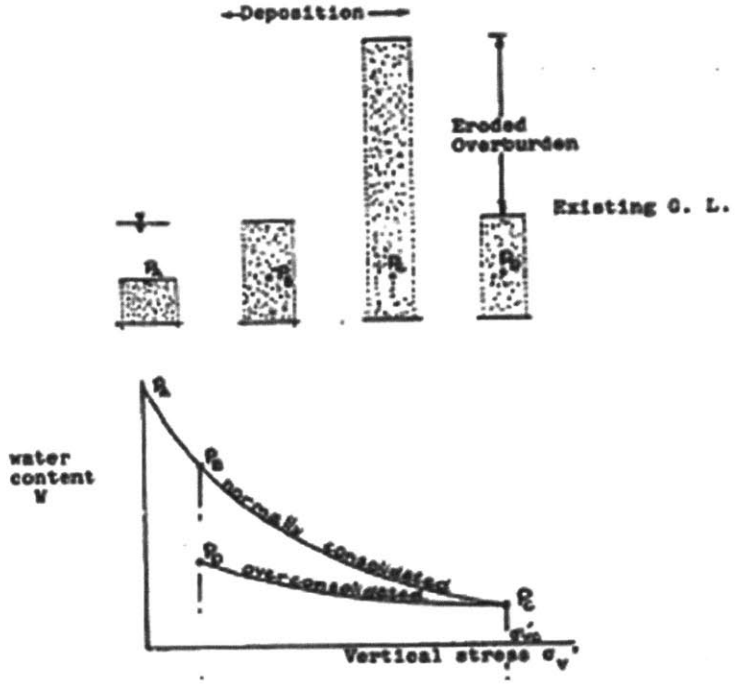

Figure 2-1 Simplified Concept for Normally Consolidated and Overconsolidated Clay (Singh, 1971)

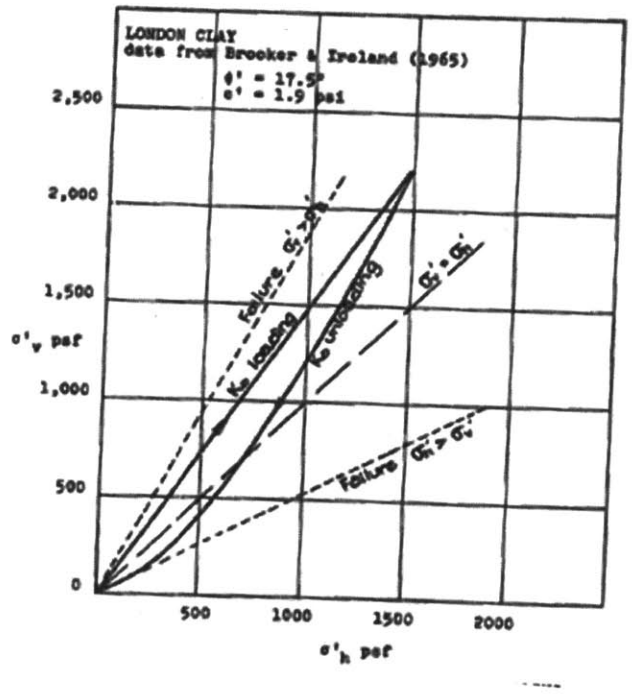

Figure 2-2 Stress Path during Ko Loading and Unloading (Brooker & Ireland, 1965)

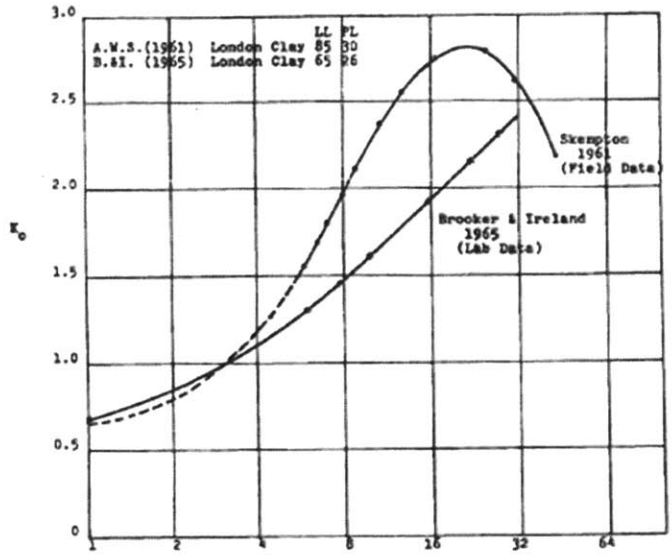

Figure 2-3 Comparison of Field and Laboratory Unloading Curves for London Clay (Singh, 1971)

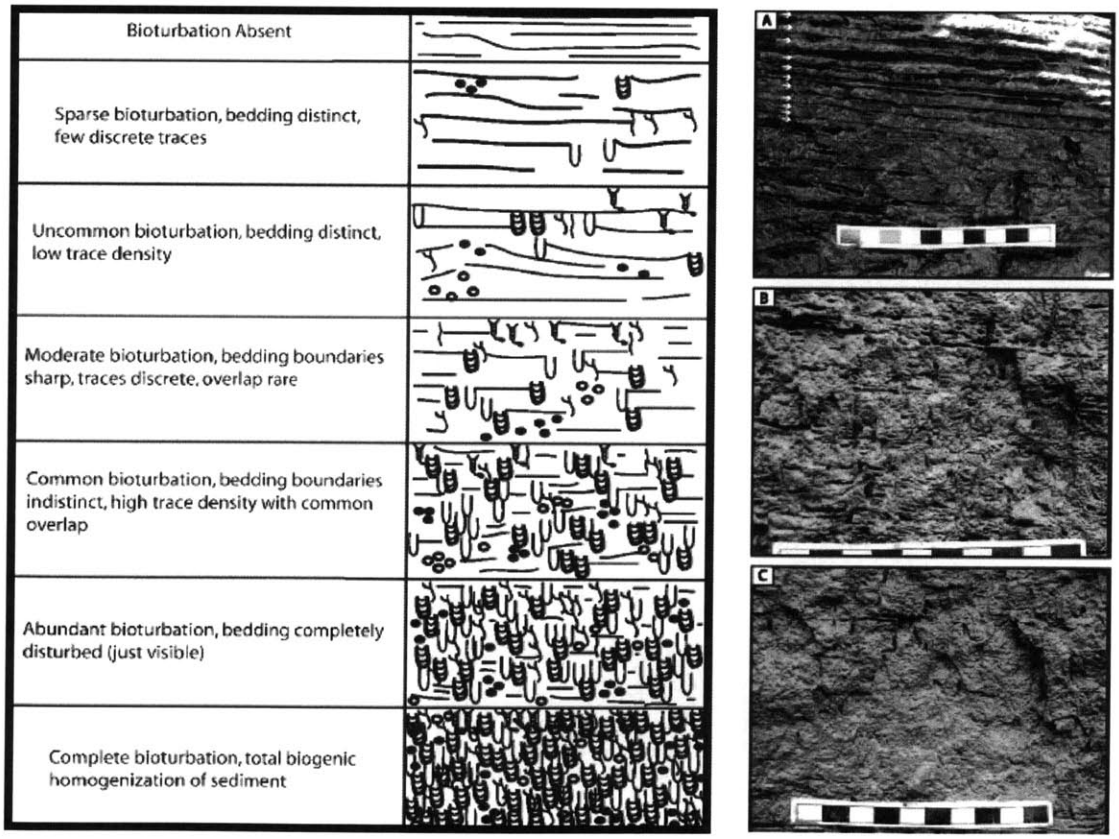

a) b)

Figure 2-4 Bioturbation – grain rearrangement. a) Bioturbation grades b) Degrees of bioturbation in seasonal deposits of Sepody River. (adapted from (Pearson & Gingras, 2006)

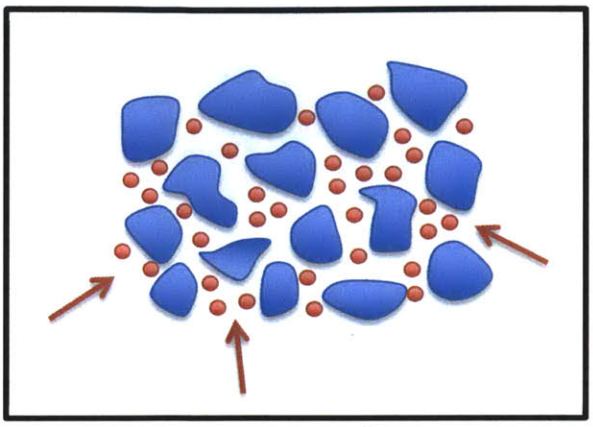

Figure 2-5 Elutriation – fine-grained particles infiltrate into the pores.

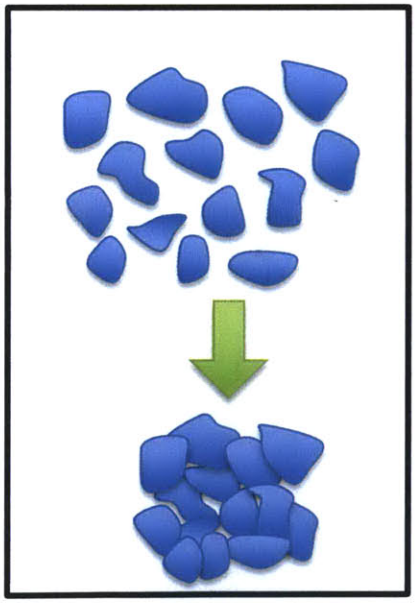

Figure 2-6 Conceptual process of the compression/compaction of grains pushed together and interlocked

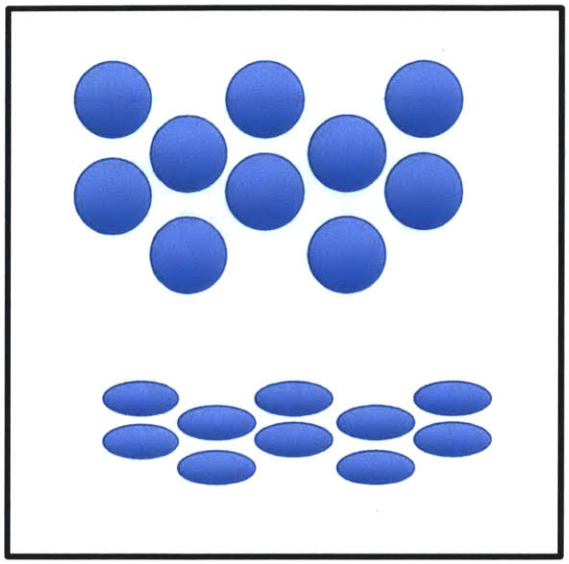

Figure 2-7 Deformation - Particles get deformed

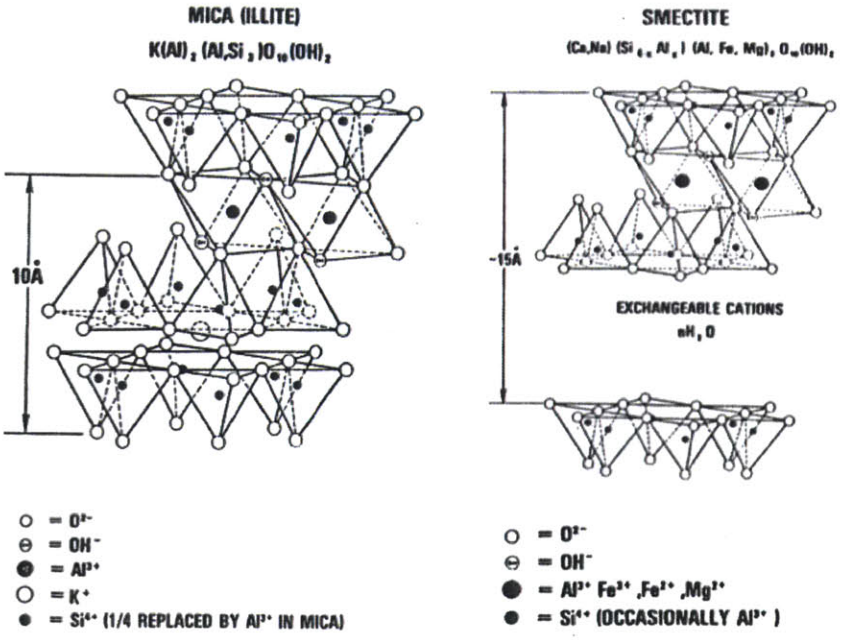

Figure 2-8 Illite and Smectite chemical structure and composition.

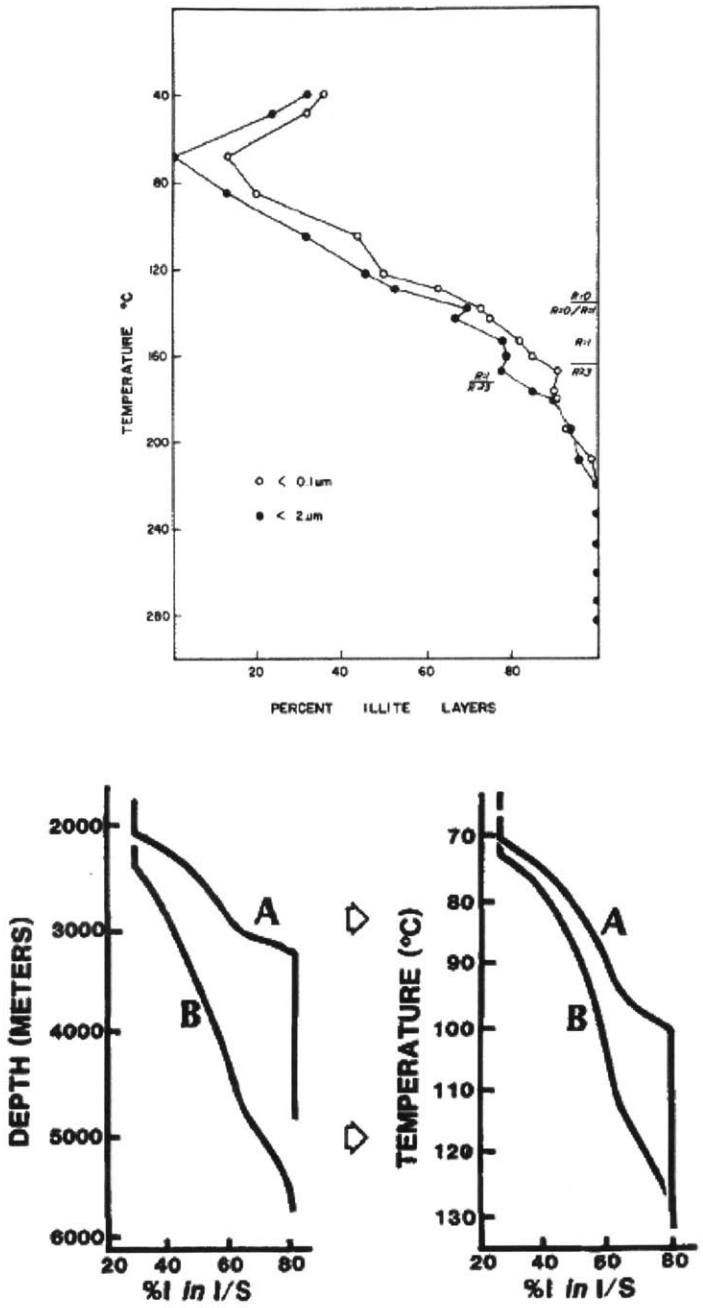

Figure 2-9 Proportion of I/S vs. depth and temperature. (A) Oligocene well (B) Miocene well. (adapted from Hower, 1981)

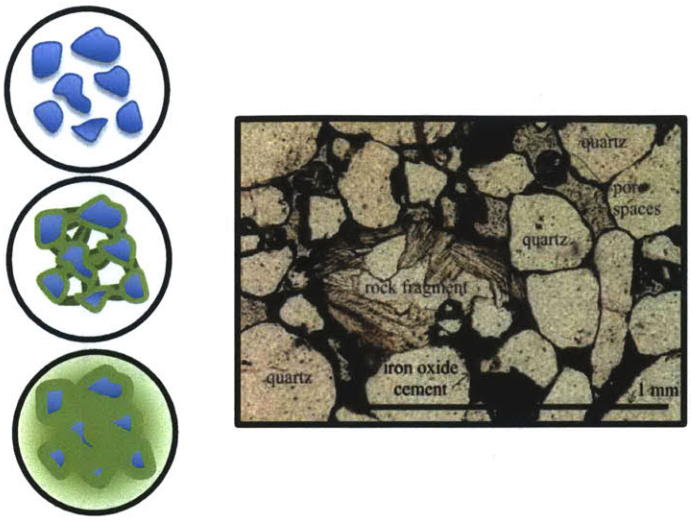

Figure 2-10 Cementation a) Conceptual mechanism b) Rock fragment cementation

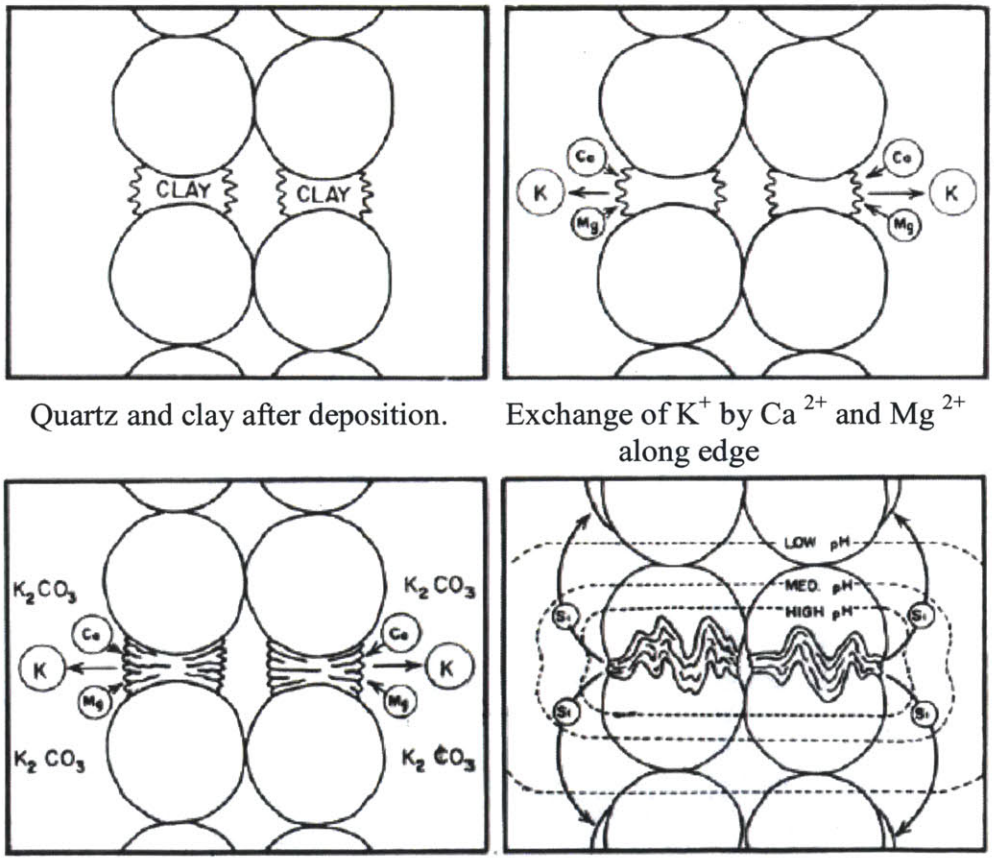

Quartz and clay after deposition.

Exchange of K^+ by Ca^{2+} and Mg^{2+} along edge

Exchange along cleavage. K_2CO_3 formed and pH increases in clay-rich areas.

With the increase of pressure, Si4+ dissolved in high pH moves to low pH areas and

Figure 2-11 Quartz cementation with pH (from Thomson 1959)

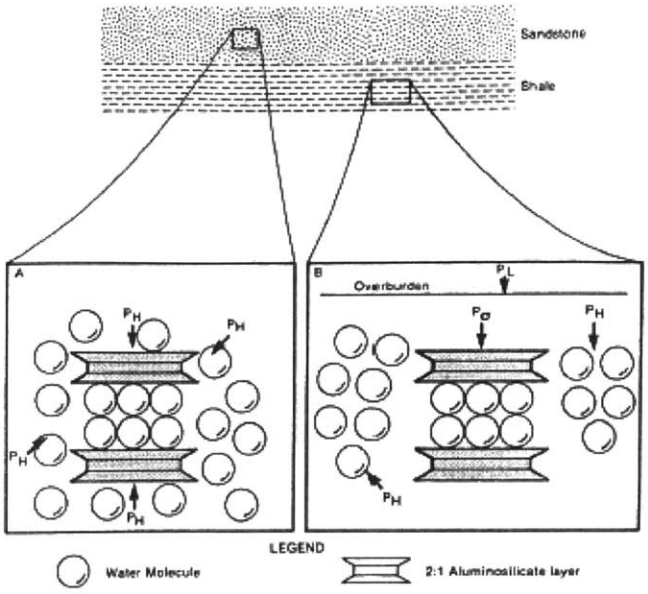

Figure 2-12 Pressure acting on smectite layers depending on the material. (Eslinger & Pevear, 1988)

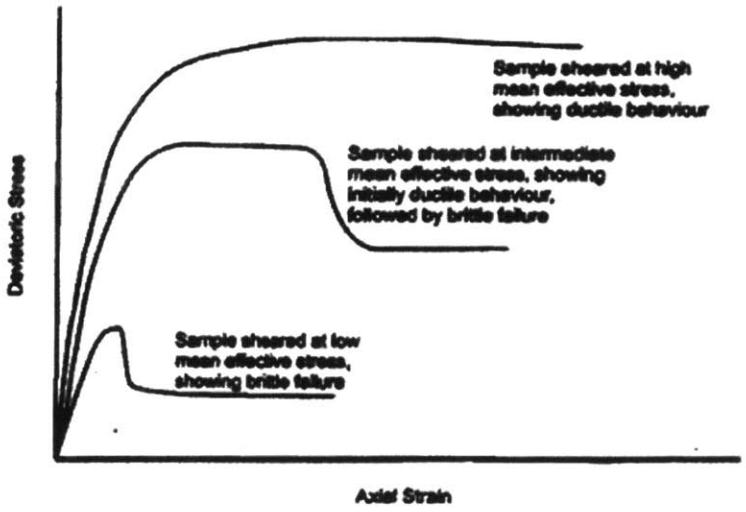

Figure 2-13 Conceptual description of stress-strain response for clay shales (Petley, 1999)

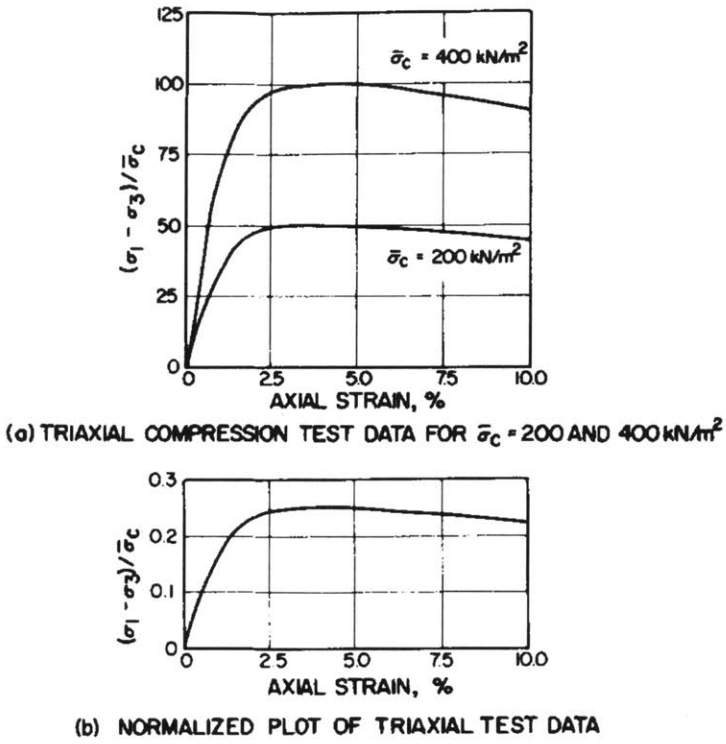

Figure 2-14 Example of normalized behavior using idealized triaxial compression test data for homogeneous clay. (Ladd & Foot, New Design Procedure for Stability of Soft Clays, 1974)

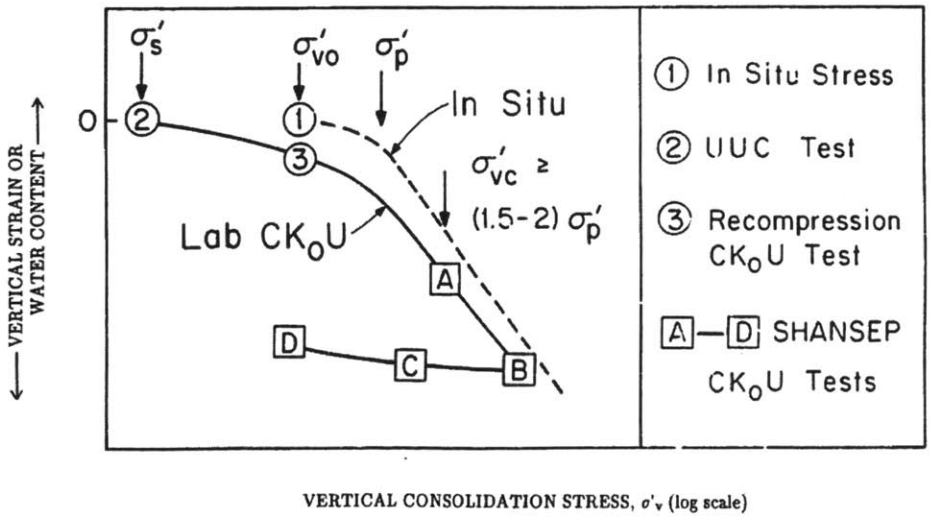

Figure 2-15: Consolidation procedure for laboratory CK_0U testing (from Ladd, 1991)

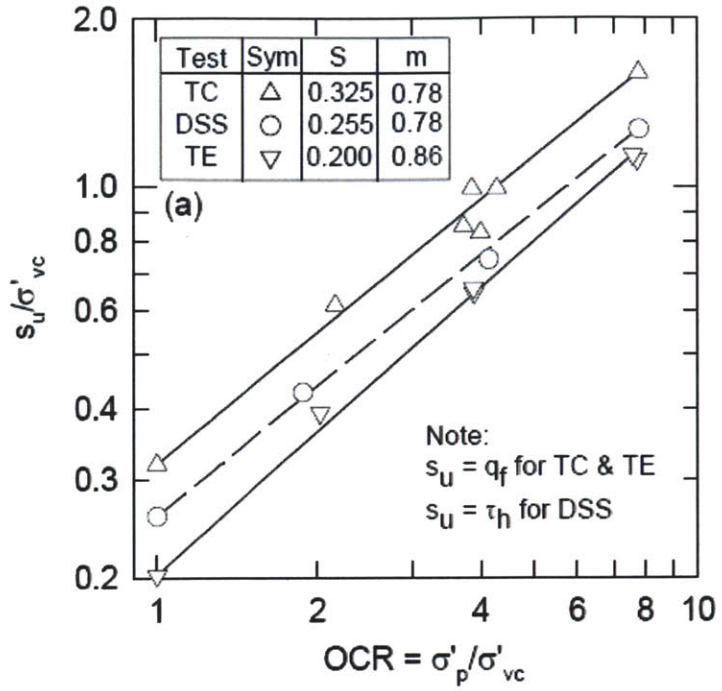

Figure 2-16: Normalized undrained shear strength versus OCR for AGS Plastic Marine Clay via SHANSEP (from Koutsoftas & Ladd, 1985)

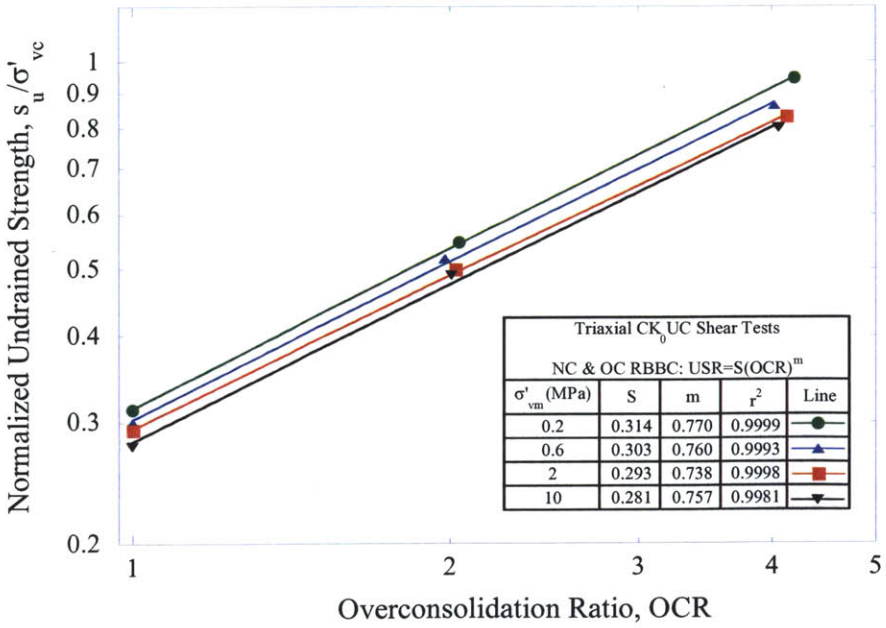

Figure 2-17 Normalized undrained strength versus OCR for RBBC from selected CK_0UC triaxial tests illustrating the effect of stress level

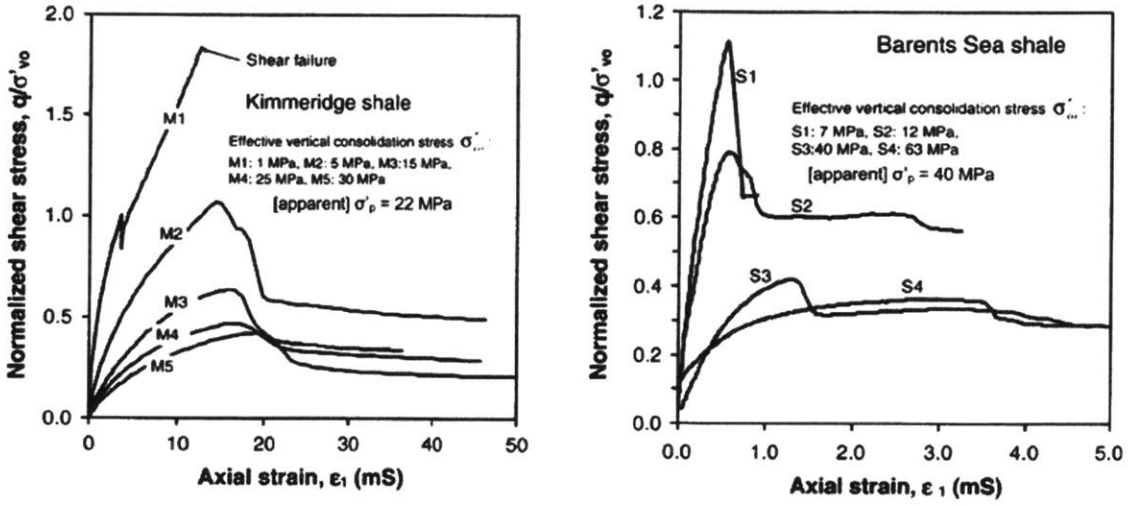

Figure 2-18 Normalized shear stress versus (q/σ'_{vc}) axial strain (milistrain, mS) for CIUC tests on Kimmeridge Shale and Barents Sea Shale (Gutierrez , Nygard, Hoeg, & Berre, 2008)

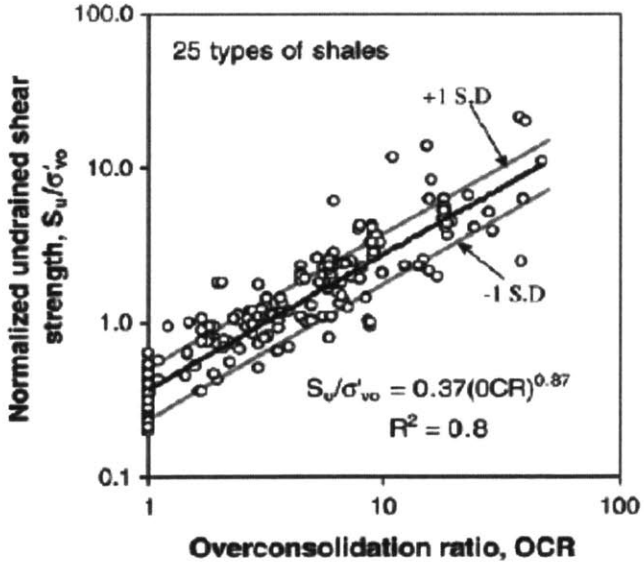

Figure 2-19 Normalized undrained shear strength versus OCR for 25 types of shales. (Gutierrez , Nygard, Hoeg, & Berre, 2008)

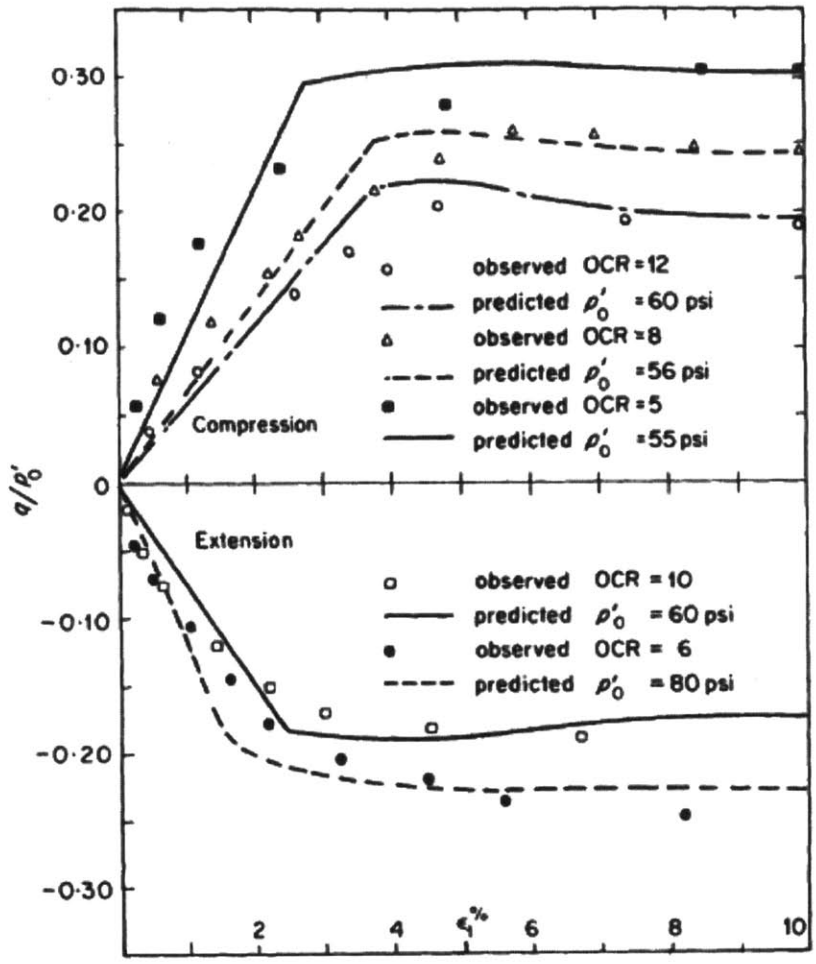

Figure 2-20 Normalized stress-strain responses of three samples in compression tests and two samples in extension tests. (Banerjee & Stipho, 1979)

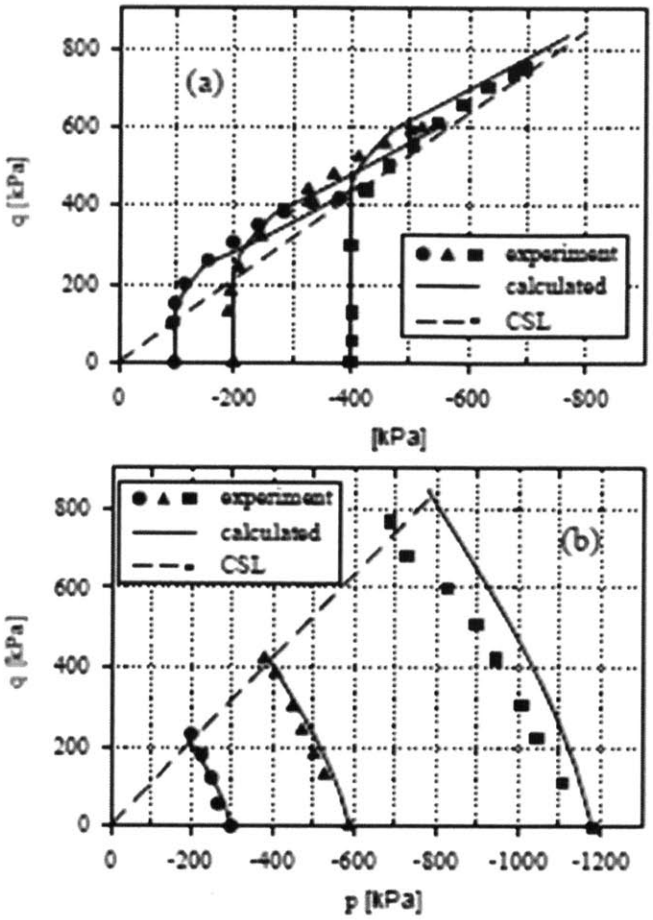

Figure 2-21 Undrained triaxial stress paths comparison (Schädlich & Schweiger, 2011)

3 MATERIALS

This chapter describes the materials used for testing in this research and the material processing procedure. Section 3.1 describes the resedimentation procedure, index properties and consolidation characteristics of Resedimented Boston Blue Clay (RBBC). Section 3.2 describes Maine Clay as the intact material used in the testing program.

3.1 Resedimented Boston Blue Clay

Natural soil specimens are variable in many different aspects such as, homogeneity, stress history and extraction disturbance. This variability can lead to difficult data interpretation due to different material sources and lack of sufficient reference behavior. The resedimentation process was used in order to eliminate spatial variability and provide uniform samples with well-defined one-dimensional stress history. This section provides an overview of Resedimented Boston Blue Clay (RBBC), one the test material employed in this program.

Boston Blue Clay (BBC) is an illitic glacio-marine clay of low plasticity (CL) and medium sensitivity. BBC was deposited in the Boston basin about 12,000 to 14,000 years ago following the Wisconsin glacial period (Kenney, 1964). BBC is present throughout Boston with various thicknesses from 20 to 40 m. A stiff overconsolidated crust (OCR = 2 - 5) forms the upper 12 to 20 m of the deposit while underneath the clay is close to normally consolidated (Santagata, 1998). Some variability can be expected in soil from different locations and consequently RBBC's made from different natural sources even though the depositional history and general

characteristics of BBC are similar around the Boston area. The index properties of clay depend on many aspects, such as the mineralogy, the particle size distribution and the chemistry of the pore fluid.

Natural BBC has been the source material for resedimentation at MIT since 1961 and there is an extensive database on the engineering properties of this material. RBBC engineering properties are very similar to many natural clay deposits, including stress-strain anisotropy, low to medium sensitivity, significant strain rate dependence, and fairly typical consolidation characteristics. These key characteristics have made this soil an ideal research material to investigate fundamental aspects of soil behavior without having to take into account the variability of natural soils.

The origin of the natural material defines the RBBC batch series. Series III was obtained by auguring from a depth of 23 m during the construction of a parking garage near Kendall Square in Cambridge. Boston Blue Clay Series IV was the batch employed in this testing program. RBBC Series IV was obtained from the base of an excavation for MIT's Biology Building in 1992. Approximately 2500 kg of BBC was excavated at a depth of 12 m where the OCR of the clay varied from 1.3 to 4.3. (Berman, 1993) The procedure employed to obtain the soil powder is described in section 3.1.1.

3.1.1 Resedimentation Process

The resedimentation procedure and equipment, used at MIT for reconstituted samples since 1961, had being improved over the years. Initially, the technique produced a large soil cake that was then trimmed into smaller pieces by consolidating a dilute slurry of BBC in a rigid-walled

cylindrical column container referred as consolidometer. Ladd and Varallyay (1965) produced partially saturated samples that were subsequently saturated using a 200 kPa back pressure. Germaine (1982) improved this method to produce fully saturated, uniform samples of RBBC with a salt concentration of 16 g/l by using a mixing chamber with rotating blades to mix the powder with 100% water content under a vacuum and a lower free fall chamber with a stainless steel consolidometer which receives the sprayed slurry and consolidates the soil. Seah (1990) introduced further modifications to the layout, extrusion technique and remote data acquisition that resulted in higher productivity, better sample uniformity and allowed continuous monitoring on the consolidation process. Today, the procedure developed by Abdulhadi (2009) is used to resediment all kind of clay at MIT. Abdulhadi's approach of preparing individual batches for each test specimen reduces the load that must be applied to achieve a particular preconsolidation pressure, especially important for high stresses batches.

3.1.1.1 Procedure

The current process employed at MIT for resedimentation has been described by many researchers including Abdulhadi (2009), Adams (2011), Casey (2011), Horan (2012) and Marjanovic (2012). The basic procedure is divided into four main stages: powdering, deposition, consolidation, and sample extrusion.

a) Powdering

In order to process the soil to a state in which it is suitable for resedimentation, a powder must be produced which will pass a US#100 (0.15 mm) sieve. This procedure consists of: (1) Softening of natural BBC with tap water and mix into a thick slurry. (2) Passing the slurry

through a #10 US (2.00 mm) standard sieve to remove all non-natural material, gravel, coarse sand, and large shell fragments. (3) Oven-drying at 60°C in preparation for grinding. (4) Grounding the dried material to 95% passing a #100 US (0.15 mm) sieve by the Sturtevant Company using a roller mill. (5) Randomizing the material by two blending operations. Finally, the dry powder (RBBC Series IV) is stored in sealed 40 gallon containers. (Cauble, 1996)

b) Deposition

After carefully estimating the quantity of dry soil powder and retrieving the desired mass of BBC powder from storage, the powder is then added to a prescribed amount of salt water and allowed to hydrate for 24 hours. Then, the fully hydrate slurry is mixed thoroughly using an electric blender (KitchenAid mixer) for duration of about 30 minutes. This mixing procedure produces a homogenous slurry without lumps, ensures a through blending of the clay and allows sufficient time to the clay particles to swell. The natural salt concentration of BBC ranges from 4 to 32 g/L depending on the locations and depth, therefore choosing a value in the mid-range of the natural salinity prevents excessive changes to the pore chemistry of the soil, which can alter the material properties of the specimen. (Horan, 2012). For this testing program the slurry was mixed with a pore fluid to achieve a 100% water content and a salt concentration of 16 g/L. This pore fluid consists of distilled water with salt (NaCI or Sea Salt) added to achieve a concentration of 16 g/l. Salt is added as a flocculent to minimize segregation of the soil particles during sedimentation and to achieve a soil fabric similar to that of natural BBC.. Note that the slurry water content of 100% is over twice the liquid limit of the clay (45 - 48 %) and results in a workable yet stable slurry with no free water present at the surface.

The slurry is then vacuumed (under 20 inches Hg) to get rid of any entrapped air. The slurry is poured in a Buchner flask using two lines: one line is connected to the vacuum pump while

the second line is used to suck the slurry from the mixing container as shown in Figure 3-1. The slurry is effectively de-aired as it falls into the flask. Once all the slurry is inside the Buchner flask a stopper is used to isolate the soil from atmospheric pressure for about 30 minutes.

Following vacuuming, the de-aired slurry is carefully placed in a tube, which inner diameter is about 3.5 cm, of a consolidometer from bottom to top by carefully pouring it using a funnel to minimize entrapment of air bubbles. Prior to pouring the slurry, the inside wall of the tube is lubricated with a thin film of either silicon oil or high viscosity vacuum grease. This lubrication minimizes sidewall friction during consolidation and also aids in the subsequent extraction of the clay from the tube. A floating sleeve set-up is used as described in section 3.1.1.2, and shown in Figure 3-2. The bottom of the acrylic tube is sealed off with a tightly-fitting porous stone and nylon filter, constraining the slurry to escape from the bottom. The top of the tube is closed off with another nylon filter paper and porous stone. These porous stones transfer the load applied to the sample and provide double drainage where excess pore pressure can escape. Finally, the outside container is filled with saline water to create a bath at the same salinity as the slurry to maintain a consistent pore chemistry.

c) Consolidation

The slurry is loaded incrementally in a consolidometer, described in section 3.1.1.2, which has double drainage, using a load increment ratio (LIR), $\Delta\sigma'_v/\sigma'_v = 1$ to obtain enough primary consolidation without causing extrusion. Each load increment is maintained at least until the end of primary consolidation (EOP), as determined by the Taylor Root time method. A sample plot from a typical increment can be seen in Figure 3-3. EOP is the point at which the majority of the deformation has occurred, all excess pore pressures has dissipated and secondary compression begins. This is when the next load increment can be applied. During each consolidation

increment axial deformation can be measured using an electronic displacement transducer or linear variable differential transformer (LVDT) anchored to a stationary surface in order to establish the EOP as well as to gain information on consolidation properties during resedimentation. However, measuring the displacement with a ruler and setting the increment time will be sufficient information. After the target maximum axial stress and allowed secondary compression, i.e. preconsolidation pressure σ'_p, has been reached, the resedimented specimen is rebounded to an overconsolidation ratio (OCR) of 4. The OCR is the maximum past stress divided by the current stress. At OCR = 4 the clay is close to uniform effective stress conditions, i.e. K_o = 1, and the shear strains due to specimen extrusion from the consolidometer are minimized, as confirmed by the work of Santagata (1994). A description of the equipment used during the consolidation stage of resedimentation is given in section 3.1.1.2.

Consolidation Behavior during Resedimentation

The one-dimensional consolidation behavior of RBBC during resedimentation can be analyzed as in a standard incremental oedometer test. This can be done because the soil slurry is incrementally loaded with known loads and resulting displacements as in the oedometer test. The consolidation process for a triaxial test specimen starts with very low vertical stress increment until it reaches at maximum of approximately 0.08MPa. This research produced more than 15 triaxial tests specimens. The time required to reach the end of primary (t_p) for each load increment depends on the drainage height of the sample as well as on the vertical coefficient of consolidation, c_v. The first few load increments require several days to reach t_p, however this

time is significantly reduced as the length of the specimen, or drainage height, becomes shorter at higher stresses. The EOP is reached after about 12 hours and a resulting settlement of 1.0 cm.

The water content and height of a sample is measured upon the extrusion from the consolidometer. These measurements are used to back-calculate the water content and void ratio at the end of each load increment. Abdulhadi (2009) and Casey (2011) showed a very good repeatability in the one-dimensional consolidation behavior during resedimentation. Figure 3-7 shows Casey's (2011) comparison between the compression curves of resedimentation samples and a CRS test performed by Abdulhadi (2009). Side wall friction in the consolidometer reduces the actual stress to the applied sample during resedimentation, producing a slight offset in the compression curves.

d) Extrusion

Finally, after the consolidation stage is completed the specimen is extruded from the plexiglass tube and prepared for testing. Depending on the level of stress achieved, the extrusion can be done by applying a downward force to the plexiglass tube by hand or using a small hand operated hydraulic jack (Figure 3-8). Once the soil is extruded, it is trimmed to the required dimensions for testing which is covered in the next chapter.

3.1.1.2 Equipment

A consolidometer is employed to produce specimens of reconstituted Boston Blue Clay (RBBC). This consolidometer consists of a basic structure involving a cylindrical plexiglass (acrylic) tube in which the clay consolidates between top and bottom porous stones. Nylon filter fabric is placed between the porous stones and the clay. A thin film of silicon oil is used to

lubricate the inside of the tubes in order to reduce the friction acting between the tube walls and the specimen.

The basic setup of the consolidometer is illustrated in Figure 3-2. A bottom piston topped with a porous stone and filter fabric is placed inside a long smooth acrylic tube. The bottom portion of the tube is submerged in a bath filled with water of the same salt concentration as that of the pore fluid of the clay. Load is applied to the specimen through a top piston which rests on the top porous stone. Clamps are used to ensure that the entire setup is maintained vertical during the consolidation process. For the first series of load increments up to 20 N of force, the load is applied by simply stacking weights on the top piston. For higher loads the weights are placed on a hanger that in turn transfers load to the top piston, as shown in Figure 3-4. RBBC specimens prepared in the consolidometer at low stresses require approximately 3 weeks to complete.

If the specimen requires a maximum load greater than the capacity of the hanger system on which dead weights are placed, a lever arm load frame is used for up to 8850 N and a pneumatic actuator is used to apply the higher loads. As shown in Table 3-1, the level of stresses that can be achieved depends on the maximum load system capacity (up to 50 MPa for a 50 cm^2 specimen).

3.1.2 Index Properties

Previous researchers at MIT have performed several laboratory tests to verify the index and engineering properties of RBBC Series IV. The results of this are summarized in Table 3-2. These tests include specific gravity, Atterberg limits, and grain size distribution. This section

summarizes the index properties for RBBC Series IV, material used in the experimental program presented in this thesis.

a) Grain Size Distribution

The grain size distribution of RBBC Series IV was obtained using the hydrometer test presented in the ASTM Standard D422. As shown in

Figure 3-5 by Abdulhadi (2009), the grain size fine fraction (% passing US #200 (0.075mm) sieve) for RBBC Series IV is greater than 98% . In addition, the clay fraction (% less than 2μm) average is of 56%. These results are in agreement with previous researchers as presented in Table 3-2 and therefore used in this research.

b) Atterberg Limits

The liquid limit determined by Abdulhadi (2009) using the Casagrande Cup Test Method resulted in a liquid limit, $w_l = 46.5 \pm 0.9\%$. Also, the plastic limit, $w_p = 23.5 \pm 1.1\%$, was defined using the rolling test method specified by the ASTM Standard D4318. Therefore, the RBBC Series IV is classified as a low plasticity clay (CL) according to the Unified Soil Classification System (USCS) and confirmed by the Casagrande Plasticity Chart presented in Figure 3-6.

c) Specific Gravity

The specific gravity, G_s, of RBBC Series IV have been measured by several researchers at MIT. All tests were carried out in accordance to the ASTM Standard D854. Zriek (1994), Casey (2010) and Horan (2012) testing yielded to an average value of 2.78, Sinfield (1994) tests resulted in a value of 2.81, and Abdulhadi (2009) and Cauble (1999) obtained a value of 2.81. Casey (2010) performed the specific gravity testing on RBBC specimens that were previously

used in a CK_oUC triaxial test at a maximum axial stress σ'_{ac} = 10MPa obtaining a value of 2.778 ± 0.001 which is within the range of values obtained by previous researchers. Therefore, no adjustment for the specific gravity are necessary below 62 MPa in accordance to Bishop et al. (1975), who stated that on the basis of purely elastic behavior, a maximum increase in G_s for clay particles would be approximately 0.2 – 0.3% at a consolidation stress of 62 MPa. Therefore, the specific value used in this thesis is 2.78.

3.1.3 Engineering Behavior

Several researchers at MIT have studied the engineering behavior of RBBC. This section presents a summary of the most important engineering properties of RBBC available from previous research. Abdulhadi (2009) investigated the one-dimensional behavior of RBBC Series IV up to 10 MPa and this section will therefore concentrate in the results reported in his research compared with the behavior observed by previous researches for lower stresses.

Section 3.1.3.1 gives an overview the compression and consolidation behavior obtained from 1-D (i.e., K_o) consolidation tests. Section 3.1.3.2 summarizes the undrained stress-strain-strength behavior in triaxial compression.

3.1.3.1 One-Dimensional Consolidation

The compression behavior of RBBC Series IV has been studied in previous testing programs at the MIT Geotechnical Engineering Laboratory. Figure 3-9 presents the compression curves in a e-log(σ'_{vc}) space resulted from the 1-D consolidation phase in the triaxial device and a typical Constant Rate of Strain (CRS) test performed by Abdulhadi's (2009). The preconsolidation

stresses (σ'_p) observed from the compression curves coincide with the batch preconsolidation pressures applied during resedimentation. The curves from the two tests agree very closely, indicating: (1) the repeatability among tests, and (2) the strain rate of 0.15%/hr during K_o-Consolidation phase in the triaxial device was adequate and therefore small excess pore pressures were generated during consolidation.

The values of the compression parameters resulted from Abdulhadi (2009) triaxial testing program varied from 0.147 to 0.168 for the virgin compression ratio ($CR = \Delta\varepsilon_a/\Delta\log\sigma'_v$) and the swelling ratio (SR) from 0.011 to 0.022 over the stress range for 0.15 to 10 MPA. There was no clear trend for CR related to the stress level. However, the SR was found to increase with the OCR.

Furthermore, Abdulhadi (2009) reported that the compression ratio for the CRS test decrease from about 0.18 – 0.2 at σ'_{vc} = 0.2 MPa to 0.13 at σ'_{vc} = 10 MPa. The values of CR at low pressures agree with previous researchers' reports while the values at high stresses are lower than prior studies. The swelling ratios (SR) are approximately an order of magnitude smaller than the compression ratio. It was also found that SR slightly increases from 0.012 to 0.015 with OCR = 1 to 4.

In order to obtain an overconsolidated (OC) specimen in a triaxial test performed at MIT Geotechnical Engineering Laboratory, specimens are subject to a stress path swelling employing the following empirical equation to calculate the pre-shear value of the lateral stress ratio (K_o) at the desired OCR value:

$$K_{oOC} = K_{oNC}(OCR)^n \qquad \text{Equation 3-1}$$

where $n \sim 1\text{-}\sin\varphi'_{mo}$.

Sheahan (1991) and Santagata (1994) reported that K_o decreases during the loading phase of consolidation to a value lower than K_{oNC} before increasing again and then remains fairly constant. Figure 3-10 shows the lateral stress ratio variation with stress for RBBC Series III. However, as presented in Figure 3-12, Casey (2011) and Abdulhadi (2009) found that the same overall trend for the lateral stress variation, both authors reported that K_o decreases in the OC range, until the preconsolidation pressure is achieved, and then plateaus to a fairly stable K_{oNC} once in the normally consolidated (NC) range. As shown in Figure 3-10, Abdulhadi (2009) reported that K_{oOC} increased from 0.518 at σ'_{vc} = 0.15 MPa to 0.564 at σ'_{vc} = 10 MPa. This discussion is important because the value of K_{oOC} can significantly affect the undrained strength of the clay.

3.1.3.2 Undrained Shear

Figure 3-14 presents the typical K_o-consolidated undrained triaxial compression (CK_oUC) behavior of normally consolidated (NC) and overconsolidated (OC) RBBC performed by Santagata (1998). A peak is observed in the NC at a small strain and then followed by a post peak softening. The peak value of the strength normalized to the maximum vertical stress decreases as OCR increases, while the strain softening decreases and the axial strain at failure increases. Also, a common failure envelope at large strain can be observed from Figure 3-15

Santagata (1998) proposed a relationship between the initial stiffness of RBBC to the vertical consolidation stress and void ratio at all OCRs:

$$E_{uMAX} = 270e^{-2.45}\sigma'^{0.43}_{vc}(MPa) \qquad \text{Equation 3-2}$$

Figure 3-13 shows the initial Young's Modulus (E_{Umax}) of Santagatas's testing program at OCR = 1, 2, 4 and 8 versus the mean consolidation stress on log scales.

As mentioned in Chapter 2, Abdulhadi (2009) concluded that the values of the parameter S and m in of the SHANSEP equation for triaxial compression tests on RBBC are stress level dependent. This conclusion was based on a comparison and regression analysis to the data by Sheahan (1991), Santagata (1994) and shown in Figure 3-16

3.2 Presumpscot Maine Clay

Presumpscot Maine Clay (PMC) was the natural material used in this testing program as a comparison for the resedimented material (RBBC) response. This intact material comes from Shelby Tubes, rather than resedimented material. This samples were also mechanically overconsolidated in the triaxial equipment.

The mineralogy of Presumpscot Maine Clay is known to be similar to BBC and therefore The material properties were not tested for this research. The specific gravity value used is 2.78. The clay fraction is approximately 30% though this may vary spatially and by depth. Reynolds (1991) gives typical Atterberg limits of Maine clays as liquid limit 30%, plastic limit 20%, and plasticity index 10%. The USCS classification is a low plasticity clay, CL. (Adams, 2011)

3.2.1 Procedure

In contrast with RBBC where the majority of the procedure was significantly reduced by using consolidometer (plexiglass) with the exact inside diameter suitable for triaxial testing,

around 3.40 cm (1.34 inches). The procedures performed for cutting and trimming intact samples from Shelby Tubes (2.8") of Presumpscot Maine Clay followed the suggested method by Germaine & Germaine (2009). Tubes are 2.8" diameter galvanized steel or brass and are capped and sealed at each end. First, the tubes are x-rayed and the radiographs are used to determine locations of poor sample quality which are not used for testing. Once a suitable specimen is located within the tube a section about 12 cm long, of the tube is cut with a horizontal band saw. All cut edges of the sample tube are smoothed and processed to remove metal burs for safety reasons. The soil adjacent to the cut portions of all pieces of sample tube is disturbed from the cutting process and often contains metal fragments; this is removed via scraping. The portions of the sample tube not containing the specimen to be tested are sealed with wax to retain moisture and taped back together for later use. A log sheet records to location of the cut section and the testing performed. Then, water content and hand held shear vanes measurements were took at the top and bottom of the tube. Prior to extrusion, a 0.5 mm steel wire (piano wire) is used to core the soil along the inside parameter in order to break the bond between the soil and the tube. After this, the soil can be extruded by using a cylindrical base and the soil pushed out of the tube by hand or using a hydraulic jack.

Table 3-1 Transfer Load System Capacity

Equipment	Max. Load Capacity	Level of Stress for 50 cm^2 specimen
Bench Top	400-600 N	0.12 MPa
Lever Arm Load Frames	8850 N	1.74 MPa

Table 3-2 Index properties of BBC Series IV (extended from Santagata, 1998)

Year	Researcher	Batch	wl (%)	wp (%)	Ip (%)	Gs	Clay Fraction (%)	Salt (g/l)
1994	Zriek	powder	46.4	22.5	23.9	2.78	60.1	
1994	Sinfield	powder	47	23.8	23.2	2.79		
		402	46.8	22.4	24.4			
		403	47.2	23.3	23.9			
1996	Cauble	powder				2.81		
		401	46.7	21.8	24.9			
		404	47.4	21.9	25.5			10.4
		405	45.2	22.1	23.1			10
		406	45	22.6	22.4		57.6	12.5
		407	44.6	23	21.6		57.8	13.1
		408	44.7	23.9	20.8		58.7	10.1
		409	45.4	24	21.4		56.8	13
		410	46.6	25	21.6			13.4
		411	46.7	24.5	22.2		56.9	10.2
		413	45.5	24.3	21.2			9.7
		414	46.3	24.3	22			12
		415	46.1	24.7	21.4			10.5
		416	46.7	24	22.7			12.9
		417	47.2	24.5	22.7			13.2
1998	Santagata	418						
		419	47.8	23.3	24.5			
1998	Force	420	45.2	23.3	21.9			
2009	Abdulhadi	powder	46.5	23.5	23	2.81	56	11.1

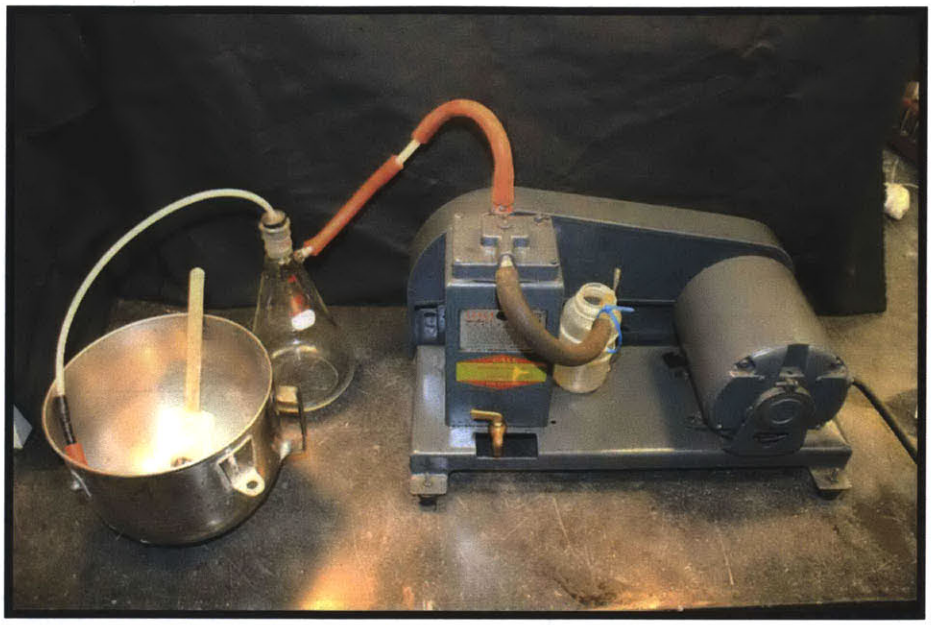

Figure 3-1 Setup to vacuum slurry

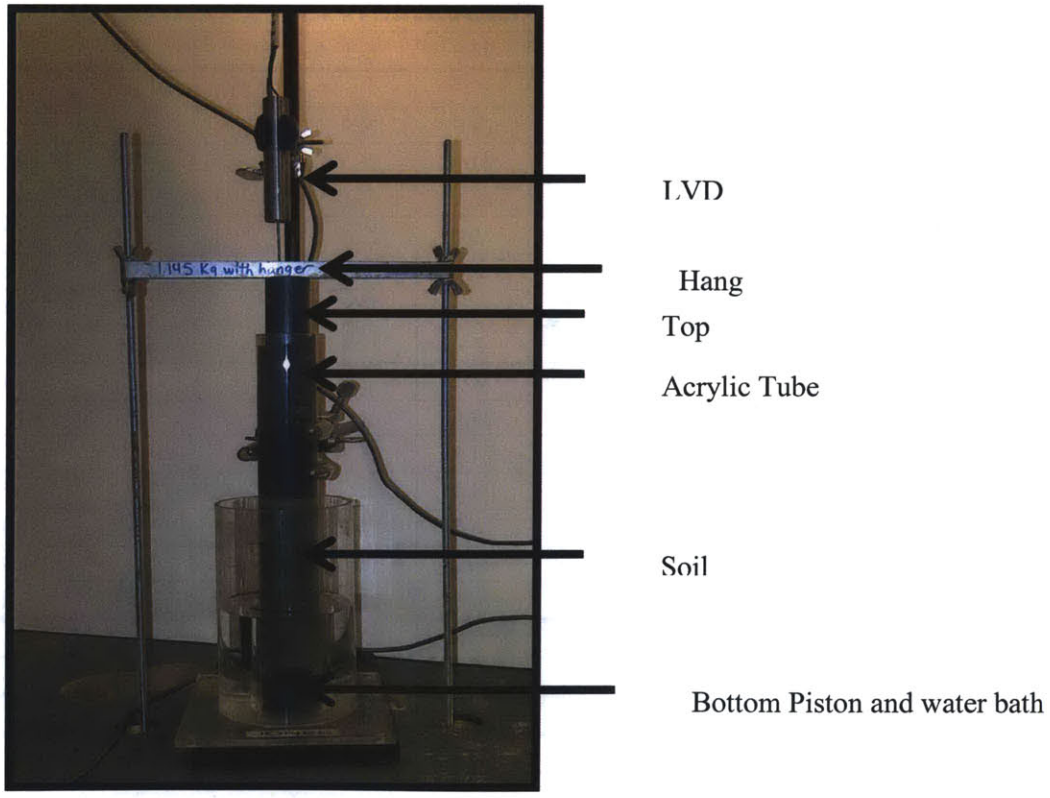

Figure 3-2 Consolidometer Setup for Low Stresses

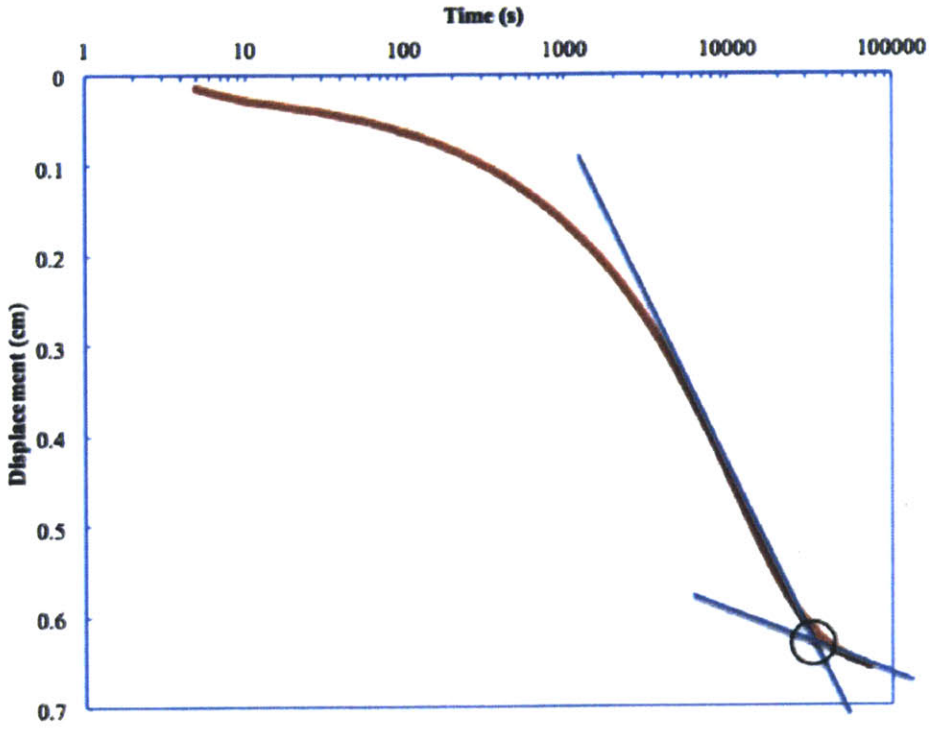

Figure 3-3 Settlement curve indicating EOP (Marjanovic, 2012)

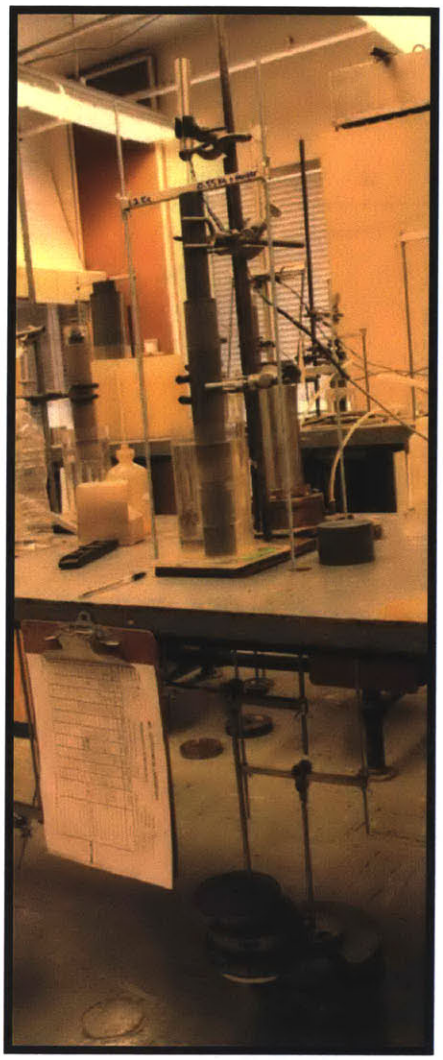

Figure 3-4 Resedimentation set-up with hanger weights applying stress for safety

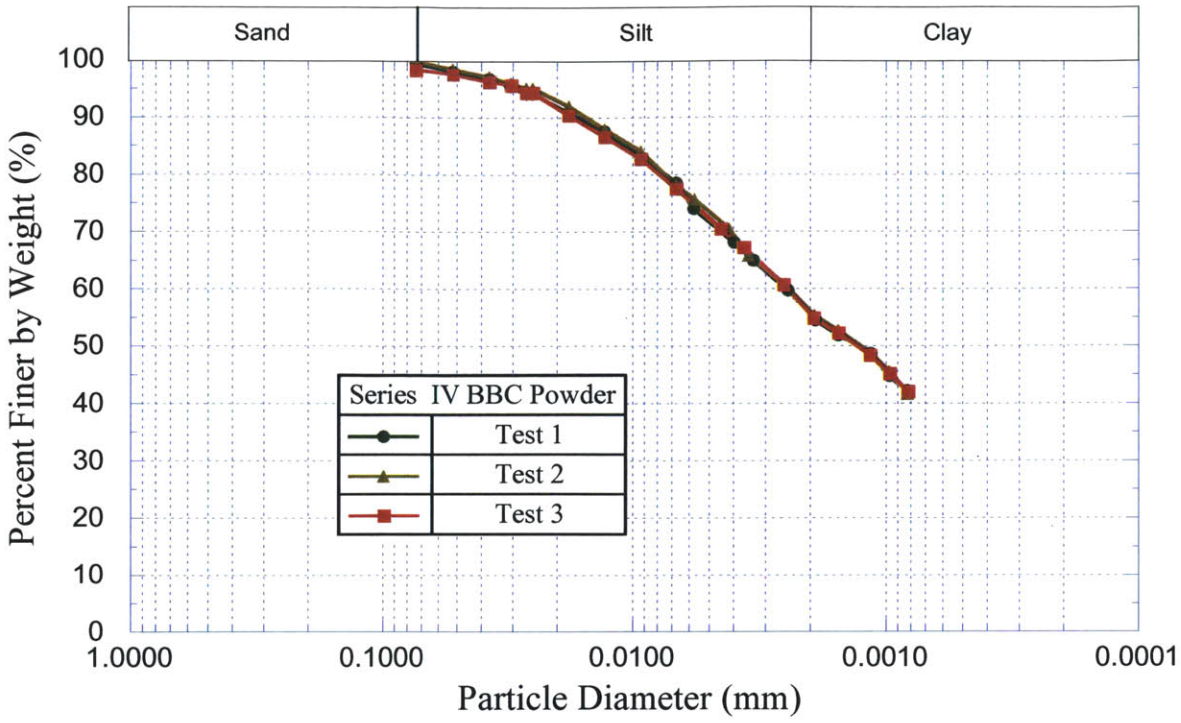

Figure 3-5 Results of grain size analyses for RBBC Series IV powder (Abdulhadi, 2009)

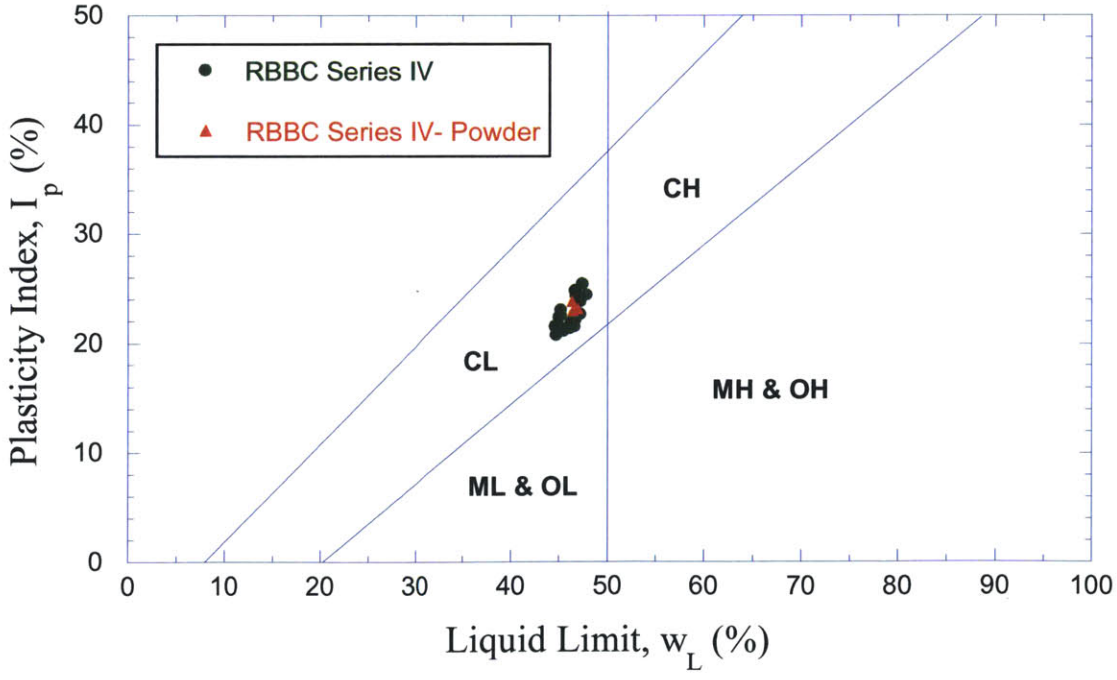

Figure 3-6 Casagrande Plasticity Chart (Abdulhadi, 2009)

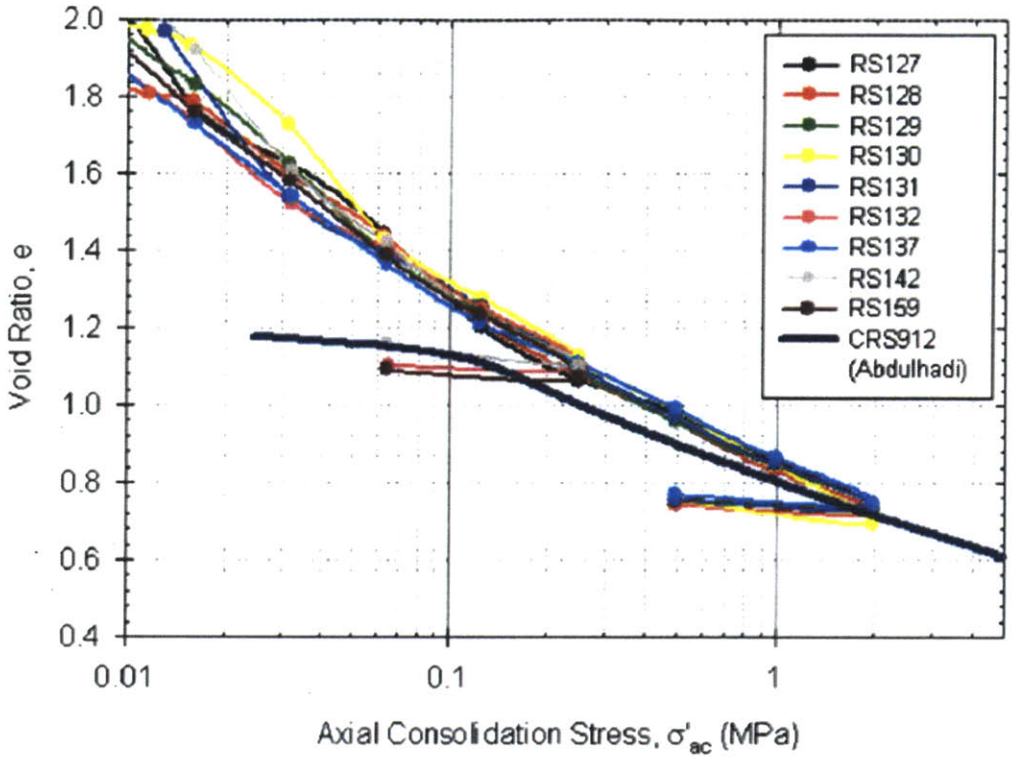

Figure 3-7 CRS vs. Resedimentation One-dimensional compression behavior comparison (Casey, 2011)

Figure 3-8 Hand-operated hydraulic jack

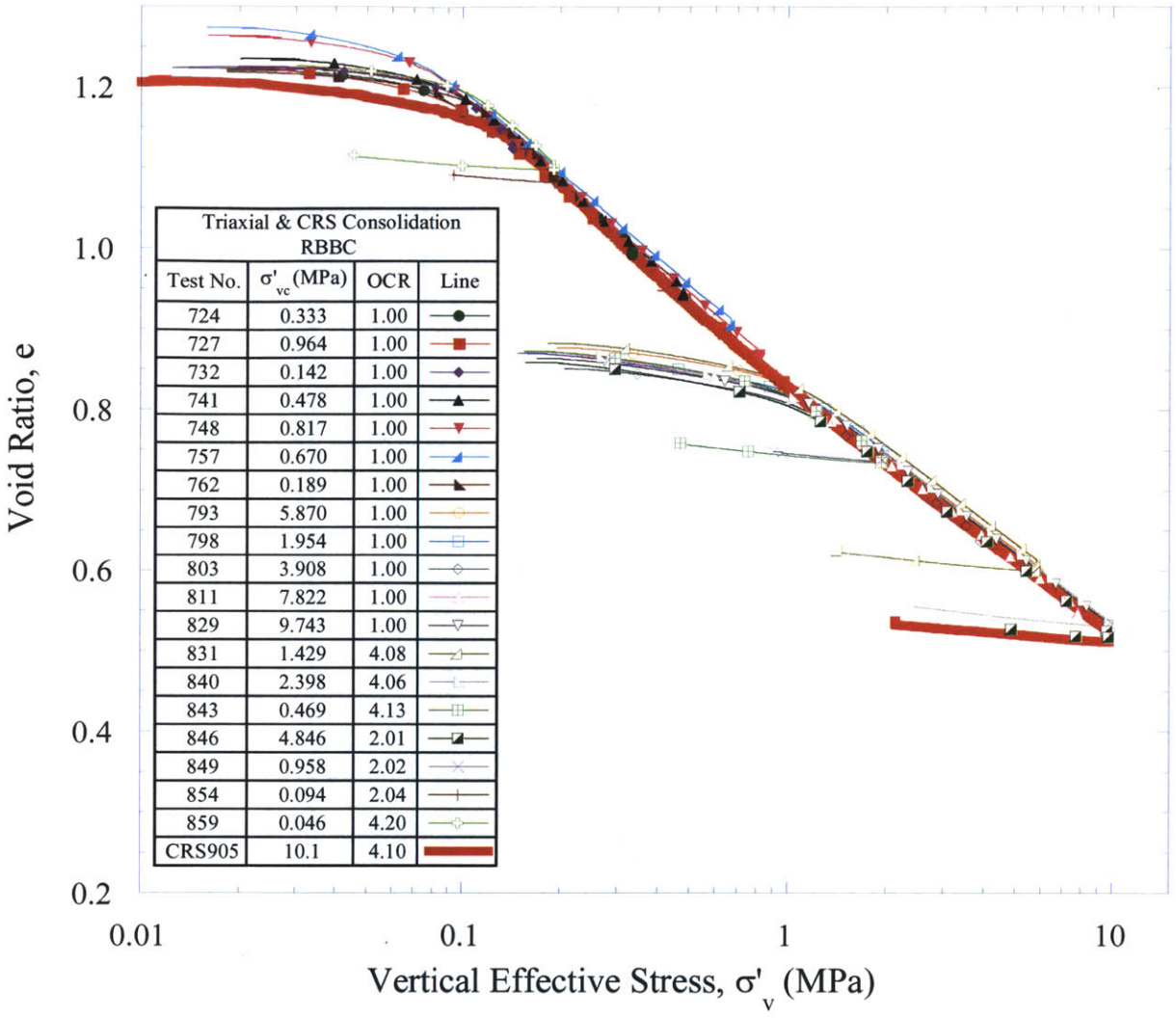

Figure 3-9 1-D compression behavior in e-logσ'v space for NC and OC RBBC from all triaxial tests compared with the CRS test (Abdulhadi, 2009)

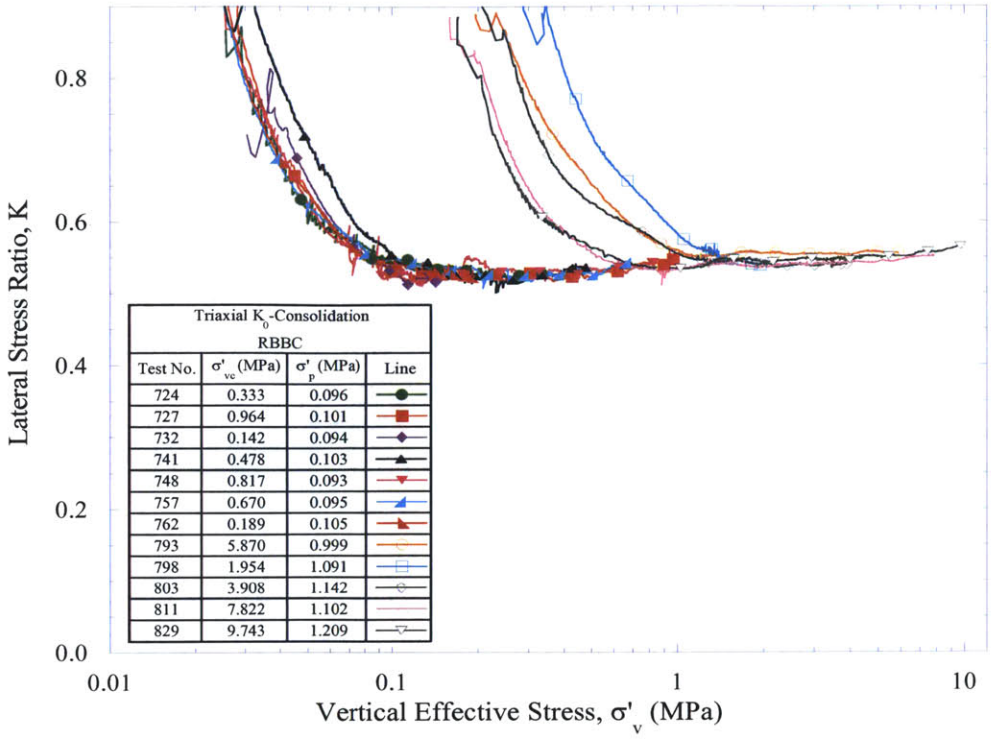

Figure 3-10 Lateral Stress Ratio variation with stress level for RBBC Series IV (Abdulhadi, 2009)

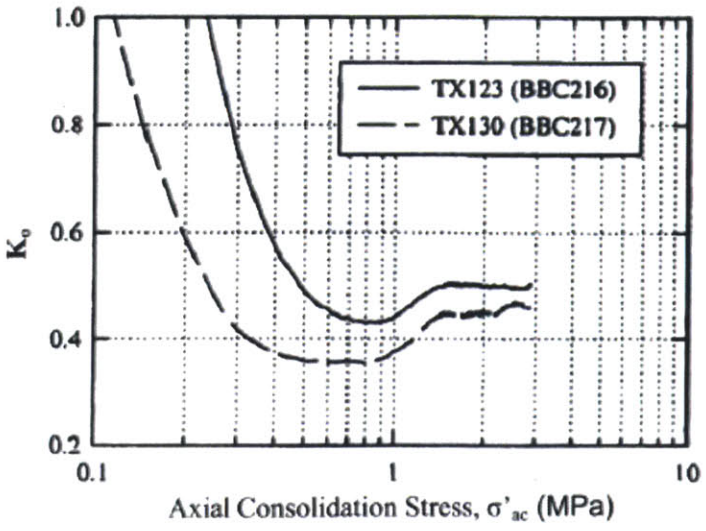

Figure 3-11 Lateral Stress Ratio variation with stress level for RBBC Series III (Santagata, 1994)

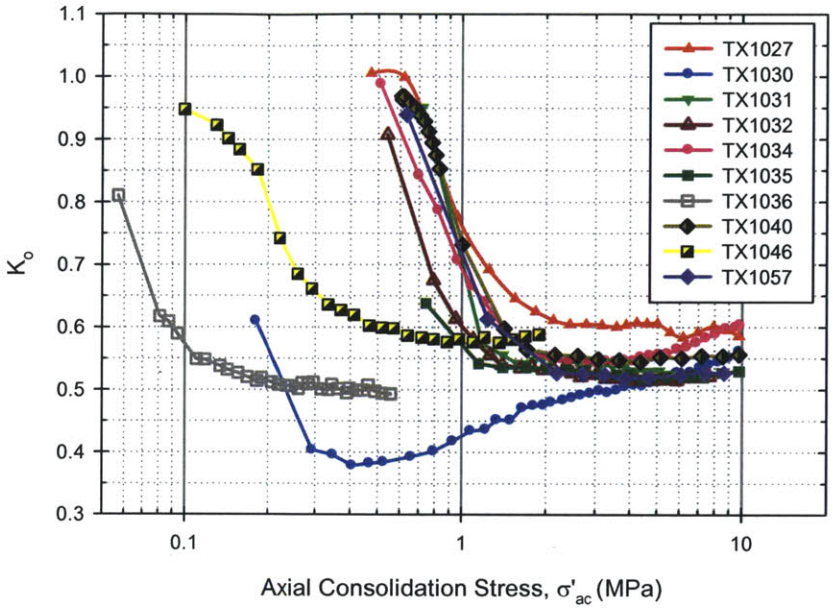

Figure 3-12 Lateral Stress Ratio variation with stress level for RBBC Series IV (Casey, 2011)

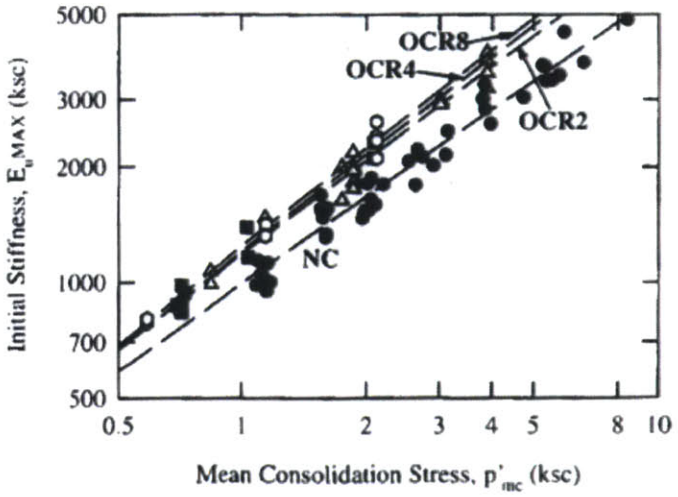

Figure 3-13 Relationship between initial stiffness of RBBC and mean consolidation stress in undrained triaxial compression (Santagata, 1998)

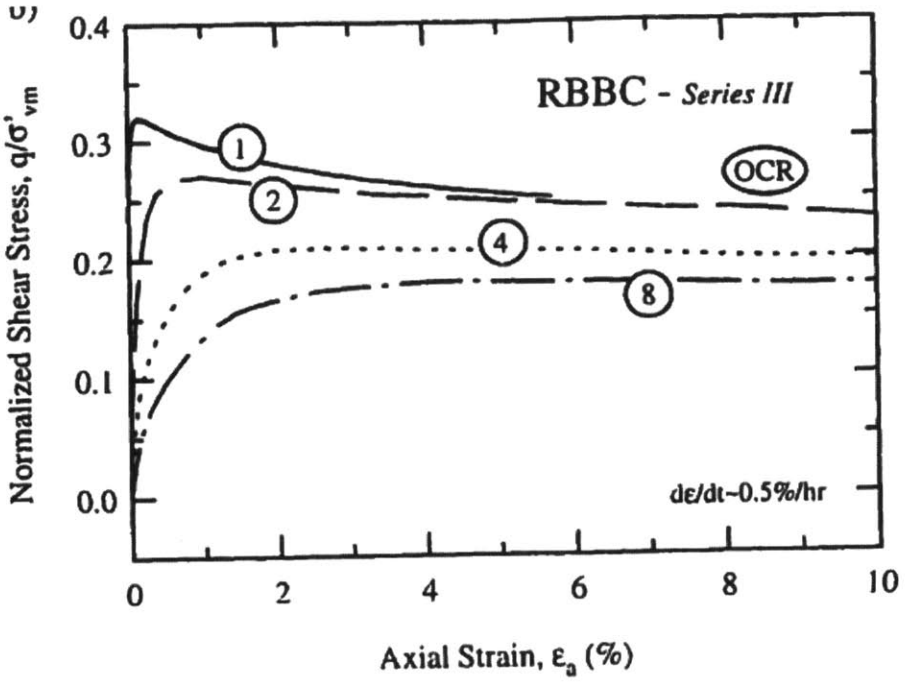

Figure 3-14 Normalized shear stress-strain behavior RBBC III (Santgata, 1994)

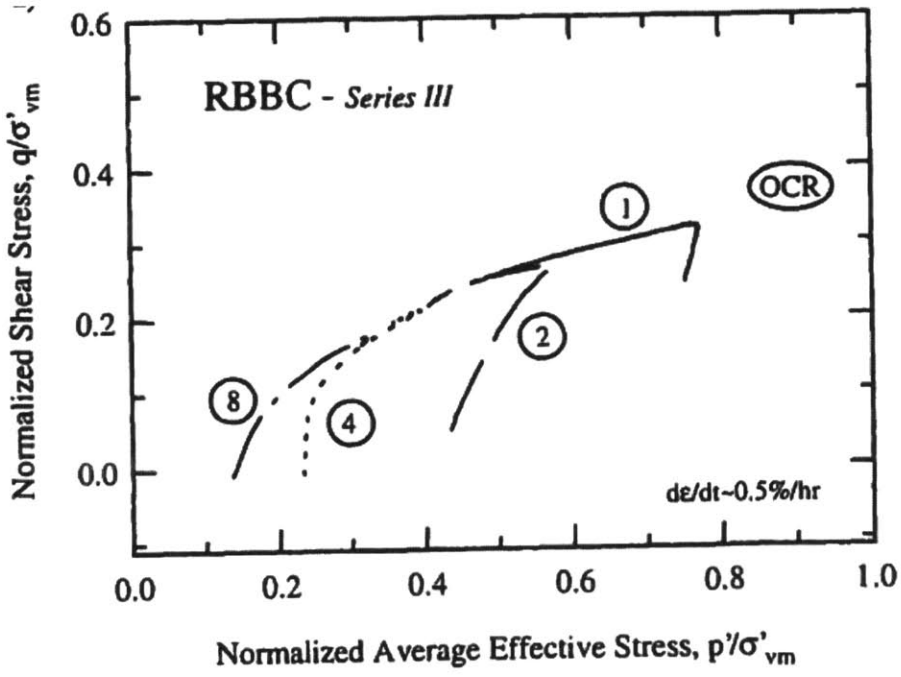

Figure 3-15 Normalized effective stress paths of RBBC III (Santagata, 1994)

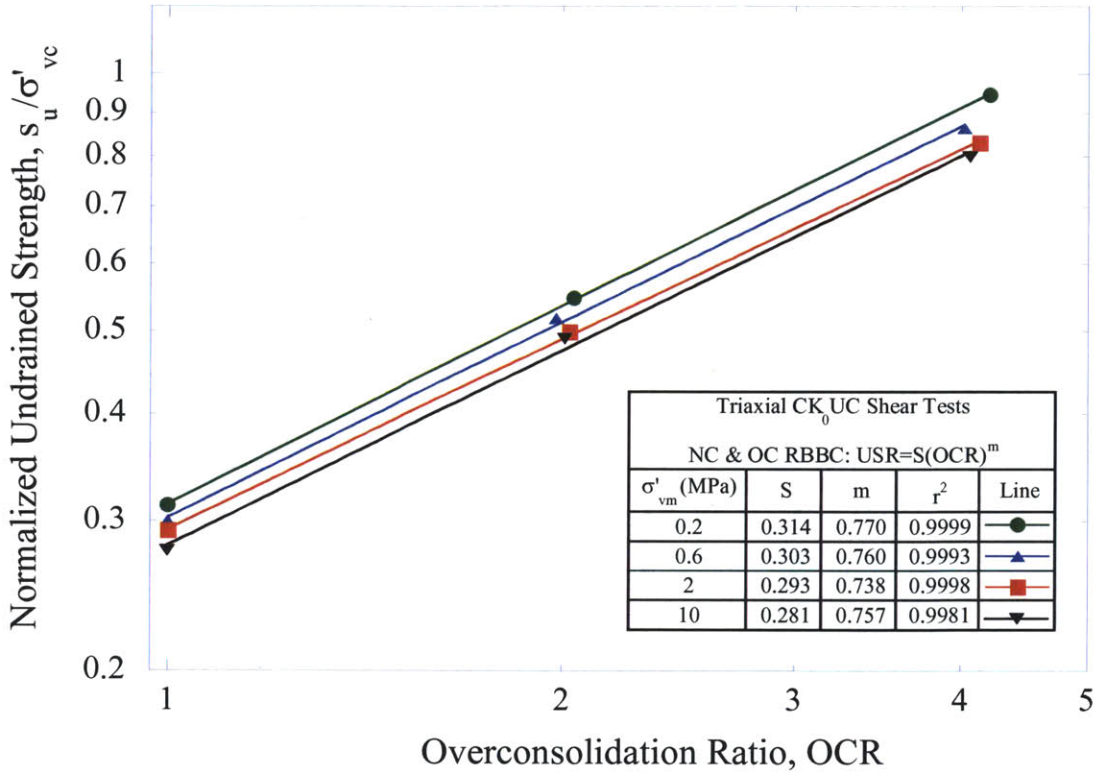

Figure 3-16 Normalized undrained strength versus OCR for RBBC from selected CK_oUC triaxial tests illustrating the effect of stress level (Abdulhadi, 2009)

4 EQUIPMENT AND TESTING PROCEDURES

This chapter provides an overview of the testing equipment and procedures used to conduct the experimental program. The MIT Triaxial Apparatus was the main device to investigate the mechanical behavior of heavily overconsolidated clays. Section 4.1 describes the MIT Automated Stress Path Triaxial equipment. Section 4.2 presents the computer control system, measurement devices and central data acquisition system used in conjunction with the triaxial apparatus. Finally, Section 4.3 gives a detailed description of the testing procedures performed in this research.

4.1 MIT Automated Stress Path Triaxial Cell

The majority of the tests conducted for this research were conducted in the low stress MIT Automated Stress Paths Triaxial Cells. This equipment was originally developed at the MIT Geotechnical Laboratory by Sheahan and Germaine (1992). Figure 4-1 shows a schematic representation of the computer controlled triaxial apparatus. The MIT Automated Stress Path Triaxial Cell consists of the following: triaxial cell, load frame, pressure volume actuators, motors, control box, and the MIT Data Acquisition System. MIT-01, MIT-03 and MIT-04 were the three stations used for this research.

The low stress triaxial apparatus has a plexiglass chamber with a maximum pressure capacity of about 1.5 MPa. The triaxial cells have customized features such as linear ball bearing bushings and rolling diaphragm seal or O-ring seal to reduce piston friction, fixed top cap for testing clays, top and bottom drainage lines, ball valves, copper tubing, internal load cell, and silicon oil as cell pressure fluid to eliminate leakage through the membrane in long tests. Figure 4-2 shows a schematic of the low stress triaxial chamber and Figure 4-3 shows a photograph of the triaxial chamber. The pore pressure and cell pressure are controlled by MIT-designed Pressure Volume Actuators (PVA) and measured by high performance diaphragm type transducers (200 psi (1.4 MPa) capacity) placed on the base of the cell. The axial strain is measured externally with an LVDT. A load cell (500 lb (2.2 kN) capacity) is located inside the chamber to measure the deviatoric stress. Two thin membranes to seal the specimen are unlubricated latex Trojan brand condoms.

The liquid used to fill the chamber is Dow-Corning "200 fluid", 20 centistokes silicone oil. Some of the advantages of using this particular oil are: 1) it is a nonconductive liquid which enable an internal load cell, 2) it is a transparent liquid, 3) it does not degrade the seals or latex membranes used in testing, and 4) insoluble with water so no osmotic pressures.

The entire triaxial cell is mounted on a bench top Wykeham-Farrance screw driven load frame with a 1 tonne (9.8 kN) capacity. Figure 4-4 shows the bench top of MIT-01.The cell and back pressures are controlled by the MIT-designed Pressure-Volume Actuators (PVA). The volumetric strain is computed using an LVDT that monitors the motion of the back pressure PVA piston. The system is inside an environmental enclosure within the main testing room, an air-conditioned laboratory.

4.2 Computer Control and Data Acquisition System

The automation of existing equipment at the MIT Geotechnical Laboratory started in the early 1990s using a process termed adaptable automation by Sheahan and Germaine (1992). This process includes modifying existing manual system components for automation and adding innovative new components to complete the automation, flexibility and quality control of the systems. This section will give an overview of the hardware and software required for the automation of the triaxial devices employed in this research program. For a more detailed description refer to Sheahan (1991) and Sheahan & Germaine (1992).

The software used for automated control is a program written in QBASIC and run on a personal computer. Figure 4-5 shows the personal computer, control box and screen of MIT-03 Low Stress Triaxial apparatus. The control program gives a series of options to perform specific tasks at different stages of a triaxial test, from initial pressure up to undrained shear. Figure 4-6 shows the control program options screen. The essential feature of this system is the feedback control loop for the driving systems. In summary, the measurement devices send a voltage signal to the computer and this is converted into engineering units; then the software compares the actual stress-strain state with a pre-computed target state and computes a corrective action for the electric motors to keep the stress-strain state on schedule. (Sheahan, et al., 1990)

4.2.1 Measurement Devices

The measurement devices used in a triaxial test include four different types of transducers: pressure transducers, load cells, LVDTs for axial displacements and string pots transducers. These transducers need a common input voltage of 5.5 volts of Direct Current provided by a

regulated power supply. Below, is a brief description of each of the four transducers used in this testing program.

Pressure Transducers: The cell and pore pressure in the triaxial equipment are measured by Data Instruments AB/HP type pressure transducers. This type of transducer measures absolute pressures by the deflection of a steel diaphragm instrumented with strain gages to eliminate barometric pressure changes. The capacity of the low pressure triaxial transducers is 200 psi (1.4 MPa). Figure 4-7 shows one of the pressure transducer used in this investigation.

Load Cell: The load cell used to measure the deviatoric stresses is a Data Instruments JP type shear beam load cell with a capacity of 500 lb (2.2 kN). Figure 4-8 shows one of the load cells use at the MIT Geotechnical Laboratory. This load cell contains an S-Shaped steel section instrumented with a strain gauge.

Axial Displacement Transducers: A Linear Variable Differential Transformer (LVDT) with a range of 2.5 cm manufactured by Trans-Tek Inc. (Series 240) measures the axial displacement. The LVDT tube generates a magnetic field through which a ferromagnetic core moves. An output voltage results from a change in the axial displacement of the core.

Volume Change Transducers: Two different transducers are used in the MIT Geotechnical Laboratory, LVDTs and string pots. A 10 cm range LVDT (Trans-Tek Inc. Series 240) measures the displacement of the back pressure PVA piston. The volume change is computed by multiplying the displacement times the area of the piston. A string pot (linear position transducer) manufactured by Celesco (SP1 type) can also be used to measure the displacement of the piston. The string pot transducer produces an electrical output signal proportional to the wire rope extension, which rotates an internal capstan and sensing device (precision potentiometer),

when an axial movement occurs. The key advantage of using a string pot is that it provides a 30 cm range (larger than required).

4.2.2 Control System

The electronic information from the transducers is transmitted to a series of instrumentation forming the control system. The output voltage of the measurement devices is sent to a multichannel analog to digital converter (MADC), which translates the signal to number of bits with a minimum of 18 bit resolution. This MADC converter, developed at MIT by Sheahan (1991), is placed on a circuit board inside the computer. Then, the control program determines the new command signal and sends it to the driving systems. The new command signal is converted to an analog signal with commercial board manufactured by Strawberry Tree Inc (12 bit resolution with a 10 volt range). The analog signals are sent to the electric motor which then drives the piston of the MIT-designed PVA or the vertical load. Figure 4-9 shows a diagram of the control system hardware components. The electric motors used in the MIT load frames are Electro-craft Model E286, while Model E372/352 drives the 0.5 Tonne actuators.

The MIT-designed PVA consists of a motor driven ball screw actuator, manufactured by Duff-Norton that converts the rotary motion of the electric motors into linear motion of a piston. The piston then displaces the fluid from a cylinder, which controls the cell and pore pressures. The triaxial PVAs have a volume capacity of about 45 cm^3 and a pressure capacity of 14 MPa. Figure 4-10 shows a pore and cell pressure PVA.

4.2.3 Central Data Acquisition System

The Central Data Acquisition System (CDAQ) in the MIT Geotechnical Laboratory allows multiple and simultaneous voltage output readings. In the case of triaxial testing, the user specifies the schedule of recording and gives a name to the file for each phase of test. This file is stored on a computer for the users to retrieve at their convenience. The details of the data acquisition system are well described by previous researchers at MIT (e.g. Sheahan (1991), Abdulhadi (2009), and others). For the reader's reference a brief overview of the system is given in this section.

The CDAQ at MIT consist of a 486 microprocessor PC with a Windows based operating system, and an HP3497A data acquisition unit manufactured by Hewlett Packard. The system has a 5.5 digit integrating analog to digital converter and an auto–ranging amplification scale (0.1, 1, 10 and 100 Volts). The current system is capable to monitor 180 channels simultaneously, provide analog to digital conversion and store data at rates up to 1 Hz. This high quality system permits recording of direct measurements from all the measurement devices in the triaxial without any signal amplification.

4.3 Testing Procedures

Procedures developed by Dr. John Germaine for MIT Graduate Subject 1.37: Geotechnical Measurements and Exploration – Assignment 9, were followed throughout the testing program meant for this investigation. These procedures have being described by previous researchers at MIT: Sheahan (1991), Sheahan & Germaine (1992), Santagata (1998) and Germaine &

Germaine (2009). The following section will provide an overview of each stage using a standard MIT automated stress path triaxial apparatus at the MIT Geotechnical Laboratory.

4.3.1 System Setup

An MIT triaxial test first stage is the system setup. This stage consists in a series of steps from system checks to cell preparation in order to ensure a successful test. First, the pressure-volume controllers have to be refilled with oil, for the cell, and distilled water, for the back pressure. Then the PVA pistons should be moved to positions suitable for the test. For the purposes of this investigation the pistons were located at the minimum range to ensure enough stroke for the conduction of the test.

While the cell preparation is conducted, the porous stones are ultrasounded for 15 minutes to get rid of any oil or soil from previous tests. The piston should be retracted and locked, with a split collar, to a higher position ensuring enough space for the specimen and porous stones. Then the drainage system is checked for possible leakage or clogging and the zero value for the pore pressure transducer is recorded. The internal load cell is connected to the cell to record the zero reading after a warm up period.

After the system is checked, the cell is prepared for the specimen set-up. First, the top cap and bottom pedestal sides are cleaned thoroughly and greased with high vacuum grease. Second, to provide protection against leakage, rubber sleeves are placed on the top cap and pedestal to secure the porous stones in alignment with the specimens, and then two rolling latex membranes, sealed with greased O-rings, are placed on the top of the rubber sleeve. Four O-rings are placed

on a stretcher which is located over the pedestal. Figure 4-11 shows a schematic of the sealing arrangement.

4.3.2 Specimen Preparation and Setup

After the sample is extruded, in accordance to section 3.1.1.1 and 3.1.2, for RBBC and Presumpscot Maine Clay respectively, the specimen is trimmed to the required dimensions for testing. In the case of the Presumpscot Maine Clay intact samples, the specimen preparation required trimming the sample to a cylindrical specimen using a miter box. This procedure is also conducted in accordance to Germaine & Germaine (2009). First, the extruded sample is placed in an orthogonal miter box and cut with a wire saw, creating a flat surface perpendicular to the axis of the sample tube. Then, the sample is cut in a cylindrical miter box using a wire saw and rotating the cylinder about 5° for each cut. The cylindrical miter box employed for reducing the diameter of the specimen has two settings: 1) coarse size, to reduce the specimen to a slightly larger diameter than required, and 2) fine, used to define the final diameter. Finally, the specimen surface is cleaned and finalized with a razor blade. Figure 4-12 and Figure 4-13 show the specimen trimming. For the majority of the tests conducted on RBBC the time necessary for this procedure was significantly reduced by using consolidometer (plexiglass) with the exact inside diameter suitable for triaxial testing, around 3.40 cm (1.34 inches).

The sample is wrapped in wax paper and transferred to a specimen mold, to cut of the specimen to its final height of 8 cm. The specimen dimensions and mass are measured and recorded using a caliper and digital scale, respectively.

After placing a porous stone with a filter paper on the bottom pedestal, the specimen is mounted on the bottom platen. A second porous stone and filter paper is placed on the top of the specimen and the piston/top cap is lowered until it makes contact with the specimen. The two latex membranes are rolled up and secured with 3 O-rings.

The load cell is plugged to the electrical connector in the base of the cell and the cylindrical Plexiglass chamber is placed. The top plate of the triaxial equipment is attached and tightened with sealed bolts. The external axial displacement (LVDT) and remaining accessories are assembled. The chamber is filled with silicone oil by using less than 10 psi air pressure and the cell pressure transducer zero value is recorded when the chamber is half-filled. The triaxial cell is raised into contact with the load frame and the axial LVDT zero value is recorded. The load frame is engaged to the axial motor drive system, and the specimen dimensions, zero values and calibration factors are input into the Q-Basic triaxial setup program. Figure 4-14 shows the setup program screen where the initial values need to be input.

4.3.3 Initial Pressure-Up and Back Pressure Saturation

Triaxial testing can begin after checking that the computer values are reasonable. Before saturating the sample, the chamber and specimen need to be pressurized. The Pressure-Up, first phase of an MIT Triaxial Test, consists of applying enough cell pressure to establish a small positive pore pressure. The Initial Pressure-Up option is selected from the computer program, and with the drainage lines closed, a cell pressure of about 25% of the vertical effective stress of the sample is applied. In the author's testing program this was achieved around 1 ksc for RBBC and 0.25 ksc for Presumpscot Maine Clay (0.25 σ_p', where $\sigma_p' = 4\,ksc$ stress at which the

specimens where consolidated in the lab (RBBC) and $\sigma'_p = 1\ ksc$ Presumpscot Maine Clay in-situ stress). The specimen is allowed to equilibrate overnight with the drainage lines closed.

The next day, the cell and pore pressure, are recorded to obtain the sampling effective stress. The second phase is the back pressure saturation. The drainage lines are opened and the pore pressure is increased by increments of 0.25 ksc and 0.50 ksc. The initial sampling effective stress is maintained constant while increasing the pore pressure to the target stress. After the first tests conducted by the author, a target back pressure of 3.50 ksc was defined to avoid cavitation in the system. Then a B-value ($\Delta u/\Delta\sigma_3$) parameter check is conducted when the targeted back pressure has been reached.

The B-value check in a MIT Triaxial Apparatus is computed automatically by the control program. The B-value check option is selected and pressure increment of 0.25 ksc up to 0.50 ksc is applied with the drainage valves closed. For saturated soils an increase in cell pressure should cause an equal reaction at the pore pressure. The B-value is computed by the control program after 2 minutes and then a final value is reported. Previous researchers reported that B-value above 85% is sufficient for saturation in tests conducted at MIT Triaxial Testing. (Kontopoulus, 2012). When a satisfactory B-value is achieved the axial and volumetric strains due to "saturation" are recorded.

4.3.4 Consolidation

Before starting the K_o-Consolidation stage, it is important to reset the volumetric strain to the same value as the axial strain. The specimen is then K_o-consolidated into the virgin compression range to a defined maximum vertical stress, σ'_{vm}. In the author's testing program

most of the tests were consolidated to values of σ'_{vm}= 16.0 – 16.5 ksc (1.4 -1.6 MPa), ensuring a radial stress, σ_r, below 14 ksc (1.5MPa) maximum value allowed by the chamber. The loading axial strain rate for all of the tests in this thesis was $\dot{\epsilon}_a$= 0.15%/hr. This rate prevents pore pressure from building up in the specimen during consolidation. The K_o-Consolidation option from the control program increases the cell pressure maintaining a zero lateral strain. Once the maximum vertical stress is reached the specimen is held at constant stresses for at least 24 hours to allow secondary compression.

4.3.5 Swelling

In order to get create overconsolidated specimen, the specimen is unloaded to the desired OCR using the stress path consolidation option in the control program. The stress path unloading was performed at a negative axial strain rate of $\dot{\epsilon}_a$= - 0.15%/hr and followed by another 24 hours of aging. Target total vertical (σ_{vc}) and radial stresses (σ_r) are required in order to conduct a stress path unloading. With the desired OCR, the target axial effective stress is calculated by:

$$\sigma'_{vc} = \frac{\sigma'_{vm}}{OCR}$$

Then, the radial effective stress can be calculated by estimating the lateral stress ratio, $K_o = \sigma'_h/\sigma'_v$, using the equation proposed by Schmidt (1966):

$$K_{oOC} = K_{oNC}(OCR)^n$$

Where for RBBC, the exponent n ≈ 0.426.

However for the author's testing program K_{oOC} was limited to 1 (hydrostatic conditions), to avoid problems with the algorithm routine because K_{oOC} >>>1 causing a negative shear stress, q, and consequently a stress path below hydrostatic conditions. This resulted in inputs for total stress of $\sigma_{vc} = \sigma_r$ at K_{oOC} =1

Observations

During this investigation, the researcher encountered some issues when conducting a triaxial test on heavily overconsolidated specimens. For instance, as the OCR target values were very high and consequently the computed vertical and radial stresses resulted in very small values, there were some problems with the control program associated with transduce stability and the stiffness of the soil.

These issues included the accuracy of the recorded zero values for all measurement devices. A small difference in the zero values can have a significant impact on the calculation of stresses. Furthermore, since the swelled specimen is significantly stiffer at the end of swelling than at Ko-Consolidation, some constants in the algorithm of the control program needed to be tuned to be able to keep very small stable stresses during aging (or secondary compression). This is especially important because the variation of stresses was in the same order of magnitude as the target stresses. Given the limitations encountered at very low stresses, the author performed a few tests in the MIT Medium Stress Triaxial Equipment to get higher OCR. Since, just one test is presented in the results chapter of this thesis and the equipment, as well as the overall procedures, is very similar to the low stress triaxial equipment. Furthermore, this is already well

described by previous researchers (e.g. Abdulhadi, 2009 and Casey, 2011) and therefore will not be repeated in this section.

4.3.6 Shearing

Before shearing, a leak check is conducted by closing the drainage lines and monitoring the pore pressure for 30 minutes. Then, if no internal or external leak is detected, i.e. the pore pressure is constant, the specimen is sheared in compression mode with no drainage allowed at a constant axial deformation rate of $\dot{\epsilon}_a$= 0.5%/hr until 15% axial strain. A strain rate of $\dot{\epsilon}_a$= 0.5%/hr was used in most of the tests except for two test performed by the author to determine the influence of higher shear strain in the development of failure planes.

4.3.7 Specimen Removal

Finally, when the test is completed a clamp is placed to lock the piston and minimize the axial deformation while the apparatus is disassembled. The chamber is emptied and the plexiglass is removed from the cell. All the equipment is thoroughly cleaned up and the O-rings are carefully removed to release the specimen from the cell. Porous stones are also removed to be cleaned with the ultrasound and stored in a water bath for future use. The final dimensions and mass of the specimen are measured using a caliper. With these measurements phase calculation are performed and the water content and dry mass of the specimen are determined. The water content for this program was determined on the entire specimen to keep failure planes intact.

4.3.8 Data Processing

The data files from each of the stage of the test are collected from the MIT Geotechnical Data Acquisition System. These files are converted into engineering values using a QBasic program, originally written by Sheahan (1991) similar to the computer control program. The reduction program uses as input the normalized zero readings, calibration factors of the different measurement devices, the specimen dimensions and other information about the test. The program takes the voltages readings in the data file and creates an output file with effective stresses, strains, pore pressures, mean (p') and shear stresses (q) are computed with time. For the undrained shear data, the program has the option to normalize the values to a specific state of stress.

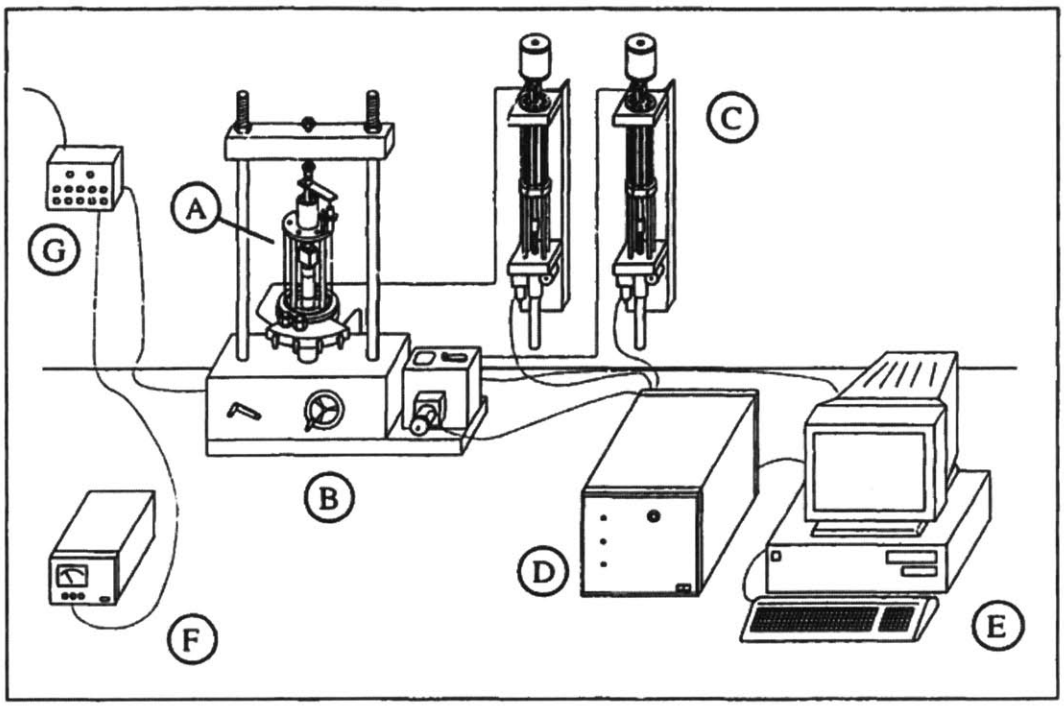

A - Triaxial Cell
B - Load Frame
C - Pressure/Volume Controllers
D - Motor Control Box
E - Personal Computer
F - DC Power Supply
G - Data Acquisition Channels

Figure 4-1 Schematic of MIT automated stress path triaxial cell (from Santagata, 1998)

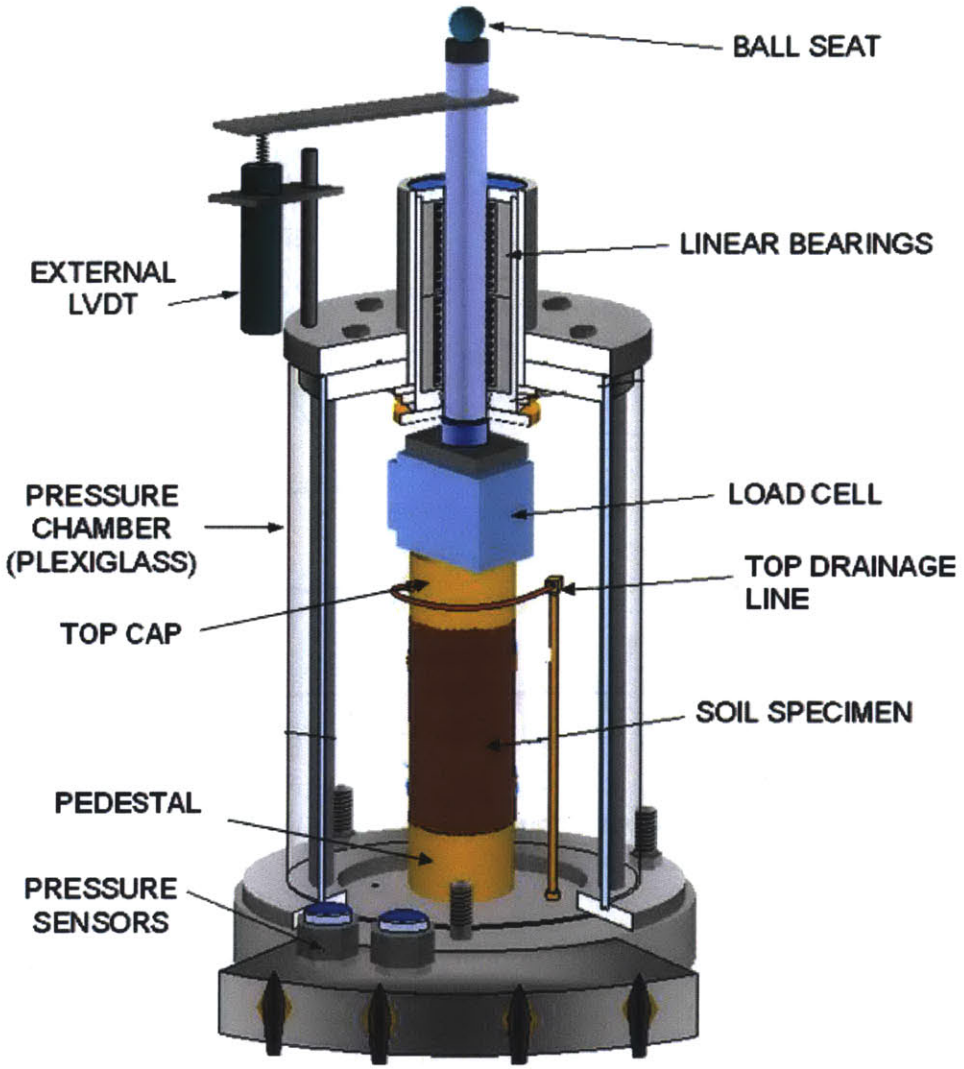

Figure 4-2 Schematic of low pressure triaxial chamber (from Santagata, 1998)

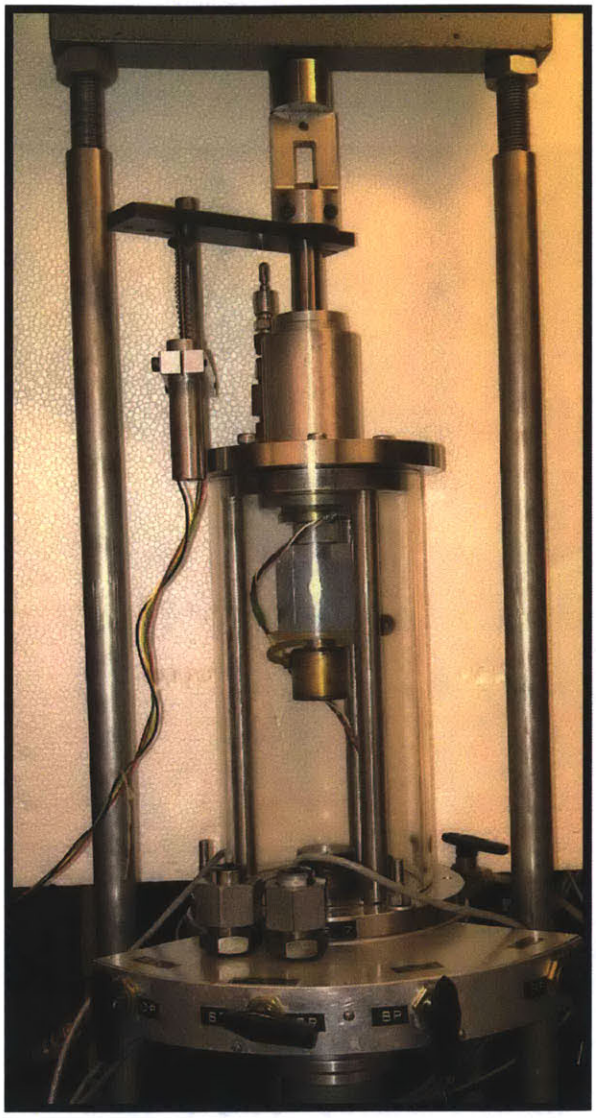

Figure 4-3 Photograph of the low stress triaxial chamber

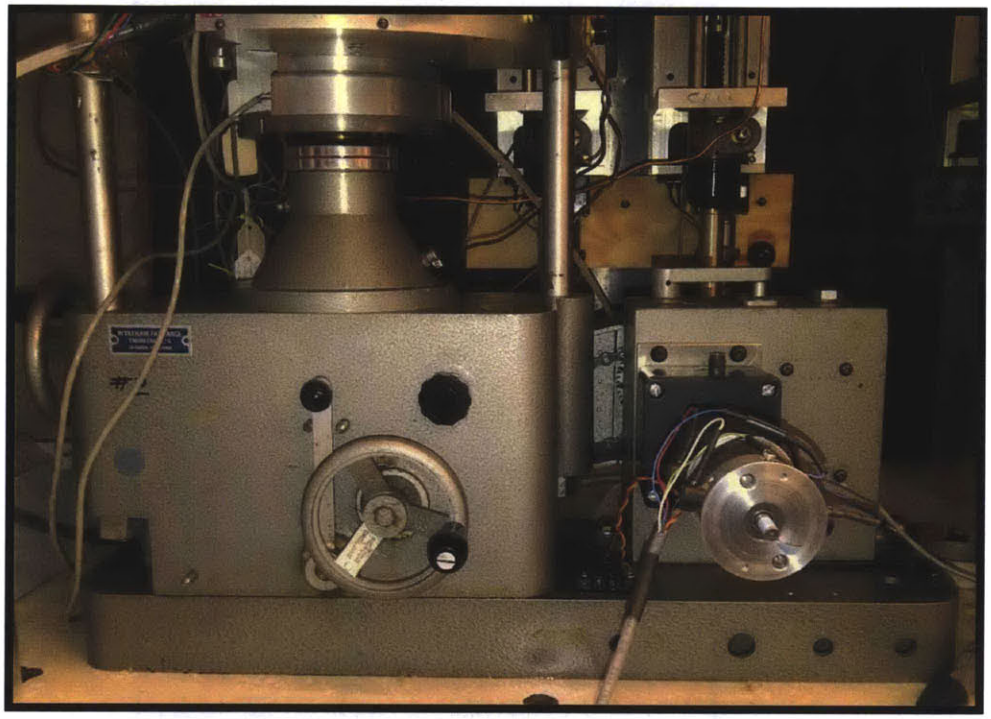

Figure 4-4 Photograph of the bench top load frame with motor for axial loading.

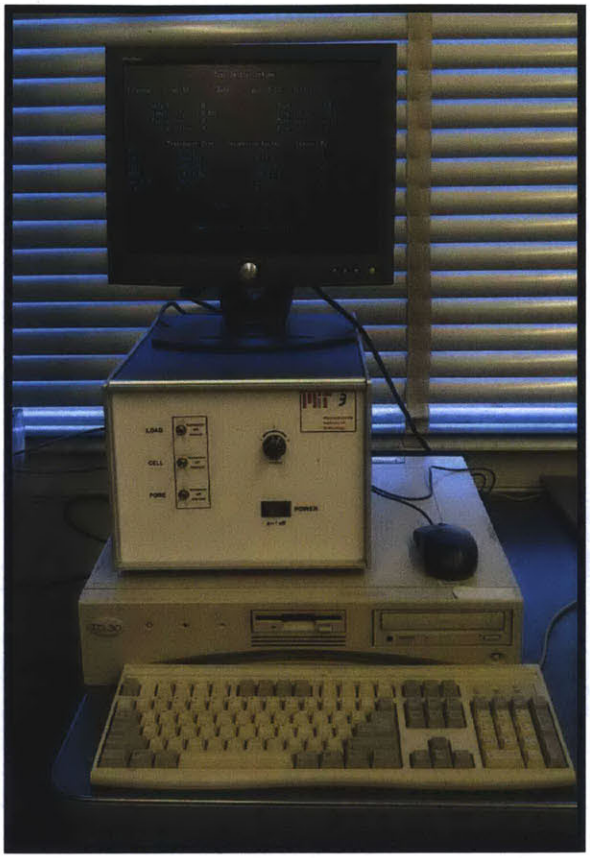

Figure 4-5 Personal Computer, Control Box and Control Program Screen

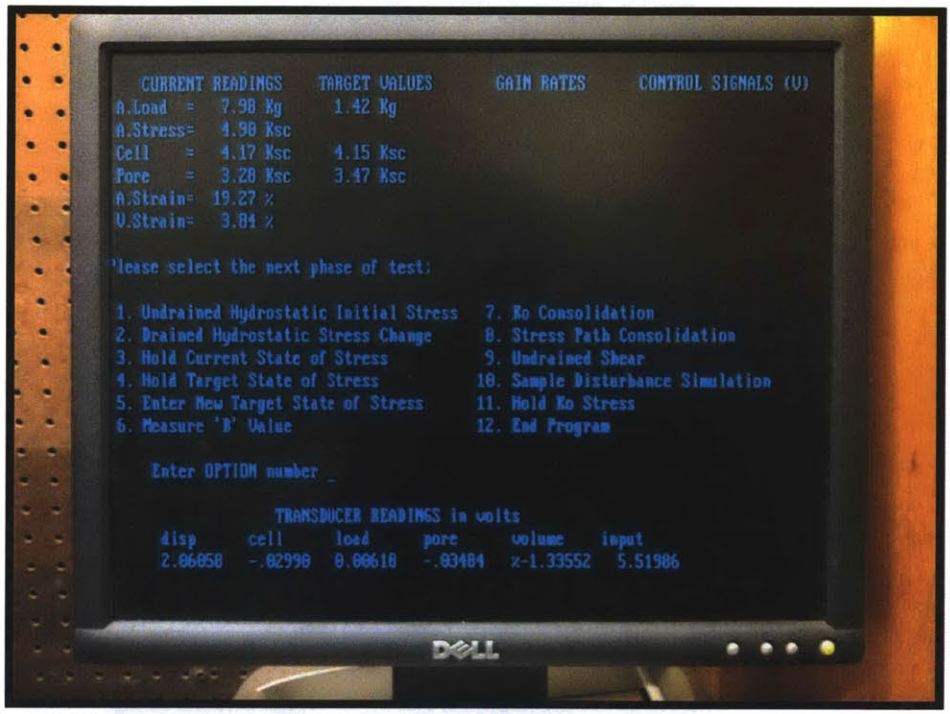

Figure 4-6 Control Program Options Screen

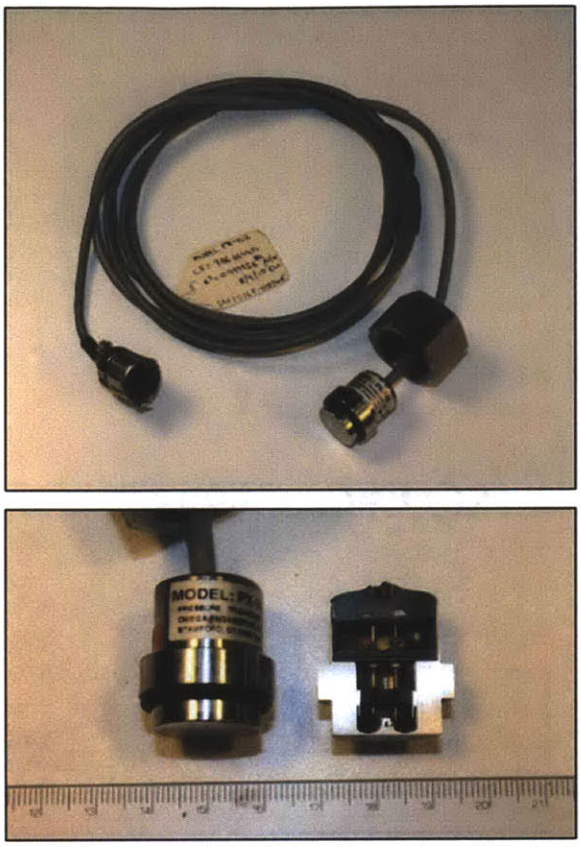

Figure 4-7 Top: Pressure Transducer, Bottom: Close up of pressure transducer and also a section through a pressure transducer to help demonstrate its operation (Horan, 2012)

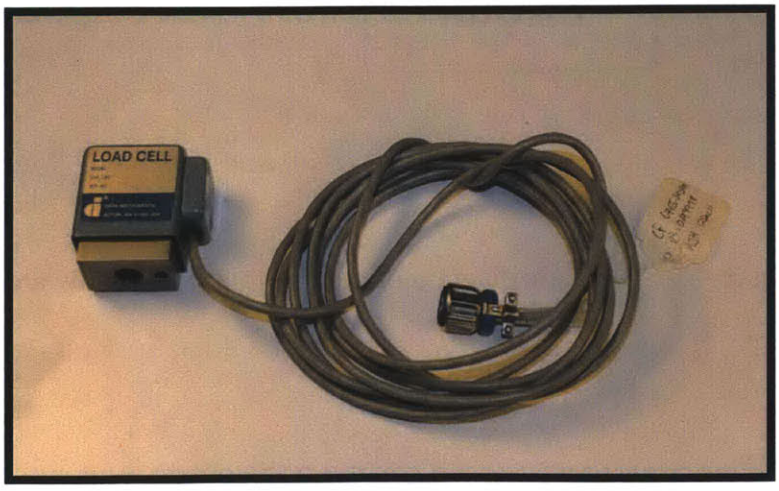

Figure 4-8 Data Instruments JP Load cell (500 lb) (Horan, 2012)

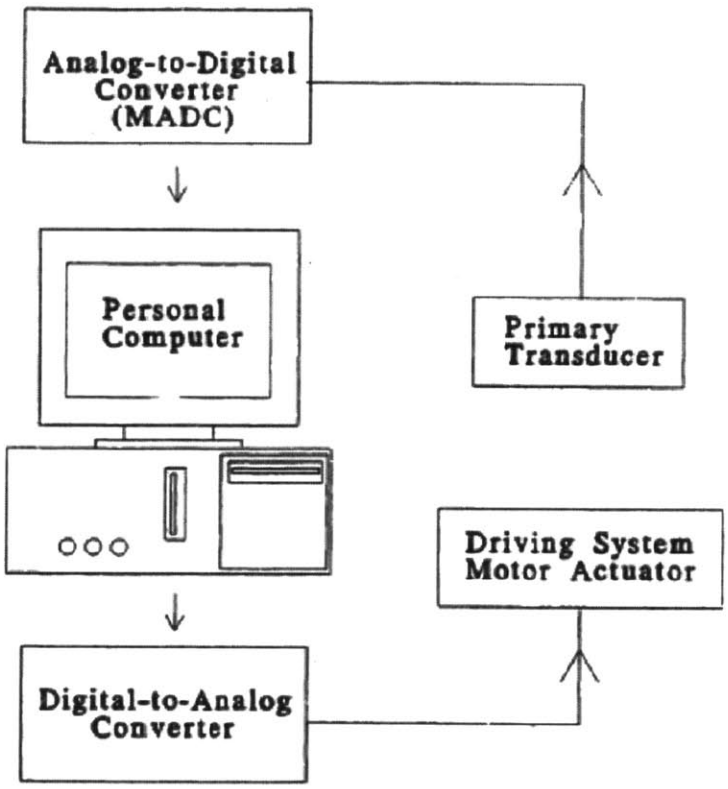

Figure 4-9 Schematic diagram of the control system hardware components

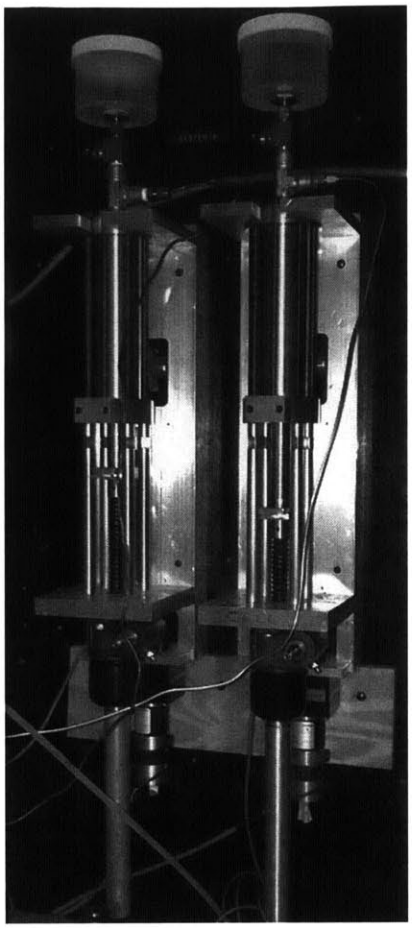

Figure 4-10 MIT-designed Pressure Volume Actuator (PVA)

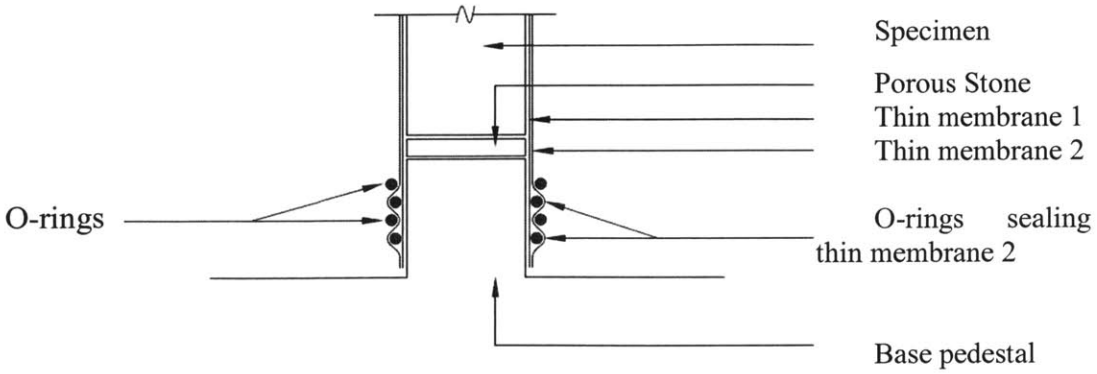

Figure 4-11 Low presssure triaxial sealing arrangement (Horan, 2012)

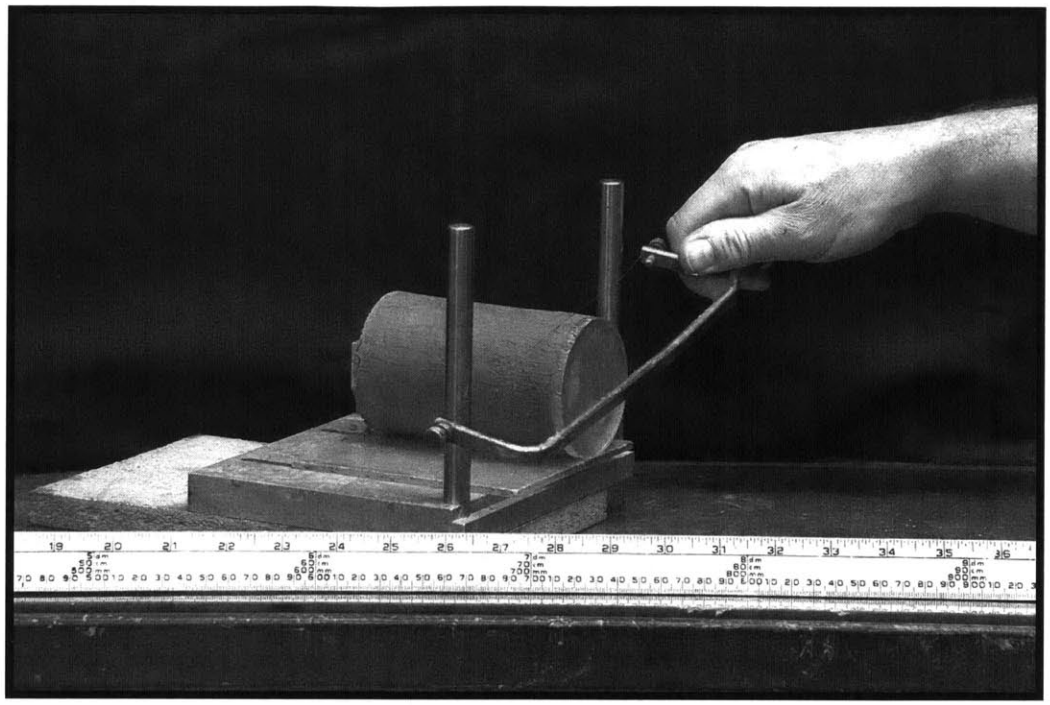

Figure 4-12 Perpendicular flat surfaces being cut on the sample in a miter box (Germaine & Germaine, 2009)

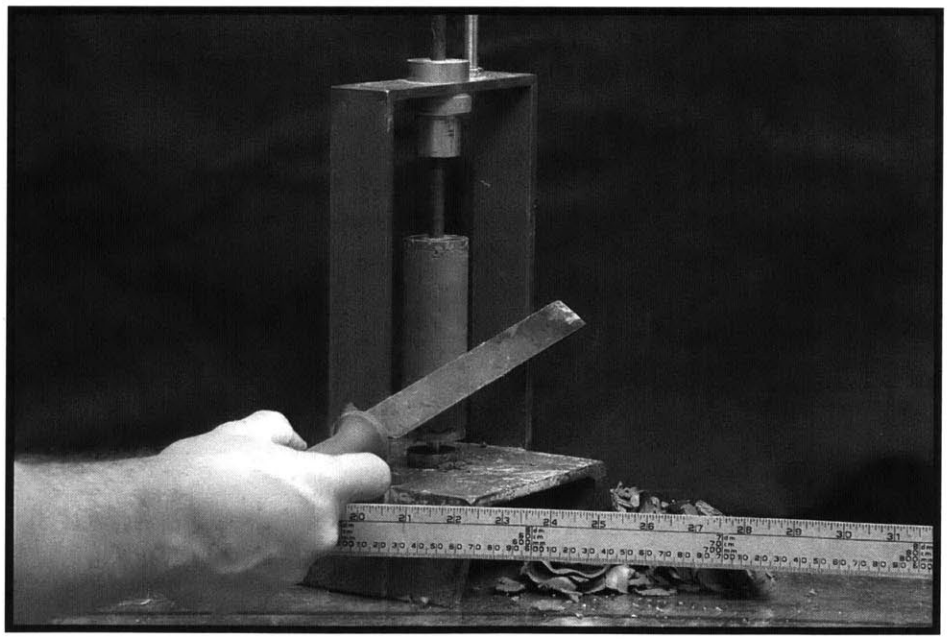

Figure 4-13 Final trimming in cylindrical miter box (Germaine & Germaine, 2009)

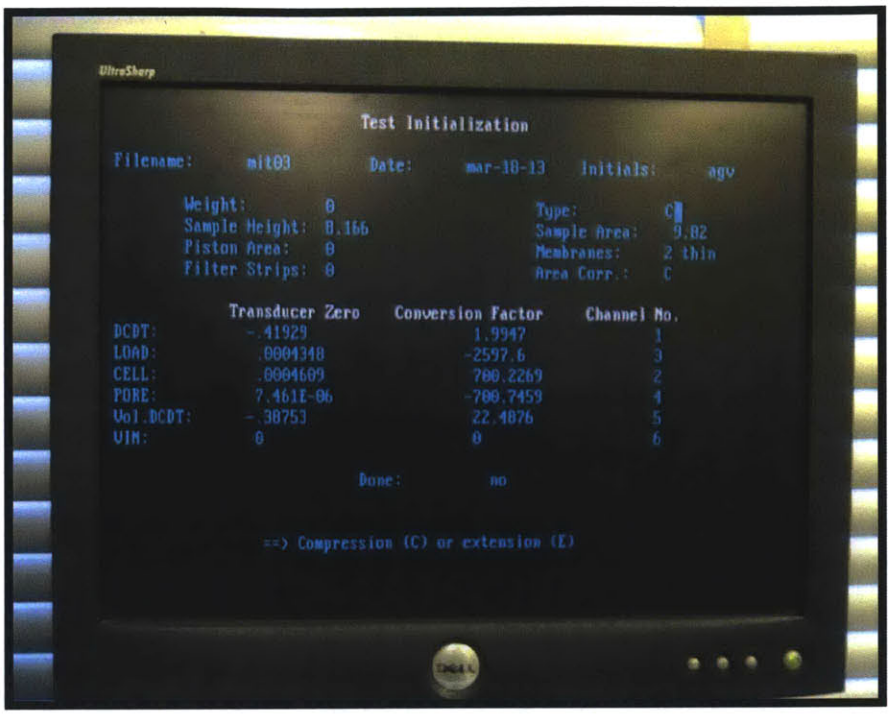

Figure 4-14 Set-up Program Screen

5 RESULTS AND ANALYSIS

5.1 INTRODUCTION

A testing program was developed to characterize the one dimensional compression and triaxial compression undrained shear behavior of Resedimented Boston Blue Clay (RBBC) and Intact Presumpscot Maine Clay (PMC) at very high overconsolidation ratios. This chapter presents the results for a series of K_o-Consolidated undrained compression triaxial test (CK_oUC) on RBBC and PMC at different overconsolidation ratios.

Section 5.2 describes the general interpretation methods used to analyze all of the test presented in this thesis. Section 5.3 presents the results from CK_oUC tests on RBBC. The triaxial compression test series studied the 1-D consolidation and undrained shear compression behavior at different overconsolidation ratios. A detailed analysis on specimens at OCR of 8 and 50 is presented as part of this section. The stress level and strain rate effect discussion is reported in section 5.3.2.3. A total of 15 tests were performed as part of the testing program. However, 5 of these tests are not presented because of experimental problems.

The results from K_o-consolidated undrained triaxial compression tests on Presumpscot Maine Clay are presented in 5.4. A total 10 tests were conducted in PMC. Of these, 4 are not presented because of experimental issues such as the LVDT in the volume PVA actuator out of range.

Section 5.5 summarizes and compares the results for a series of OC triaxial tests on RBBC conducted by the author, with three tests at OCR = 1, 2 and 4 reported by Abdulhadi (2009). This

section integrates both researchers' results to give the reader an overall understanding of the OCR effect on RBBC.

5.2 GENERAL INTERPRETATION

This section describes the general procedures for analyzing the results of this testing program. As explained previously in section 4.3.8, the data files are retrieved from the data acquisition and converted to engineering values in a reduce program. The reduction program was written in QBasic and requires the user to input the specimen dimensions, zero values and calibration factors to perform all the calculations. This file is called "reduce file" and is used to convert the voltages to engineering values for the consolidation and undrained sheared phases of the test. The user must check that the results are in agreement with the recorded values during the test. This reduction procedure is standard for all triaxial test at the MIT Geotechnical Laboratory and is explained in detailed by Sheahan (1991). The results files are then imported into Microsoft Excel for a first inspection and after into SigmaPlot 11.0 for detailed graphing. Section 5.2.1 discusses the general interpretation for the consolidation behavior and section 5.2.2 describes the methods used for the interpretation of the undrained shear behavior.

5.2.1 Consolidation Behavior

In order to analyze the 1-D consolidation behavior of the entire testing program conducted for this research a common procedure was followed. Each test had a corresponding reduce file, containing all the setup information, and a result file, with the engineering values measured during the tests, which was first analyzed in Microsoft Excel. The calculations are based on the

initial specimen dimensions and the reduce program incorporates corrections for the specimen and the stiffness of the membranes.

Phase calculations were performed for each test to obtain the initial void ratio and saturation of the specimen. Error in specimen dimensions and weight result in a saturation value out of the tolerance range ± 2% as occurred for test TX1138. To obtain the preconsolidation pressure the strain energy method (Becker et al 1987) was used. Some differences with respect to the batch consolidation pressure were encountered for some particular tests. This difference can be attributed to factors such as secondary compression (which tends to increase σ'_p), the side-wall friction (which tends to increase σ'_p), disturbance caused during extrusion, and/or simply inexact application of the maximum vertical stress.

The CR values were computed as the slope of loading portion of the compression curve and the initial void ratio. The SR values were determined by connecting the compression curve points at the end of loading and the end of unloading (after secondary compression).

The maximum vertical stress (σ'_{vm}) and minimum vertical stress (σ'_{vc}) values were computed as the average values during aging. On the other hand, the last reading for volumetric strains, axial strains, and lateral stress ratio were the values included in the summary table. The OCR was computed as $\sigma'_{vm}/\sigma'_{vc}$ for almost all of the test.

Observations:

Some of the issues encountered during the analysis of the consolidation behavior are due to human error or equipment issues. For instance, errors in specimen dimensions and weight result in a saturation value out of the tolerance range ± 2% as occurred for test TX1138.

Equipment limitations, such as if the LVDT used to measure the displacement of the piston in the pore pressure PVA is out range, caused the volumetric strain not to be equal to the axial strain, meaning that some lateral strain occurred during consolidation. However, the effect on the undrained shear behavior wasn't affected significantly.

In addition, small errors in the zero values can cause a major impact at lower stresses during the swelling phase of the test. For example, if the load cell zero value is below its real value this can cause the applied stress to keep trying to be reduced when in reality it reached zero applied stress and hydrostatic conditions. In this cases the average of the radial stress (σ'_{cc}) instead of the vertical stress.

5.2.2 Undrained Shear Triaxial Compression

During the shear phase of the triaxial the calculations performed by the reduction program are based on the preshear specimen dimensions while the membrane correction is still based on the setup dimensions of the specimen. Note that the parabolic area correction is used for the undrained shear triaxial compression.

The "results" file for the undrained shear phase computes the shear and mean stresses, the excess and shear pore pressures, the secant modulus, the A parameter, and the friction angle. However, it is difficult to choose a peak undrained strength in overconsolidated tests because of the shape of the stress-strain curves do not show a well-defined peak as NC test. Consequently, the maximum value function from Microsoft Excel was used to find the peak strength. Accordingly, strain softening of the stress strain curves is quite mild.

As a consequence of the backlash in the axial loading gear system during load reversal (from unloading, for swelling; to loading for shearing), the initial strain measurements are slightly affected and hence, a correction was made to the data. The shearing starting point was determined graphically by defining the point in the origin.

Regarding the secant modulus, reasonable results were obtained only beyond 0.05% axial strain, since the measurements were performed employing an external LVDT. It is challenging to define a failure envelope with a cohesion intercept because of the non-linearity trend of the envelope with increasing the overconsolidation ratio.

5.3 RESEDIMENTED BOSTON BLUE CLAY

5.3.1 One-Dimensional Consolidation Behavior

All the triaxial tests conducted by the author were K_o-consolidated at a constant strain rate of 0.15%/hr and allowing 24 hours of secondary compression. Then the specimens were swelled to a specified OCR value with -0.15%/hr followed by another 24 hours of aging. As described in section 4.3, the K_o-Consolidation algorithm ensures zero lateral strain by adjusting the cell pressure to keep the axial and volume strains equal. On the other hand, the stress path algorithm is used for the swelling portion of the test. Appendix 1 reports the test number, resedimentation batch number, applied preconsolidation pressure, and initial phase relations. Table 5-1 and Table 5-2 summarized the states at the end of both phases.

Figure 5-2 shows the compression curves in a void ratio (e) versus logarithm of the vertical consolidation stress (log σ'_v) space for all OC tests conducted by the author. This plot includes three test conducted by Abdulhadi (2009) for comparison. The majority of the tests were

consolidated to a maximum vertical stress of 1.5 – 1.8 MPa, with the exception of TX1156 that was consolidated to 5.4 MPa. As expected, the preconsolidation stresses obtained in the triaxial were roughly the resedimentation batch preconsolidation pressure values of σ'_p = 0.4 to 1.5 MPa. It can also be observed that all the compression curves, apart from TX1138, lie in a very tight band showing fine agreement and repeatability among test specimens. The test TX1138 computed void ratio value is believed to be anomalous, wrong specimen measurements could have led to these results, as it was described in 5.2.1

As reported by previous researchers, the virgin consolidation behavior from the author's testing program also displays a log-linearity with CR values of about 0.16. Figure 5-3 shows the SR values versus OCR and stress level. This plot shows how the SR value is affected by both parameters OCR and the maximum stress level. The SR value for the different OCR was computed for specimens with the same stress level, considering values at the end of consolidation and at state with OCR = 10 for three of the author's triaxial tests. For comparison, the previous values are plotted in conjunction with Abdulhadi (2009) reported SR values for RBBC specimens at different stress levels and the same OCR. As expected, the soil increases its swelling potential with stress level as well as with overconsolidation. These values of SR are one order of magnitude smaller than the average CR for the triaxial tests conducted by the author.

The change in the lateral stress ratio during the K_o-consolidation and swelling stages is shown in Figure 5-4. The average K_c (K_o at the end of consolidation), for the 10 test reported, is 0.556. It can be observed that the lateral stress ratio rises during the swelling phase to approximately of $K_{o\,OC}$ equal to 1. The repeatability of the K_o is somewhat good in comparison with previous researchers. However, the overall trend of the tests conducted by the author agrees

with Abdulhadi (2009) reported behavior. The lateral stress ratio decreases with loading until the preconsolidation pressure is achieved and then plateaus at a constant value ranging from 0.50 to 0.60. Table 5-1 and Table 5-2 report the values of K_o at the maximum stress. Note that Abdulhadi (2009) reported that the K_c increases with the stress level.

5.3.2 Undrained Triaxial Compression

5.3.2.1 Behavior of OCR = 8

Shear Stress-Strain Behavior

The stress-strain curves for the three CK_oUC triaxial tests conducted on specimens to a nominal OCR of 8 are shown on Figure 5-5. The post peak portions of the stress strain curves are fairly parallel. As presented in the summary plot in Figure 5-6, the peak undrained shear stress increases as the preshear consolidation stress (σ'_{vc}). Figure 5-7 presents the normalized shear stress-strain (q/σ'_{vc}) behavior with axial strain (ε_a). A close up view up to ε_a = 8% is shown in Figure 5-8. Figure 5-9 exhibits the normalized stress-strain curve with axial strain on a logarithmic scale. The undrained shear strength exhibits a directly proportional behavior with the preshear consolidation stress (σ'_{vc}) level and maximum stress (σ'_{vm}) level as shown in Figure 5-6 and Figure 5-10, respectively. Figure 5-11 exhibits that the undrained strength ratio (s_u/σ'_{vc}), or USR, drops approximately 7% when varying the preshear stress from 0.12 to 0.24 MPa. Note that the specimens were unloaded to a K_c = 1, the only test that supersedes this value was TX1134 because of experimental issues as discussed previously. Figure 5-12 shows the USR with K_c. Shear planes appeared during undrained shearing of two tests as it is described in Table

5-1, and shown in Figure 5-1. The strain at peak stress (ε_f) ranges from 8% to 12% with no particular correlation as Figure 5-13 shows.

Stiffness

Figure 5-14 presents a summary of the normalized secant modulus (E_u/σ'_{vc}) at different strain levels versus the preshear consolidation stress for the three tests overconsolidated to an OCR = 8. Figure 5-15 exhibits the stiffness behavior with axial strain in a log-log plot. The stiffness behavior is not quite affected by the small increase in stress level. The normalized initial stiffness decreases with increasing the stress level. The stiffness values converge at larger strains.

Effective Stress Behavior

Figure 5-16 shows the effective stress paths from the undrained shear for the three test conducted at a nominal OCR = 8. A close up view of the normalized stress paths (q/σ'_{vc} versus p'/σ'_{vc}) shown in Figure 5-17 demonstrates that the three stress paths raise towards the envelope with parallel paths until reaching the peak stress at different locations.

The variation in friction angle at peak (ϕ'_p) and maximum obliquity (ϕ'_{mo}) is shown in Figure 5-18. Assuming a zero cohesion intercept, ϕ'_p ranges from 34° to 50° while ϕ'_{mo} from 33° to 52°. These data agree with the reported behavior on the difference between ϕ'_p and ϕ'_{mo} gets smaller as OCR increases by Abdulhadi (2009).

Porewater Pressures

The normalized excess pore pressure versus axial strain behavior is presented in Figure 5-19. For the three tests discussed on this section, the *excess pore pressure* initially increases, then decreases and reach a minimum value at about ε_f. For test TX1138, where a slip surface was developed, a later increase in the excess pore pressure is shown after ε_f. However, the data recorded after a failure surface is considered unreliable. Interestingly, in the case of TX1132 the failure plane does not appear to alter the pore pressures, this can be attributed to the definition or intensity of the failure plane. It was observed a greater aperture in the failure plane developed in TX1138 specimen. The preshear consolidation stress level seems to be correlated with the minimum excess pore pressure value; meaning that as the stress level increases the minimum value becomes more negative, as well as the post peak pore pressure rate. The shear induced pore pressure increases slightly to a positive value and the decrease to a negative minimum value (Figure 5-20). The undrained shear behavior for RBBC at an OCR=8 is initially contractive, and finally *dilative*.

5.3.2.2 Behavior of OCR = 50

Two CK_oUC triaxial tests were performed on resedimented specimens and mechanical overconsolidated to a nominal OCR = 50 at different stress levels. The two the tests, TX1139 and TX1148 target the same maximum stress σ'_{vm} = 7.80 MPa. Specimens were sheared undrained at 0.5%/hr strain rate. One test, TX1148 developed a shear plane.

Shear Stress-Strain Behavior

Figure 5-22 exhibits the shear stress - strain curves for the OCR = 50 test series. The undrained shear strength appears to be correlated to the vertical consolidation stress level as summarized in Figure 5-23. The peak undrained shear stress increases from 0.1 MPa to 0.14 with a 0.1 MPa increment in the pre-shear consolidation stress (σ'_{vm}). Figure 5-24 presents the normalized shear stress-strain behavior (q/σ'_{vc} - ε_a). In addition, Figure 5-25 shows the normalized shear stress-strain curves on a close up view to ε_a = 2% strain linear scale, while and Figure 5-26 present the results on a logarithmic scale. The undrained shear strength values with respect to the vertical consolidation stress are shown in Figure 5-23. The undrained shear strength increases proportionally to the maximum vertical consolidation stress level as presented in Figure 5-27. Figure 5-28 shows that the USR varies from 3.1 to 4.2 for both tests. Figure 5-29 reports that the undrained strength ratio (s_u/σ'_{vc}) decreases as the K_c value increases. Figure 5-30 shows that the strain at peak stress (ε_f) varies from 11.5% to 14% between the two tests.

Stiffness

A summary of the normalized secant modulus (E_u/σ'_{vc}) at different strain levels versus the preshear consolidation stress for test series overconsolidated to an OCR = 50 is presented in Figure 5-31. The stiffness behavior with axial strain in a log-log plot is shown in Figure 5-32. Even though the two curves are offset throughout the test, the stiffness behavior is not largely affected by the small increase in stress level. The stiffness values incline to converge at larger strains.

Effective Stress Behavior

As in the OCR = 8 series, the effective stress paths (ESPs) for the OCR = 50 tests are characterized by the initial generation of positive excess pore pressures as the shear stress increases and the ESPs reach the effective stress envelope (ESE). Once the ESPs intersect the ESE, the path continues along the envelope. The effective stress paths from the undrained shear for the two test conducted at a normal OCR = 50 are presented in Figure 5-33. Figure 5-34 shows a close up view of the normalized stress paths (q/σ'_{vc} versus p'/σ'_{vc}).

Figure 5-35 shows the friction angle at peak stress ϕ'_p (32° - 39°) and maximum obliquity ϕ'_{mo} (41° - 72°) dependence to the vertical consolidation stress level. The maximum obliquity is reached at much lower strains than peak stress. However, this difference can be attributed to the small errors at very low stresses that were targeted to achieve such a high OCR.

Porewater Pressures

Figure 5-36 shows the normalized excess pore pressure development versus axial strain and Figure 5-37 plots the normalized shear induced pore pressure versus strain. The excess pore pressure initially increases and then decreases to a minimum value occurring near or at ε_f. The shear induced pore pressure also exhibits a similar behavior as the excess pore pressure. Figure 5-38 shows a close up view of the shear induced pore pressure at lower strains. Note that the plots discussed in this section are normalized to the vertical consolidation stress levels. As for OCR = 8 tests series, the undrained shear behavior is initially contractive, and finally *strongly dilative* for RBBC at an OCR=50.

5.3.2.3 Behavior of OCR = 32 - Stress Level vs. Strain Rate Effect

Three CK_oUC triaxial tests were conducted on resedimented specimens and mechanically overconsolidated to a nominal OCR = 32 and sheared at different strain rates. Two tests, target the same maximum stress σ'_{vm} =1.6 MPa, while T1156 was consolidated to a significantly higher vertical consolidation stress σ'_{vm} = 5.4 MPa. TX1141 and TX1156 were sheared undrained using 0.5%/hr while TX1140 was tested at 4.0%/hr strain rate. All of the tests at this OCR developed shear planes.

Shear Stress-Strain Behavior

The stress-strain curves for the three CK_oUC triaxial tests conducted on specimens mechanically overconsolidated to a nominal OCR of 32 with maximum vertical consolidation stresses σ'_{vm} = 1.6 - 5.4 MPa, but using different strain rates during shearing (0.5%/hr and 4.0%/hr) are reported on Figure 5-39.

Figure 5-40 summarized the undrained shear strength versus strain rate. The peak undrained shear stress decreases from 0.132 MPa to 0.118 with a 3.5%/hr rate increment ($\dot{\varepsilon_a}$) and from 0.13 to 0.30 MPa with a 3.8 MPa increment in the vertical consolidation stress (σ'_{vm}). The normalized shear stress-strain behavior (q/σ'_{vc} - ε_a) is presented in Figure 5-41. Besides, Figure 5-42 and Figure 5-43 exhibits the normalized shear stress-strain curves on a close up view to ε_a = 4% strain linear scale and on a logarithmic scale, respectively.. The normalized undrained shear strength (s_u/σ'_{vc}) shows a decline as the strain rate increases, and also as the vertical consolidation stress increases as reported on Figure 5-44. The drop in the USR is more sensitive to the stress level than to the change in strain rate. Figure 5-45 presents the USR versus lateral

stress ratio, since the three values of K_c are very similar it can be inferred that the USR was affected predominantly because of the stress level. Figure 5-46 shows that the strain at peak stress (ε_f) varies from 13% at a 0.5%/hr to 10% at a 4%/hr.

Stiffness

Figure 5-47 summarizes the normalized secant modulus (E_u/σ'_{vc}) at different strain levels versus stress for the three tests at OCR = 32. Figure 5-48 exhibits the stiffness behavior with axial strain in a log-log plot. The stiffness behavior is not largely affected by the strain rate, however a noticeable effect can be seen with stress level. The stiffness values tend to converge at larger strains for the same stress level.

Effective Stress Behavior

Figure 5-49 shows the effective stress paths from the undrained shear for the three test conducted at a nominal OCR = 32. The three ESPs climb towards the envelope with comparable paths until reaching the peak stress at different locations. Figure 5-50 reports the variation in friction angle at peak (ϕ'_p) and maximum obliquity (ϕ'_{mo}). Assuming a zero cohesion intercept, ϕ'_p is about 33 - 48° while ϕ'_{mo} ranges from 40° to 60°.

Porewater Pressures

Figure 5-51 presents the normalized excess pore pressure versus axial strain behavior. For all of the tests, the *excess pore pressure* initially increases, then decreases and reach a minimum value. As expected, it is observed that the high strain rate cause higher pore pressures. Likewise, the stress level behavior tends to increase the excess pore pressure and then decrease, but in this case the peak is delayed. Figure 5-52 and Figure 5-53 shows that the shear induced pore pressure increases slightly to a positive value and the decrease to a negative minimum value. The specimen tested at higher strain rate induced more pore water pressure at the initial stages of shearing. As the tests discussed in the previous sections, the undrained shear behavior for RBBC at an OCR=32 is initially contractive, and finally *dilative*.

5.4 PRESUMPSCOT MAINE CLAY

5.4.1 One-Dimensional Consolidation Behavior

As for RBBC, all the triaxial tests conducted on Presumpscot Maine Clay (PMC) were K_o-consolidated at a constant strain rate of 0.15%/hr and swelled, allowing 24 hours of aging after each phase. Appendix 1 reports the test number, resedimentation batch number, applied preconsolidation pressure, and initial phase relations. Table 5-3 summarized the states at the end of both phases.

The compression curves in a void ratio (e) versus logarithm of the vertical consolidation stress (log σ'_v) space for all OC tests are shown in Figure 5-54. The 6 tests were consolidated to a maximum vertical stress of 1.0 – 1.8 MPa and swelled to a specified OCR. The

preconsolidation stresses obtained in the triaxial were roughly around $\sigma'_p = 0.2 - 0.3$ MPa. It can also be observed that some compression curves lie in a very narrow band showing fine agreement; this means that the material and grain size distribution was similar for the various intact samples.

Two of the tests performed on PMC are clearly outliers from this band; the computed void ratio value is believed to be anomalous. An error during specimen measurements could have led to these results, as it was described in 5.2.1.

The virgin consolidation line shows a log-linearity with CR values of about 0.15 and SR = 0.008, fairly similar to RBBC. The values of SR are one order of magnitude smaller than the average CR for the triaxial tests conducted by the author.

Figure 5-55 shows the lateral stress ratio variation with vertical stress during the Ko-consolidation and swelling stages. The average K_c (K_o at the end of consolidation) for the 6 test reported is 0.48. It can be observed that the lateral stress ratio rises during the swelling phase to an approximate of $K_{o\ OC}$ equal to 1. For being intact samples, the repeatability of the K_o is satisfactory. The lateral stress ratio decreases with loading until the preconsolidation pressure is achieved and then plateaus at the same value of about 0.48. Table 5-3 reports the values of K_o at the maximum stress.

5.4.2 Undrained Triaxial Compression

This section presents results from triaxial tests in which OC specimens were sheared undrained in compression at a constant axial strain of 0.5%/hr after K_o-consolidation and stress path swelling to vertical consolidation effective stresses, σ'_{vc}= 0.03-0.21 MPa. A total of 9 tests

were performed on Intact Presumpscot Maine Clay (PMC). However, 3 tests were non-K_o consolidation tests and are not presented in this thesis for clarity. This section will discuss 6 tests at nominal OCR values from 5 to 62.

Shear Stress-Strain Behavior

Figure 5-56 shows the stress-strain behavior for the six CK_oUC tests conducted on specimens with OCR = 5 – 62. These data indicate that the peak undrained strength is between 0.2 and 0.3 and is not related with the OCR value, as summarized in Figure 5-57 and Figure 5-58. The scatter on these plots can be attributed to the difference in stress levels across the tests presented in this section. However, Figure 5-59 shows the normalized shear strain behavior (q/σ'_{vc} - ε_a), indicating that as OCR increases the peak value of strength normalized to preshear vertical consolidation stress increases. Additionally, Figure 5-60 and Figure 5-61 exhibits the normalized shear stress-strain curves on a close up view to ε_a = 2% strain linear scale and on a logarithmic scale, respectively. Figure 5-57 reports values of the undrained shear strength from 0.2 to 0.31 MPa versus the preshear consolidation strength and versus the maximum vertical stress in Figure 5-62. The normalized undrained shear strength (s_u/σ'_{vc}) also shows a very good relationship with OCR as it can be observed on Figure 5-63. Figure 5-64 presents the USR versus lateral stress ratio. Figure 5-65 reports the strain at peak stress (ε_f) varies from 8% to 13% at different overconsolidation ratios. As shown in Figure 5-66 maximum obliquity was reached much earlier than failure in all cases.

Stiffness

The normalized secant modulus (E_u/σ'_{vc}) at different axial strains versus OCR for the PMC test series is summarized in Figure 5-67. Figure 5-68 presents the stiffness behavior with axial strain in a log-log. From this figure, it can be observed that the stiffness increases with OCR.

Effective Stress Behavior

The effective stress paths from the undrained shear are presented in Figure 5-69. As for RBBC, the ESPs rise towards the envelope until reaching the peak stress at different locations. The variation in friction angle at peak (ϕ'_p) and maximum obliquity (ϕ'_{mo}) versus OCR is presented in Figure 5-70. Assuming a zero cohesion intercept, it can be observed that ϕ'_p increases with OCR, while ϕ'_{mo} ranges from 33° to 48°.

Porewater Pressures

The normalized excess pore pressure versus axial strain behavior is presented in Figure 5-71. The excess pore pressure initially increases and then decreases in all cases. After reaching a minimum the pore pressures stayed around a constant value. Figure 5-73 shows the normalized shear induced pore pressure generation with strain during shearing. In all the six tests, the pore pressure initially increases indicating a contractive behavior and then the 6 specimens tend to dilate with shearing after very small strains. A close up view of the behavior at small strains is presented in Figure 5-72 and Figure 5-74.

5.5 OVERVIEW OF OVERCONSOLIDATED COMPRESSION BEHAVIOR

This section presents results from a set of triaxial tests in which OC specimens were sheared undrained in compression at a constant axial strain of 0.5%/hr after K_o consolidation ($\sigma'_{vm} \approx 1.6$ MPa) and stress path swelling to vertical consolidation effective stresses, σ'_{vc}= 0.03-0.23 MPa. A total of 15 tests were performed on Resedimented Boston Blue Clay (RBBC). However, this section presents 5 tests that were conducted by the author in conjunction with some tests results performed by Abdulhadi in 2009 with similar conditions but with lower OCRs.. This section will discuss 8 tests at nominal OCR values from 1 to 50.

Shear Stress-Strain Behavior

Figure 5-75 shows the stress-strain behavior for 8 CK_oUC tests conducted on specimens with OCR = 1 – 50. These data indicate that the peak undrained strength is between 0.10 and 0.56 MPa and is significantly related with the OCR value, as summarized in Figure 5-76. The undrained strength decreases as OCR increases. Figure 5-77 shows the normalized shear strain behavior (q/σ'_{vc} - ε_a), indicating that as OCR increases the peak value of strength normalized to preshear vertical consolidation stress increases. Moreover, Figure 5-78 and Figure 5-79 shows the normalized shear stress-strain curves on a close up view to ε_a = 2% strain linear scale and on a logarithmic scale, respectively. Figure 5-80 reports values of the undrained shear strength ratio from 0.29 to 3.0 MPa versus overconsolidation ratio. The normalized undrained shear strength (s_u/σ'_{vc}) also shows a fair relationship with OCR and agrees with SHANSEP equation theories as it can be observed on Figure 5-81. Figure 5-82 shows the USR normalized to the normally

consolidated USR value as a function of OCR. The normalized undrained shear strength is related to the K_c value as reported on Figure 5-83. Figure 5-84 reports the strain at peak stress (ε_f) varies from 0.5% to 13% at different overconsolidation ratios. As shown in Figure 5-85 the maximum obliquity was reached much earlier than failure in all cases of OCR > 8, in contrast the opposite occurred for NC and OC specimens up to OCR = 4.

SHANSEP Equation in Heavily Overconsolidated RBBC

As mentioned previously, Figure 5-81 shows the undrained shear strength ratio versus OCR for the author's and Abdulhadi selected tests. The regression equation (R^2=0.9844) reported that the SHANSEP parameters S is equal to 0.3189, and m is equal to 0.6090. It can be concluded that the SHANSEP equation accurately models the undrained strength as a function of OCR, but that high OCR values increase the parameter S while decreasing the parameter m.

Stiffness

The normalized secant modulus (E_u/σ'_{vc}) at different axial strains versus OCR for the PMC test series is summarized in Figure 5-86. The normalized stiffness behavior versus axial strain in a log-log scale is presented in Figure 5-87 and Figure 5-88. From these figures, it can be observed that the stiffness increases with OCR.

Effective Stress Behavior

The normalized effective stress paths from the undrained shear are presented in Figure 5-89. As for PMC, the ESPs rise towards the envelope until reaching the peak stress at different locations. The stress states at peak stress and maximum obliquity cause the failure envelope to be steeper as it is observed in Figure 5-90 and Figure 5-91. The variation in friction angle at peak (ϕ'_p) and maximum obliquity (ϕ'_{mo}) versus OCR is presented in Figure 5-92. Assuming a zero cohesion intercept, it can be observed that ϕ'_p increases with OCR, while ϕ'_{mo} ranges from 30° to 43°.

The large strain states obtained at the end of shearing are presented in Figure 5-93 for the author's tests in comparison with previous work performed by Abdulhadi (2009) and Casey (2011). This figure shows the K_o-Consolidation line for 2 test from Casey and a K_o-Consolidation with swelling line from the authors testing program. The critical state line for tests with fixed ends and with OCR between 1 and 4 lie parallel to the K_o-Consolidation line. Casey's (2011) smooth end triaxial test lie in the left of this critical state line. While the authors heavily overconsolidated specimens lie in the dry side of the critical state line and do not reach either of this previous researcher defined critical state lines. This indicates that the water content of the specimen need it to be increase to reach this state.

Porewater Pressures

The normalized shear induced pore pressure versus axial strain behavior is presented in Figure 5-94. The shear induced pore pressure initially increases and then decrease for all OC specimens. After reaching a minimum the pore pressures stayed around a constant value. The

increment in the pore pressure indicates a contractive behavior and then dilation occurs. A close up view of the behavior at small strains is presented in Figure 5-95.

Table 5-1 Summary of CK_oUC Triaxial Tests on Resedimented Boston Blue Clay

	Ko - Consolidation and Swelling				At Max Shear			At Max Obliquity			E_u/σ'_{vc} @ ε_a =		
	@ Max Stress		@ Preshear										
Test #	ε_a	σ'_{vm}	ε_a	σ'_{vc}	ε_a	$\Delta u_e/\sigma'_{vc}$	q/p'	ε_a	$\Delta u_e/\sigma'_{vc}$	q/p'	0.001%	1%	Remarks
Sample	ε_{vol}	K_c	ε_{vol}	OCR		$\Delta u_s/\sigma'_{vc}$	ϕ'		$\Delta u_s/\sigma'_{vc}$	ϕ'	0.01%		
			K_c		q_f/σ'_{vc}	p'_f/σ'_{vc}	A	q_f/σ'_{vc}	p'_f/σ'_{vc}	A	0.1%		
TX1132*	10.44	1.860	8.08	0.236	9.67	0.027	0.562	2.45	0.273	0.578	1077.9	141.5	RBBC OCR=8
RS261	10.40	0.528	7.97	7.870		-0.826	34.16		0.414	35.34	956.7		Shut Down Ko-C
MIT-01			1.01		1.281	2.281	0.010	1.033	1.786	0.132	565.5		*Failure Plane
TX1134	12.47	1.113	9.97	0.128	12.10	0.485	0.538	8.52	0.530	0.544	4245.7	183.1	RBBC OCR = 8
RS282	15.32	0.604	12.69	8.664		-0.658	32.54		-0.560	33.000	1386.9		Non-Ko
MIT-04					1.380	2.569	0.140	1.340	2.457	0.164	784.8		*Failure Plane
TX1138*	12.53	1.514	10.47	0.191	7.78	0.732	0.767	7.73	0.696	0.791	5470.2	162.6	RBBC OCR = 8
RS295	12.68	0.500	10.75	7.918		-0.195	49.96		-0.142	52.24	688.6		
MIT-01			1.01		1.278	1.667	0.260	1.277	1.616	0.280	544.0		*Failure Plane
TX1139	15.37	1.667	10.97	0.033	14.07	-1.507	0.642	2.68	0.795	0.956	3654.0	206.2	RBBC OCR=50
RS296	15.46	0.560	10.17	50.236		-4.285	39.85		-0.458	72.73	1603.0		
MIT-01			1.04		4.285	6.678	-0.179	1.974	2.066	0.213	808.0		
TX1141*	13.43	1.615	9.22	0.050	12.98	-1.335	0.544	2.33	0.166	0.647	-	136.3	RBBC OCR=32
RS304	13.39	0.528	7.98	32.294		-3.018	33.15		-0.594	40.25	784.3		
MIT-04			1.06		2.667	4.902	-0.265	1.306	2.020	0.074	474.5		*Failure Plane
TX1142	14.17	1.626	11.15	0.111	10.64	0.178	0.683	2.99	0.415	0.686	-	153.8	RBBC OCR=16
RS305	14.17	0.540	10.77	14.673		-1.046	42.94		-0.478	43.350	1093.5		Clogged - cell
MIT-01			1.09		1.820	2.664	0.047	1.333	1.942	0.154	588.5		pressure line

Table 5-2 Summary of CK_oUC Triaxial Tests on Resedimented Boston Blue Clay (continuation)

	Ko - Consolidation and Swelling				At Max Shear			At Max Obliquity			E_u/σ'_{vc} @ ε_a =		Remarks
	@ Max Stress		@ Preshear										
Test #	ε_a	σ'_{vm}	ε_a	σ'_{vc}	ε_a	$\Delta u_e/\sigma'_{vc}$	q/p'	ε_a	$\Delta u_e/\sigma'_{vc}$	q/p'	0.001%	1%	
Sample	ε_{vol}	K_c	ε_{vol}	OCR		$\Delta u_s/\sigma'_{vc}$	ϕ'		$\Delta u_s/\sigma'_{vc}$	ϕ'	0.01%		
			K_c		q_f/σ'_{vc}	p'_f/σ'_{vc}	A	q_f/σ'_{vc}	p'_f/σ'_{vc}	A	0.1%		
TX1146*	12.30	1.577	8.84	0.095	11.58	-0.491	0.522	2.29	0.316	0.592	201.6	138.4	RBBC OCR = 16
RS306	12.30	0.586	8.54	16.644		-0.162	31.490		-0.381	35.830	961.3		
MIT-04			1.04		1.670	3.200	-0.145	1.030	1.740	0.150	554.9		*Failure Plane
TX1148*	13.67	1.562	8.66	0.032	11.59	-1.790	0.542	2.83	0.087	0.669	607.0	113.0	LVDT Stuck
RS311	13.64	0.563	7.38	48.273		-3.790	32.800		-0.729	41.410	523.0		during Swelling
MIT-04			1.21		3.080	5.685	-0.308	1.345	2.010	0.036	317.0		*Failure Plane
TX1149*	14.41	1.562	10.09	0.048	10.40	-1.040	0.557	2.07	0.581	0.775	-	157.1	RBBC OCR 32
RS310	14.47	0.552	9.18	32.508		-2.670	33.690		-0.199	50.480	8.1		Strain Rate 4%
MIT-04			1.08		2.457	4.410	-0.220	1.170	1.510	0.246	619.0		*Failure Plane
TX1156*	11.21	5.388	2.79	0.165	13.33	-0.001	0.744	3.47	0.512	0.868	-	54.6	RBBC OCR = 32
RS323	13.79	0.580	6.17	32.605		-1.026	48.090		0.154	60.170	235.0		High Stress
MIT-13			1.10		1.802	2.421	0.006	0.782	0.901	0.474	214.3		*Failure Plane

Table 5-3 Summary of CK_oUC Triaxial Tests on Presumpscot Maine Clay

	Ko - Consolidation and Swelling				At Max Shear			At Max Obliquity			E_u/σ'_{vc} @ ε_a =		Remarks
	@ Max Stress		@ Preshear										
Test #	ε_a	σ'_{vm}	ε_a	σ'_{vc}	ε_a	$\Delta u_e/s'_{vc}$	q/p'	ε_a	$\Delta u_e/s'_{vc}$	q/p'	0.001%	1%	
Sample	ε_{vol}	K_c	ε_{vol}	OCR		$\Delta u_s/s'_{vc}$	ϕ'		$\Delta u_s/s'_{vc}$	ϕ'	0.01%		
Loc			$K_{o\,OC}$		q/σ'_{vc}	p'/σ'_{vc}	A	q/σ'_{vc}	p'/σ'_{vc}	A	0.1%		
TX1117	11.69	1.070	10.98	0.212	6.67	-0.213	0.552	1.02	-0.069	0.332	732.2	120.4	OCR=8
SAA-F8T5	11.66	0.476	10.61	5.051		-0.745	33.52		-0.477	33.71	753.8		MIT-01
5-9 in			0.59		0.963	1.745	-0.138	0.472	1.421	-0.056	404.4		
TX1121	12.67	1.363	11.39	0.168	7.99	-0.404	0.574	1.60	-0.156	0.579	989.9	169.7	OCR=8
SAA-F8T5	12.67	0.506	11.20	8.129		-1.304	35.05		-0.854	35.53	1432.3		MIT-01
18-23 in			0.69		1.515	2.637	-0.150	1.209	2.088	-0.074	509.9		
TX1122	10.94	1.379	9.56	0.117	11.23	-0.429	0.606	1.34	0.035	0.617	1186.3	190.7	OCR=16
SAA-F8T6	10.92	0.504	9.28	11.815		-1.613	37.67		-0.710	38.08	1106.0		MIT-01
2-6 in			0.78		1.894	3.124	-0.119	1.235	2.003	0.016	579.1		
TX1126	11.79	1.365	10.15	0.084	8.66	-0.452	0.589	1.48	0.256	0.614	1465.1	255.1	OCR=16
SAA-F8T6	11.75	0.481	10.08	16.186		-2.105	36.08		-0.826	37.850	1718.3		MIT-01
17-22 in			1.15		2.398	4.070	-0.091	1.535	2.500	0.078	727.1		
TX1130	11.32	1.862	9.87	0.064	9.263	-2.240	0.592	1.11	0.071	0.659	1919.5	368.0	OCR=32
SAA-F8T2	11.68	0.430	9.85	29.215		-5.500	36.276		-1.270	41.169	1854.9		MIT-01
9-14 in			1.06		4.82	8.140	-0.227	1.950	2.960	0.020	941.5		
TX1135	10.95	1.638	9.03	0.026	13.37	-4.450	0.559	1.03	0.692	0.705	1594.7	393.7	OCR=64
SAA-F8T2	11.63	0.490	9.23	61.852		-9.640	34.00		-0.739	44.85	2251.9		MIT-01
19-24 in			1.31		7.54	13.490	-0.286	1.910	2.710	0.160	1222.7		

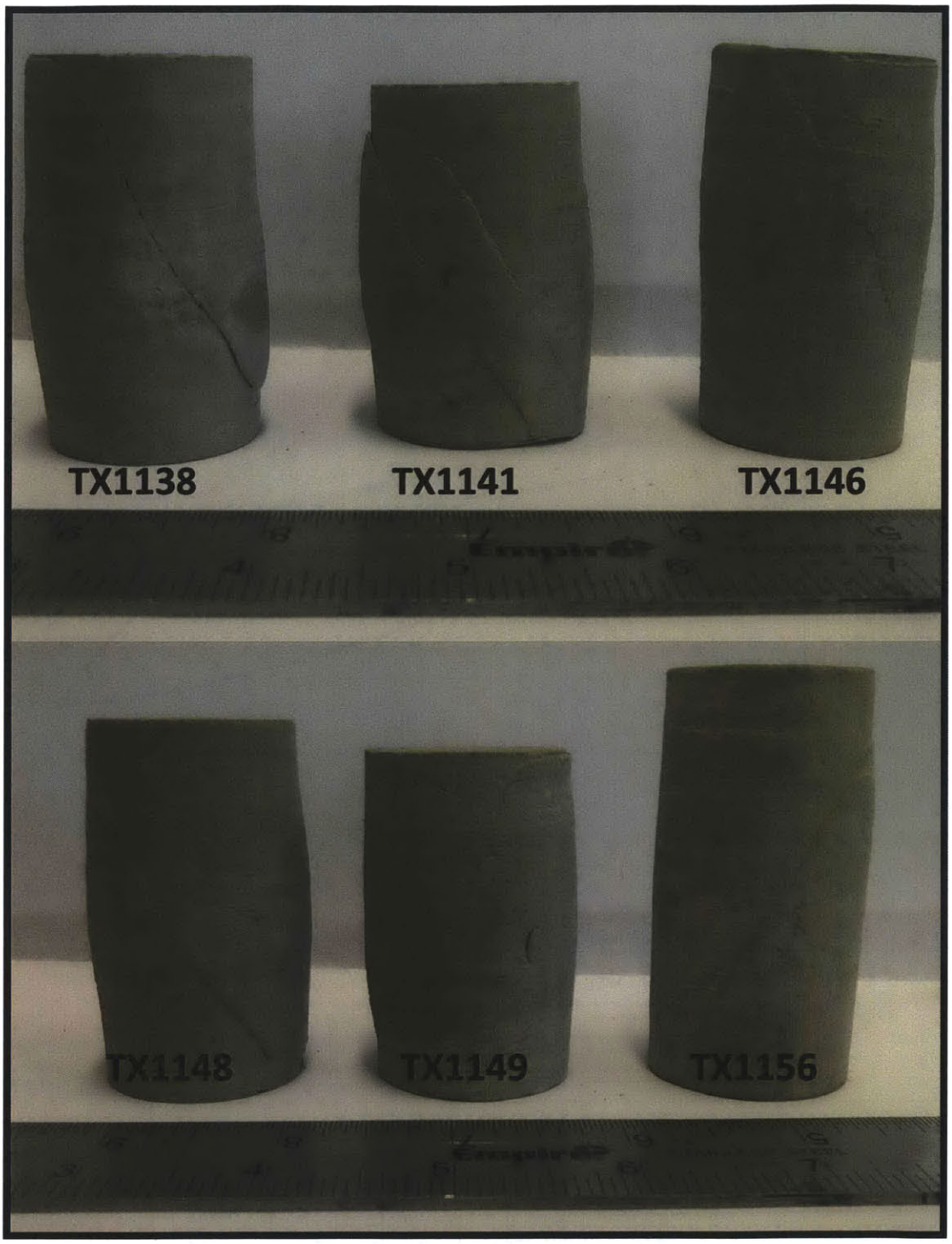

Figure 5-1 RBBC specimens after CK_oUC triaxial testing showing failure planes

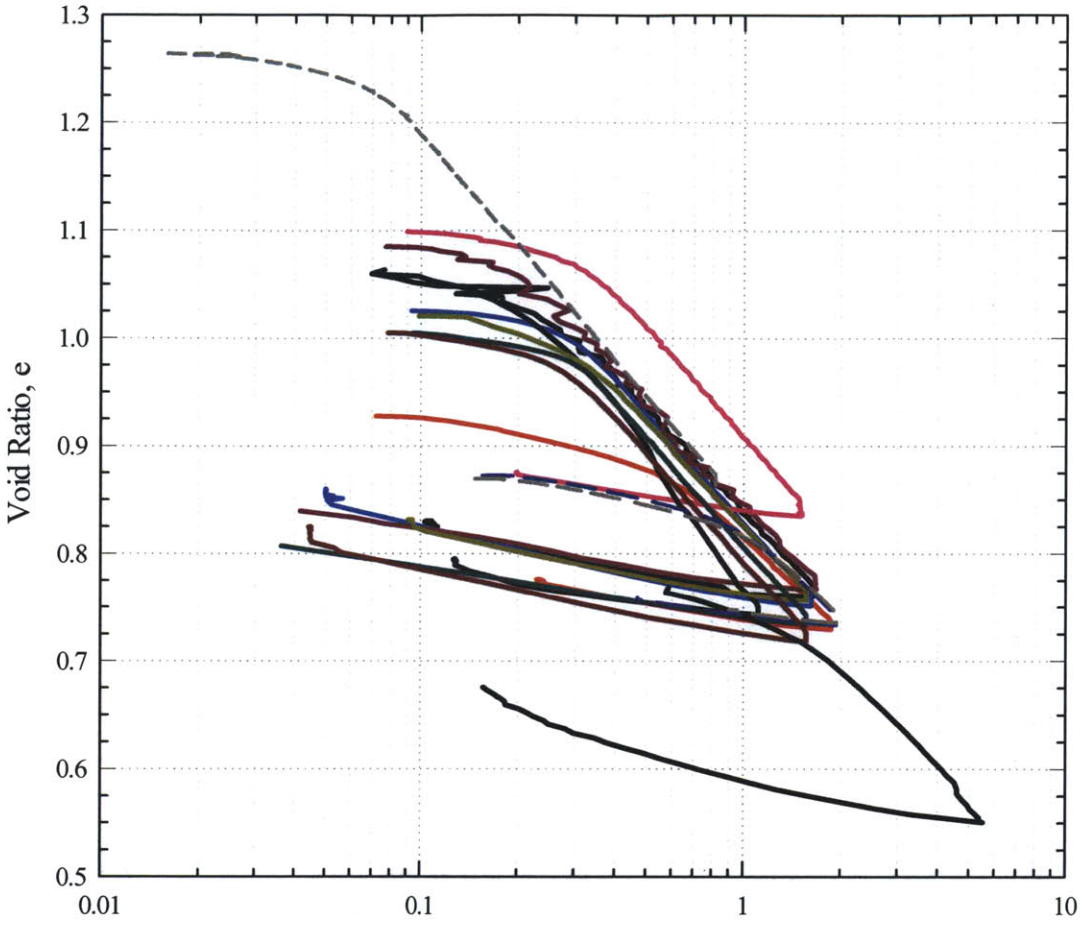

	TEST	OCR	σ'_{vc} (MPa)	σ'_{vm} (MPa)
	TX1132*	7.870	0.236	1.860
	TX1134	8.664	0.128	1.113
	TX1138*	7.918	0.191	1.514
	TX1142	14.673	0.111	1.626
	TX1141*	32.294	0.050	1.615
	TX1139	50.236	0.033	1.667
	TX1146*	16.644	0.095	1.577
	TX1148*	48.273	0.032	1.562
	TX1149*	32.508	0.048	1.562
	TX1156*	32.605	0.165	5.388
	TX798	1.000	1.954	1.954
	TX843	4.124	0.469	1.934
	TX849	2.022	0.958	1.937

Figure 5-2 I-D Compression behavior in e-log σ'_v space for all testing program on RBBC at different OCR

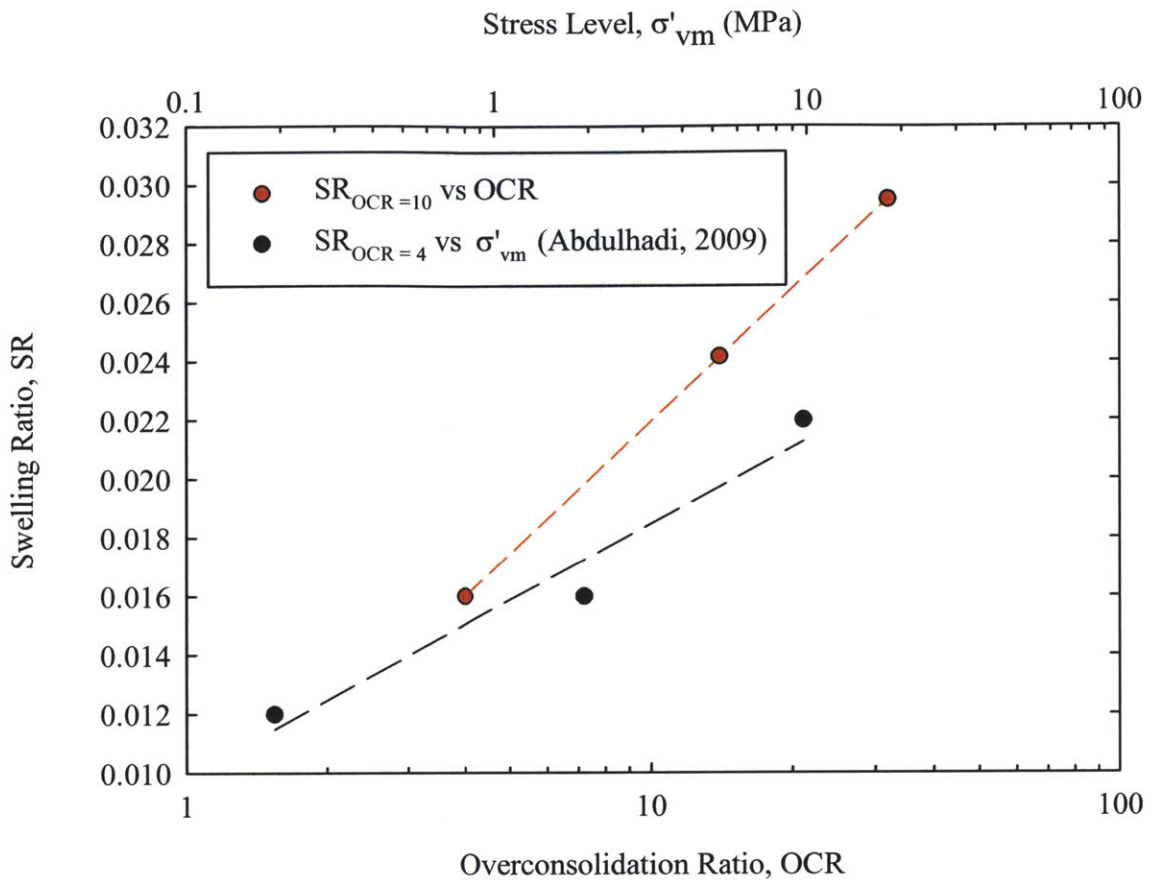

Figure 5-3 Swelling Ratio versus OCR and Stress Level

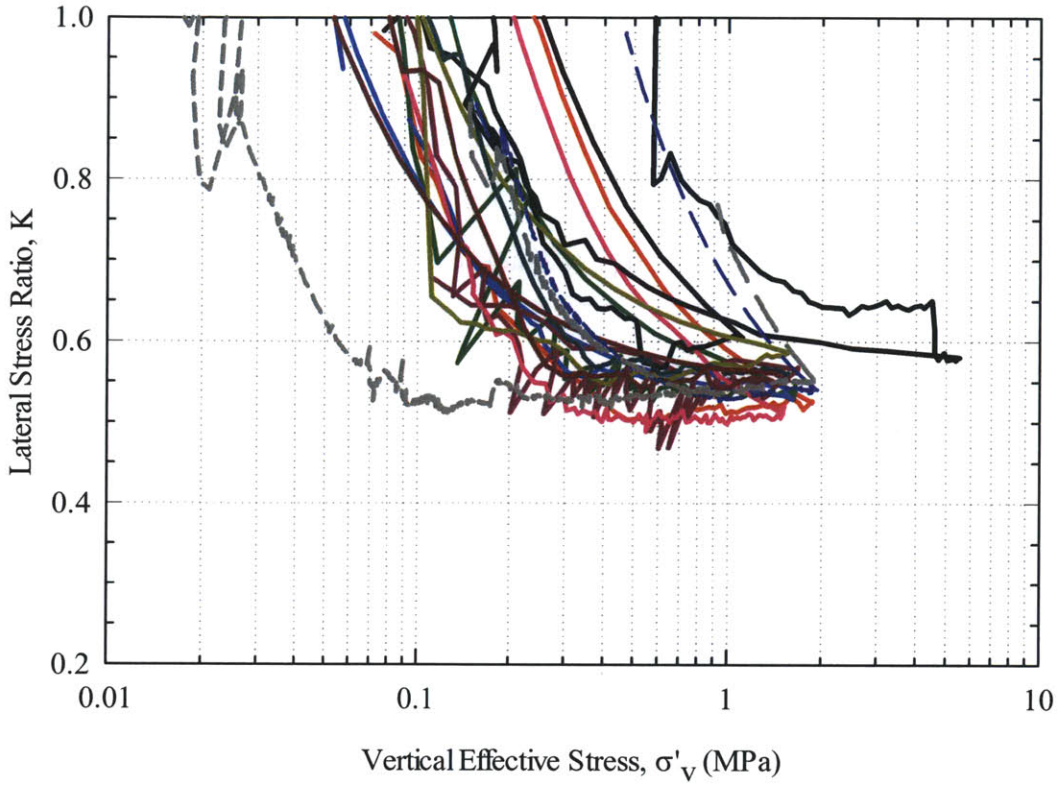

	TEST	OCR	σ'_{vc} (MPa)	σ'_{vm} (MPa)
	TX1132*	7.870	0.236	1.860
	TX1134	8.664	0.128	1.113
	TX1138*	7.918	0.191	1.514
	TX1142	14.673	0.111	1.626
	TX1141*	32.294	0.050	1.615
	TX1139	50.236	0.033	1.667
	TX1146*	16.644	0.095	1.577
	TX1148*	48.273	0.032	1.562
	TX1149*	32.508	0.048	1.562
	TX1156*	32.605	0.165	5.388
	TX798	1.000	1.954	1.954
	TX843	4.124	0.469	1.934
	TX849	2.022	0.958	1.937

Figure 5-4 Lateral stress ratio versus vertical effective stress for all testing program on RBBC at different OCR

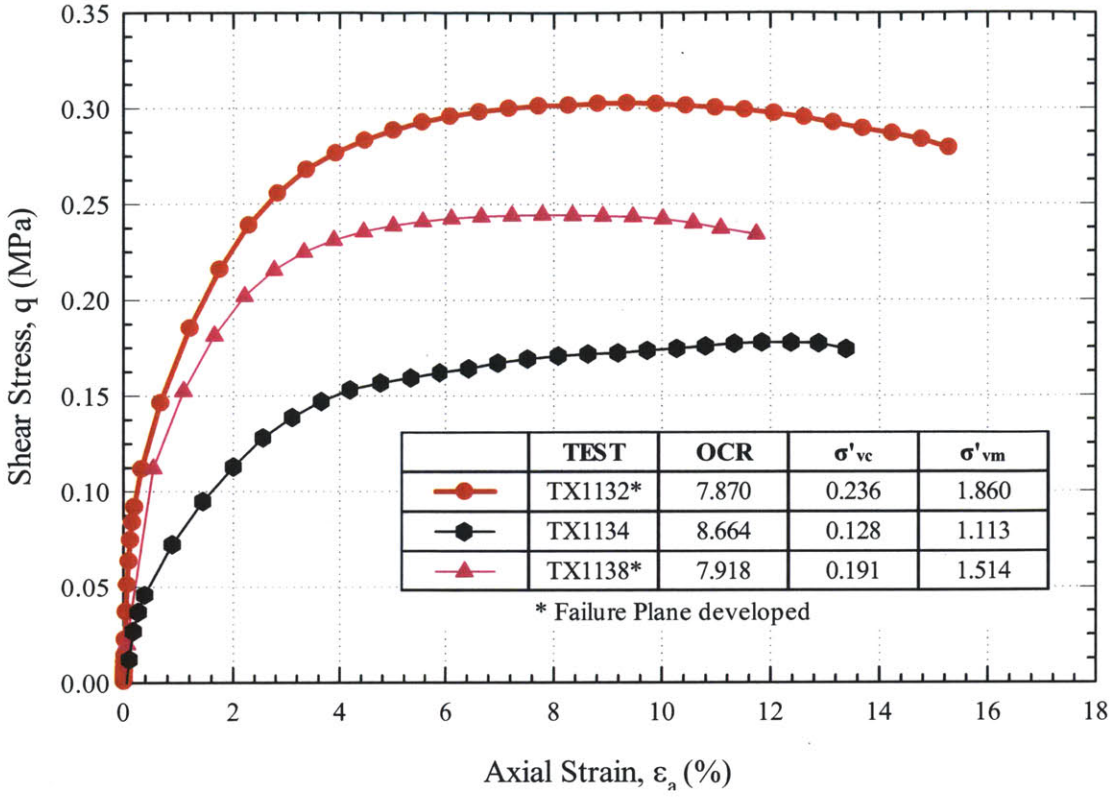

Figure 5-5 Stress-Strain curves for RBBC at OCR = 8

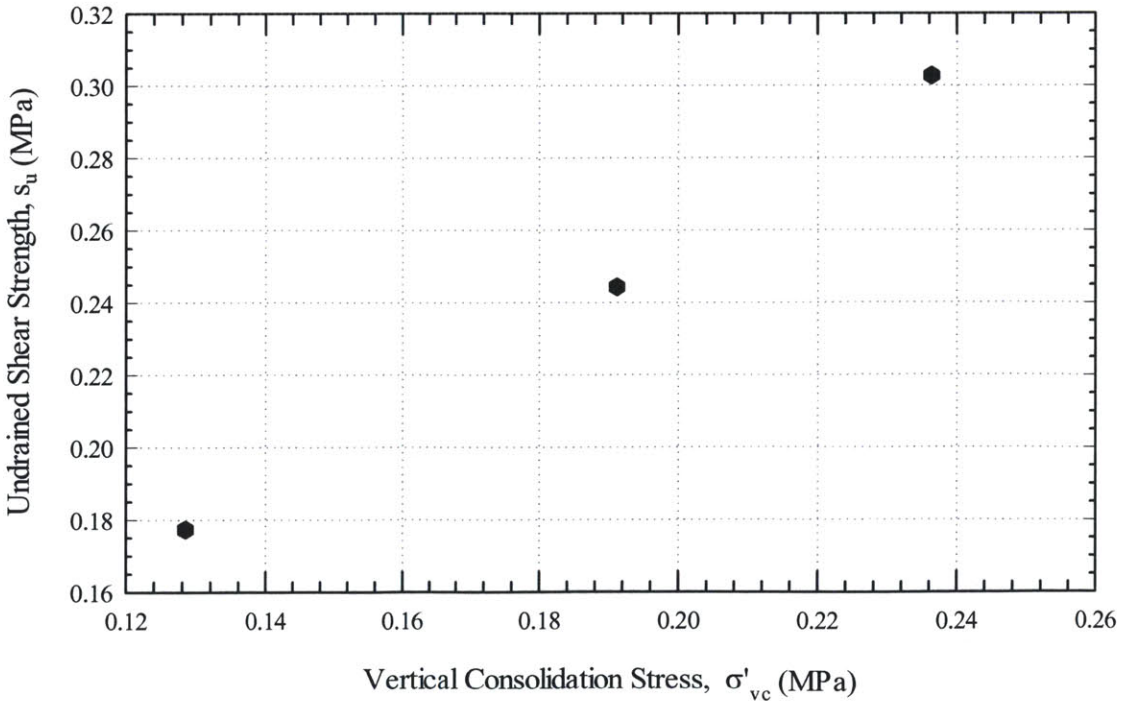

Figure 5-6 Undrained Shear Strength versus stress level for RBBC at OCR = 8

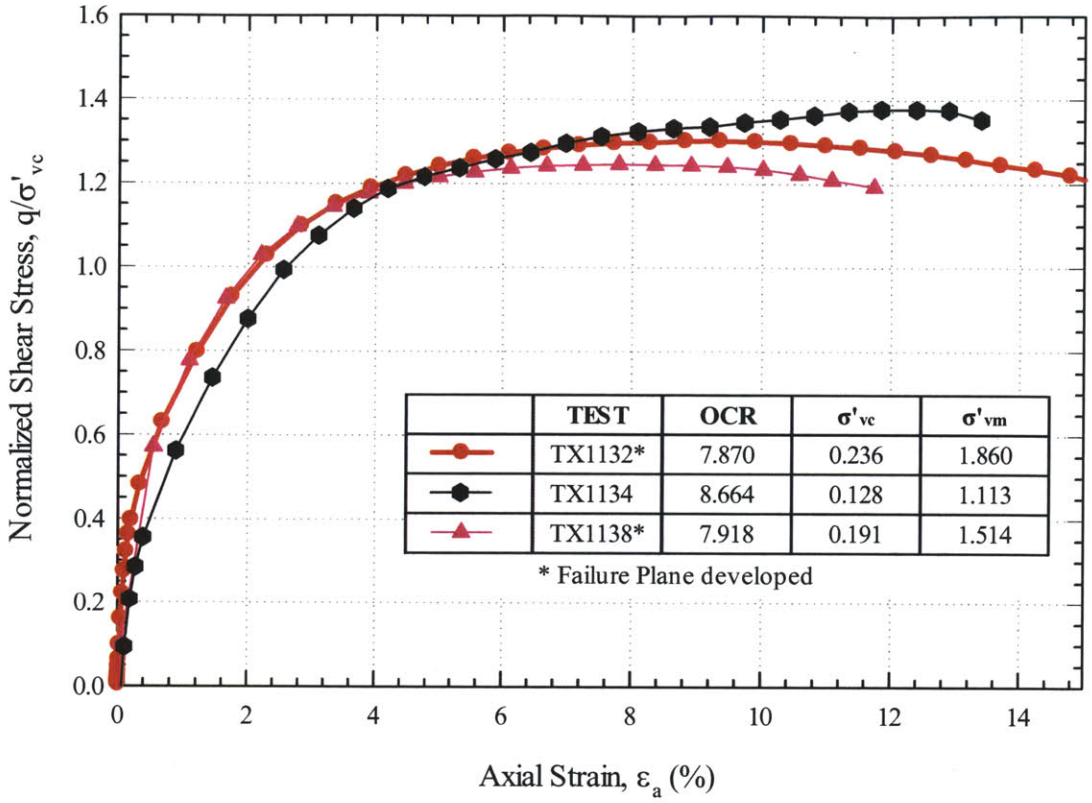

Figure 5-7 Normalized stress-strain curves for RBBC at OCR = 8

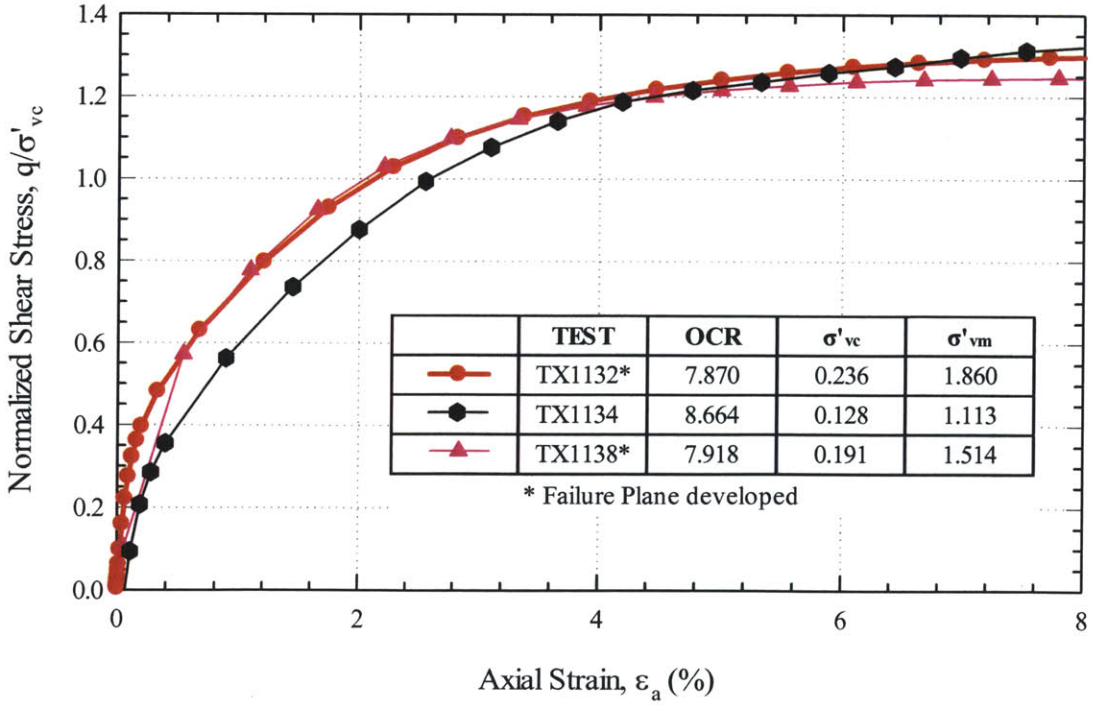

Figure 5-8 Normalized stress-strain (up to 8%) for RBBC at OCR = 8

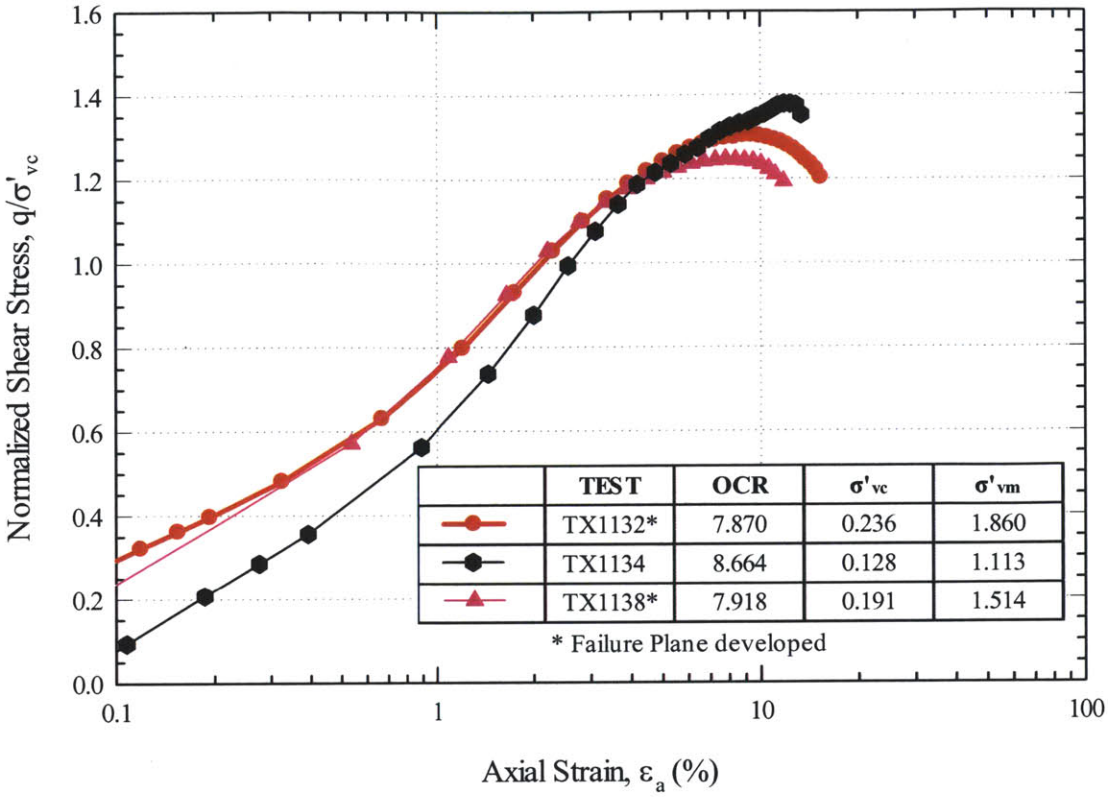

Figure 5-9 Normalized stress-(log)strain for RBBC at OCR = 8

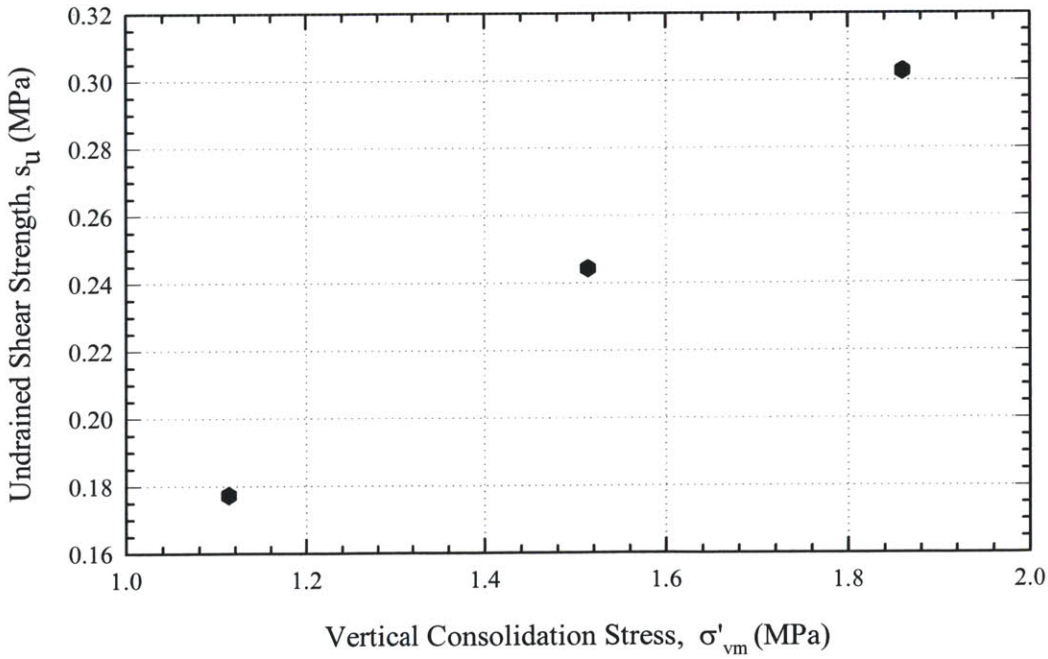

Figure 5-10 Undrained Shear Strength versus maximum stress (σ'_{vm}) level for RBBC at OCR = 8

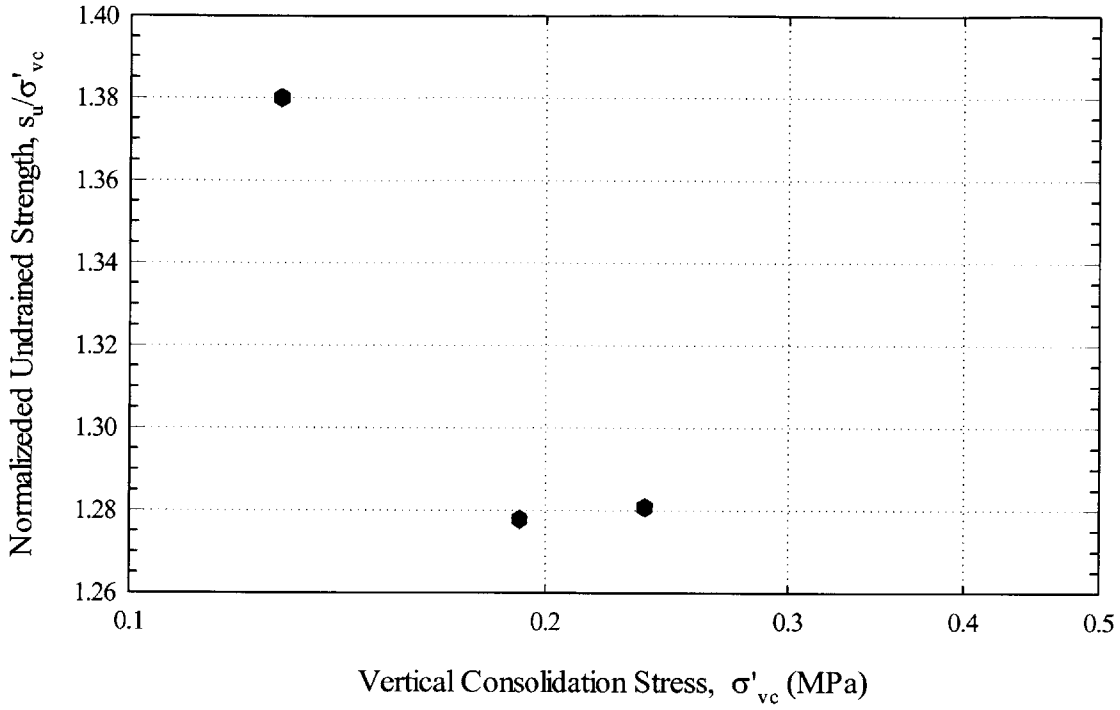

Figure 5-11 Normalized undrained shear strength versus stress level for RBBC at OCR = 8

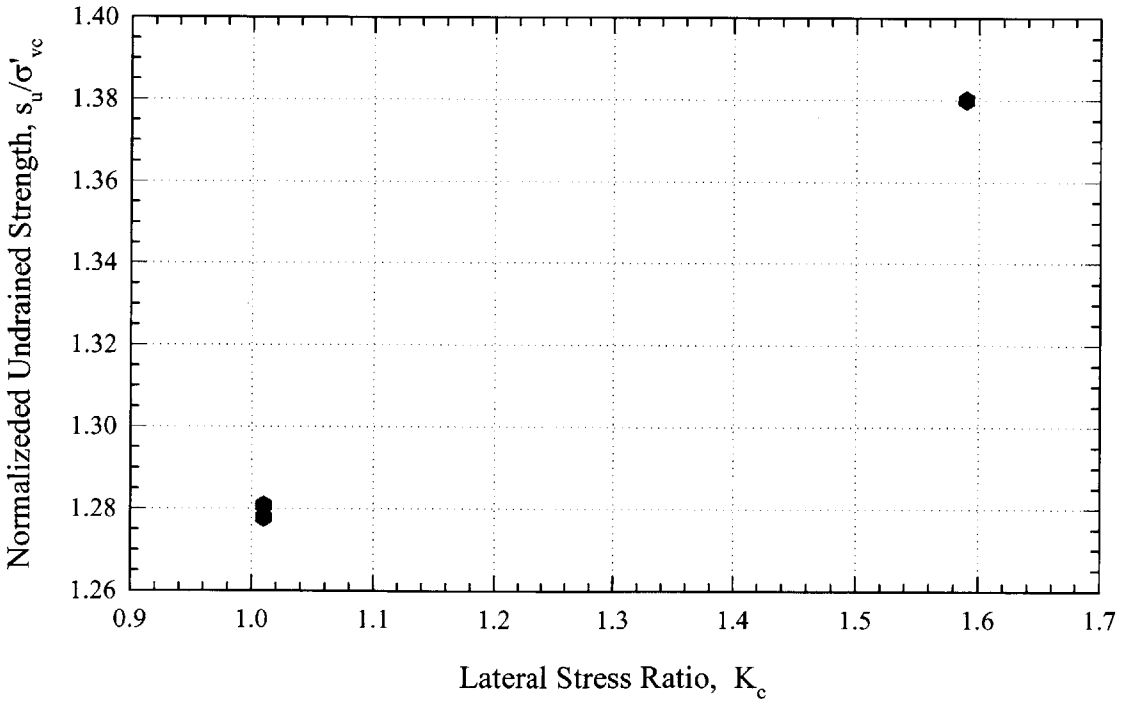

Figure 5-12 Normalized Undrained Shear Strength versus lateral stress ratio for RBBC at OCR = 8

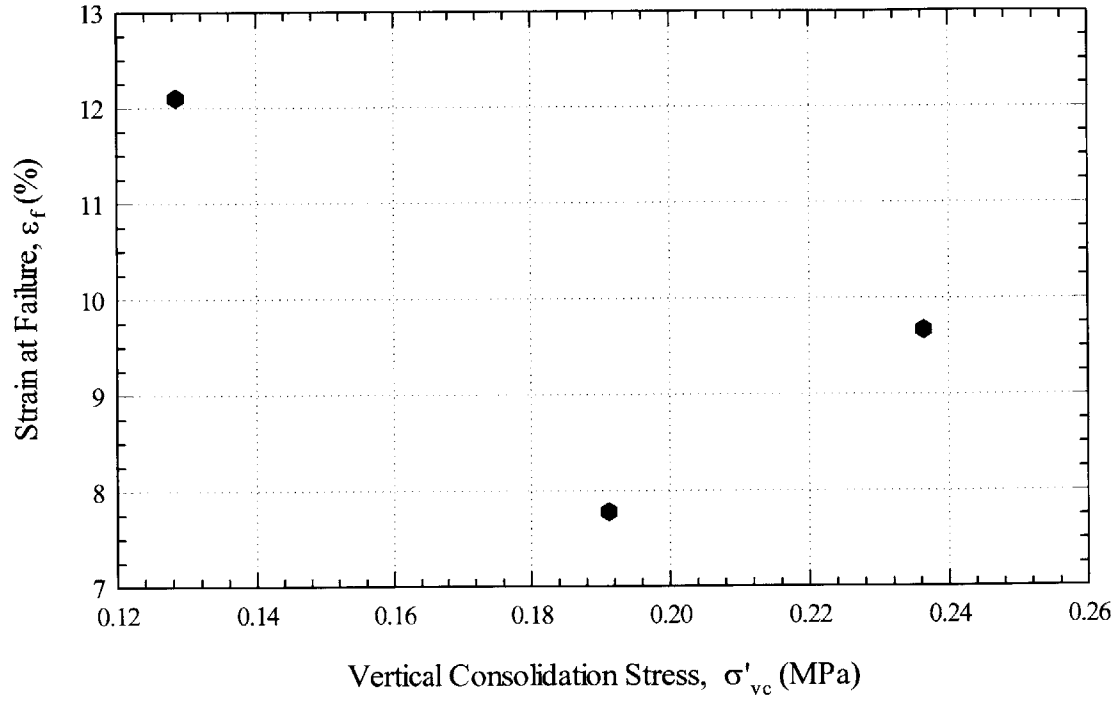

Figure 5-13 Strain at failure versus stress level for RBBC at OCR = 8

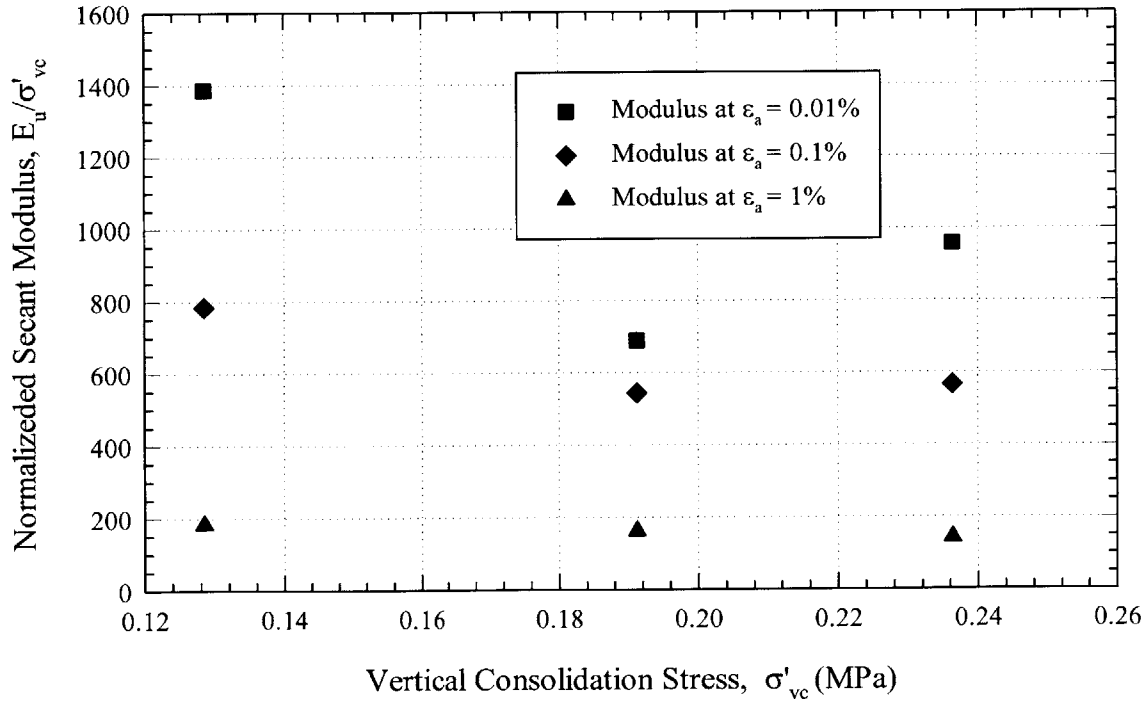

Figure 5-14 Normalized undrained secant modulus versus stress level for RBBC at OCR = 8

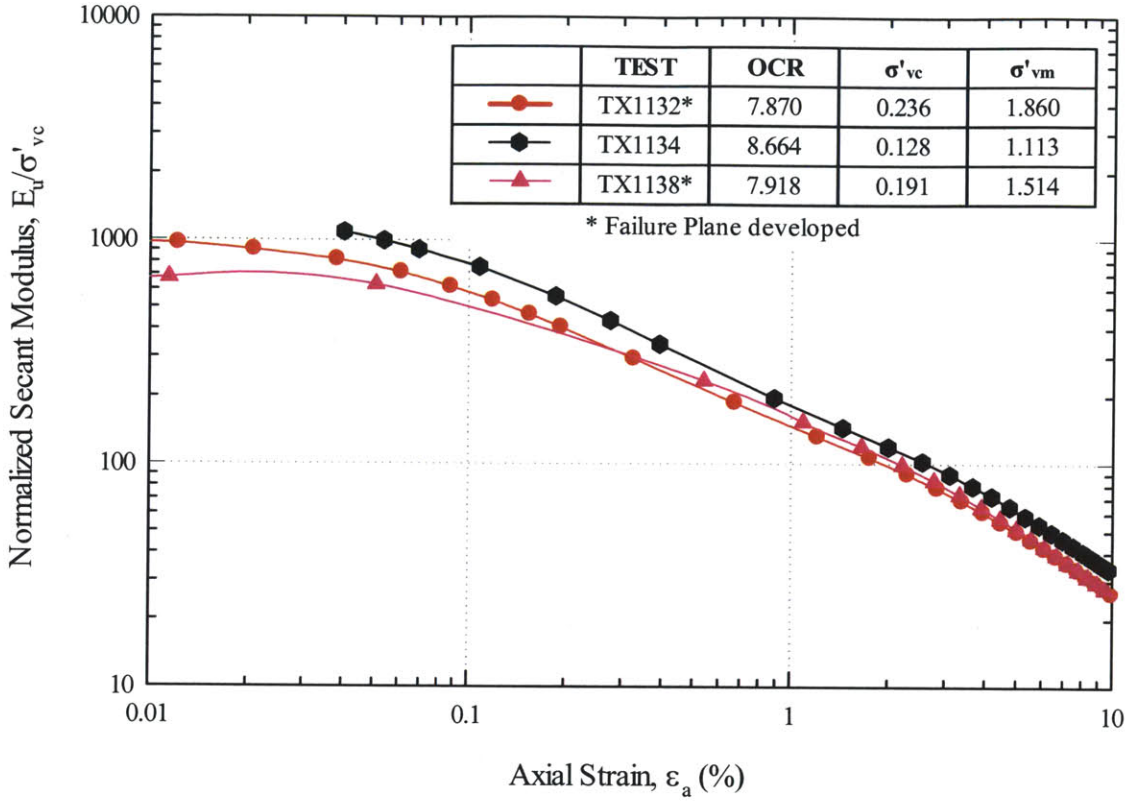

Figure 5-15 Normalized undrained secant modulus versus axial strain for RBBC at OCR = 8

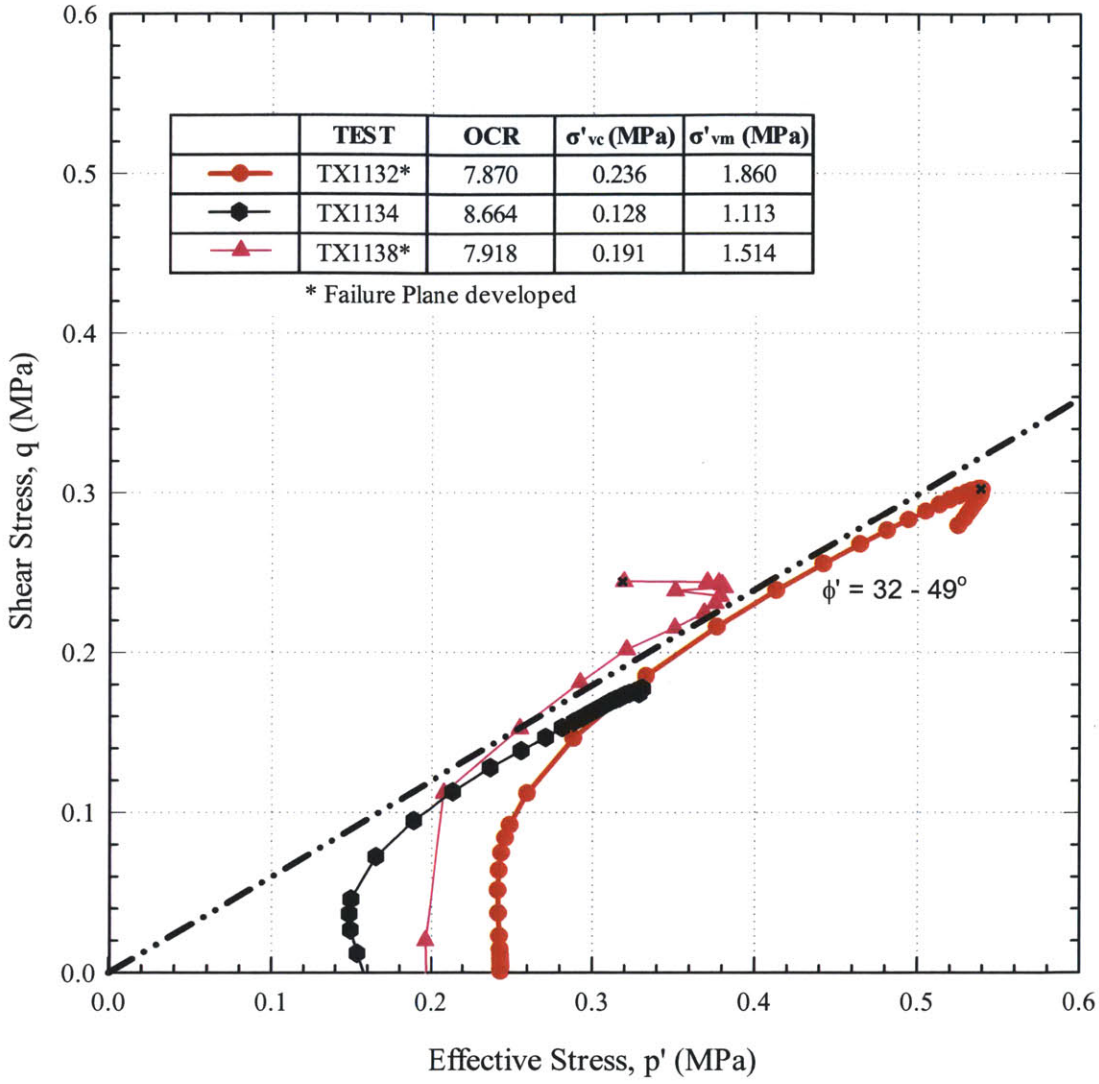

Figure 5-16 Effective Stress Paths for RBBC at OCR = 8

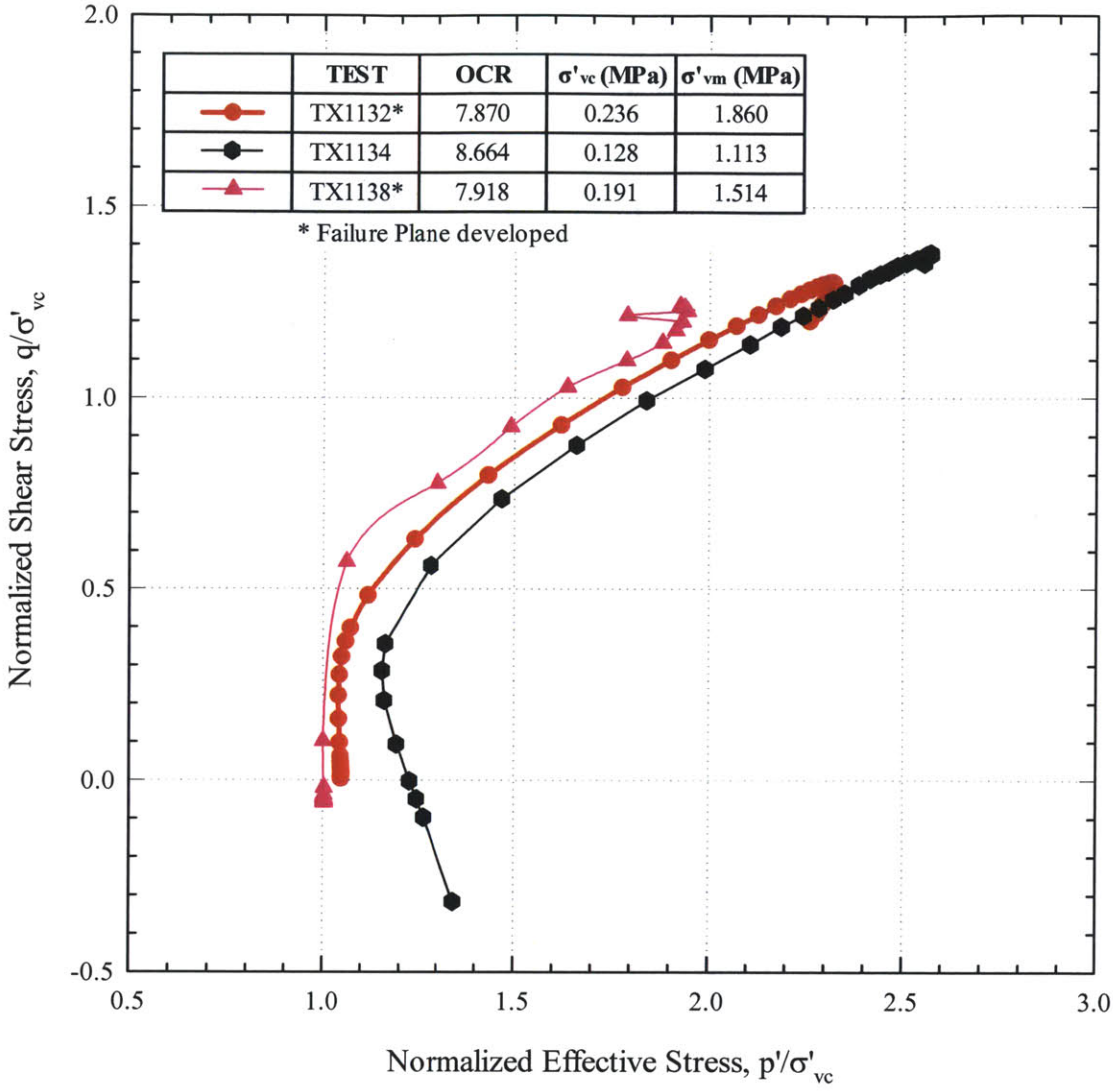

Figure 5-17 Normalized Effective Stress Paths (close up view) for RBBC at OCR = 8

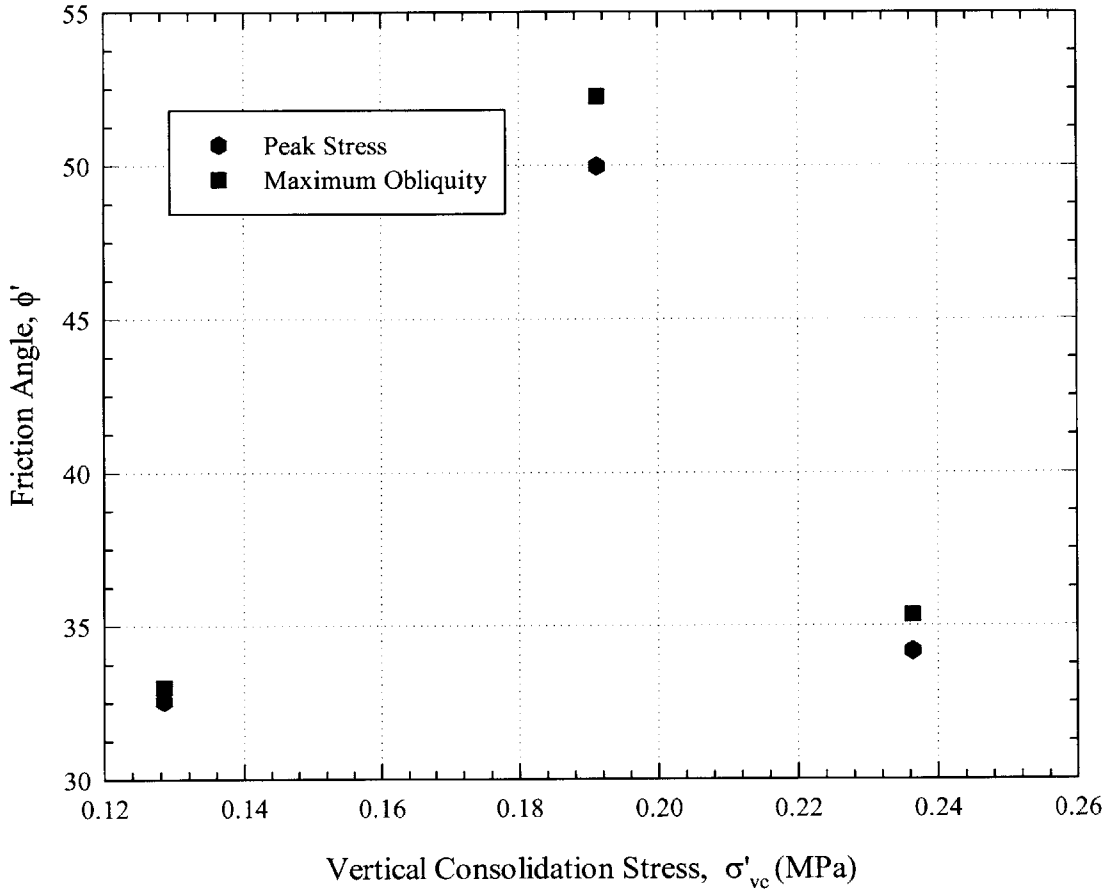

Figure 5-18 Friction angle at peak and maximum obliquity versus stress level for RBBC at OCR = 8

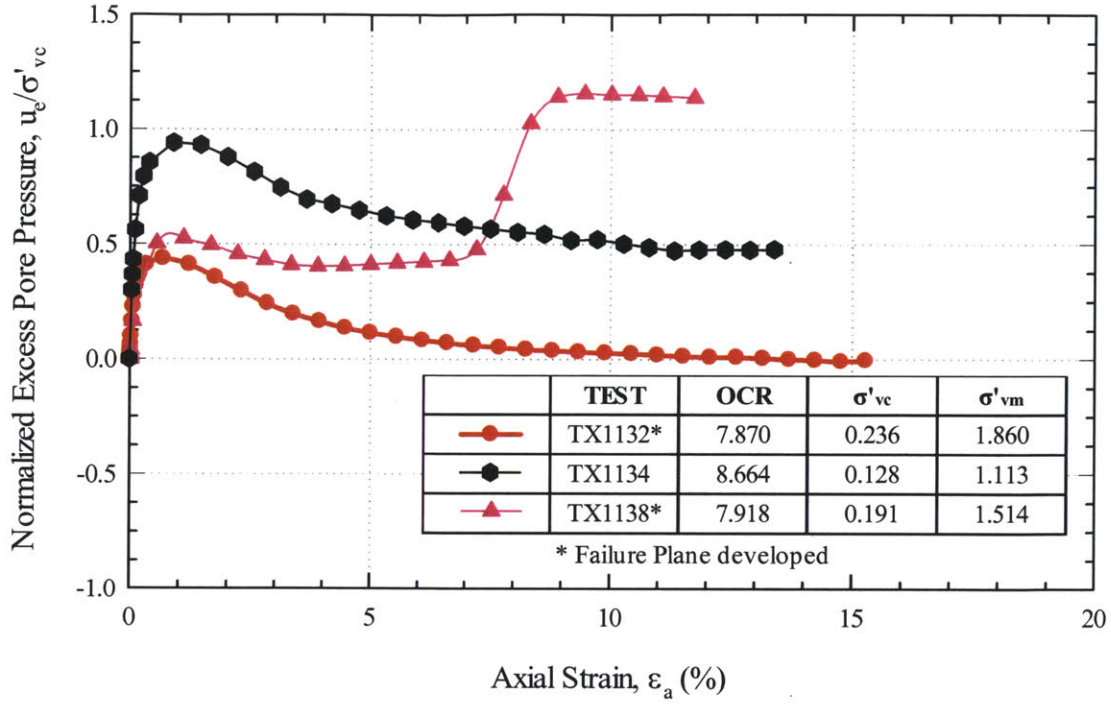

Figure 5-19 Normalized excess pore pressure versus strain for RBBC at OCR = 8

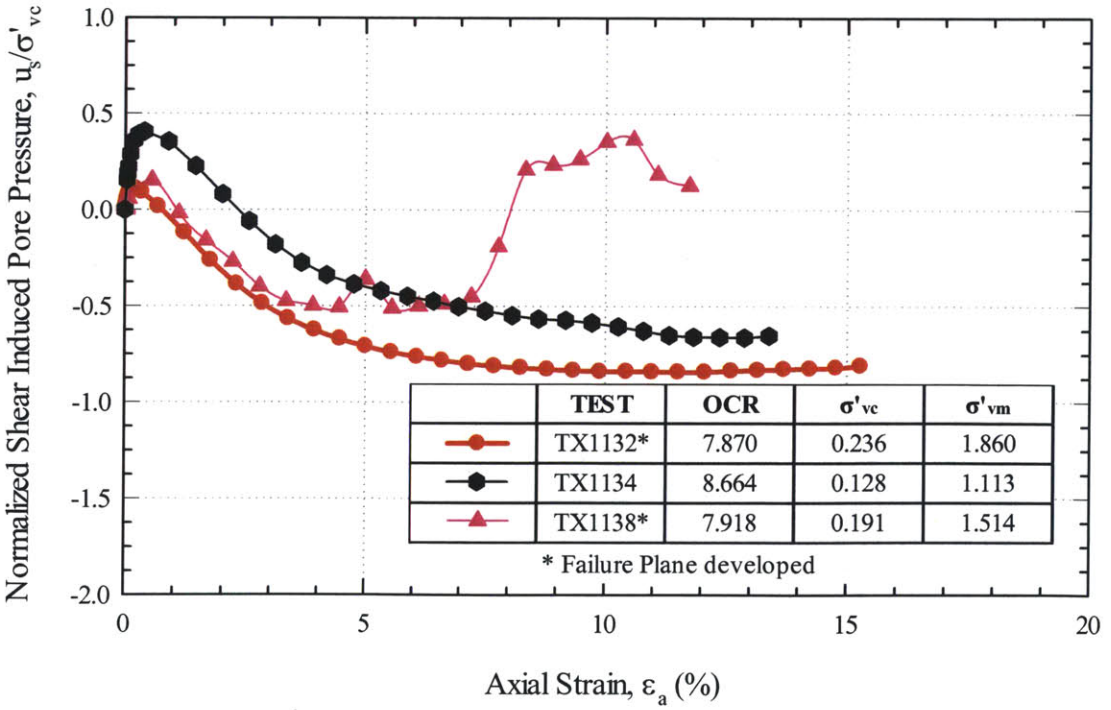

Figure 5-20 Normalized shear induced pore pressure versus strain for RBBC at OCR = 8

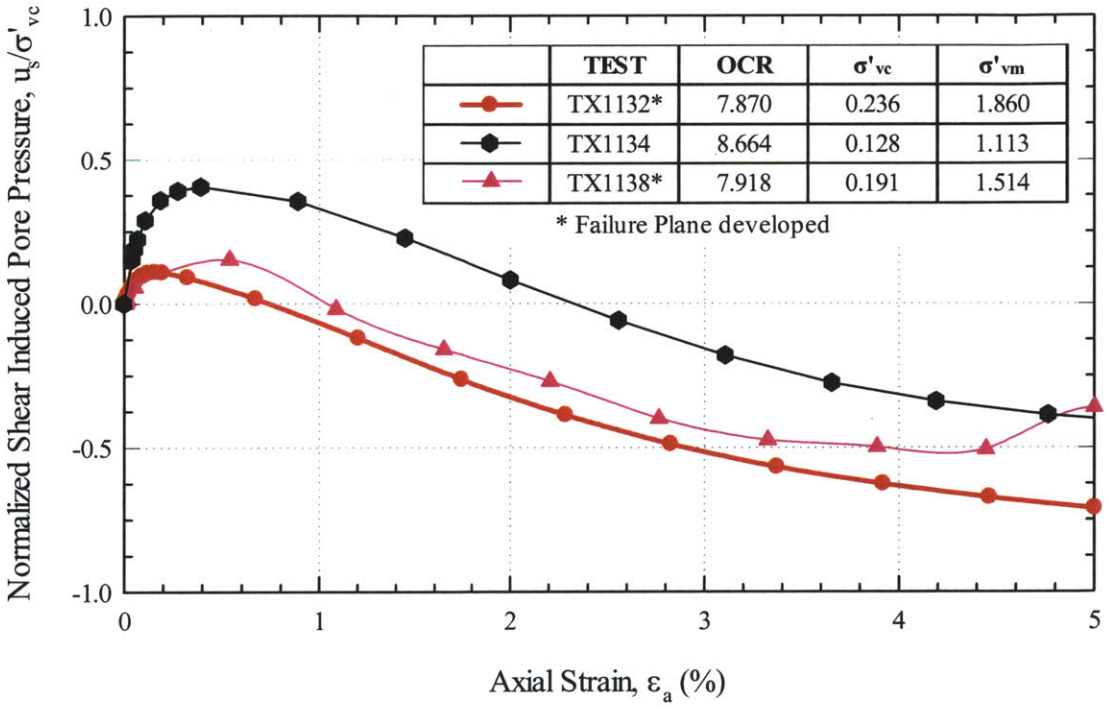

Figure 5-21 Normalized shear pore pressure versus strain (up to 5%) for RBBC at OCR = 8

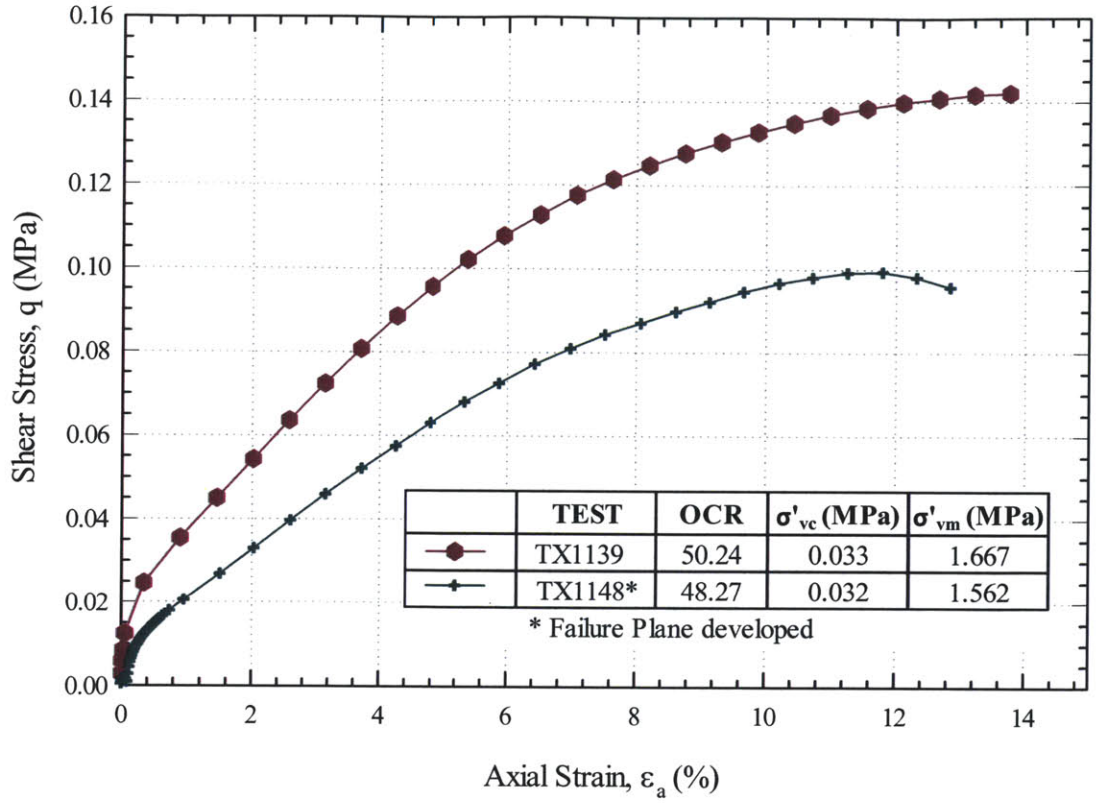

Figure 5-22 Stress-Strain curves for RBBC at OCR = 50

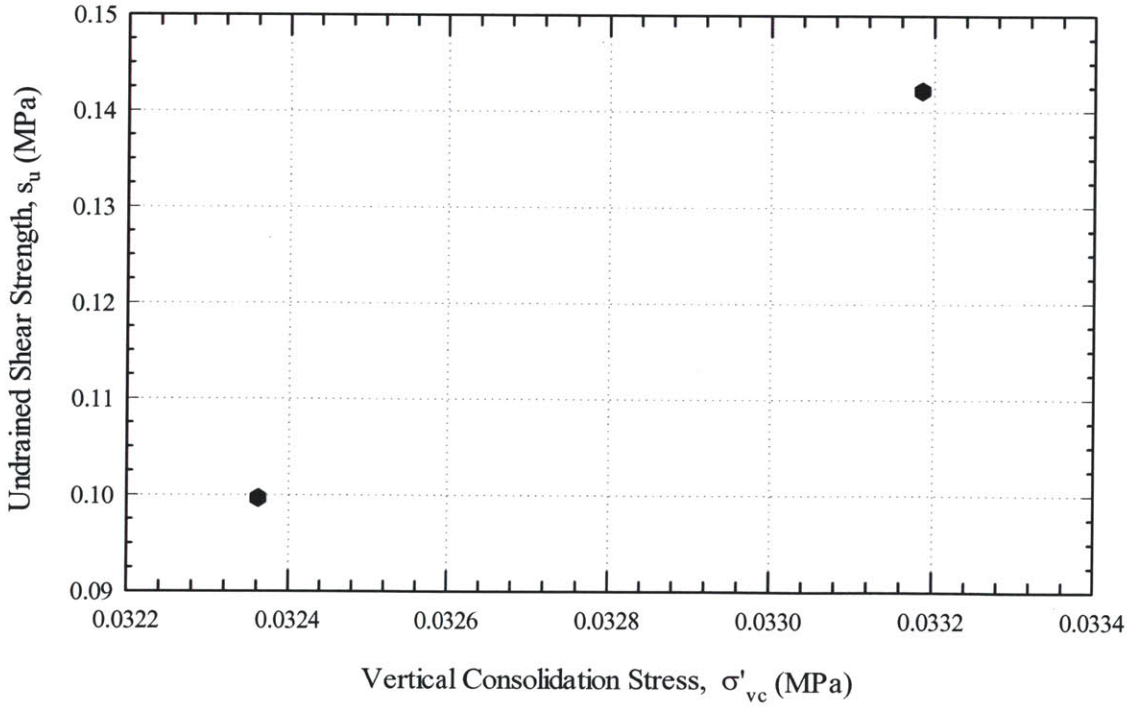

Figure 5-23 Undrained Shear Strength versus stress level (σ'_{vc}) for RBBC at OCR = 50

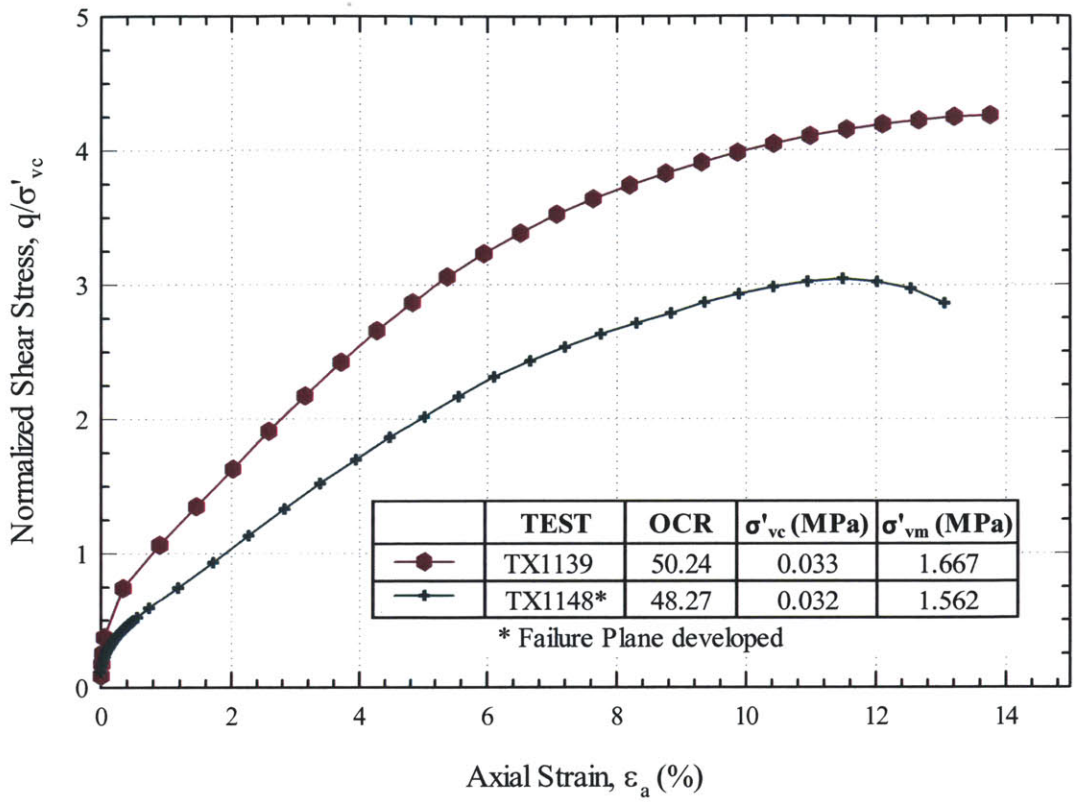

Figure 5-24 Normalized stress-strain curves for RBBC at OCR = 50

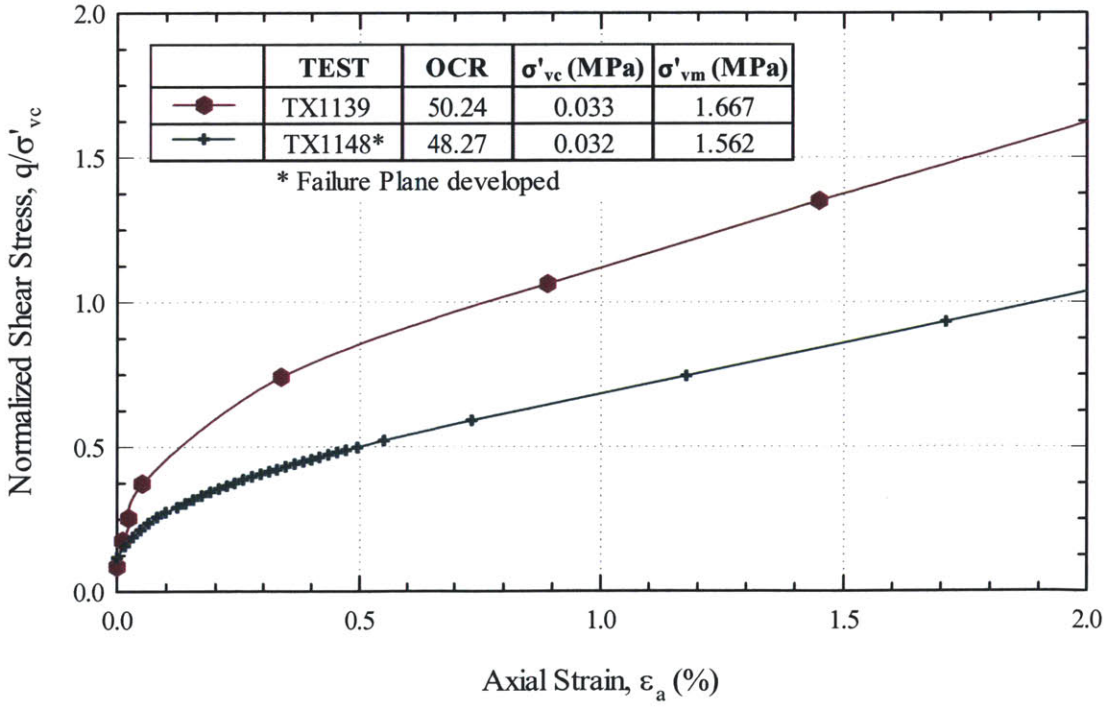

Figure 5-25 Normalized stress-strain (up to 2%) for RBBC at OCR = 50

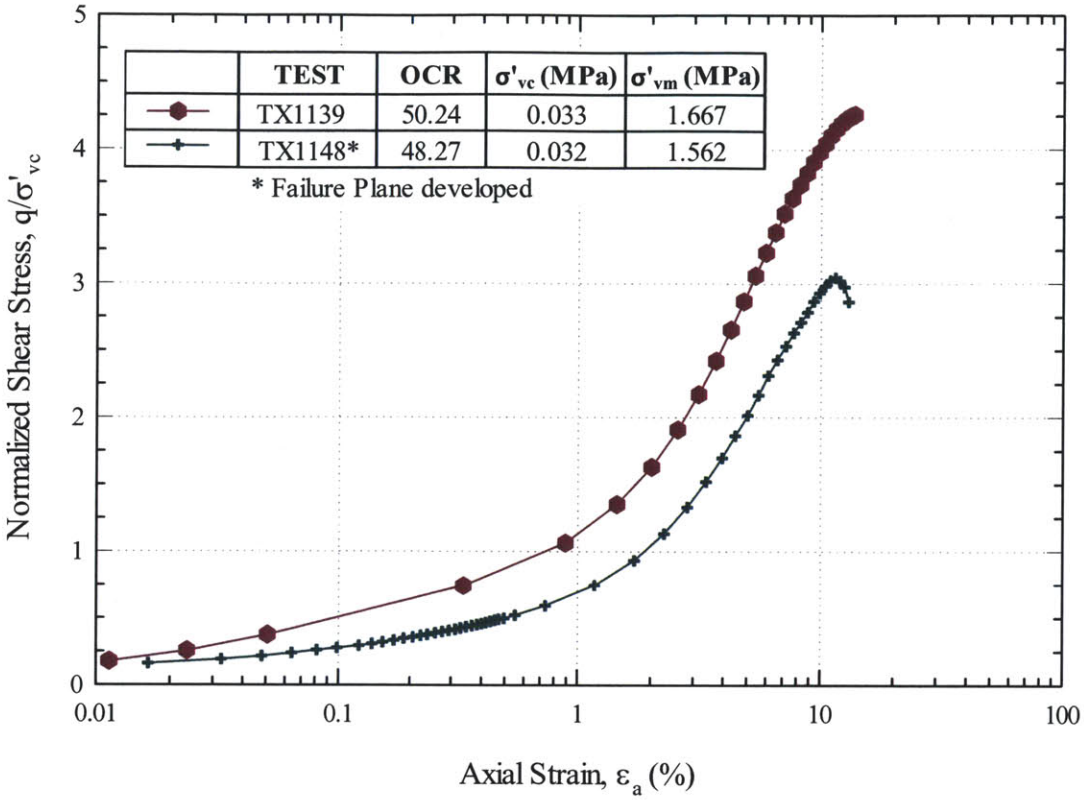

Figure 5-26 Normalized stress-(log)strain for RBBC at OCR = 50

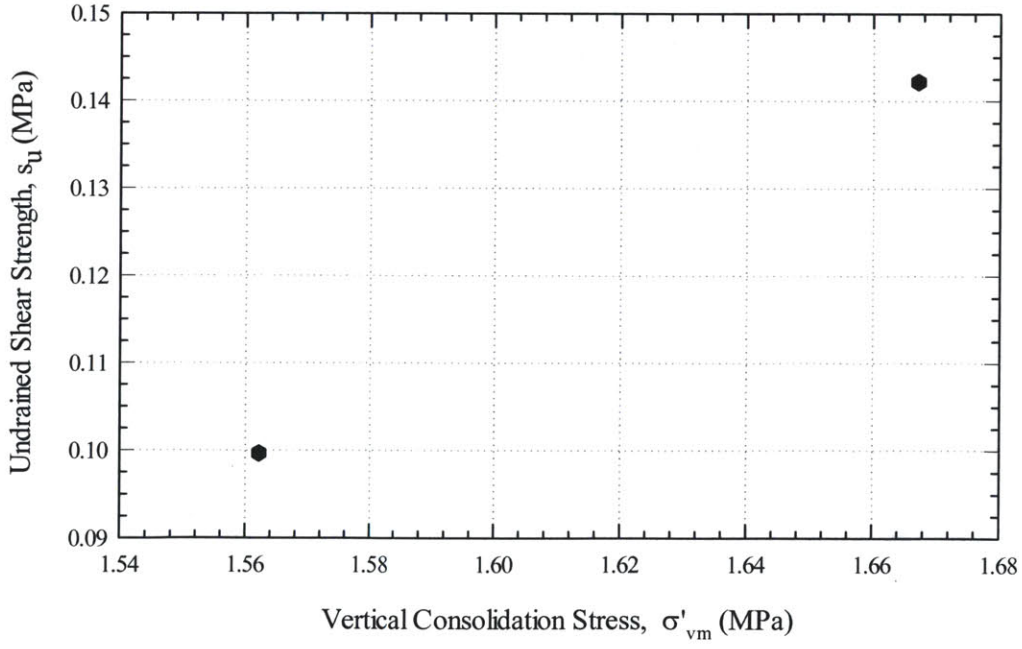

Figure 5-27 Undrained Shear Strength versus maximum stress (σ'_{vm}) level for RBBC at OCR = 50

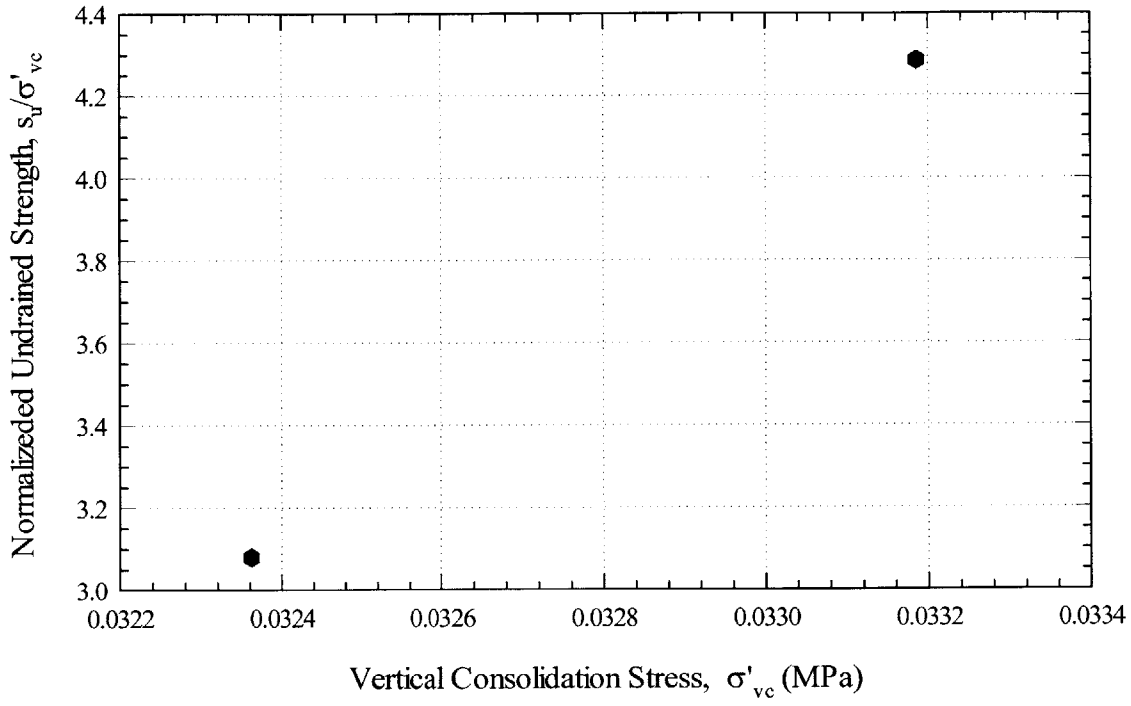

Figure 5-28 Normalized Undrained Shear Strength versus preshear stress (σ'_{vc}) level for RBBC at OCR = 50

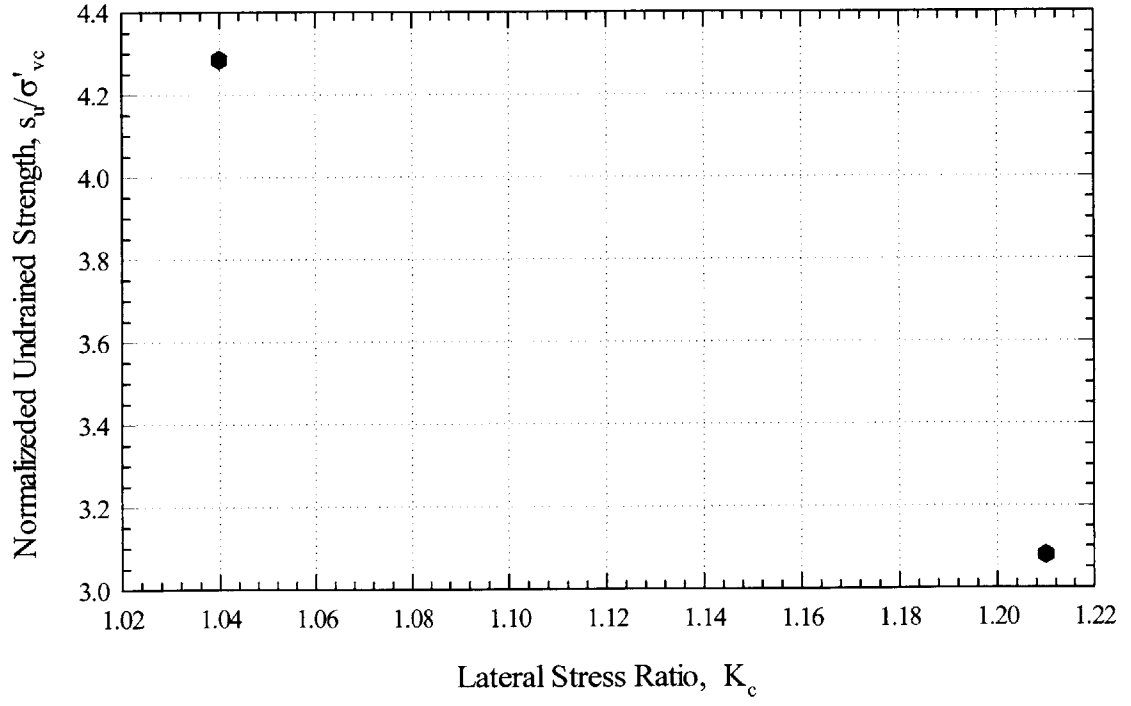

Figure 5-29 Normalized Undrained Shear Strength versus lateral stress ratio for RBBC at OCR = 50

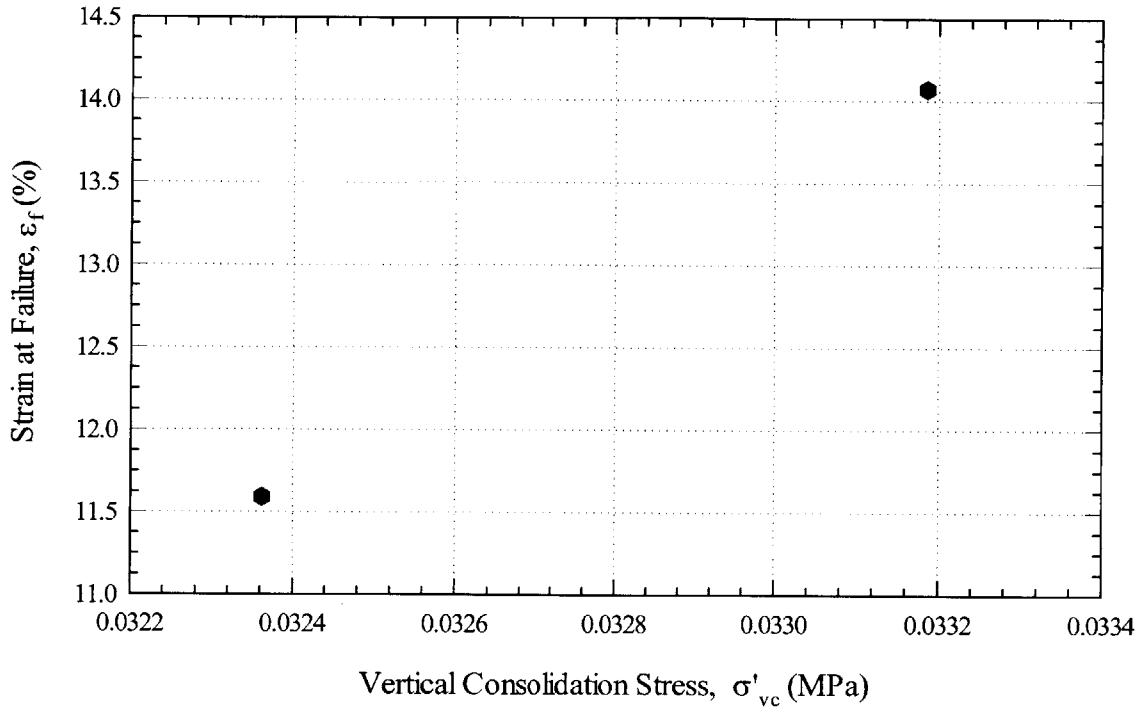

Figure 5-30 Strain at failure versus stress level for RBBC at OCR = 50

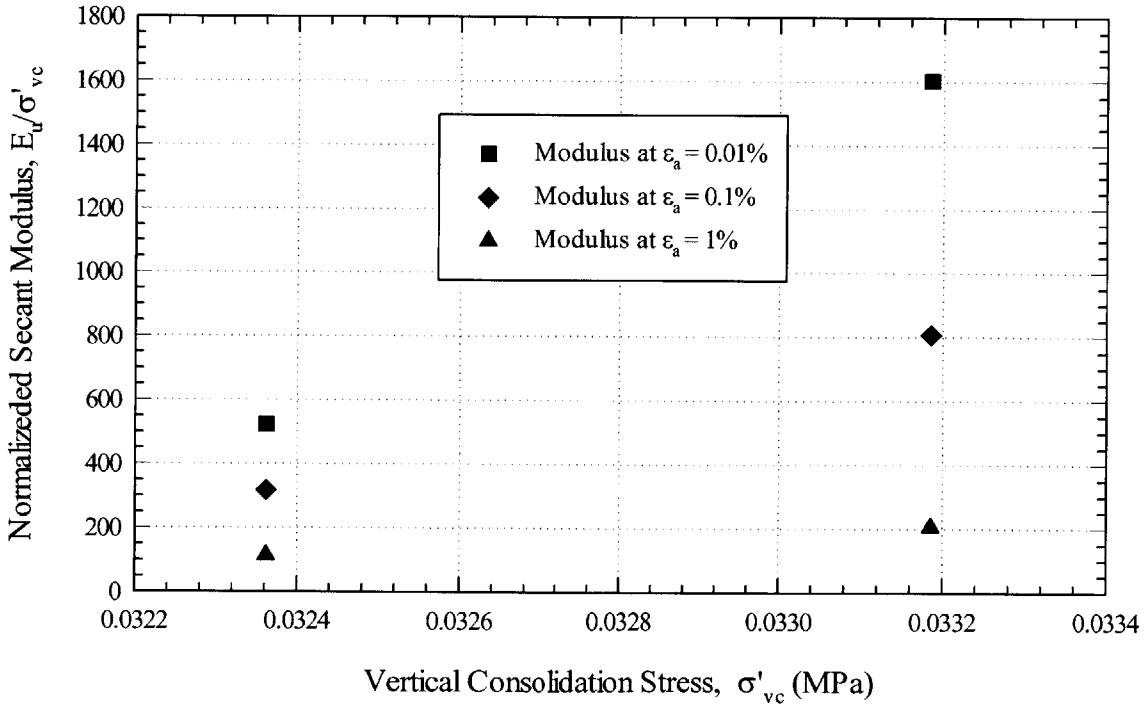

Figure 5-31 Normalized undrained secant modulus versus stress level for RBBC at OCR = 50

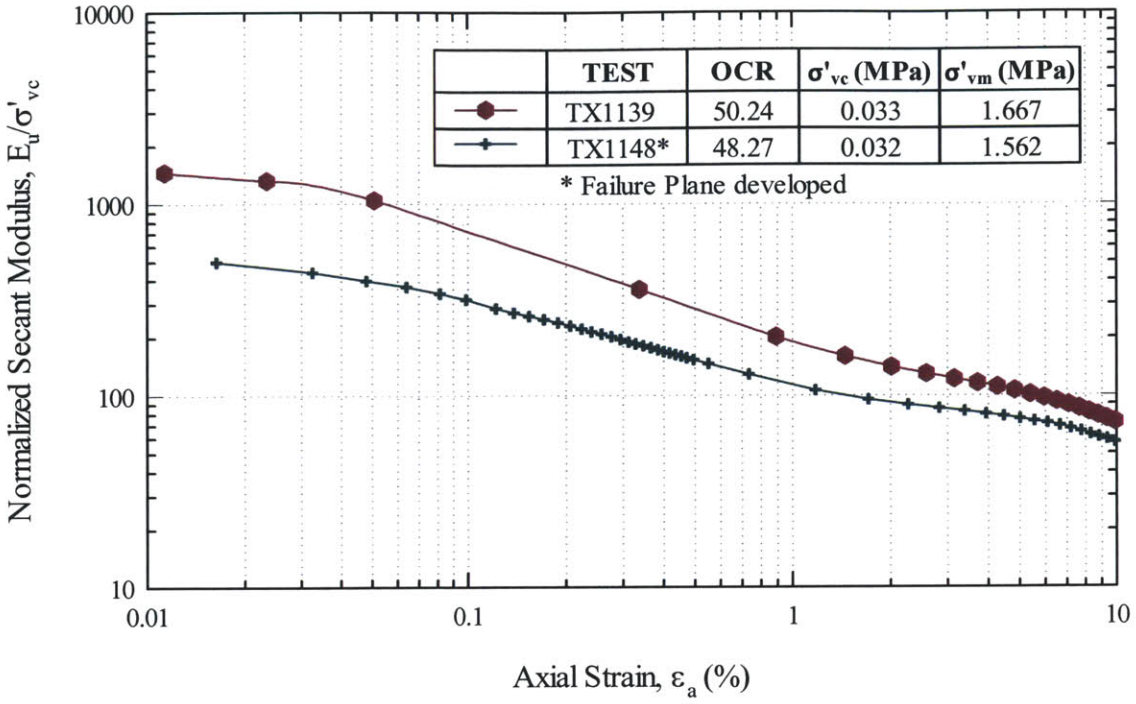

Figure 5-32 Normalized undrained secant modulus versus axial strain for RBBC at OCR = 50

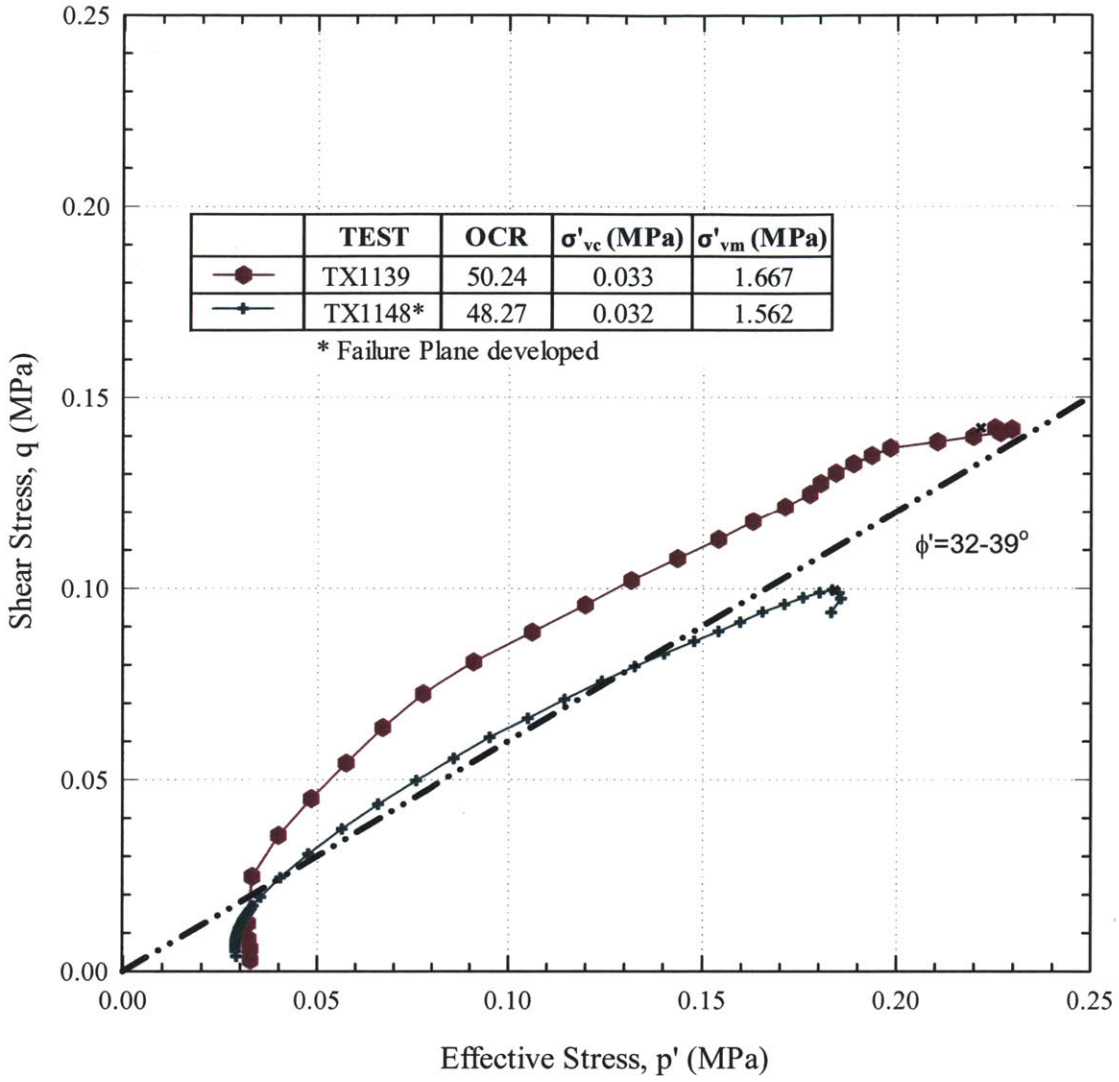

Figure 5-33 Effective Stress Paths for RBBC a OCR = 50

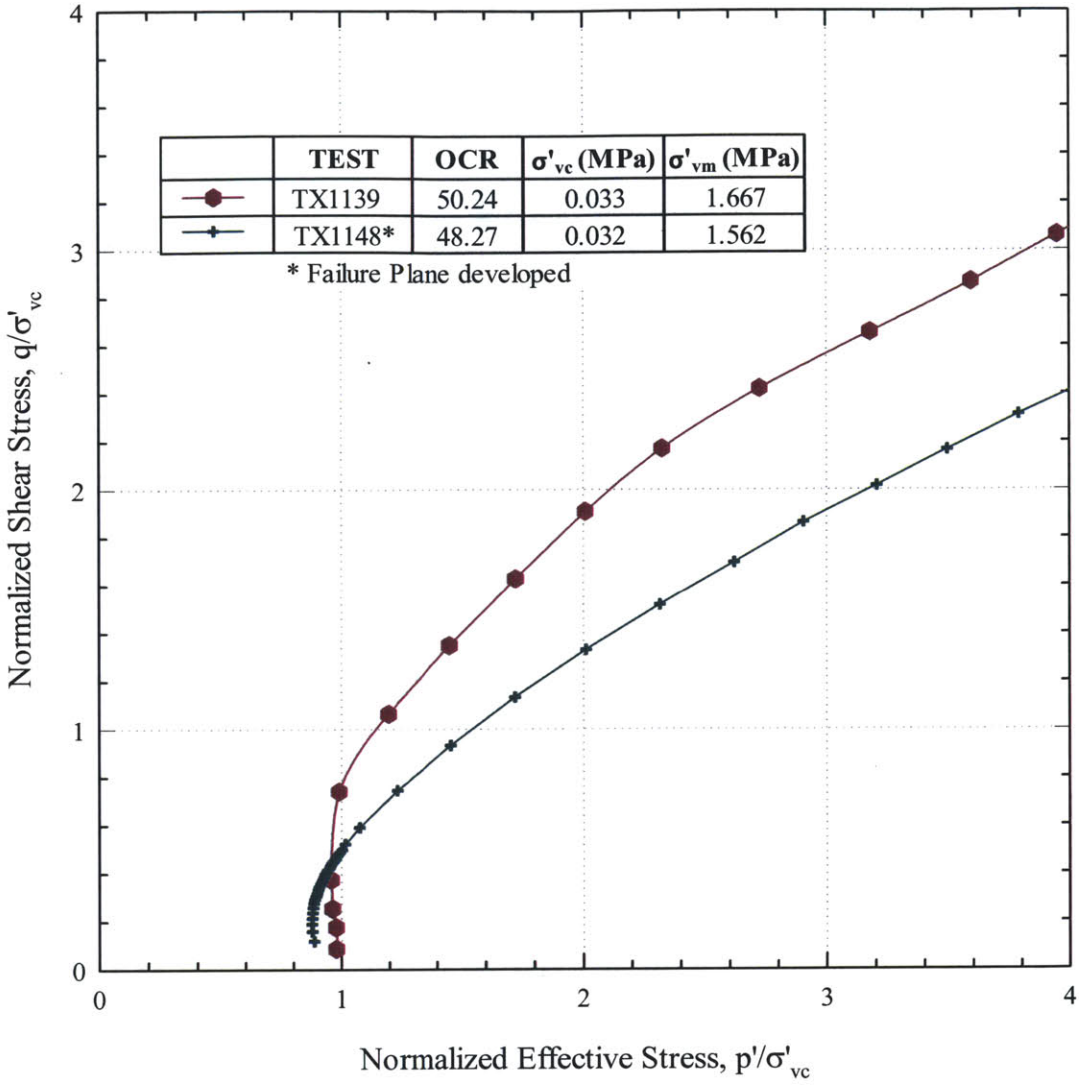

Figure 5-34 Normalized Effective Stress Paths (close up view) for RBBC at OCR = 50

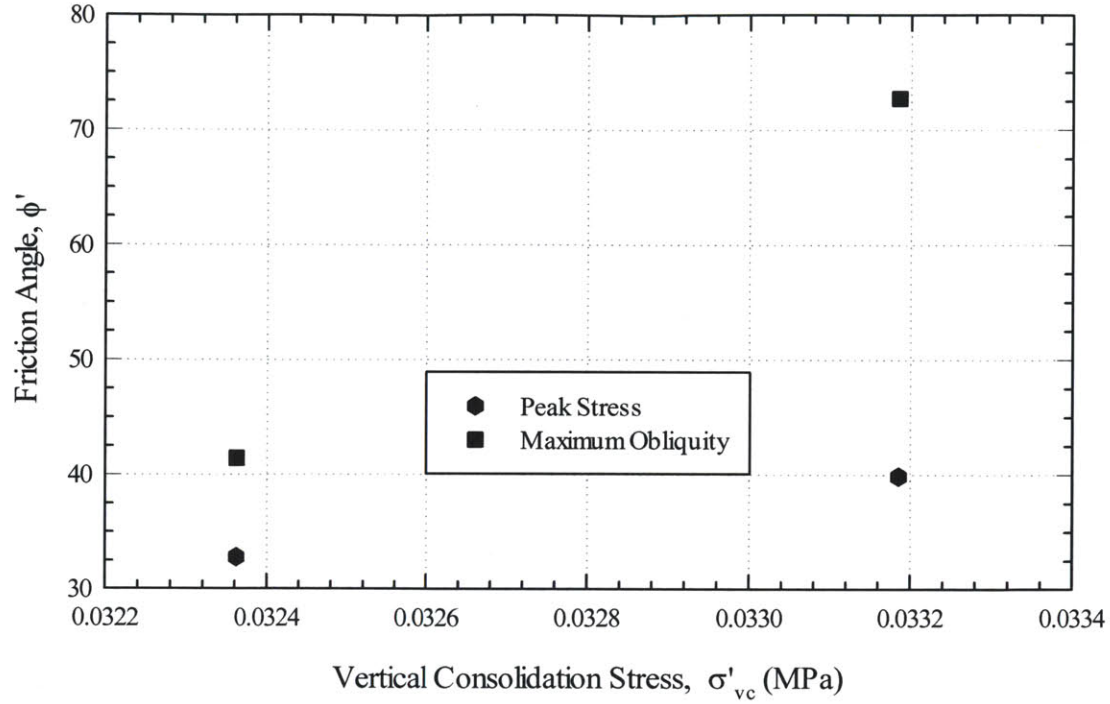

Figure 5-35 Friction angle at peak and maximum obliquity versus stress level for RBBC at OCR = 50

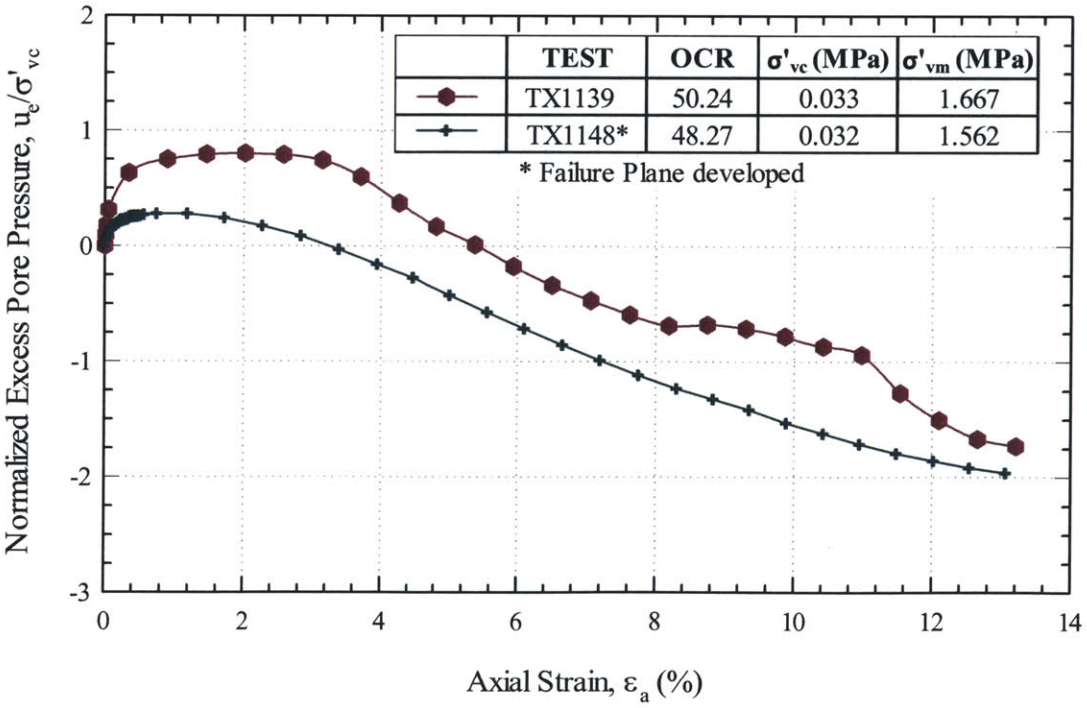

Figure 5-36 Normalized excess pore pressure versus strain for RBBC at OCR = 50

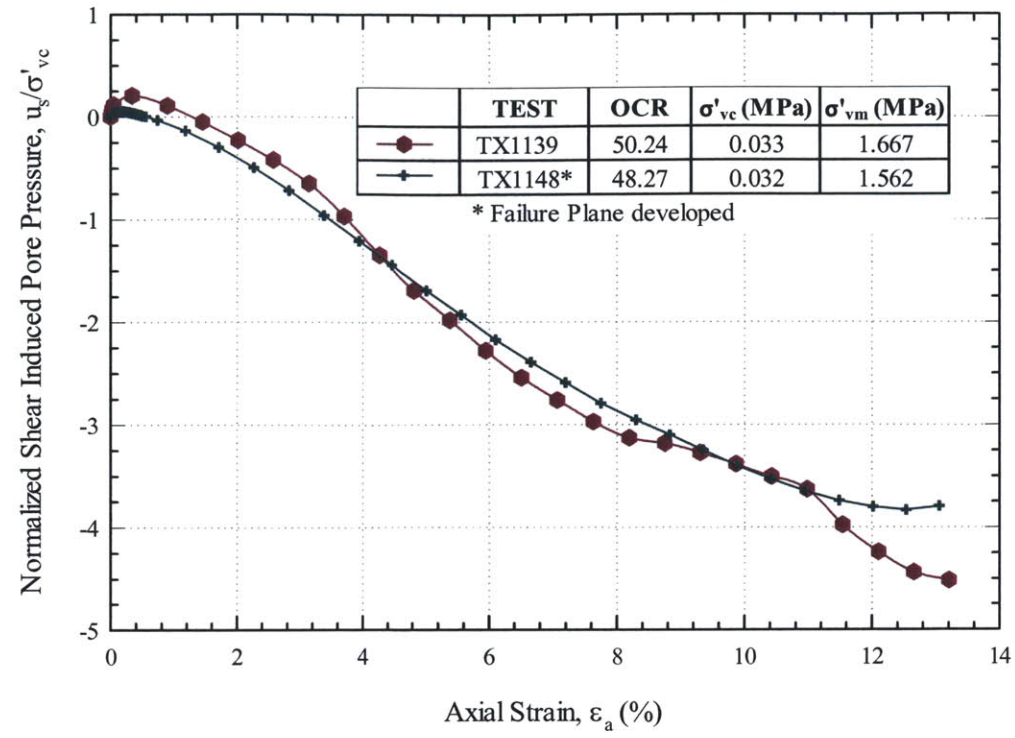

Figure 5-37 Normalized shear pore pressure versus strain for RBBC at OCR = 50

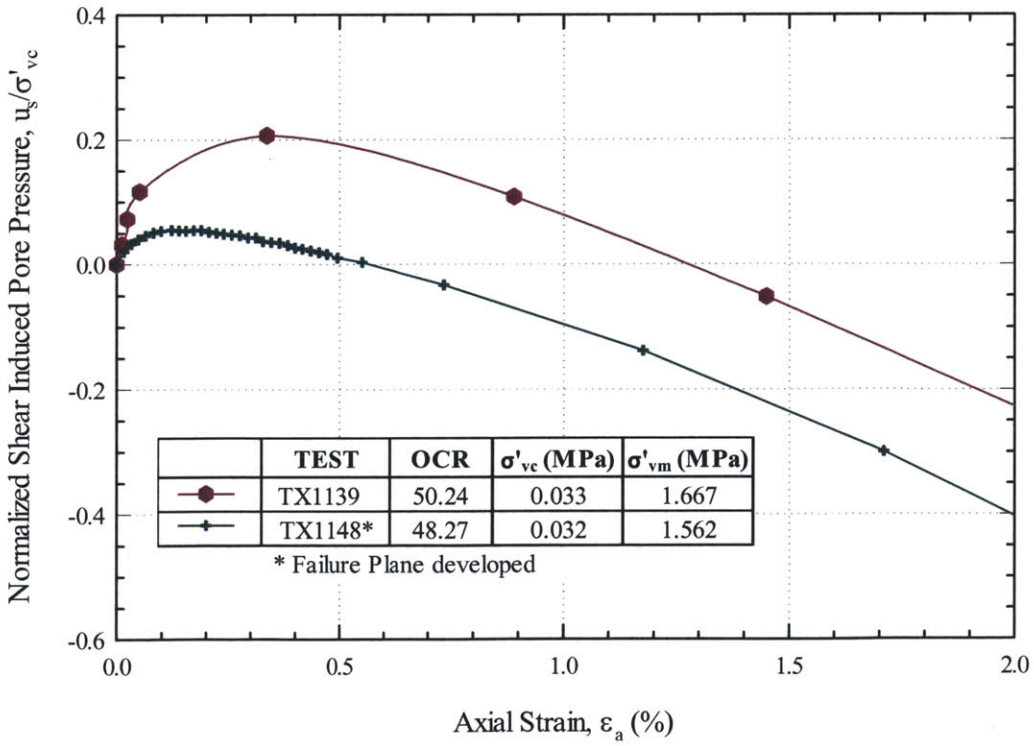

Figure 5-38 Normalized shear pore pressure versus strain (up to 5%) for RBBC at OCR = 50

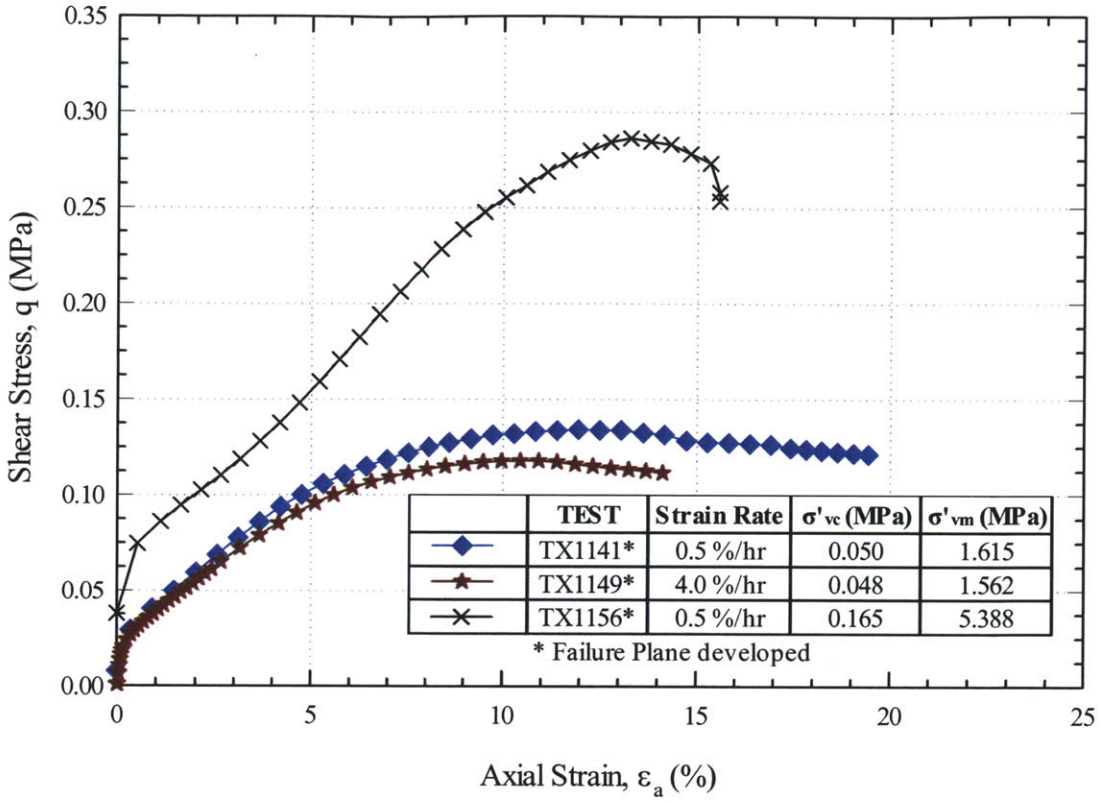

Figure 5-39 Stress-Strain curves for RBBC at OCR = 32 (Strain Rates 0.5% and 4.0%)

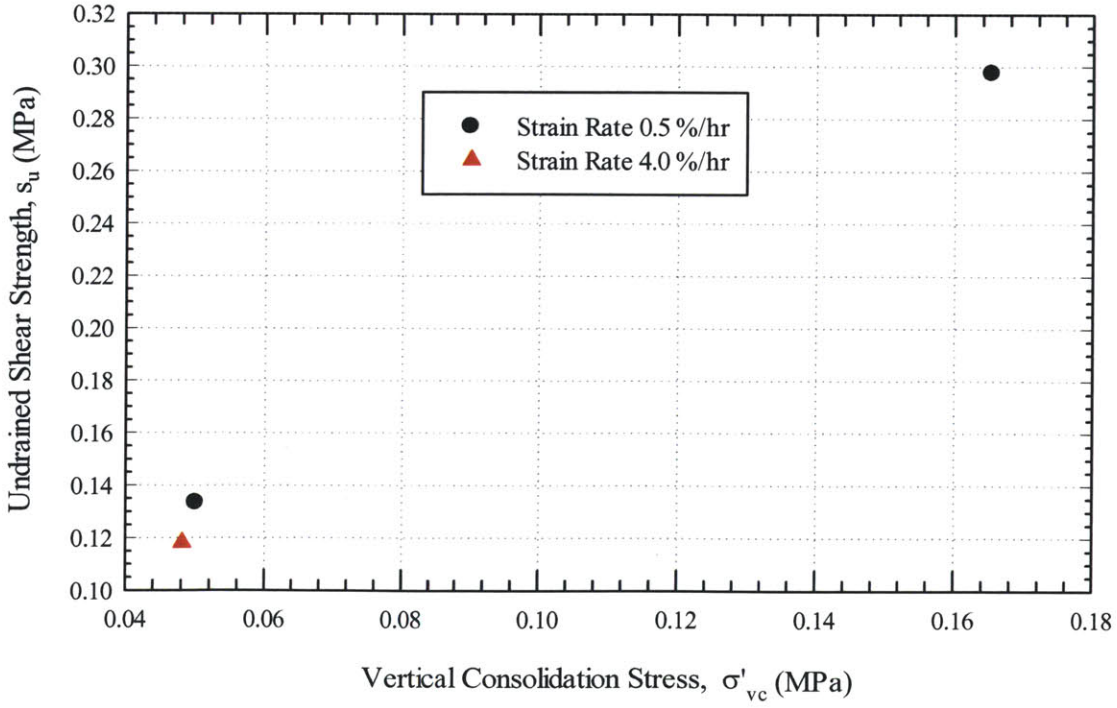

Figure 5-40 Undrained Shear Strength versus stress levels for RBBC at OCR = 32

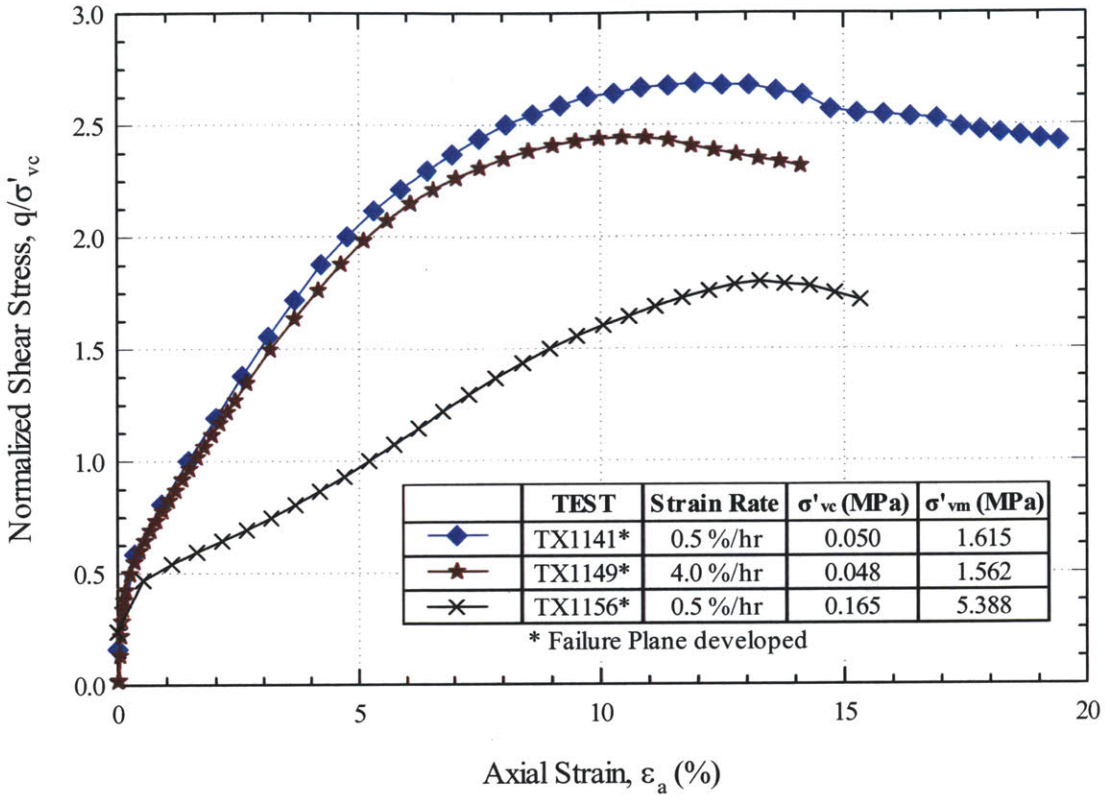

Figure 5-41 Normalized stress-strain curves for RBBC at OCR = 32

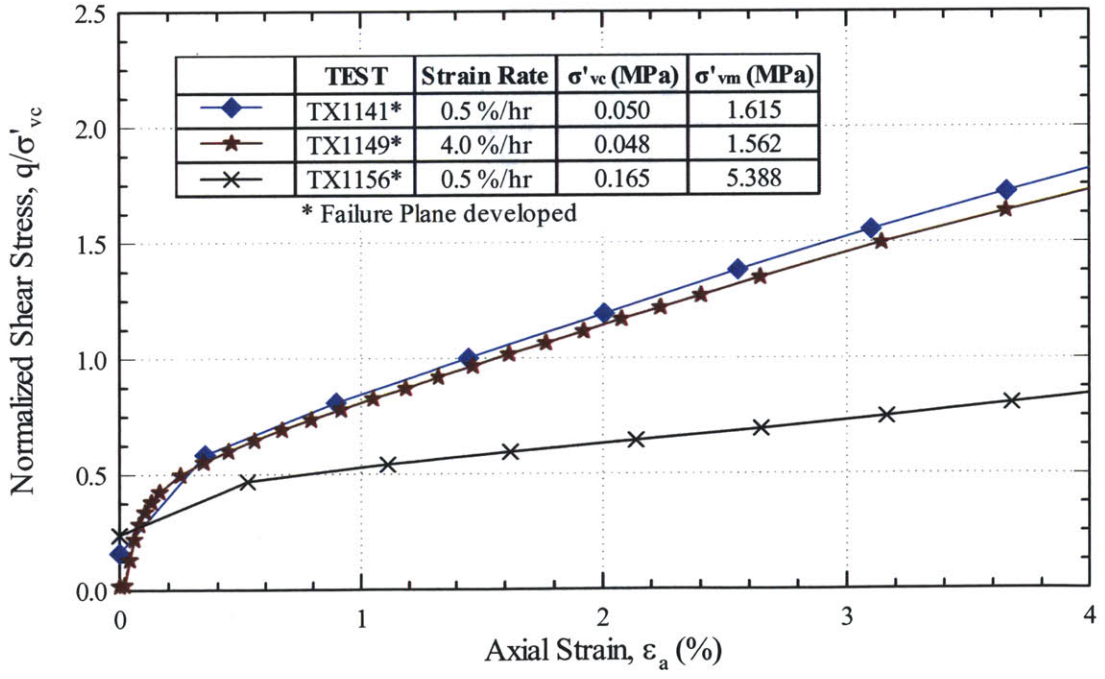

Figure 5-42 Normalized stress-strain (up to 4%) for RBBC at OCR = 32 (Strain Rates 0.5% and 4.0%)

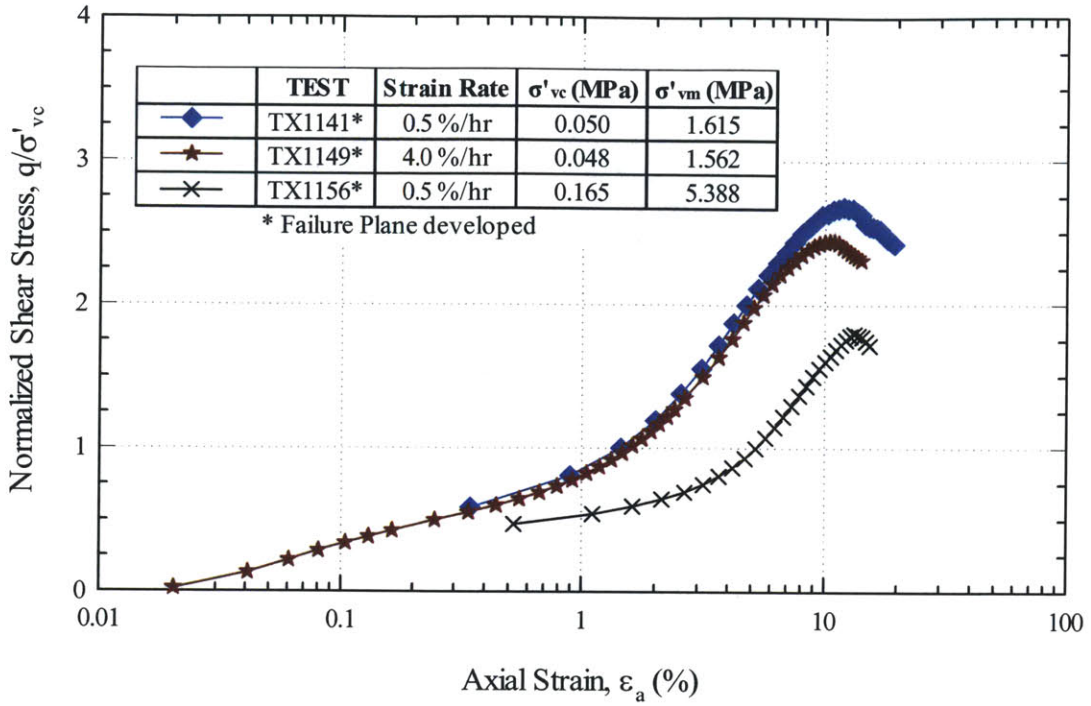

Figure 5-43 Normalized stress- (log) strain for RBBC at OCR = 32 (Strain Rates 0.5% and 4.0%)

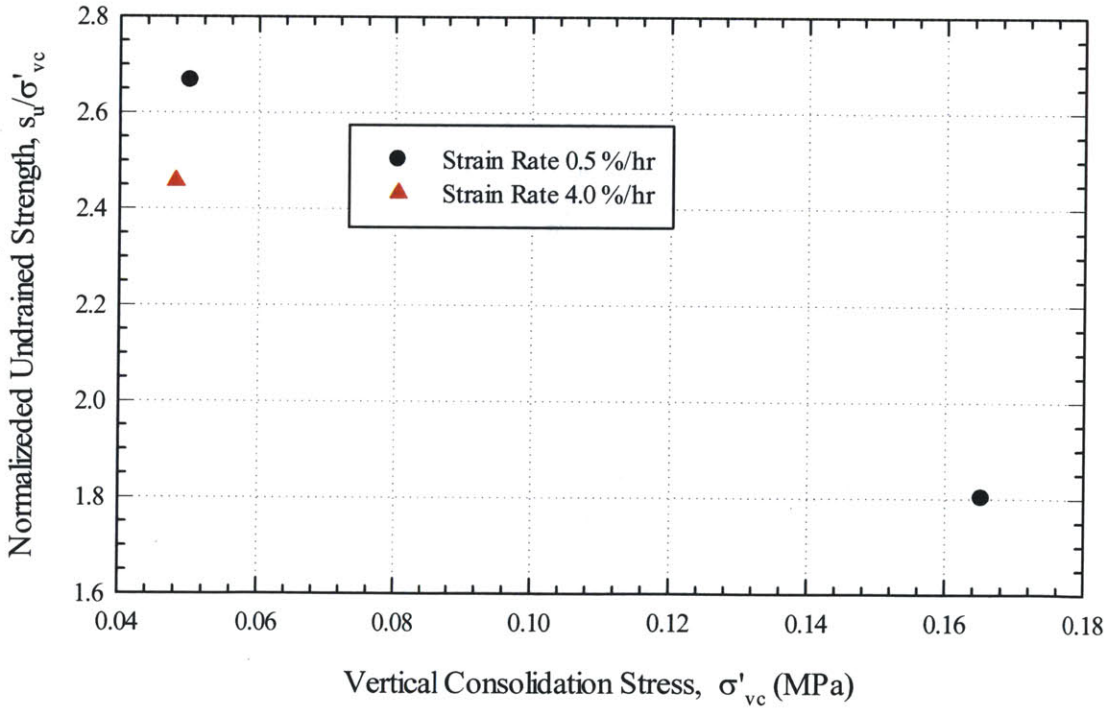

Figure 5-44 Normalized undrained shear versus stress level for RBBC at OCR = 32

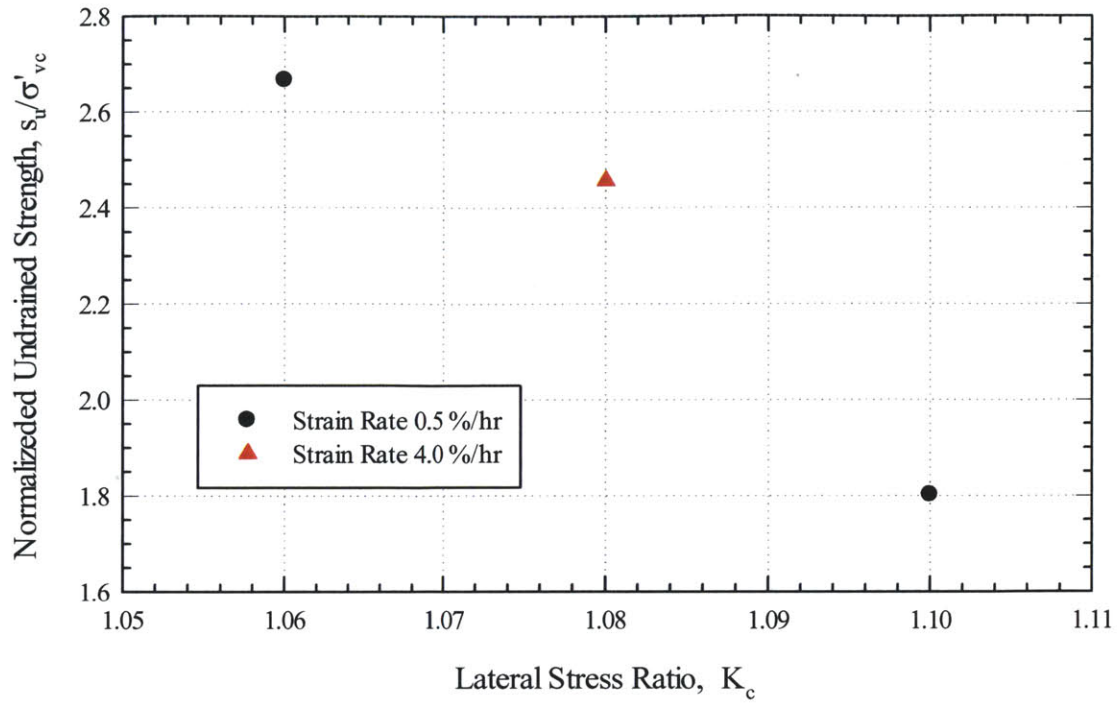

Figure 5-45 Normalized Undrained Shear Strength versus lateral stress ratio for RBBC at OCR = 32

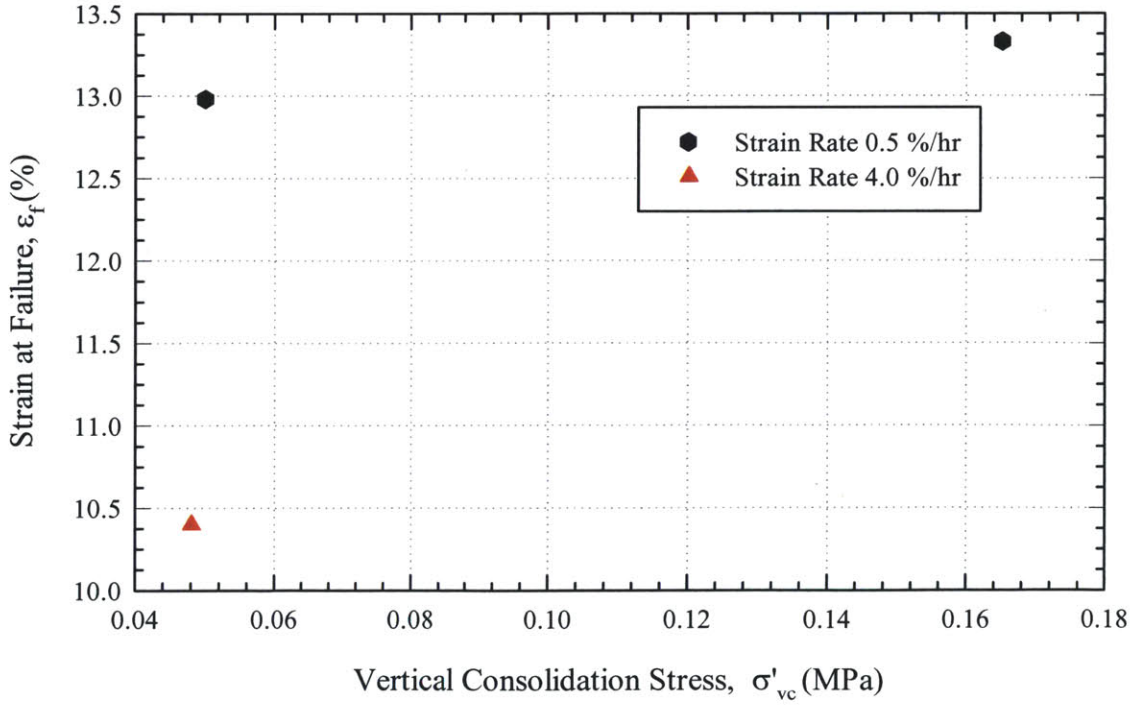

Figure 5-46 Strain at failure versus stress level for RBBC at OCR = 32

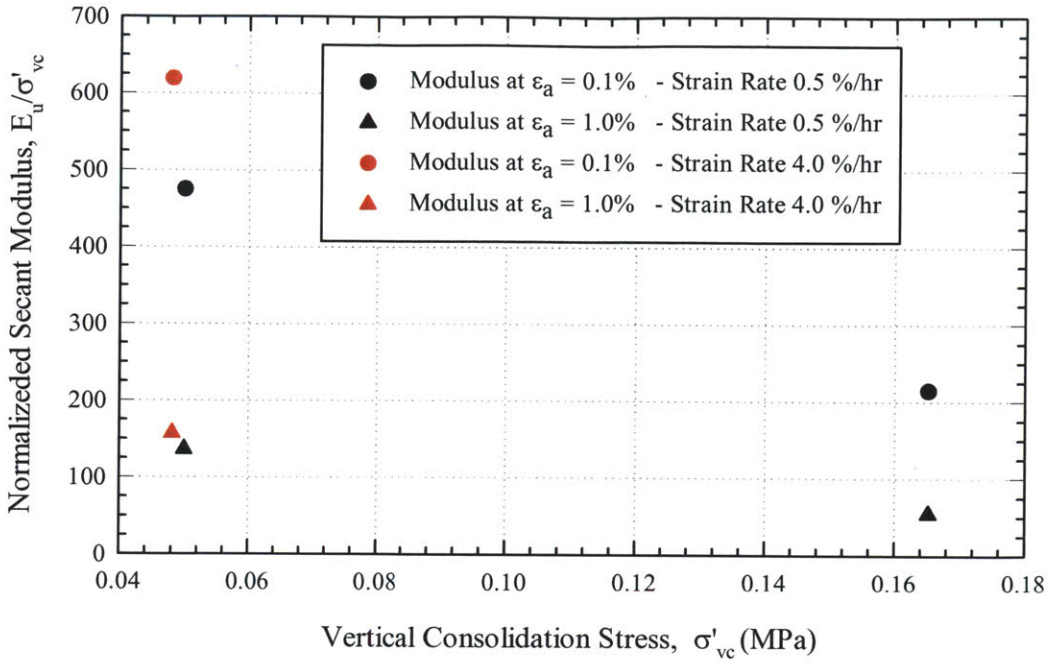

Figure 5-47 Normalized undrained secant modulus versus stress level for RBBC at OCR = 32

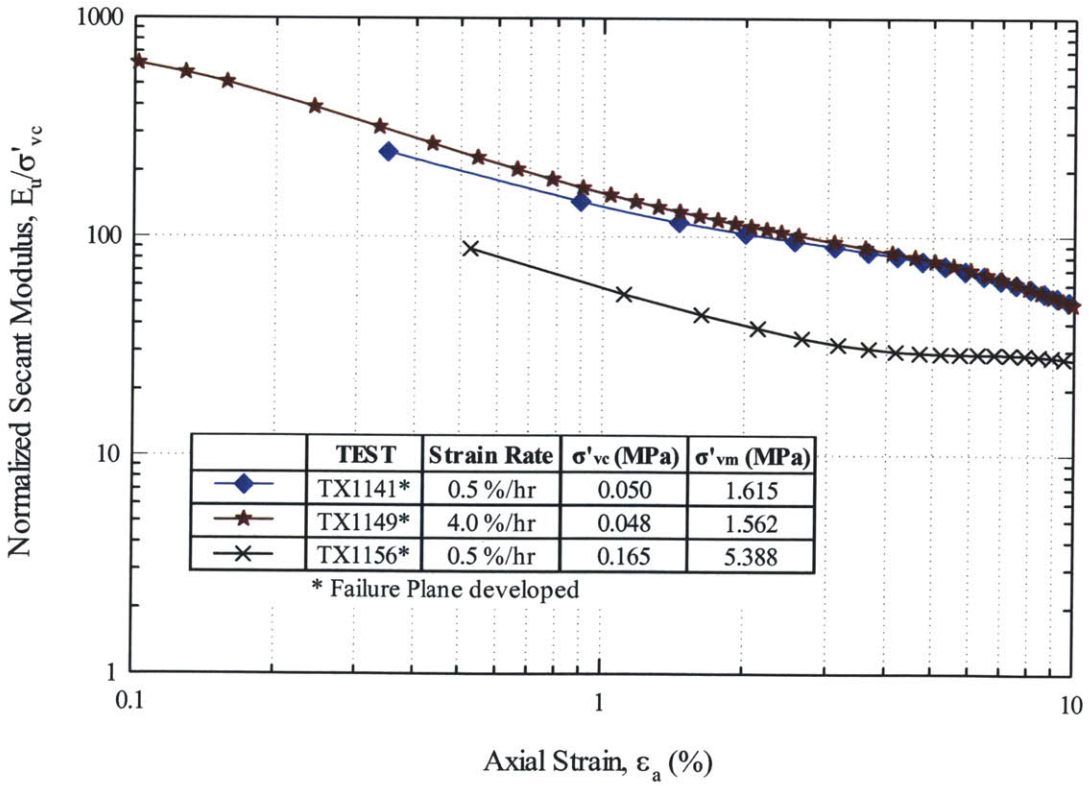

Figure 5-48 Normalized undrained secant modulus versus axial strain for RBBC at OCR = 32

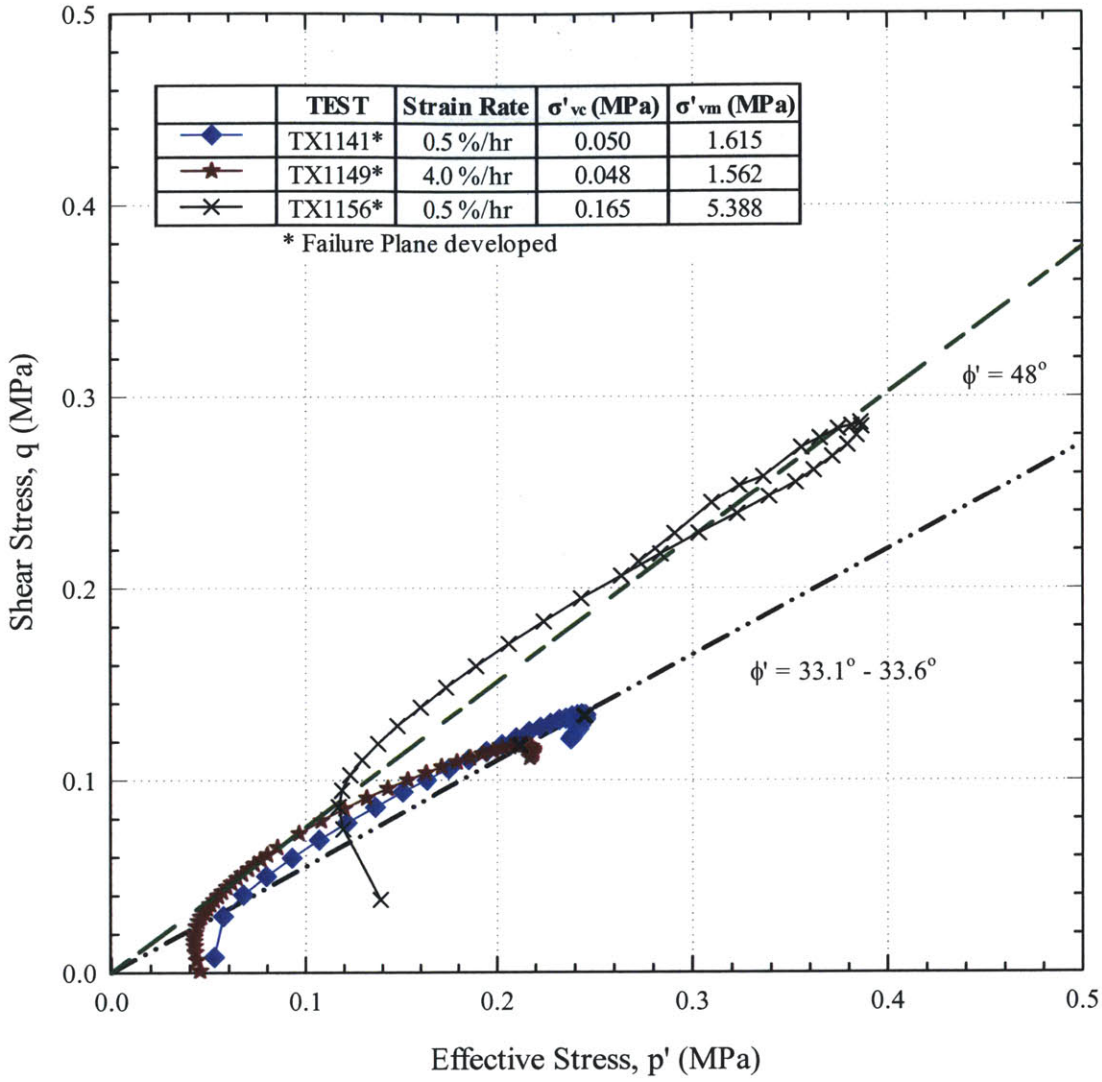

Figure 5-49 Effective Stress Paths for RBBC at OCR = 32 (Strain Rates 0.5%/hr and 4.0%/hr)

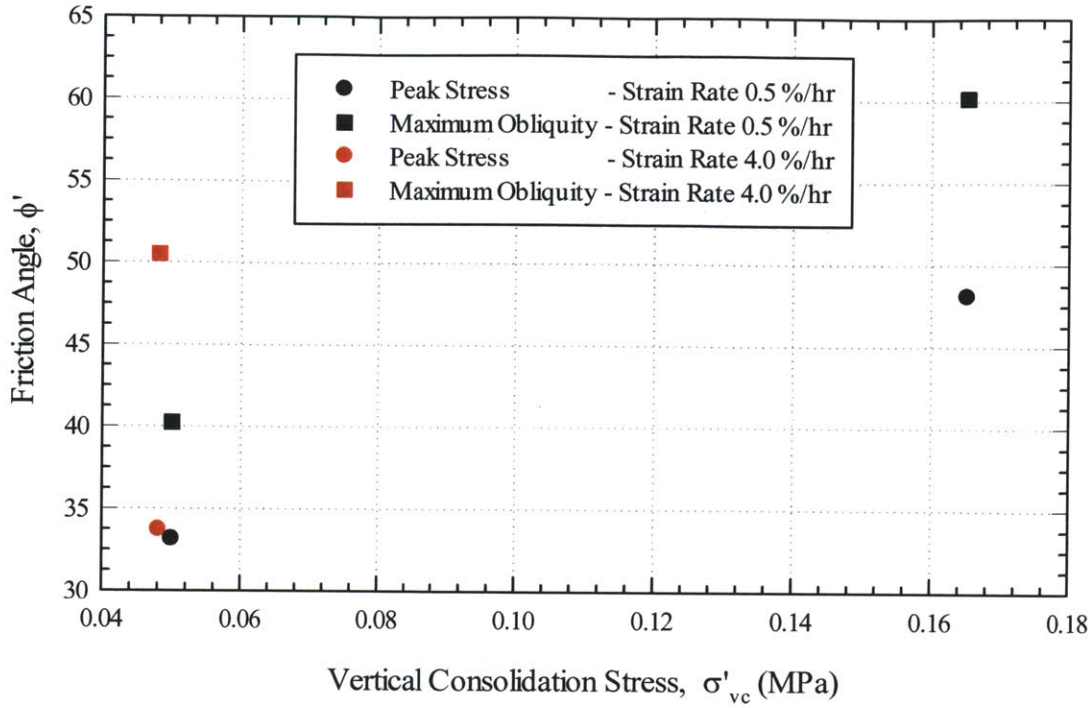

Figure 5-50 Friction angle at peak and maximum obliquity versus strain rate for RBBC at OCR = 32

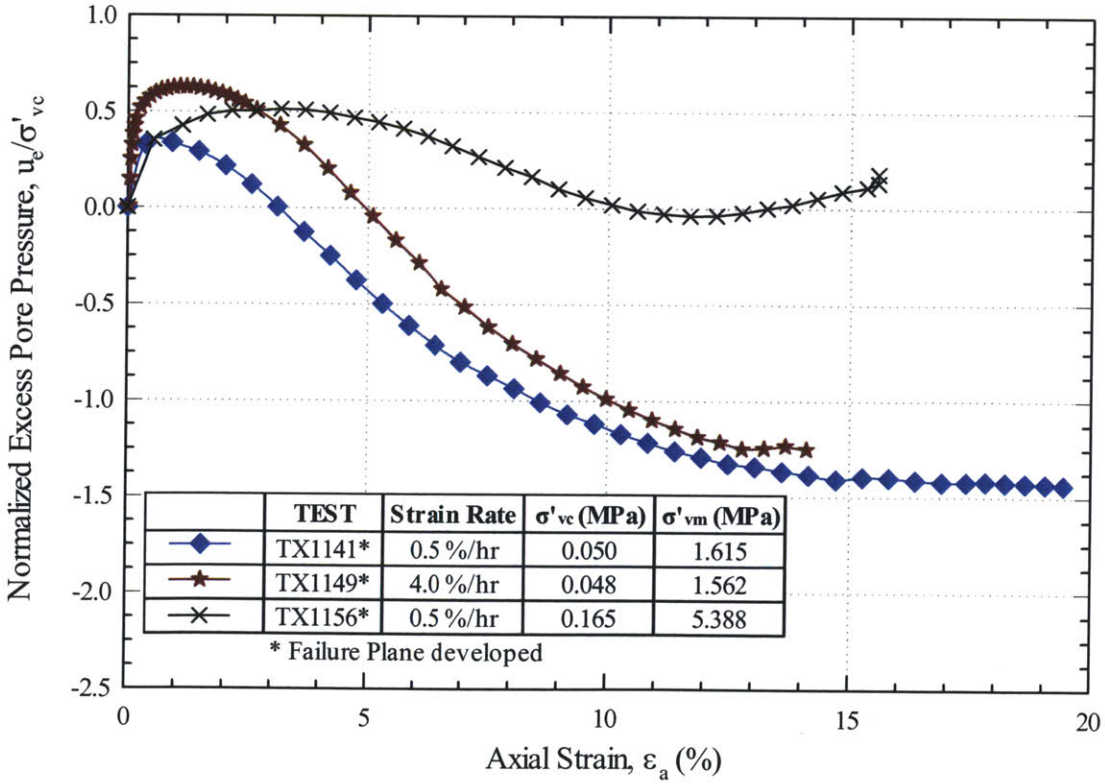

Figure 5-51 Normalized excess pore pressure versus strain for RBBC at OCR = 32

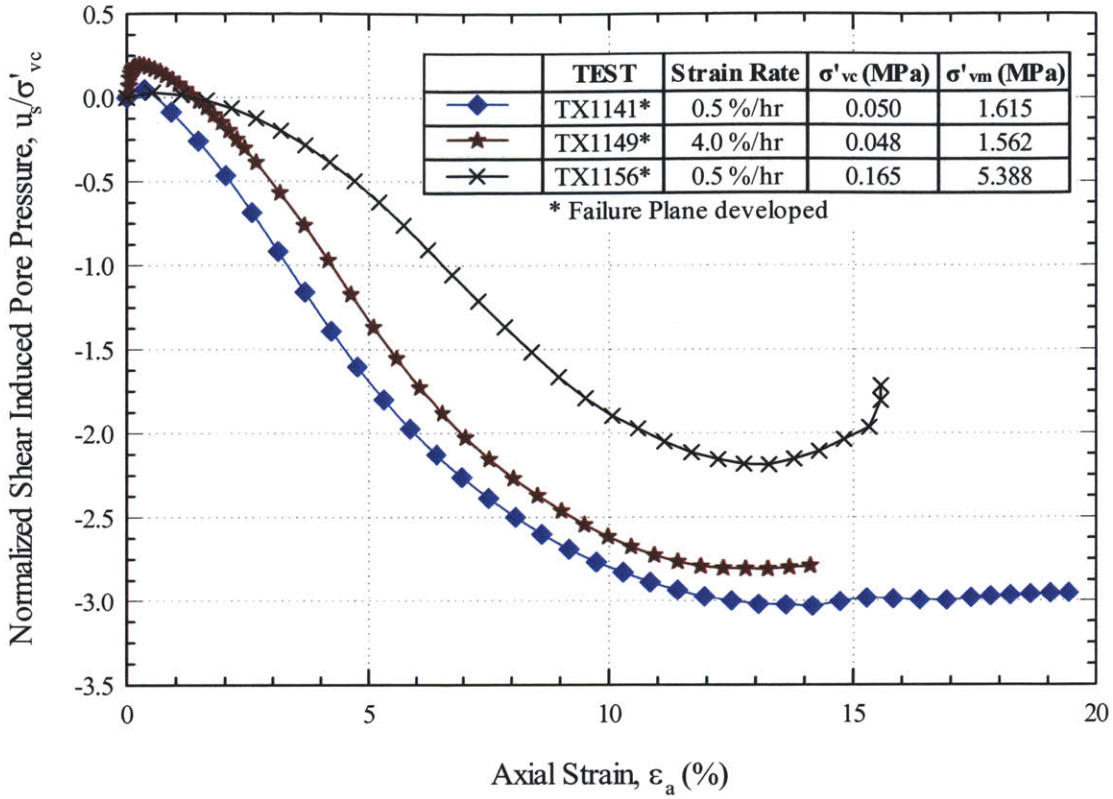

Figure 5-52 Normalized shear induced pore pressure versus strain for RBBC at OCR = 32

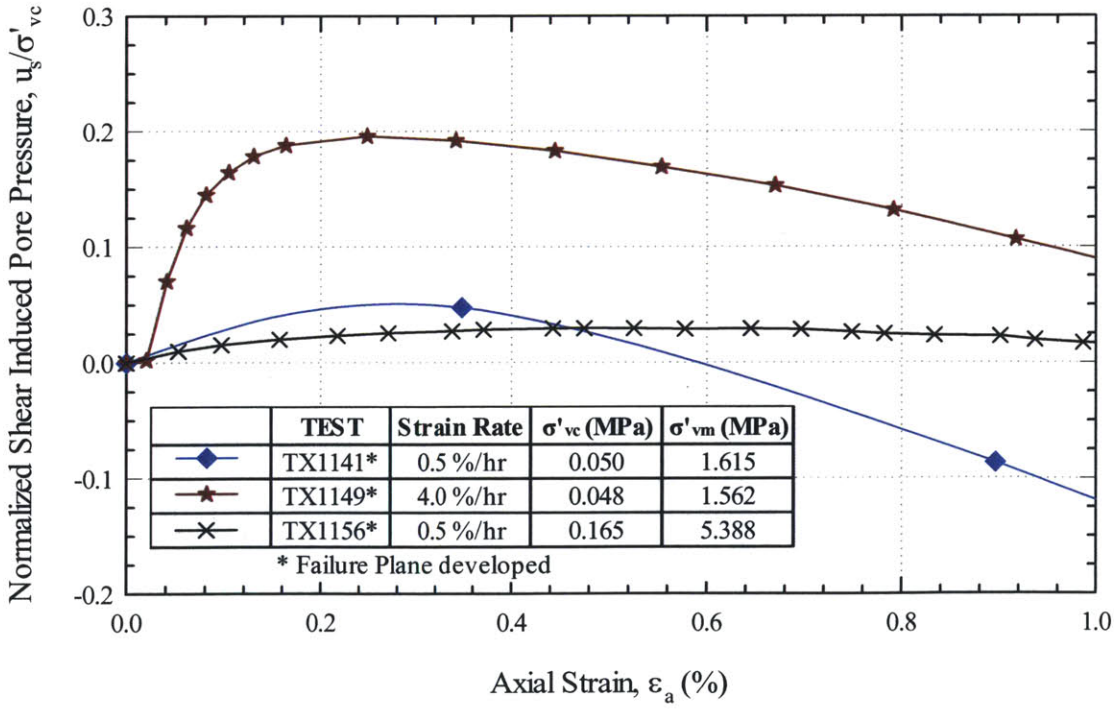

Figure 5-53 Normalized shear pore pressure versus strain (up to 1%) for RBBC at OCR = 32

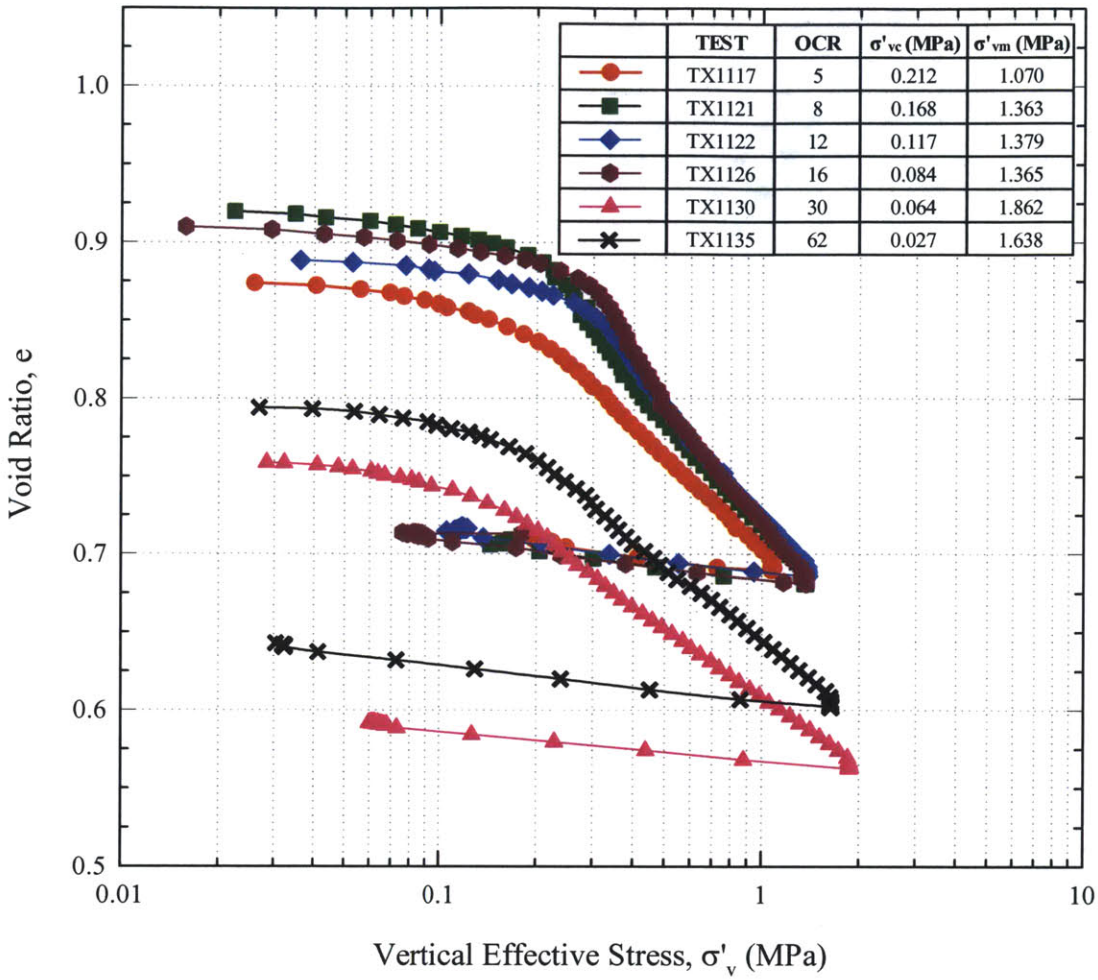

Figure 5-54 Compression behavior in e-log σ'v space for all testing program on PMC at different OCR

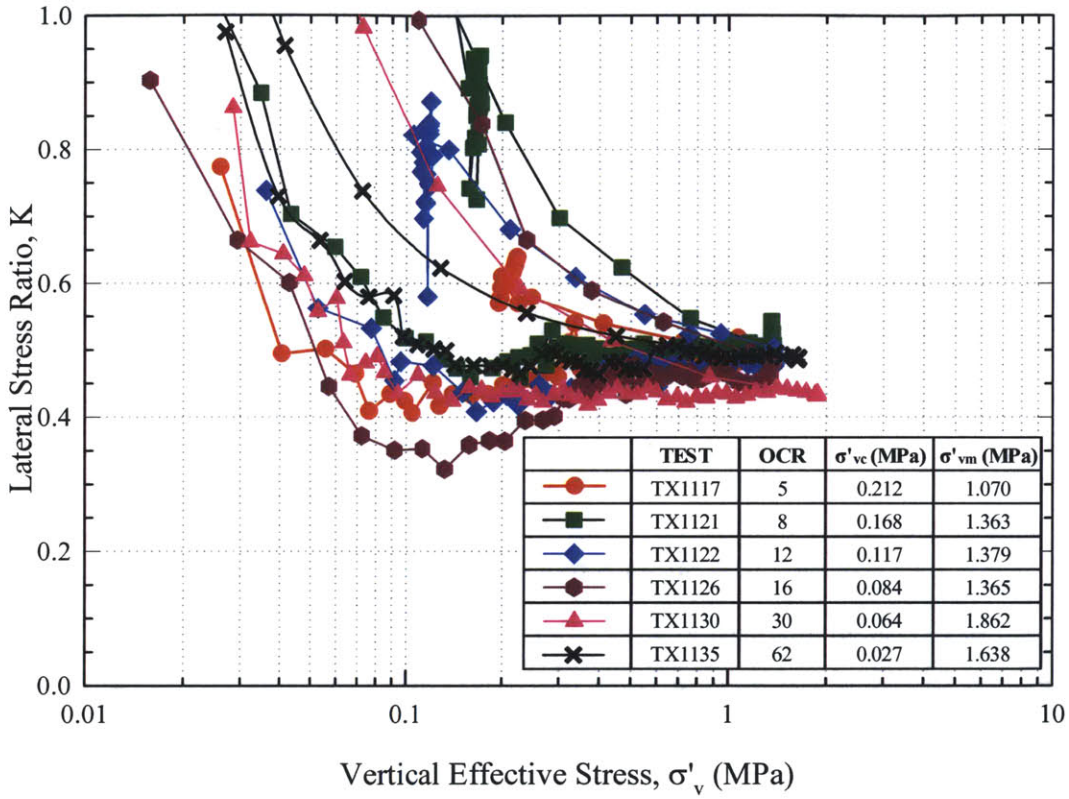

Figure 5-55 Lateral stress ratio versus vertical effective stress for all testing program on PMC at different OCR

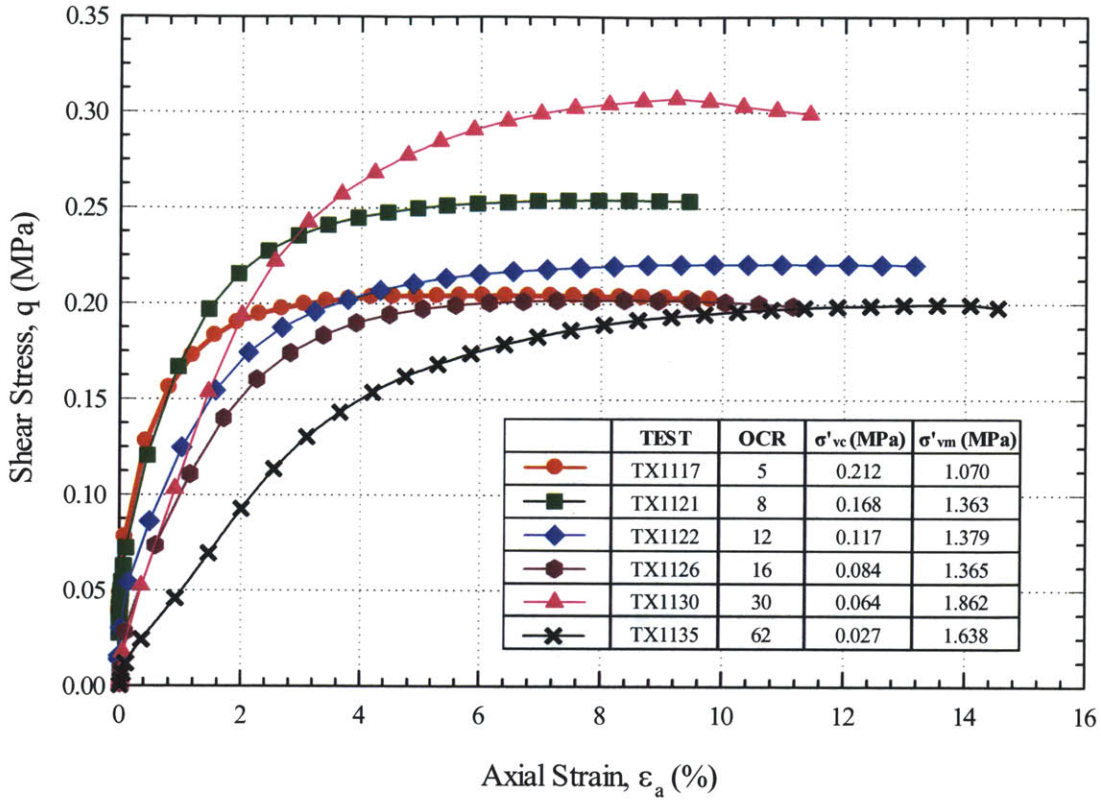

Figure 5-56 Stress-Strain curves for PMC at different OCR

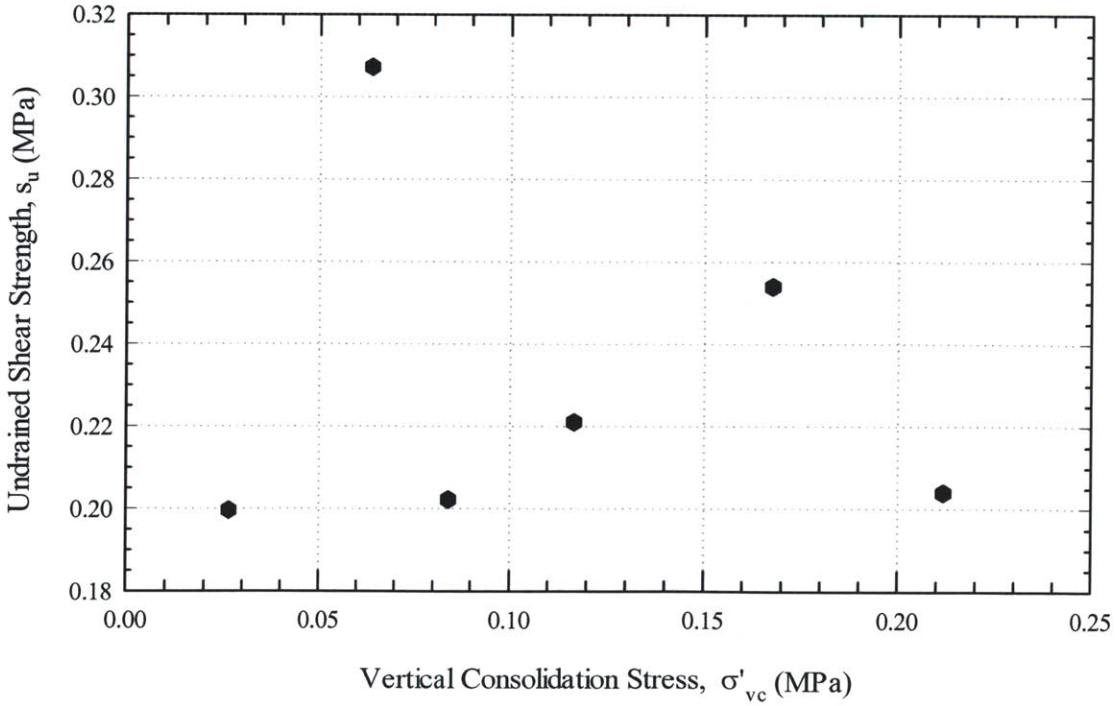

Figure 5-57 Undrained Shear Strength versus stress level for PMC at different OCR

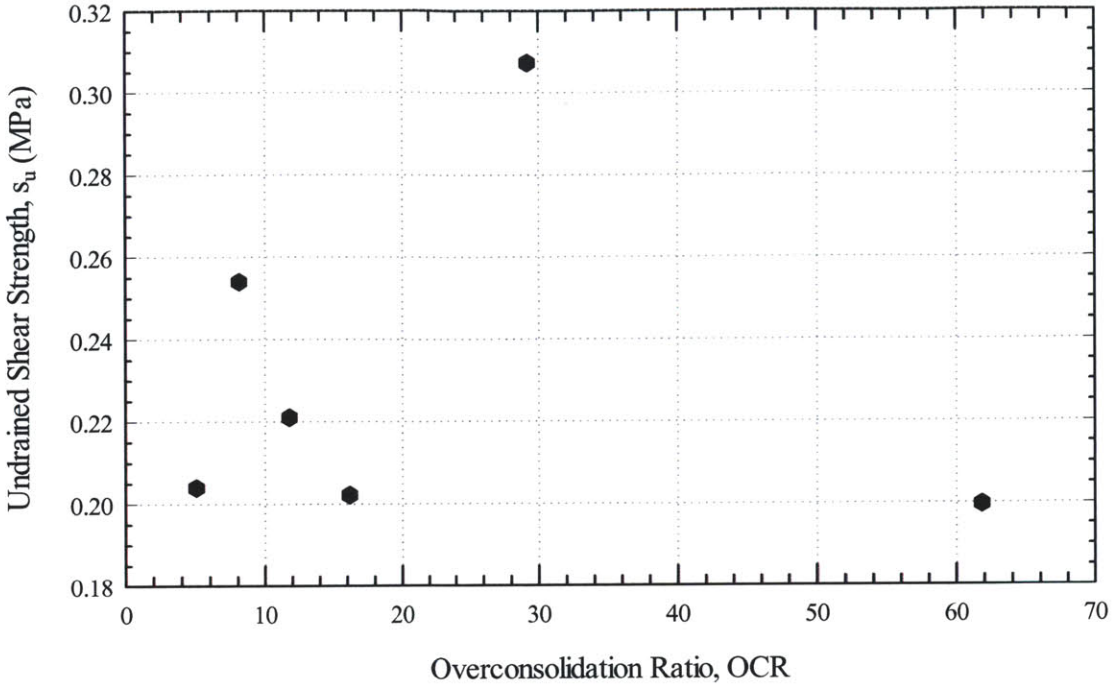

Figure 5-58 Undrained shear strength versus overconsolidation ratio for PMC

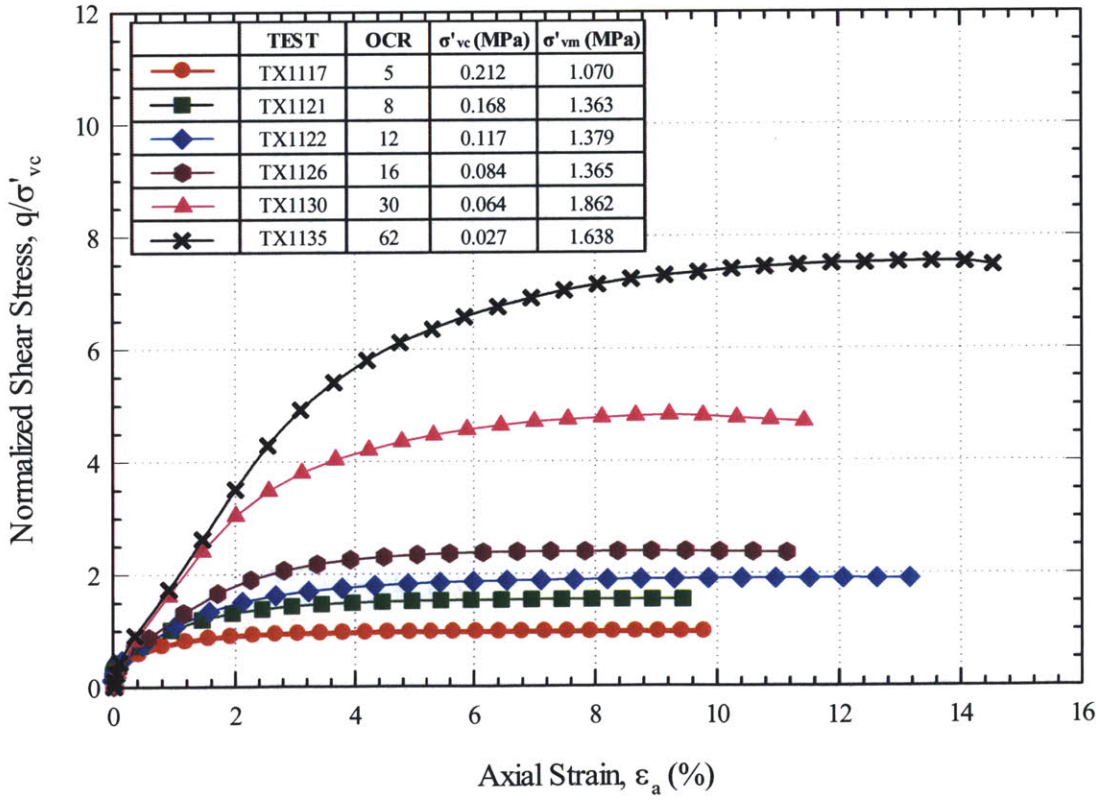

Figure 5-59 Normalized stress-strain curves for PMC at different OCR

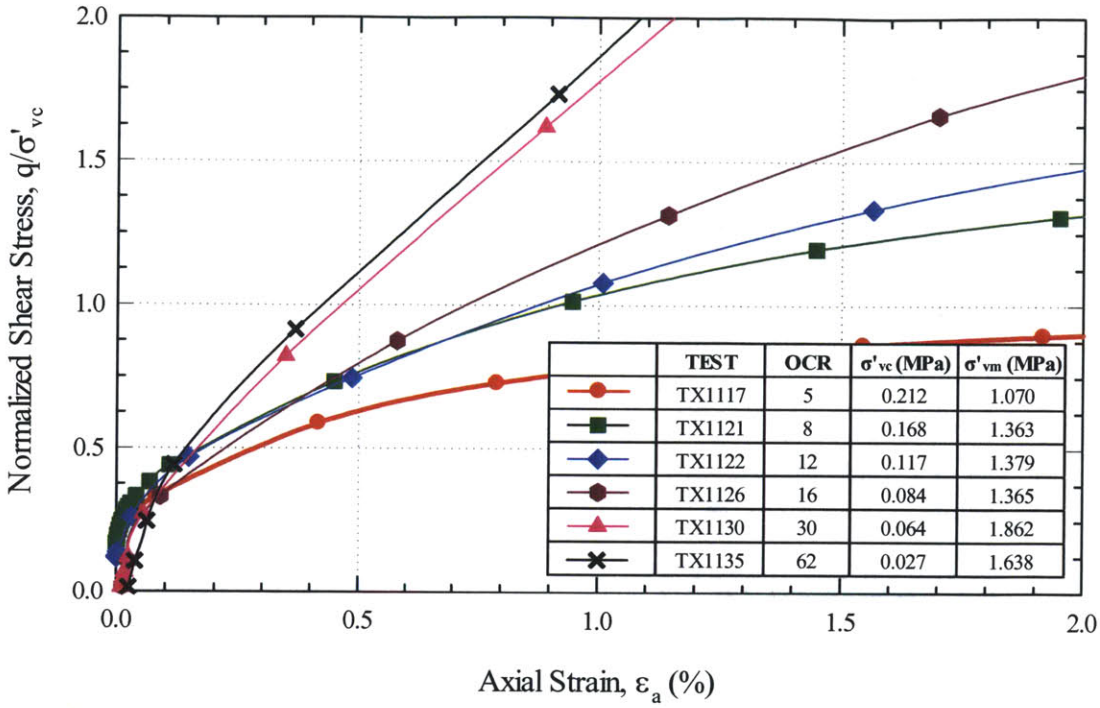

Figure 5-60 Normalized stress-strain curves (up to 2%) for PMC at different OCR

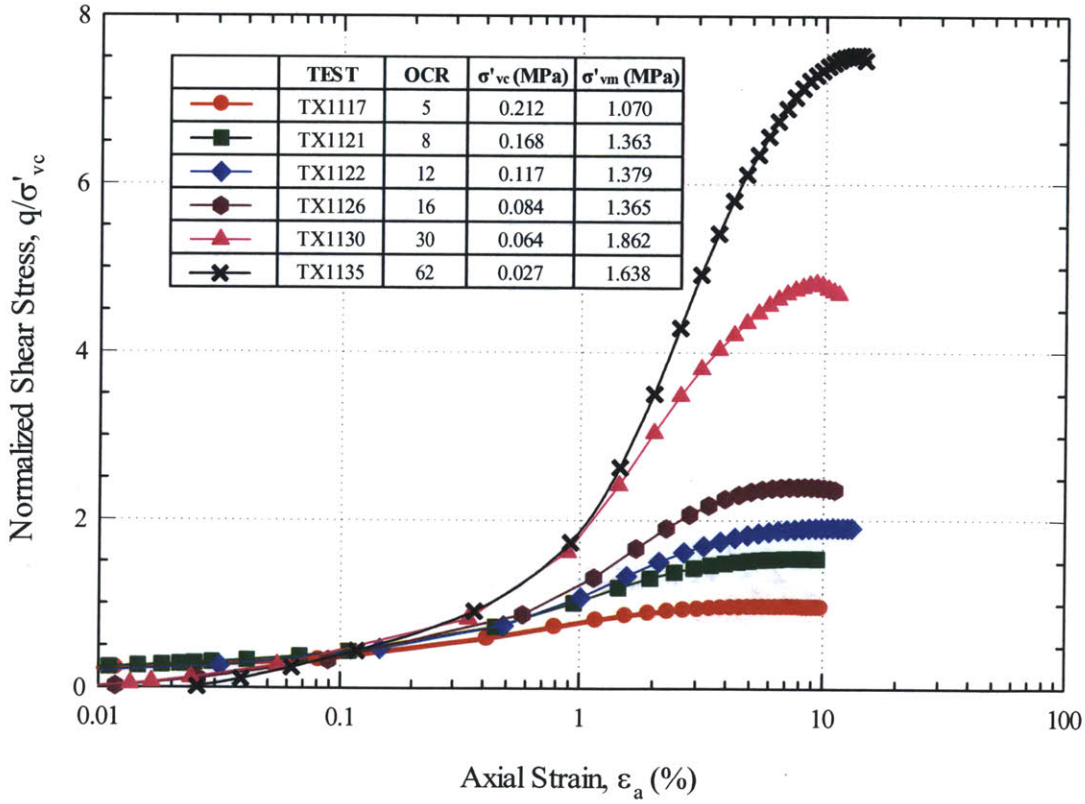

Figure 5-61 Normalized stress-(log)strain curves for PMC at different OCR

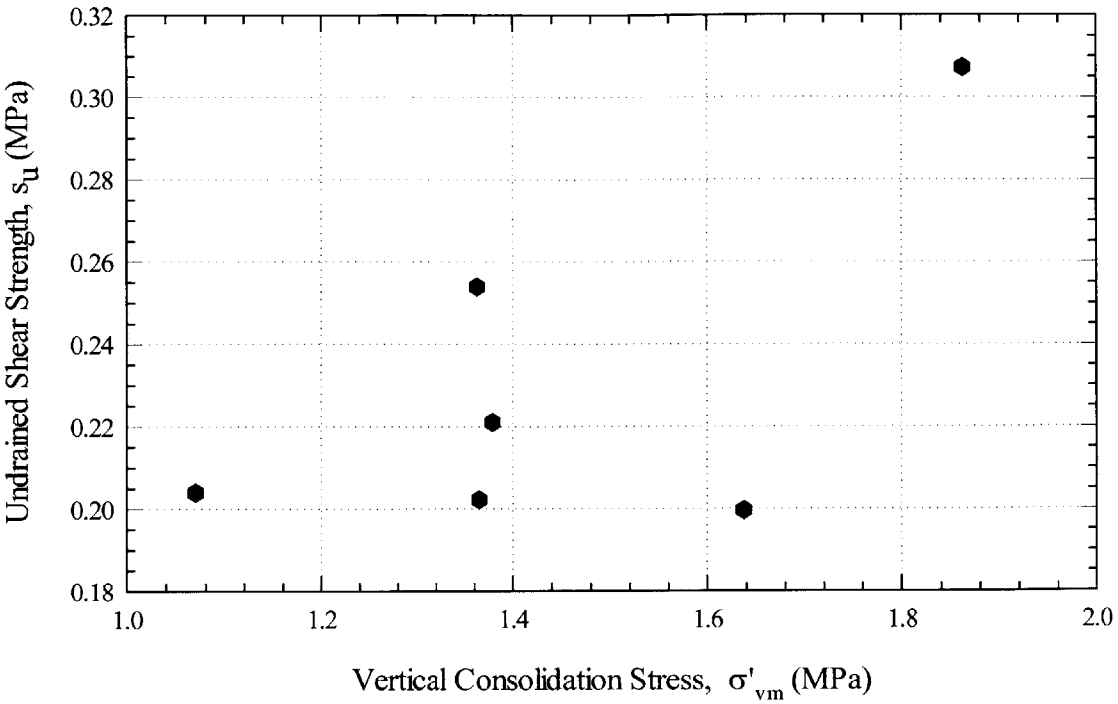

Figure 5-62 Undrained Shear Strength versus maximum stress (σ'_{vm}) level for PMC at different OCR

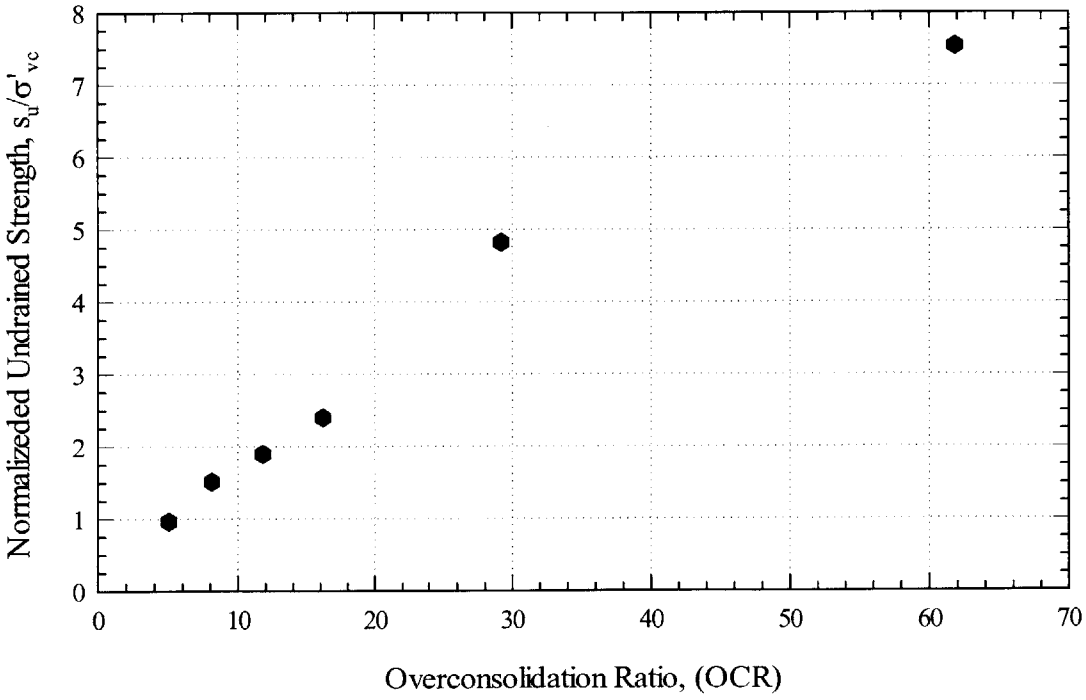

Figure 5-63 Normalized undrained shear versus overconsolidation ratio for PMC

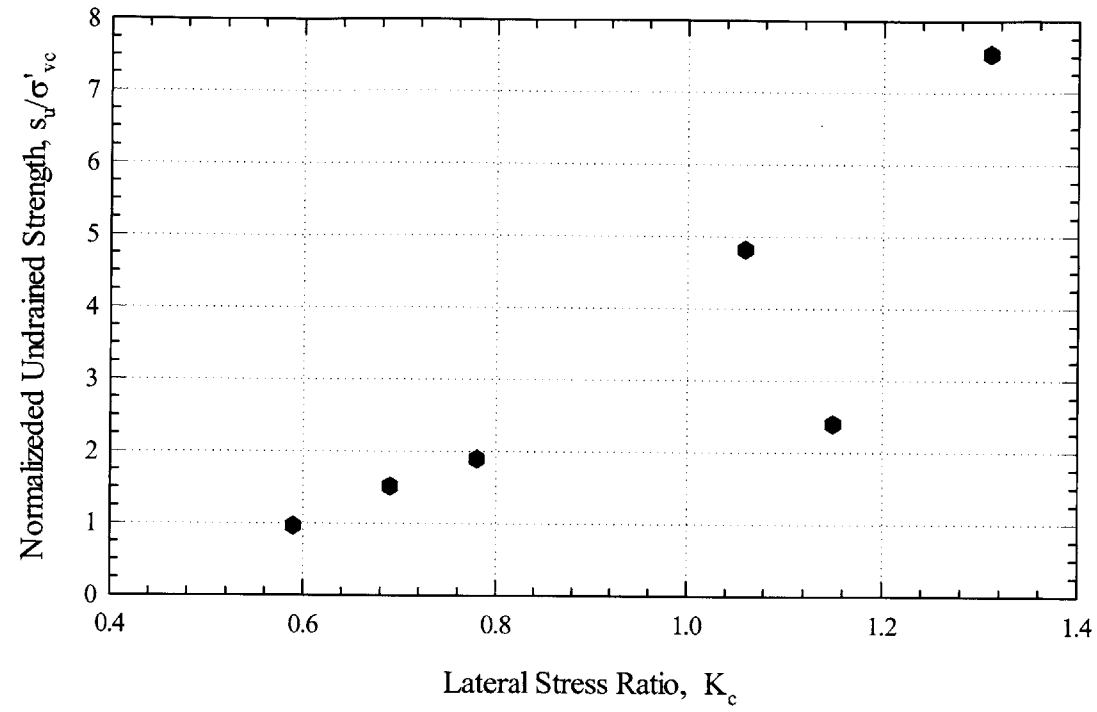

Figure 5-64 Normalized Undrained Shear Strength versus lateral stress ratio for PMC at different OCR

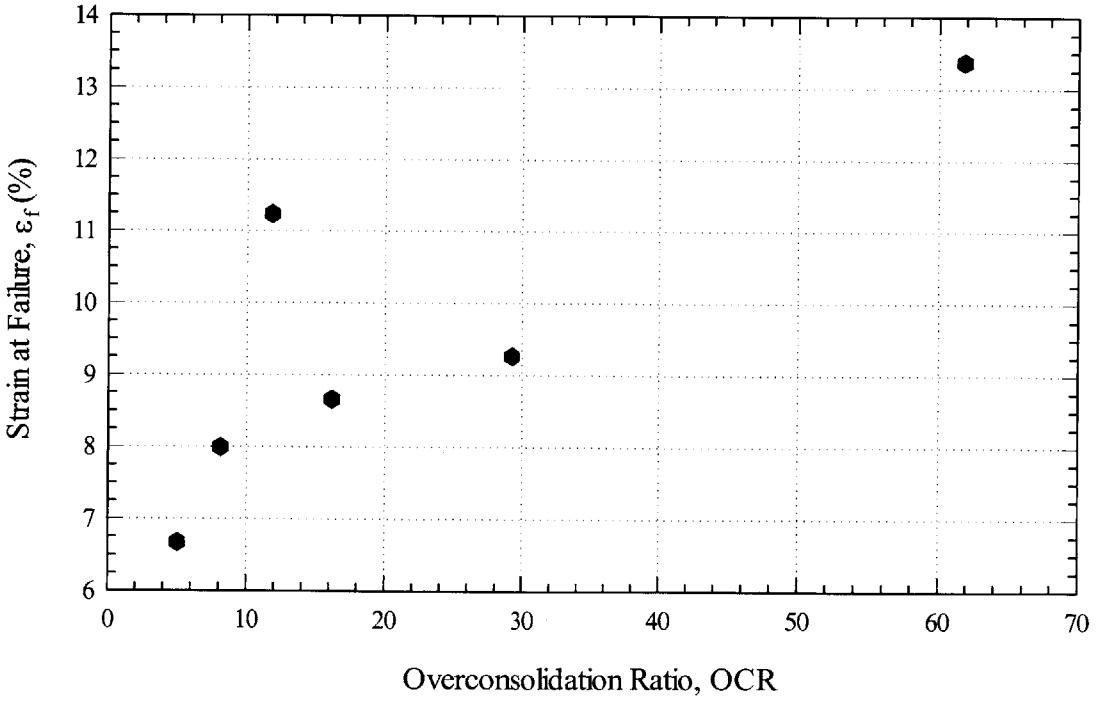

Figure 5-65 Strain at failure versus strain rate for PMC at different OCR

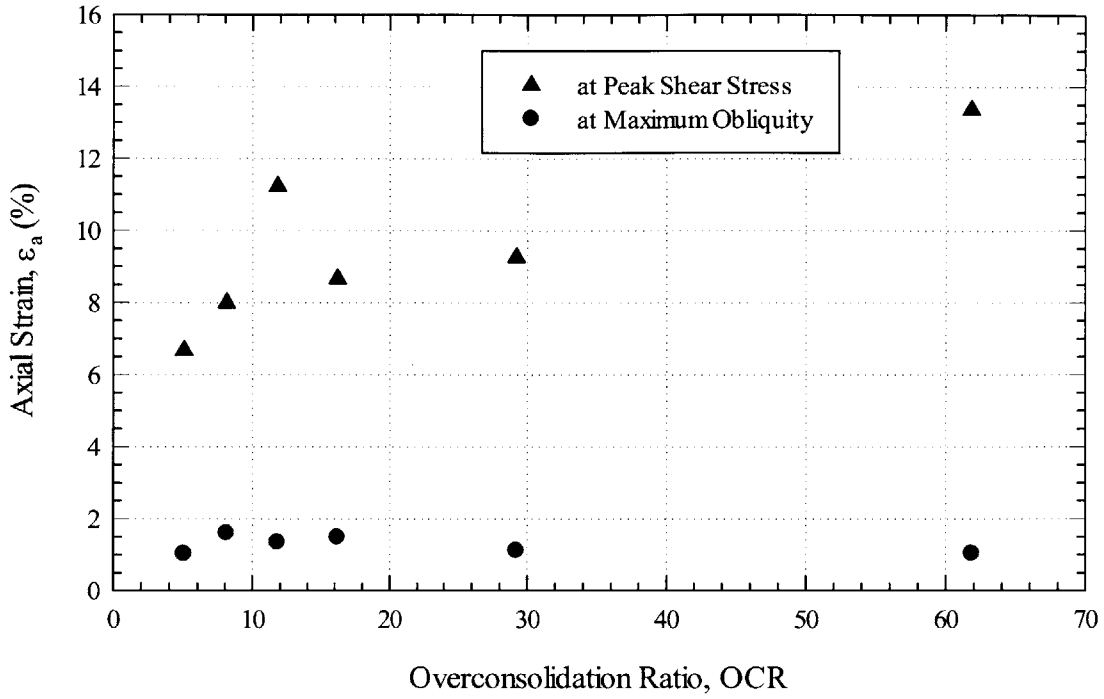

Figure 5-66 Strain at failure and maximum obliquity versus OCR for PMC

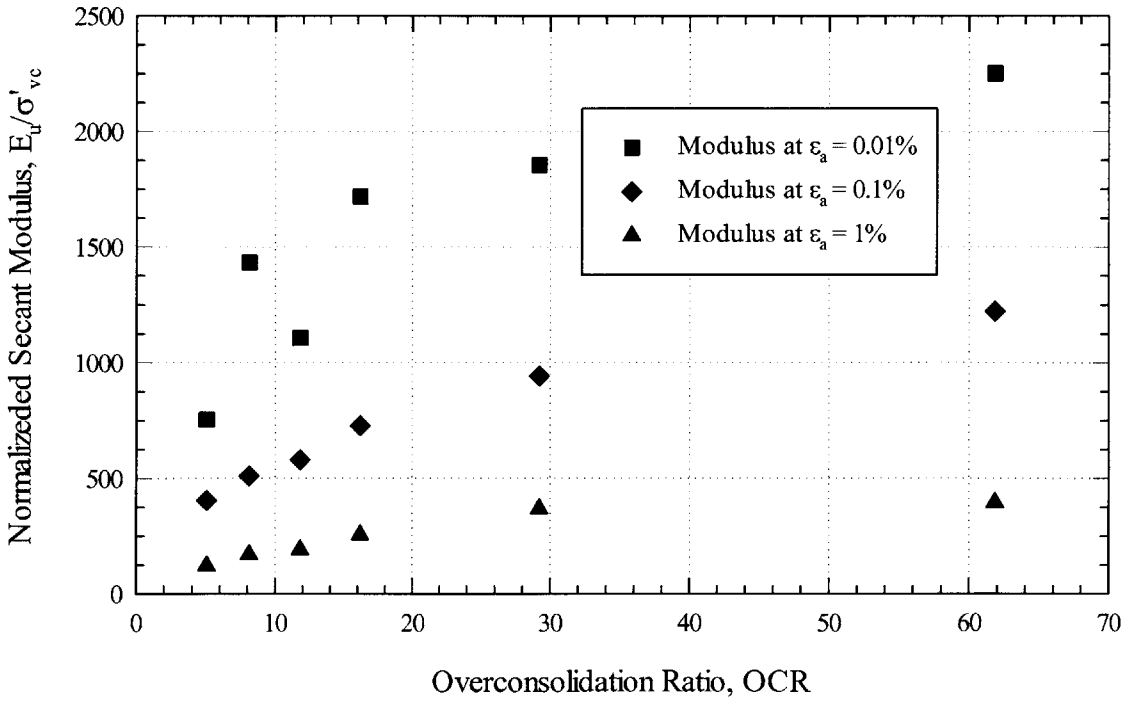

Figure 5-67 Normalized undrained secant modulus versus OCR for PMC

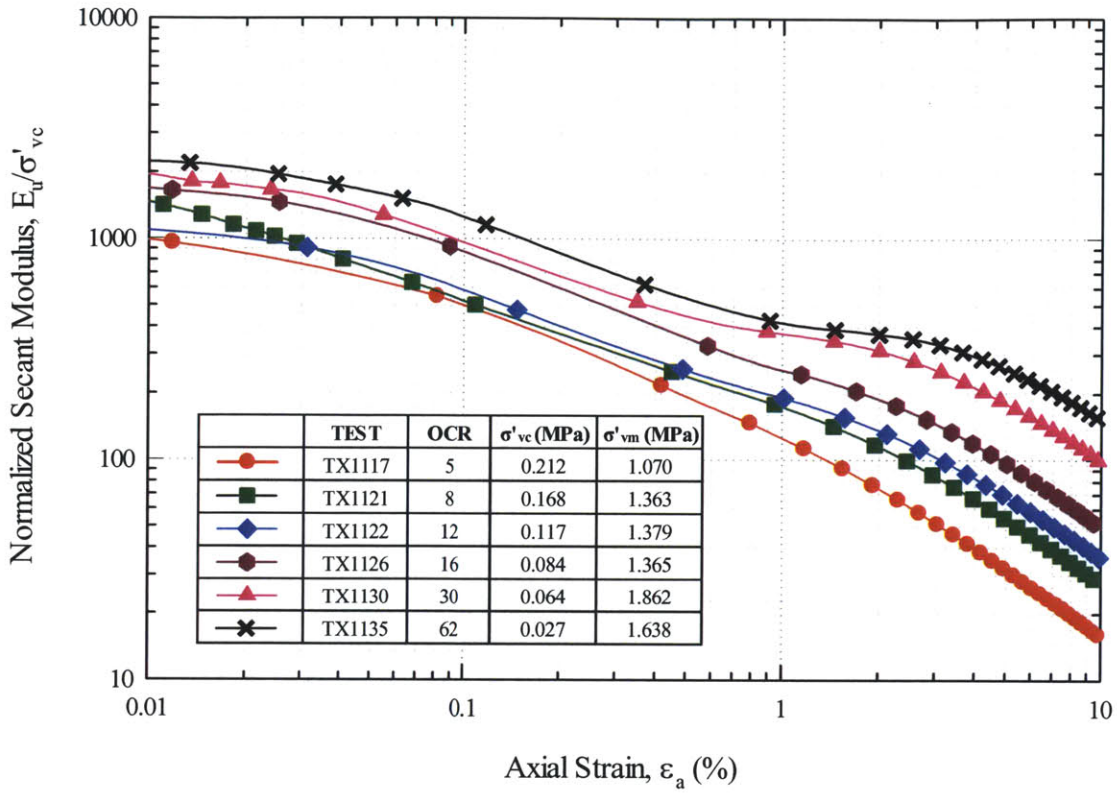

Figure 5-68 Normalized undrained secant modulus versus axial strain for PMC at different OCR

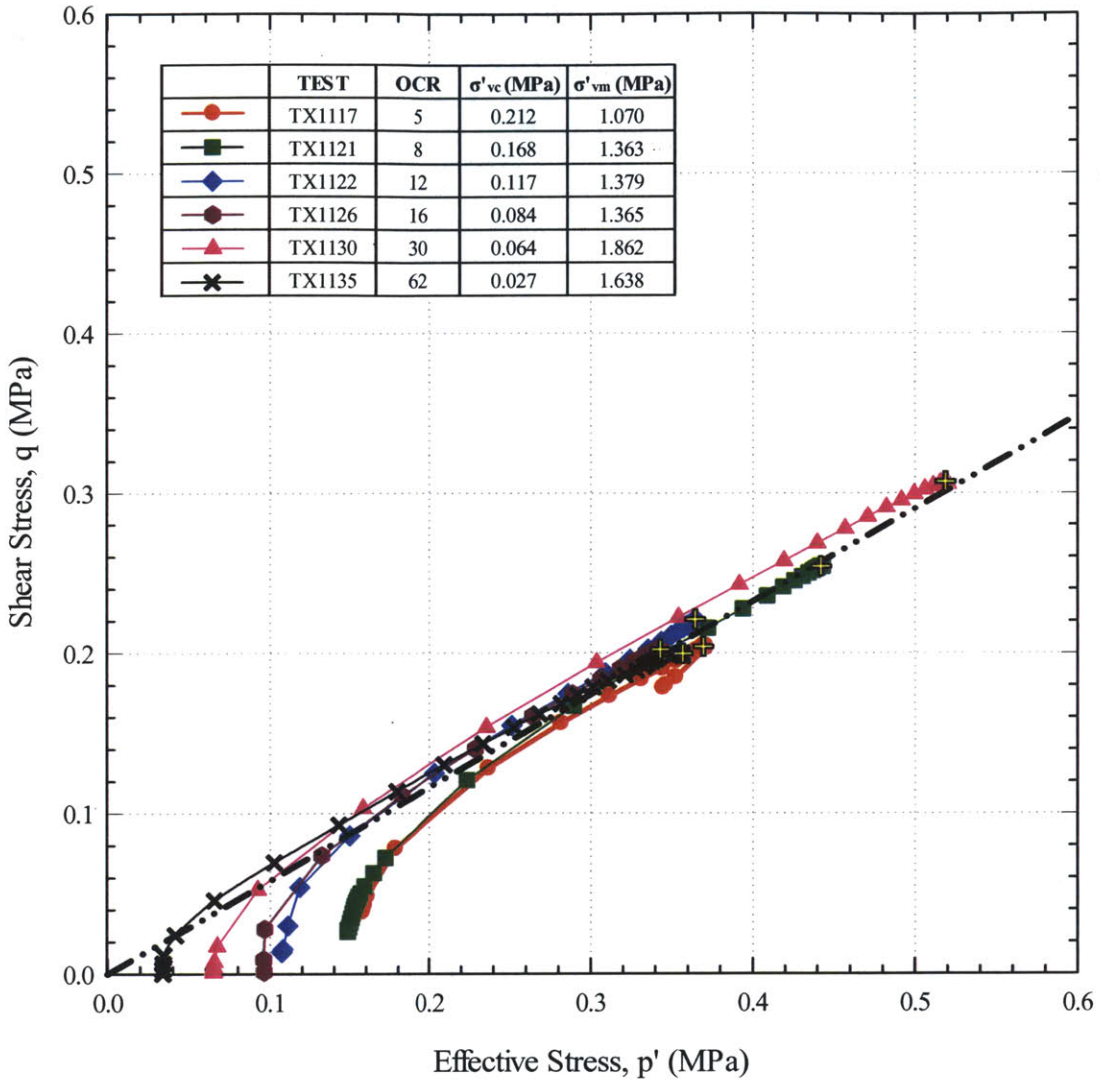

Figure 5-69 Effective Stress Paths for PMC at different OCR

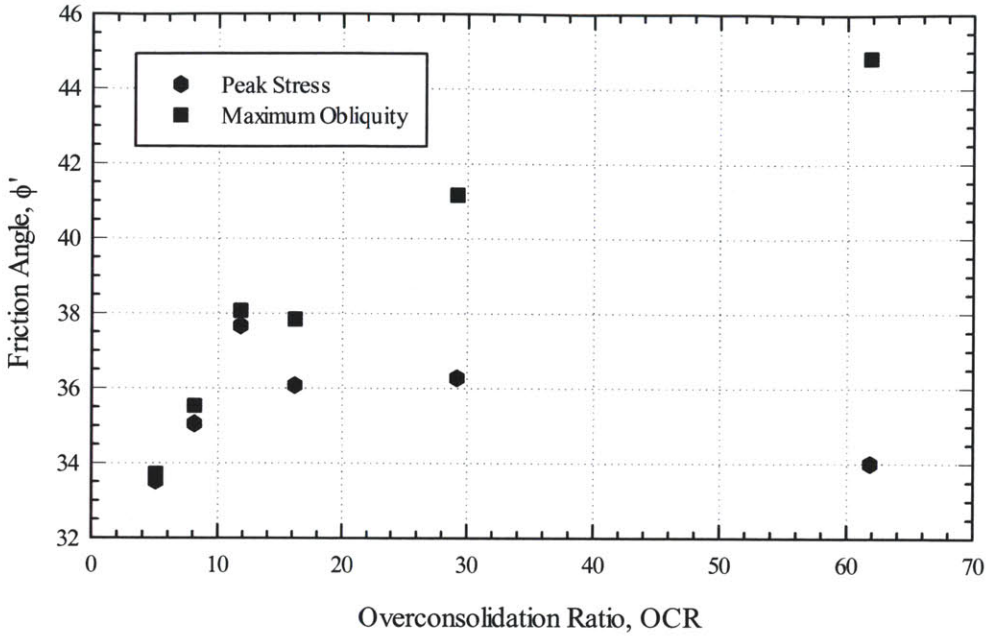

Figure 5-70 Friction angle at peak and maximum obliquity versus OCR for PMC

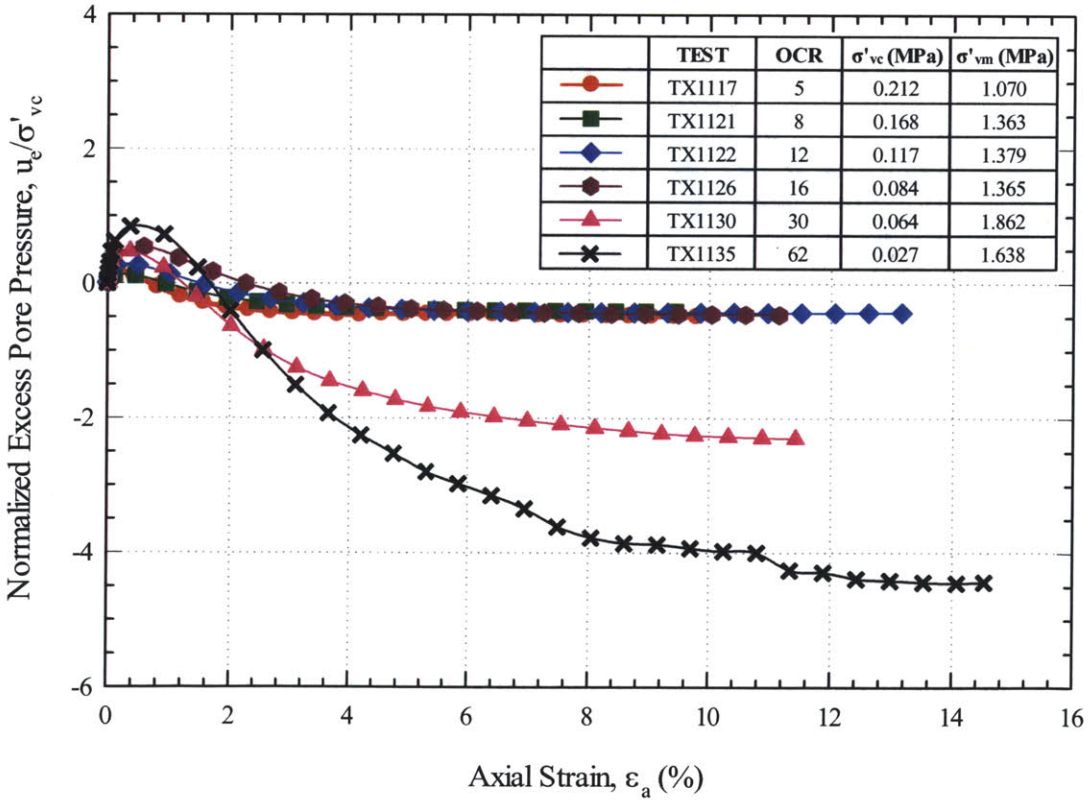

Figure 5-71 Normalized excess pore pressure versus strain for PMC at different OCR

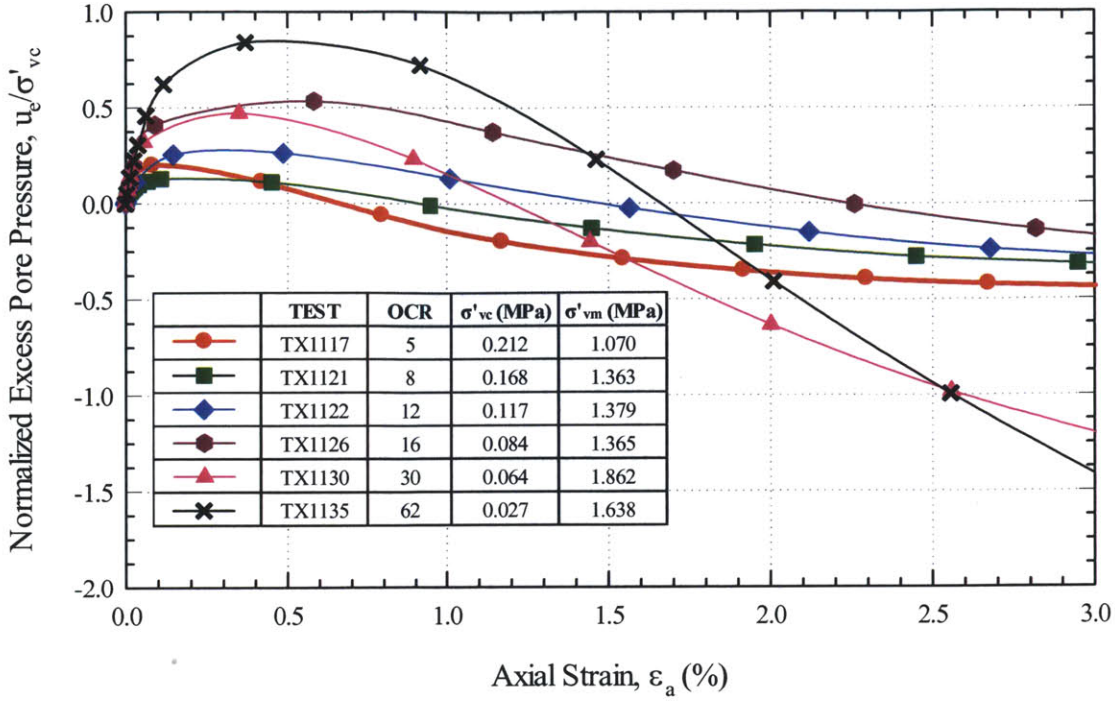

Figure 5-72 Normalized excess pore pressure versus strain (close up view) for PMC at different OCR

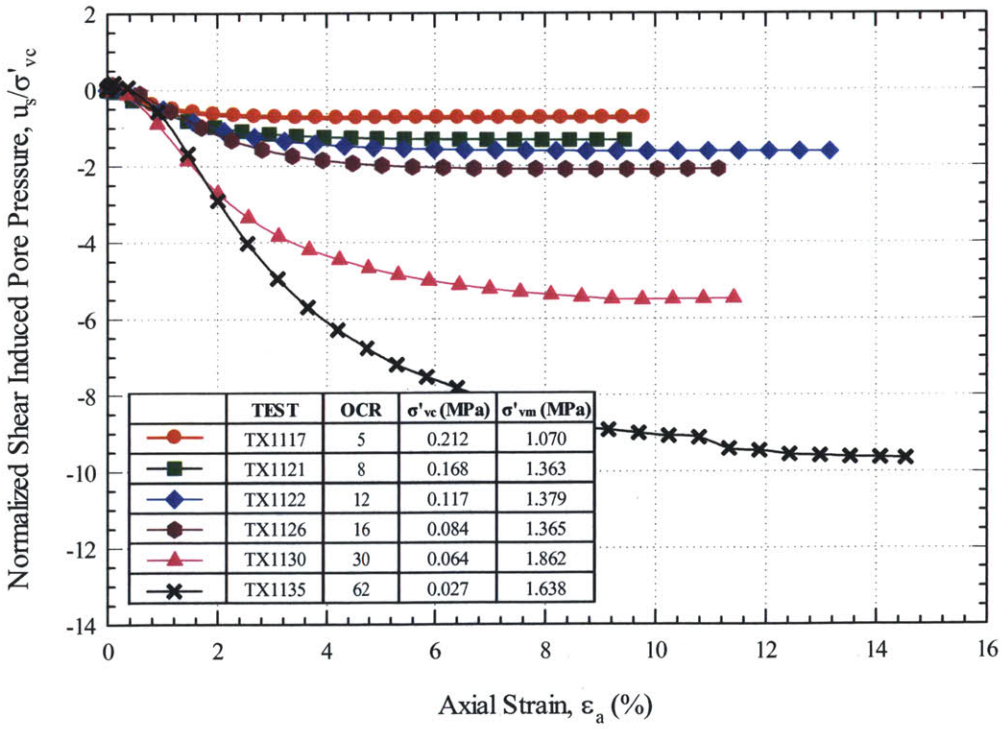

Figure 5-73 Normalized shear induced pore pressure versus strain for PMC at different OCR

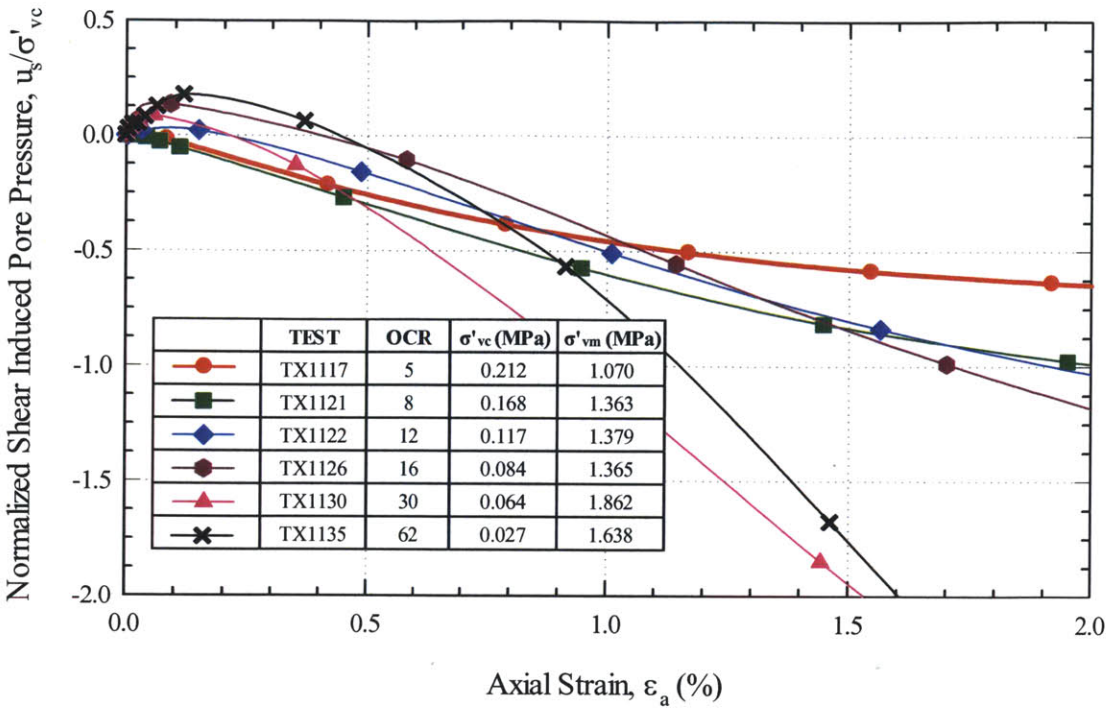

Figure 5-74 Normalized shear induced pore pressure versus strain (close up view) for PMC at different OCR

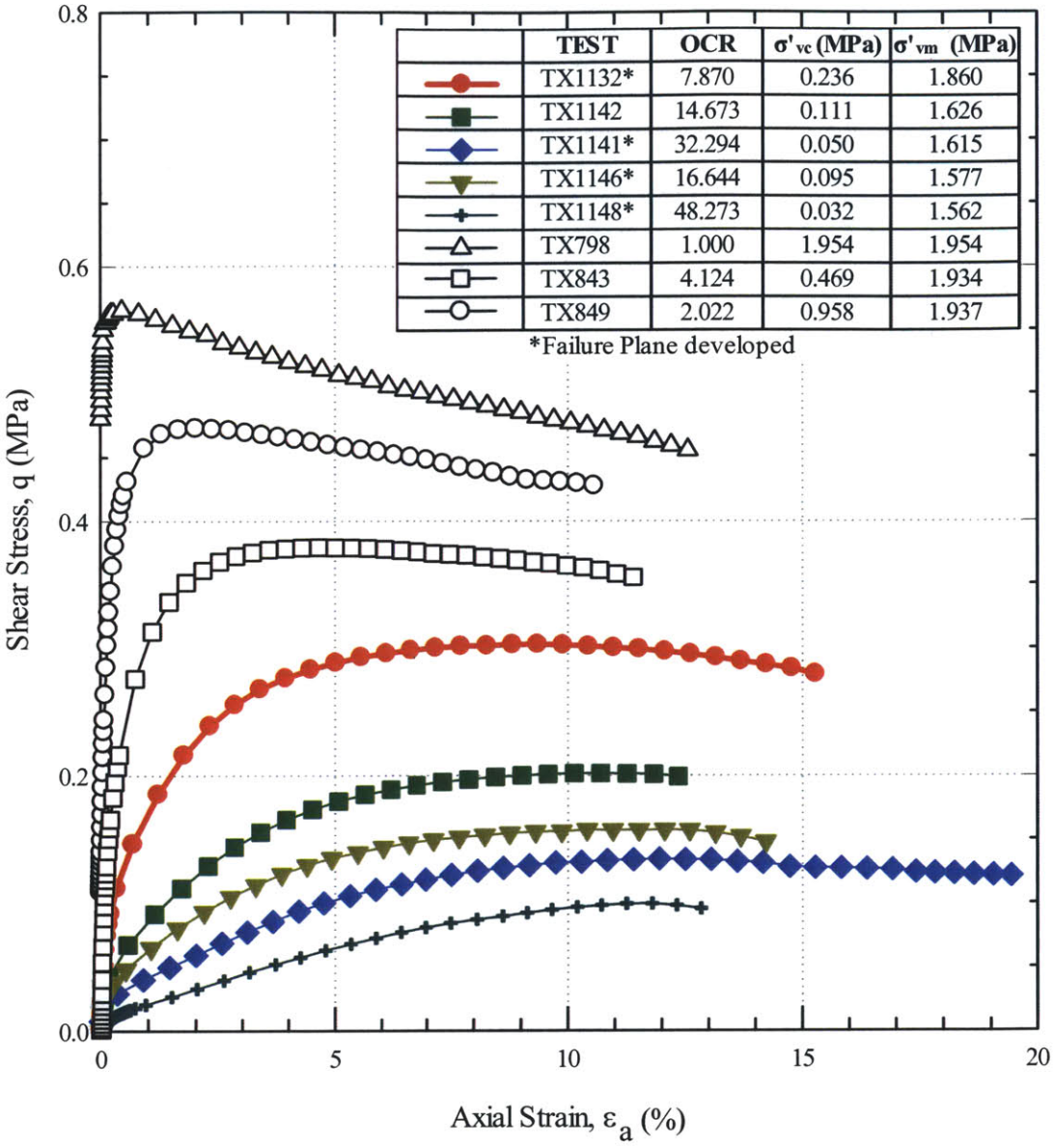

Figure 5-75 Stress-Strain curves for RBBC at different OCR

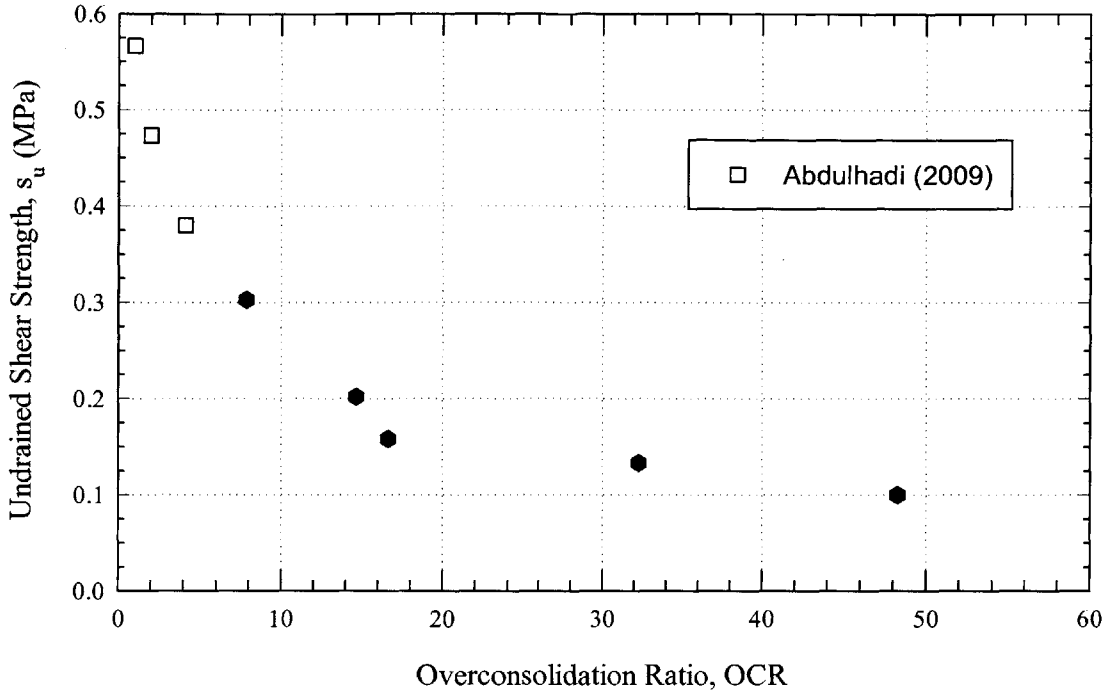

Figure 5-76 Undrained Shear Strength versus OCR for RBBC

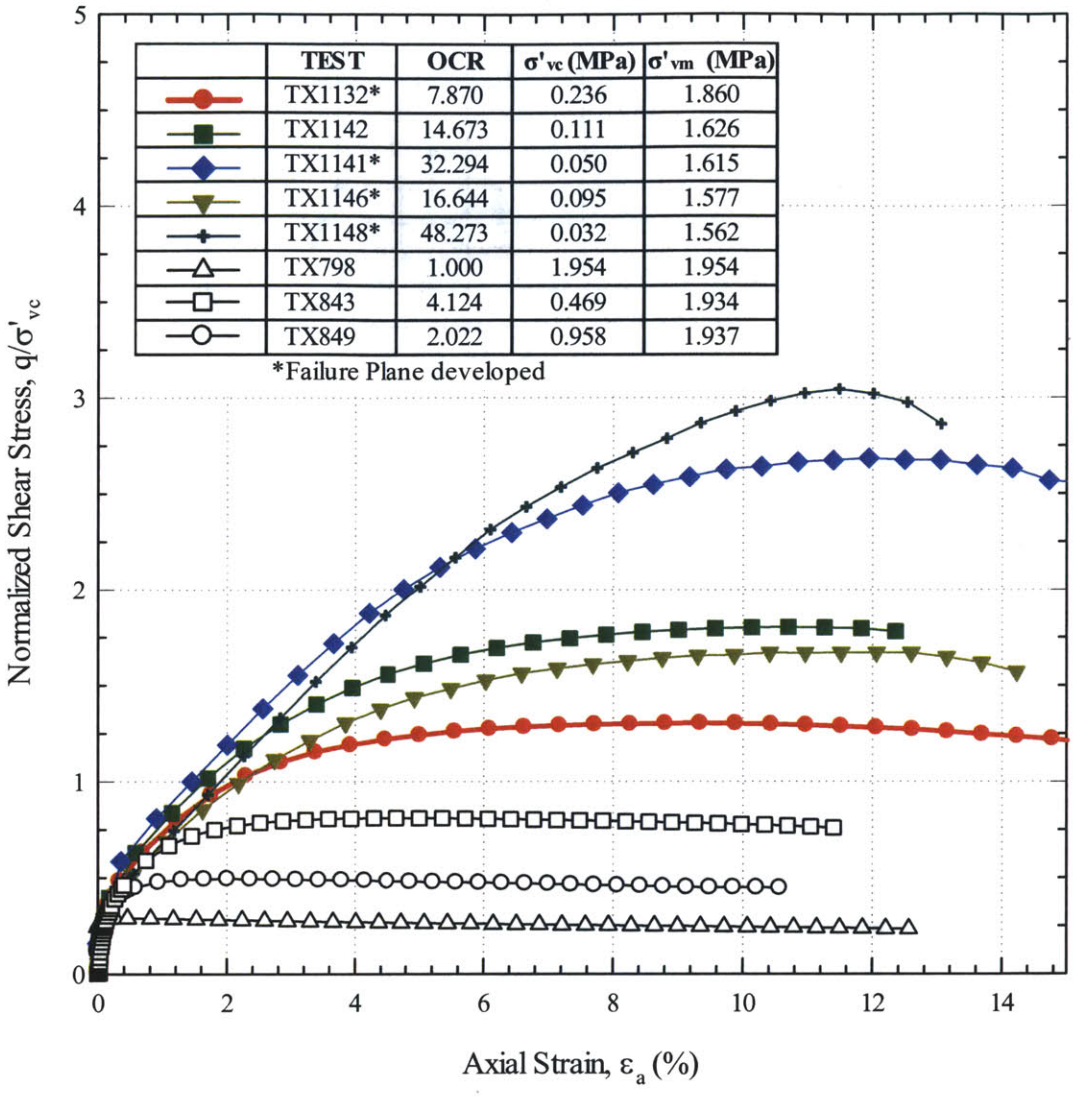

Figure 5-77 Normalized stress-strain curves for RBBC at different OCR

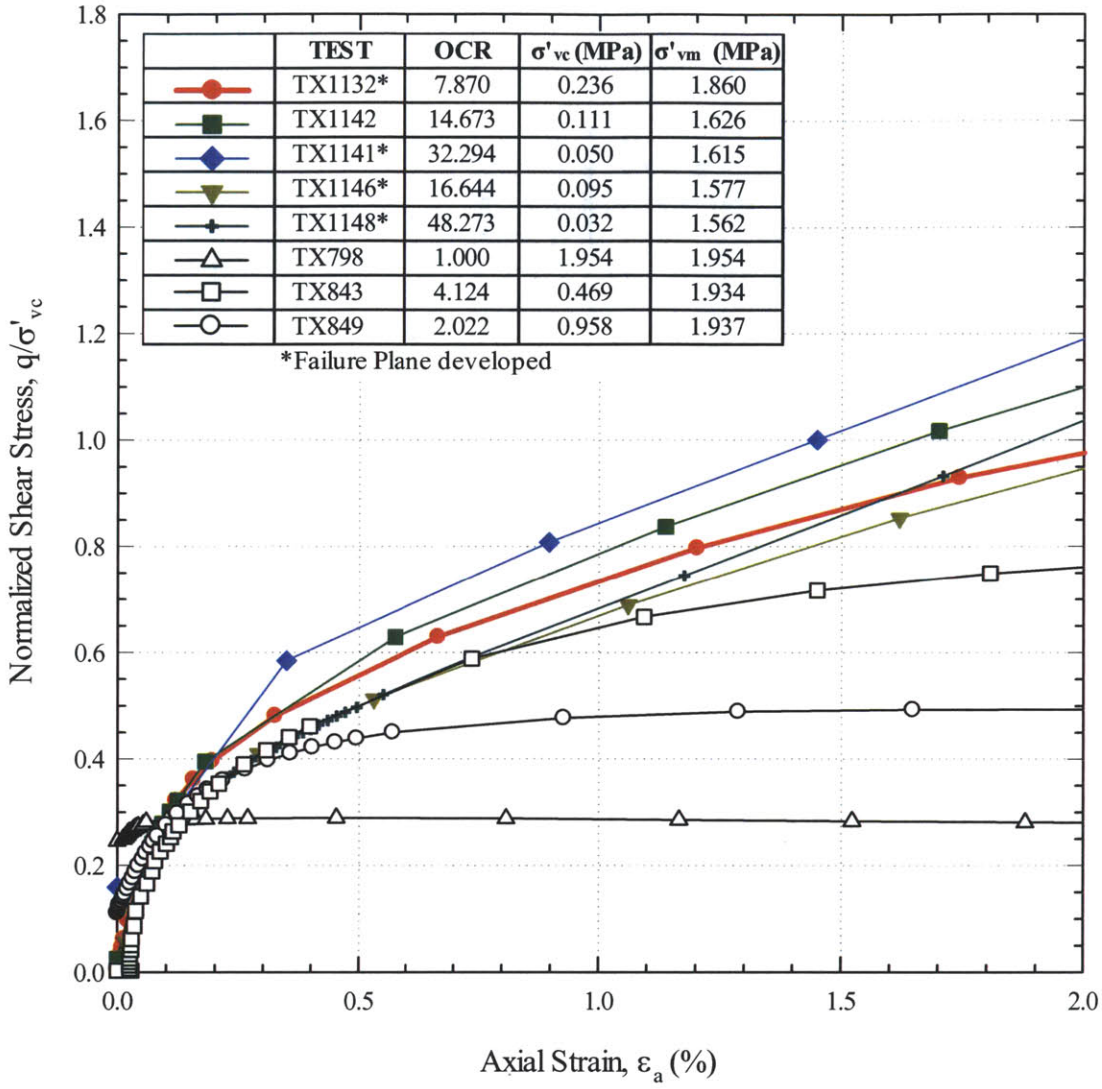

Figure 5-78 Normalized stress-strain curves (up to 2%) for RBBC at different OCR

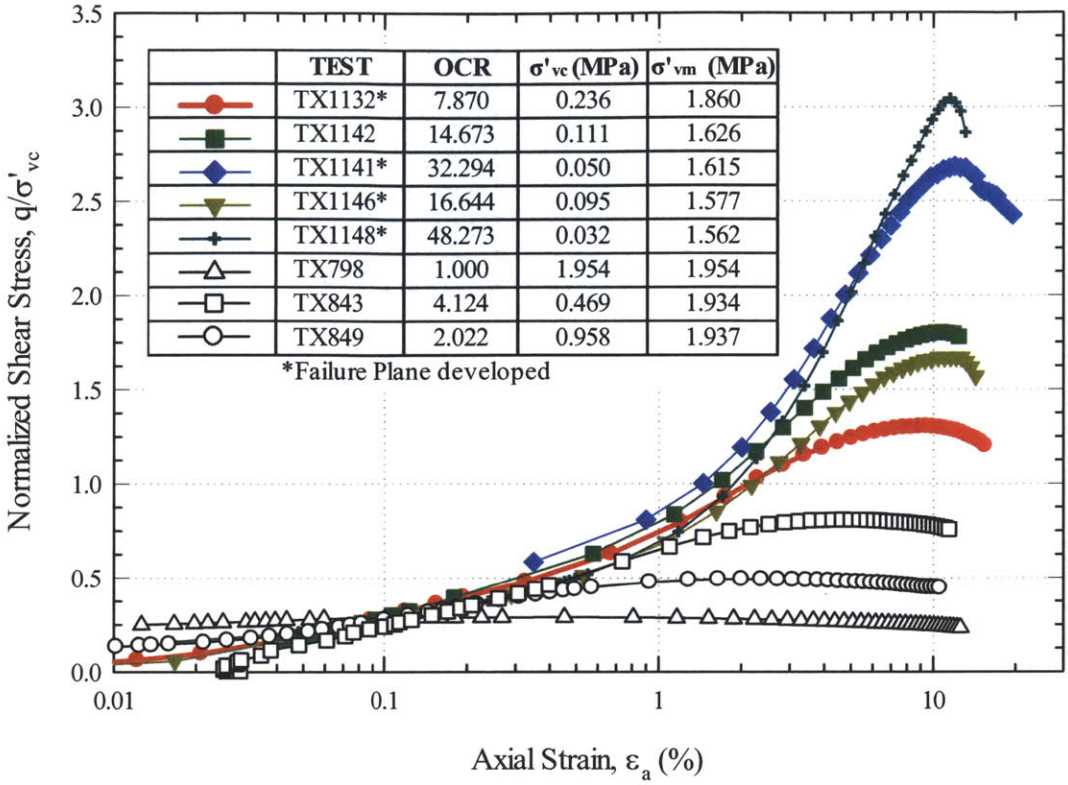

Figure 5-79 Normalized stress-(log)strain curve for RBBC at different OCR

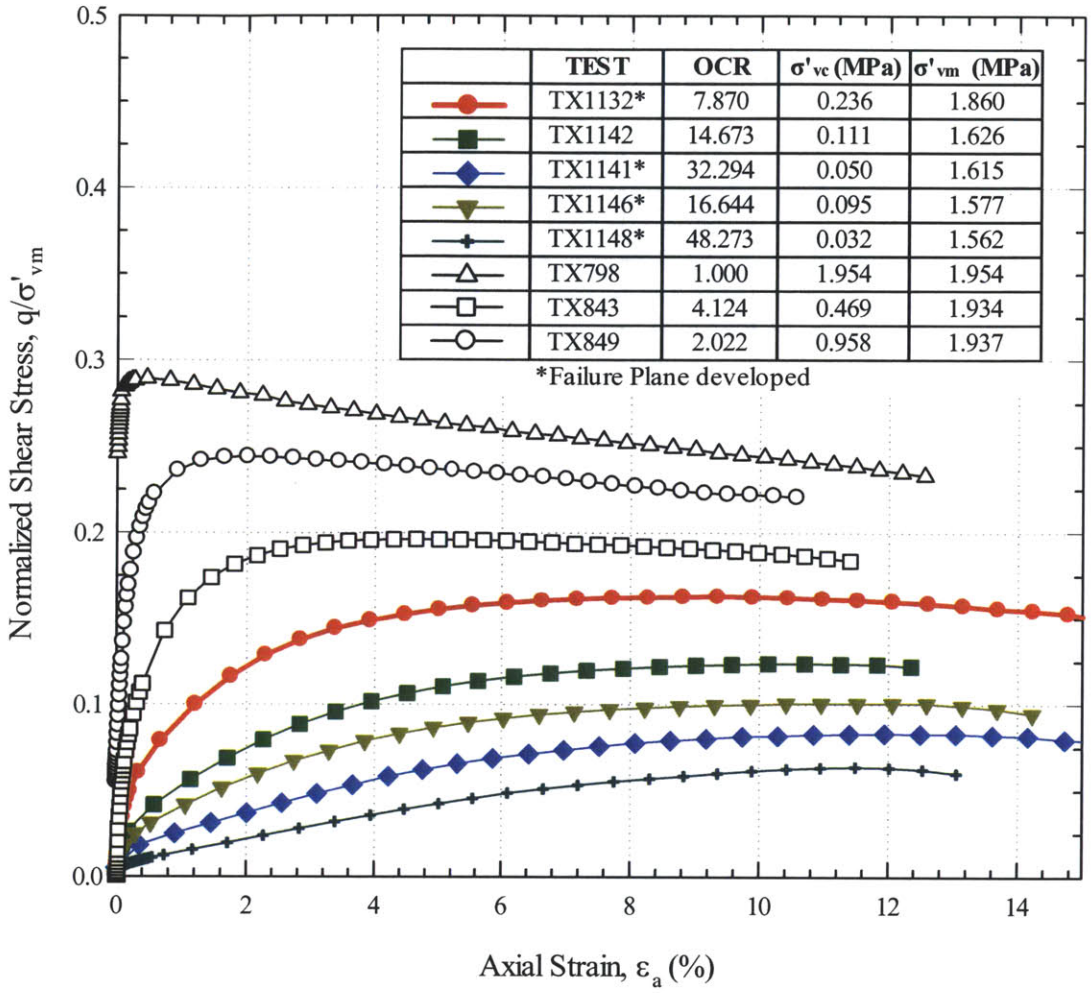

Figure 5-80 Normalized stress-strain curves for RBBC at different OCR

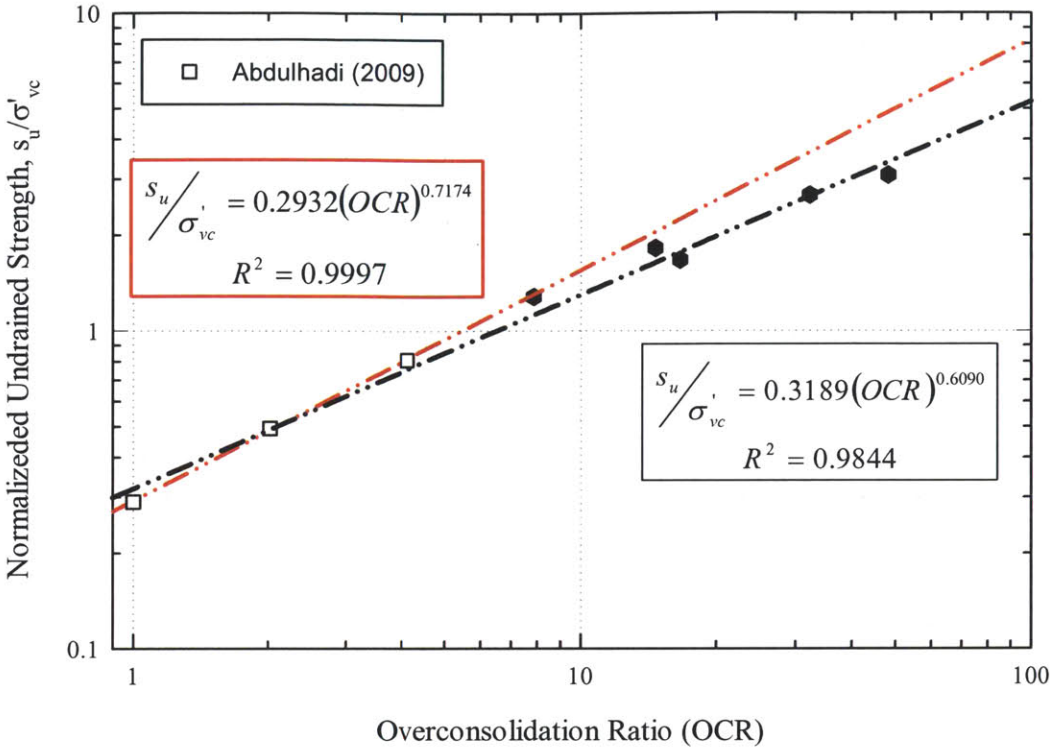

Figure 5-81 Normalized undrained shear versus overconsolidation ratio for RBBC

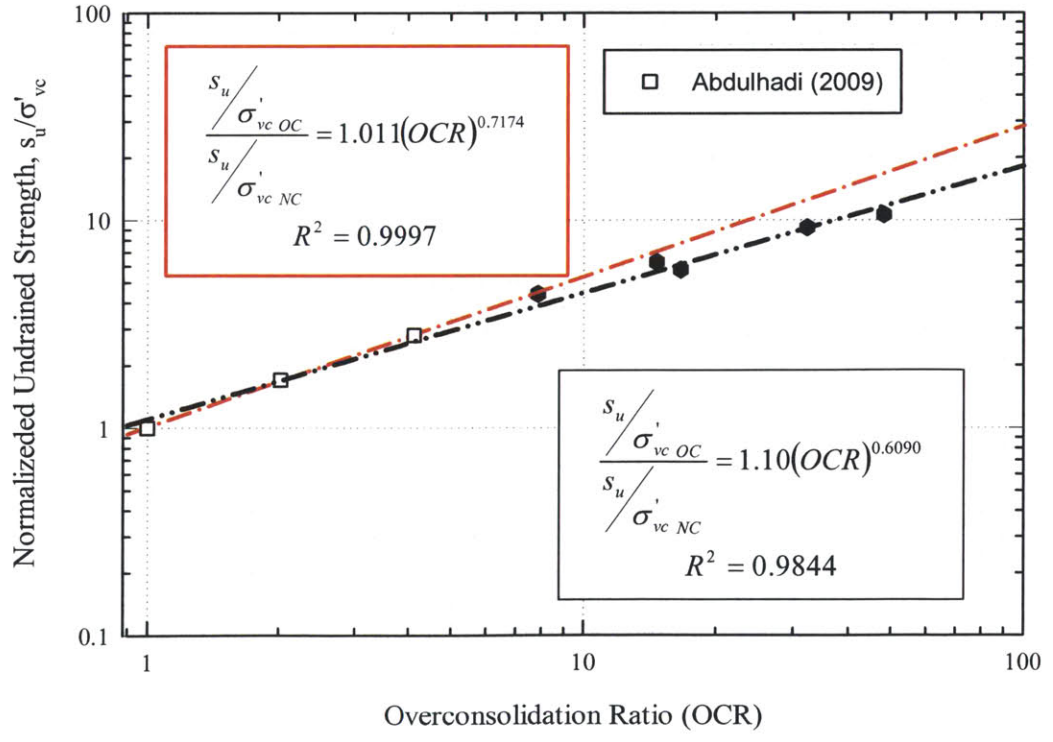

Figure 5-82 Normalized undrained shear versus overconsolidation ratio for RBBC

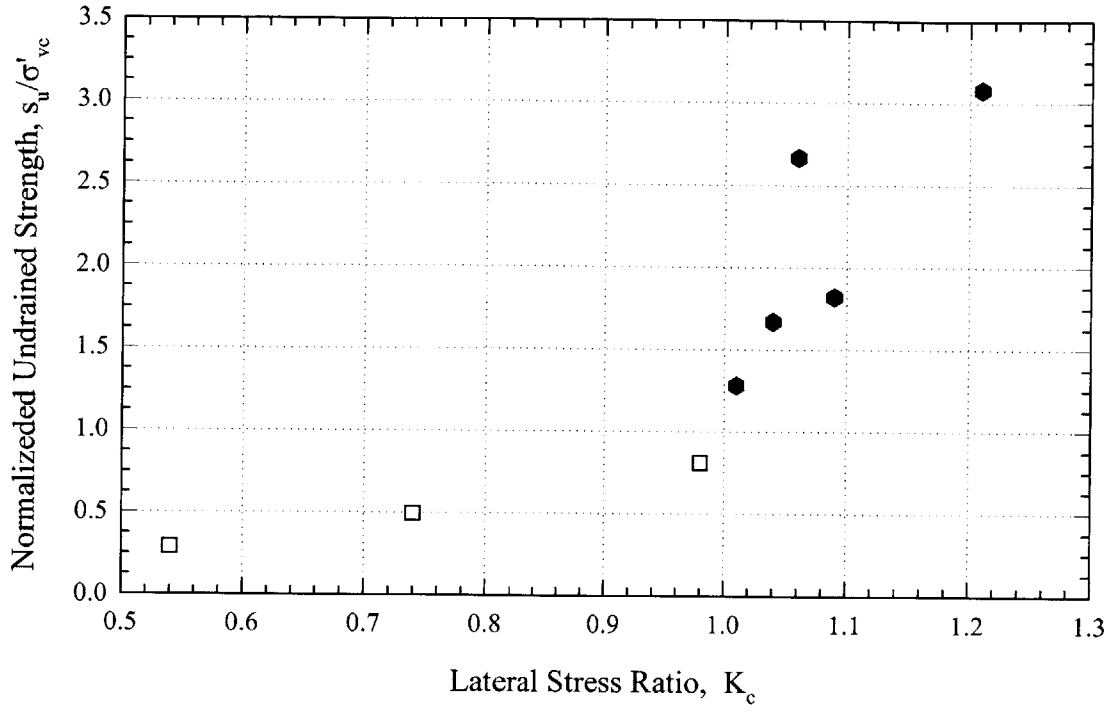

Figure 5-83 Normalized Undrained Shear Strength versus lateral stress ratio for RBBC at different OCR

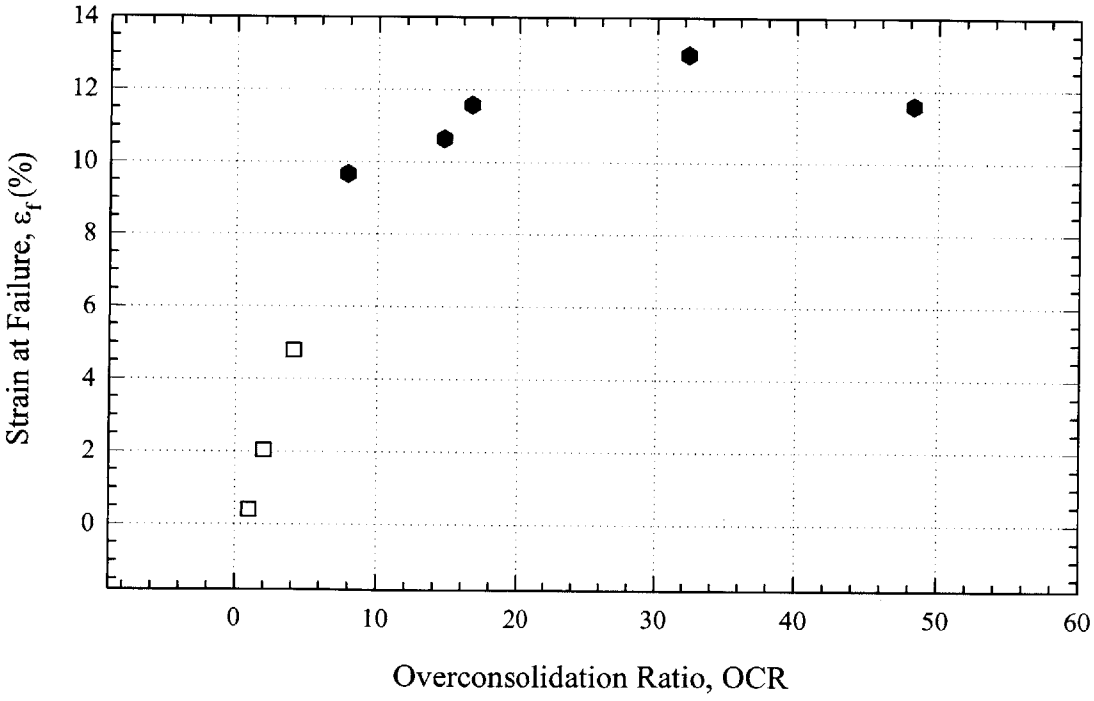

Figure 5-84 Strain at failure versus strain rate for RBBC at different OCR

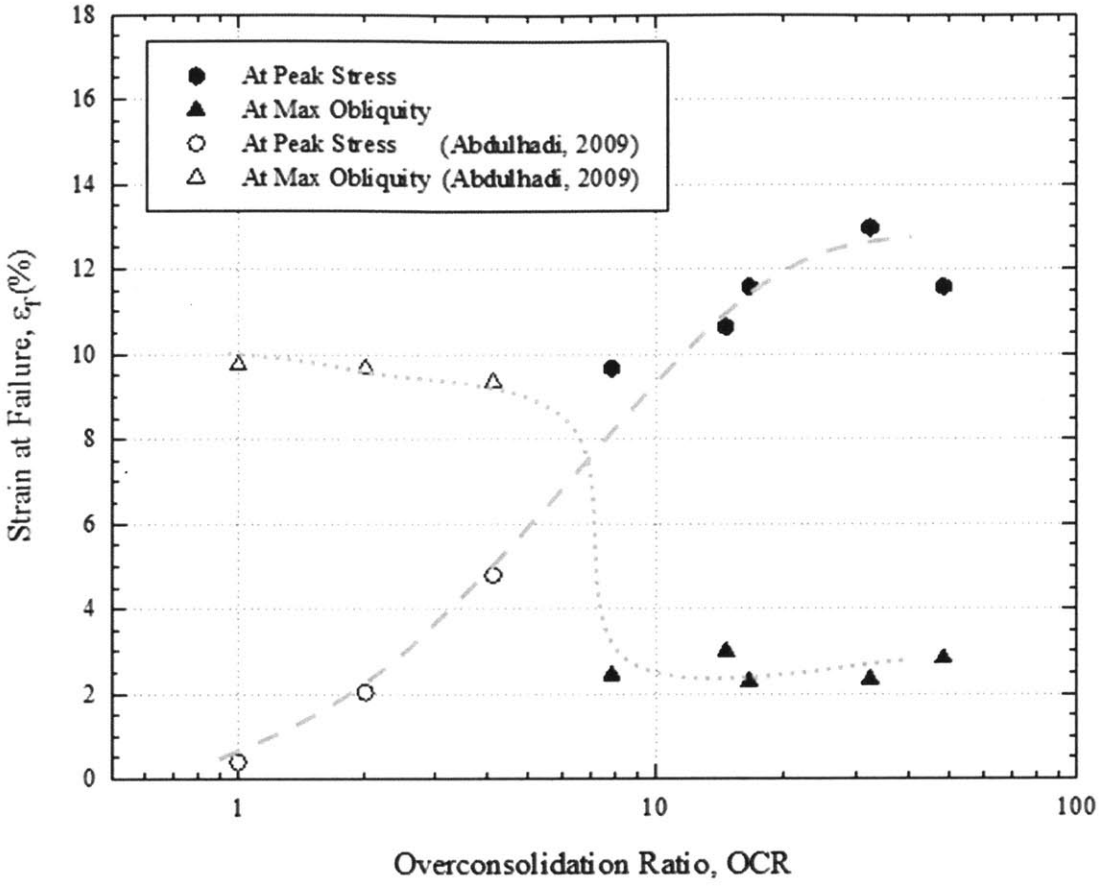

Figure 5-85 Strain at failure and maximum obliquity versus OCR for RBBC

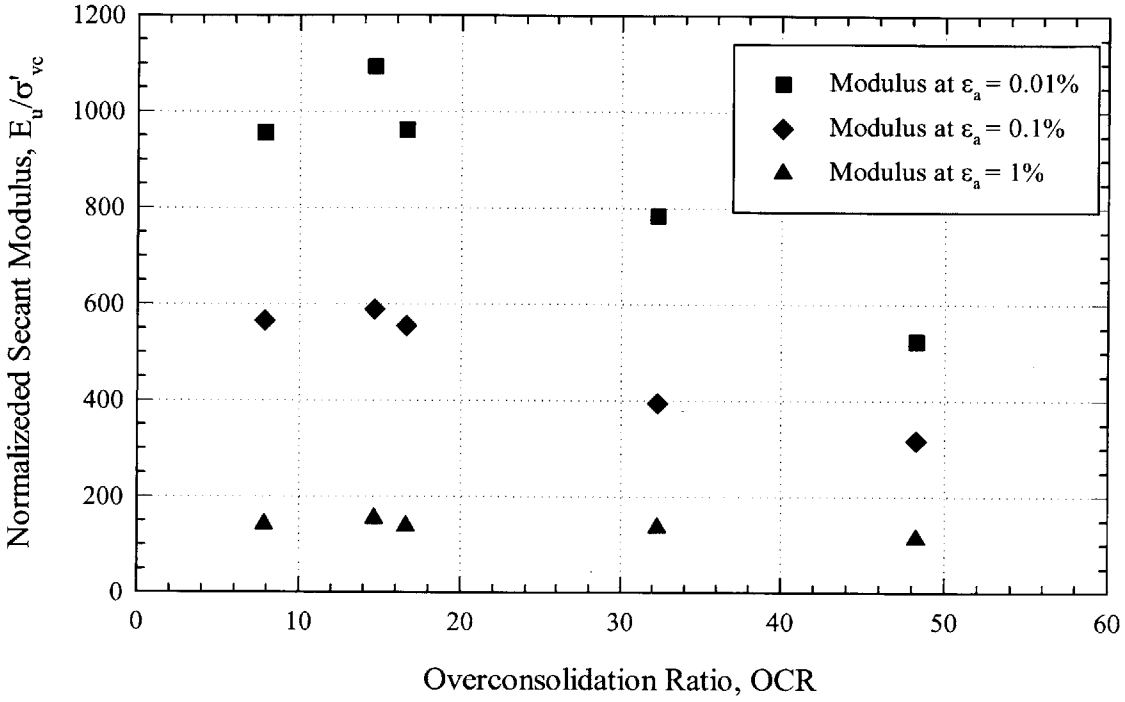

Figure 5-86 Normalized undrained secant modulus versus OCR ≥ 8 for RBBC

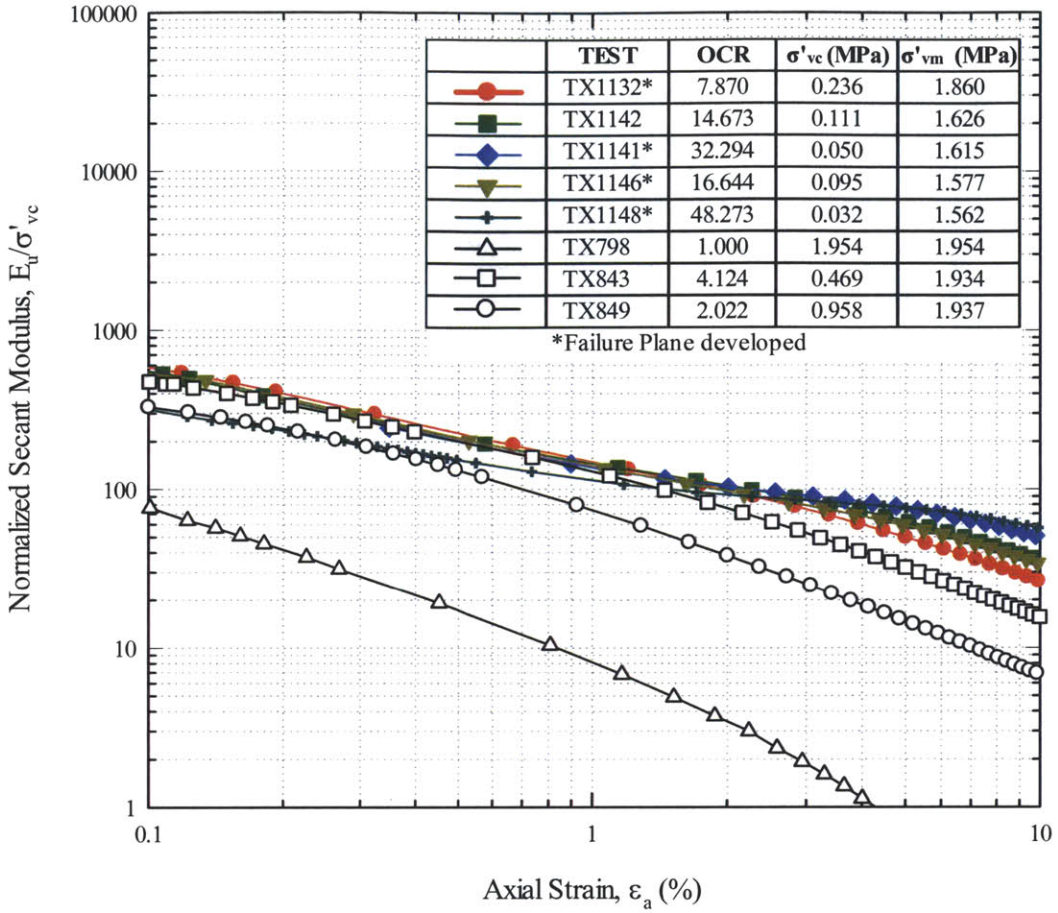

Figure 5-87 Normalized undrained secant modulus (E_u/σ'_{vc}) versus axial strain for RBBC at different OCR

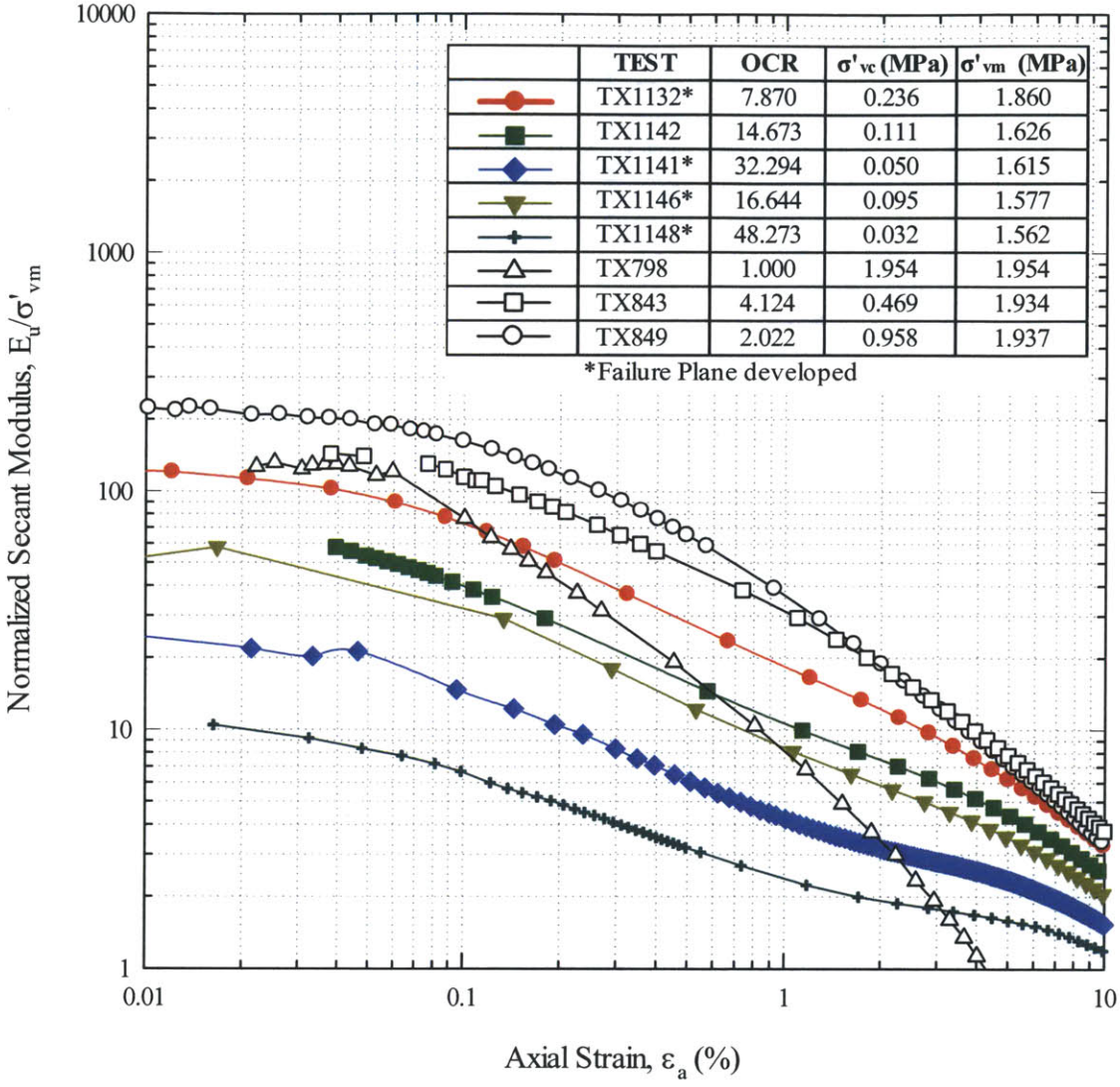

Figure 5-88 Normalized undrained secant modulus (E_u/σ'_{vm}) versus axial strain for RBBC at different OCR

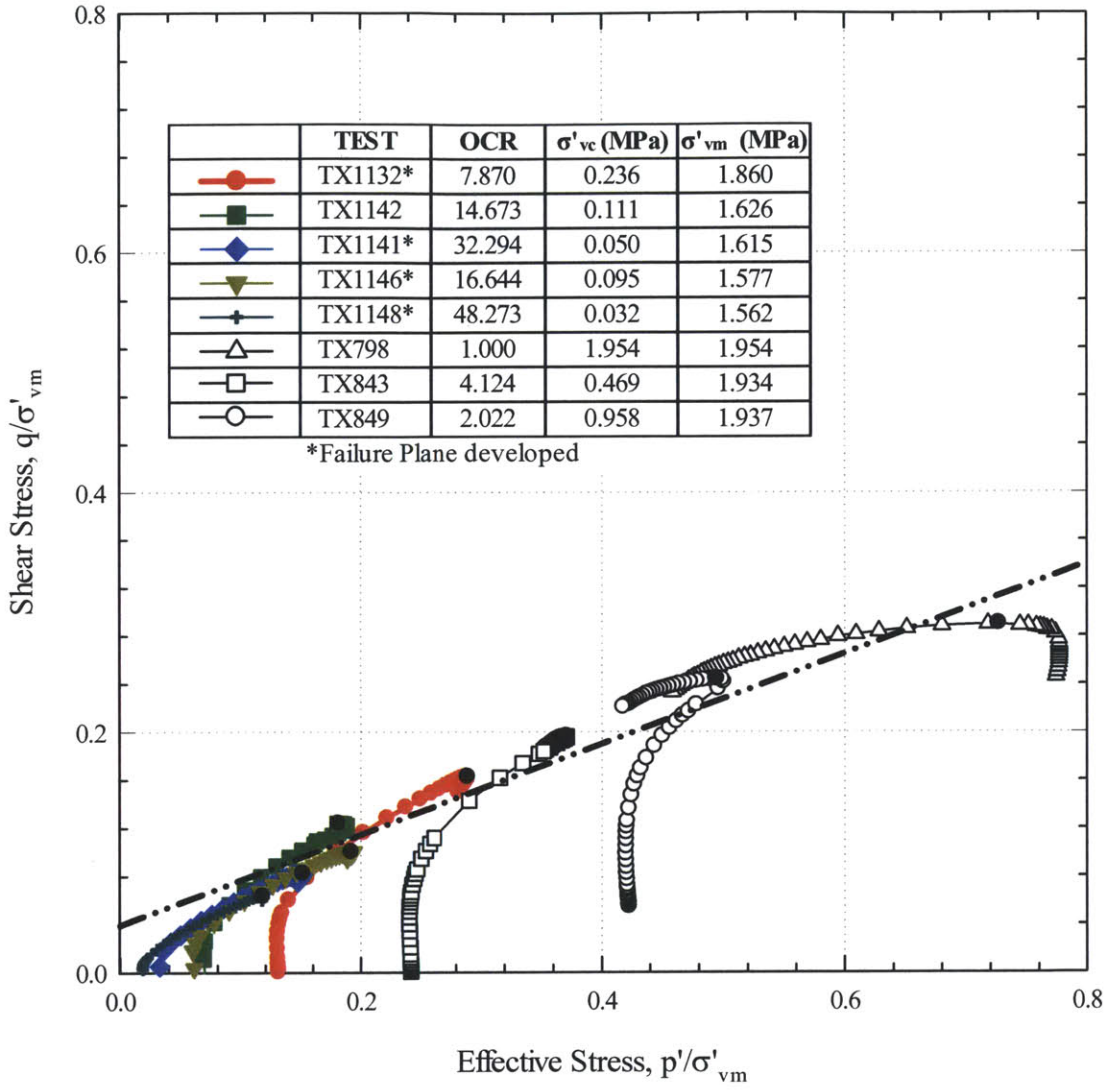

Figure 5-89 Normalized Effective Stress Paths for RBBC at different OCR

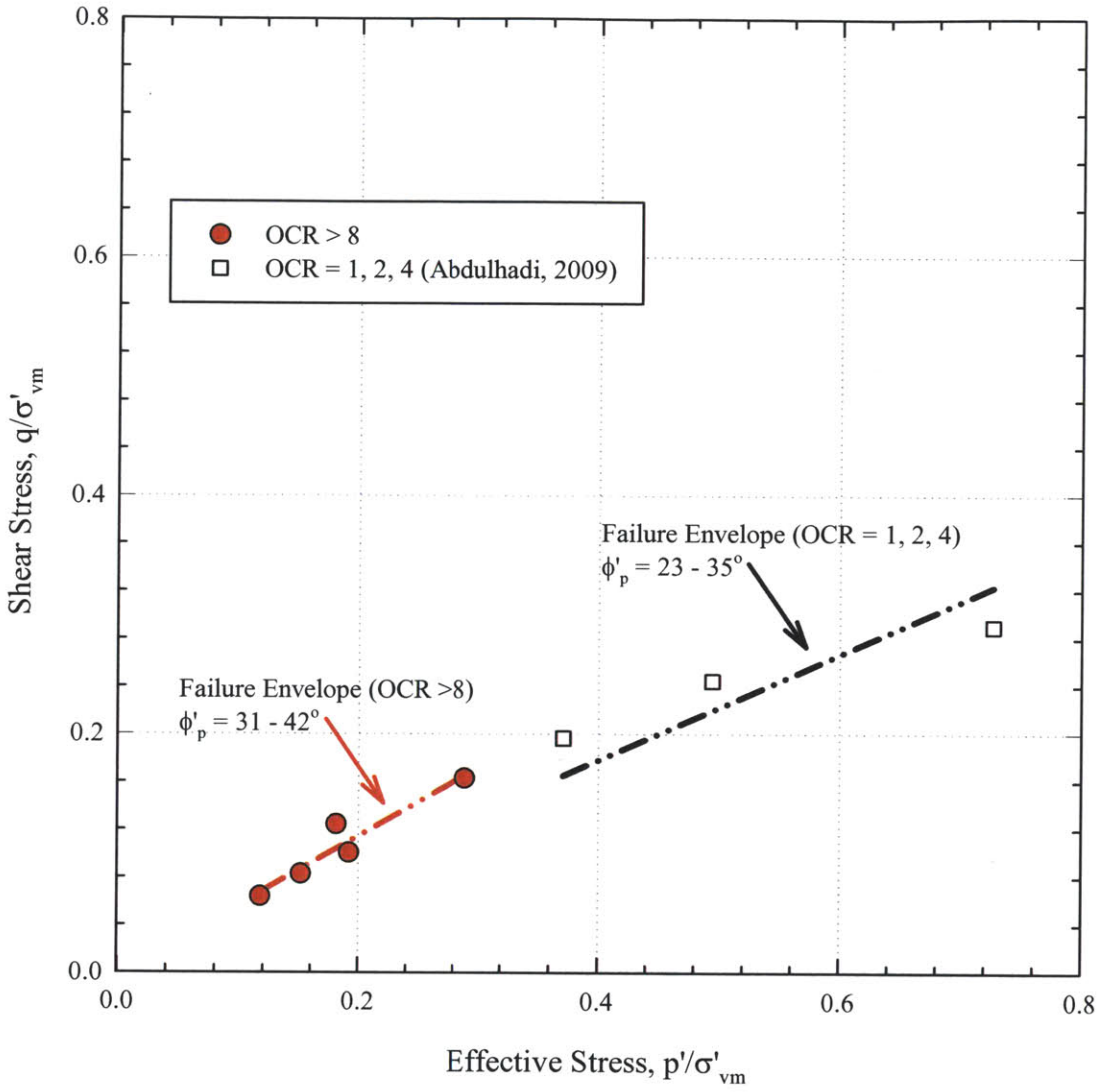

Figure 5-90 Stress states at peak for RBBC at different OCR

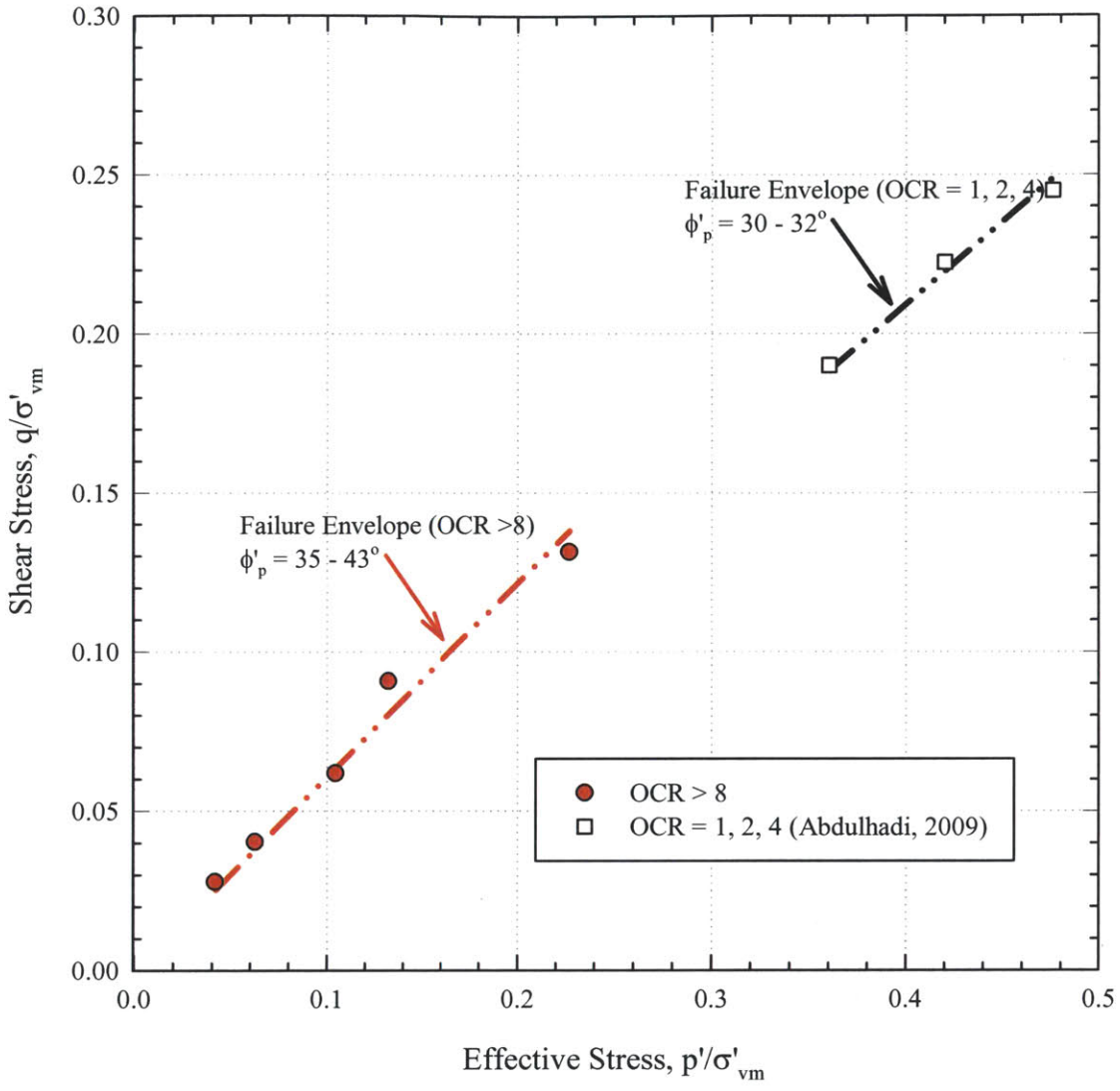

Figure 5-91 Stress states at maximum obliquity for RBBC at different OCR

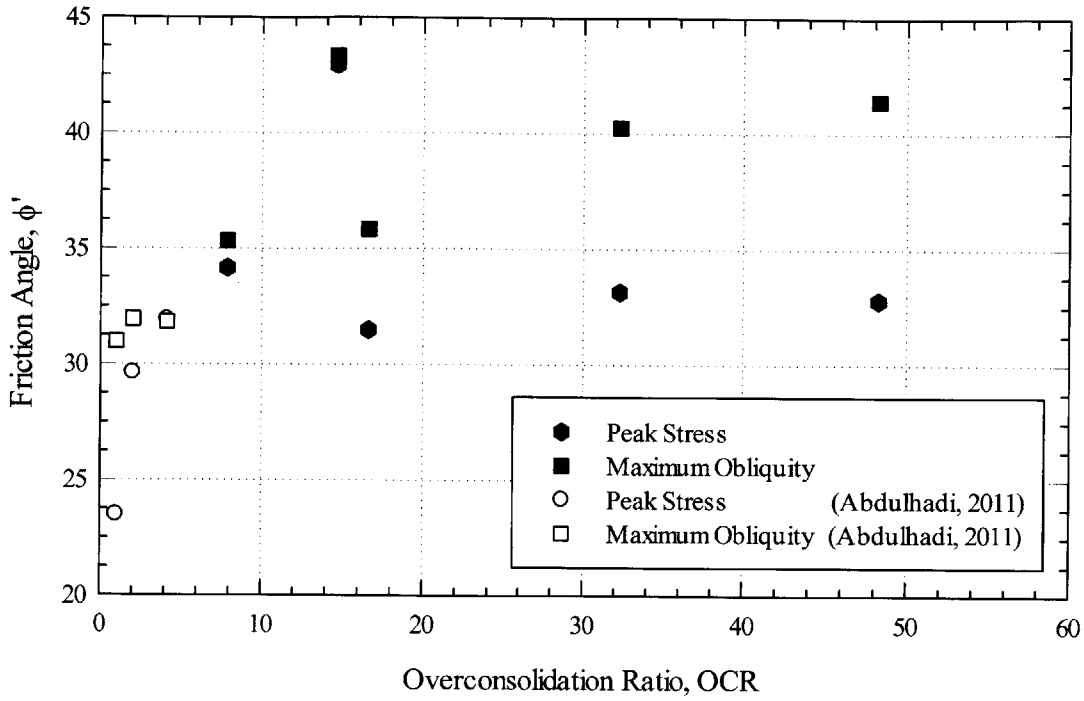

Figure 5-92 Friction angle at peak and maximum obliquity versus OCR for RBBC

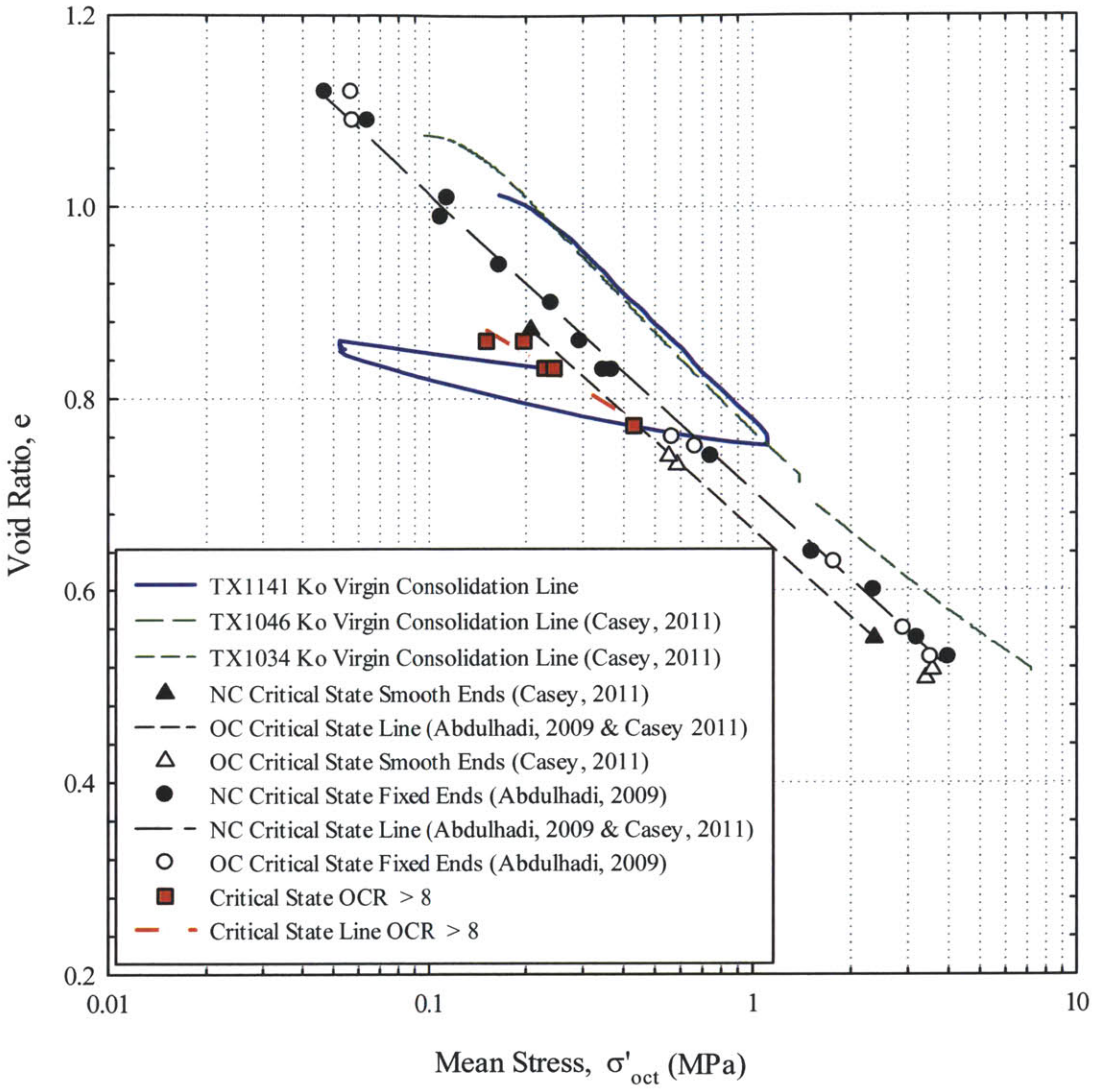

Figure 5-93 Large strains end of shearing stress states in e-log mean stress for NC and OC RBBC

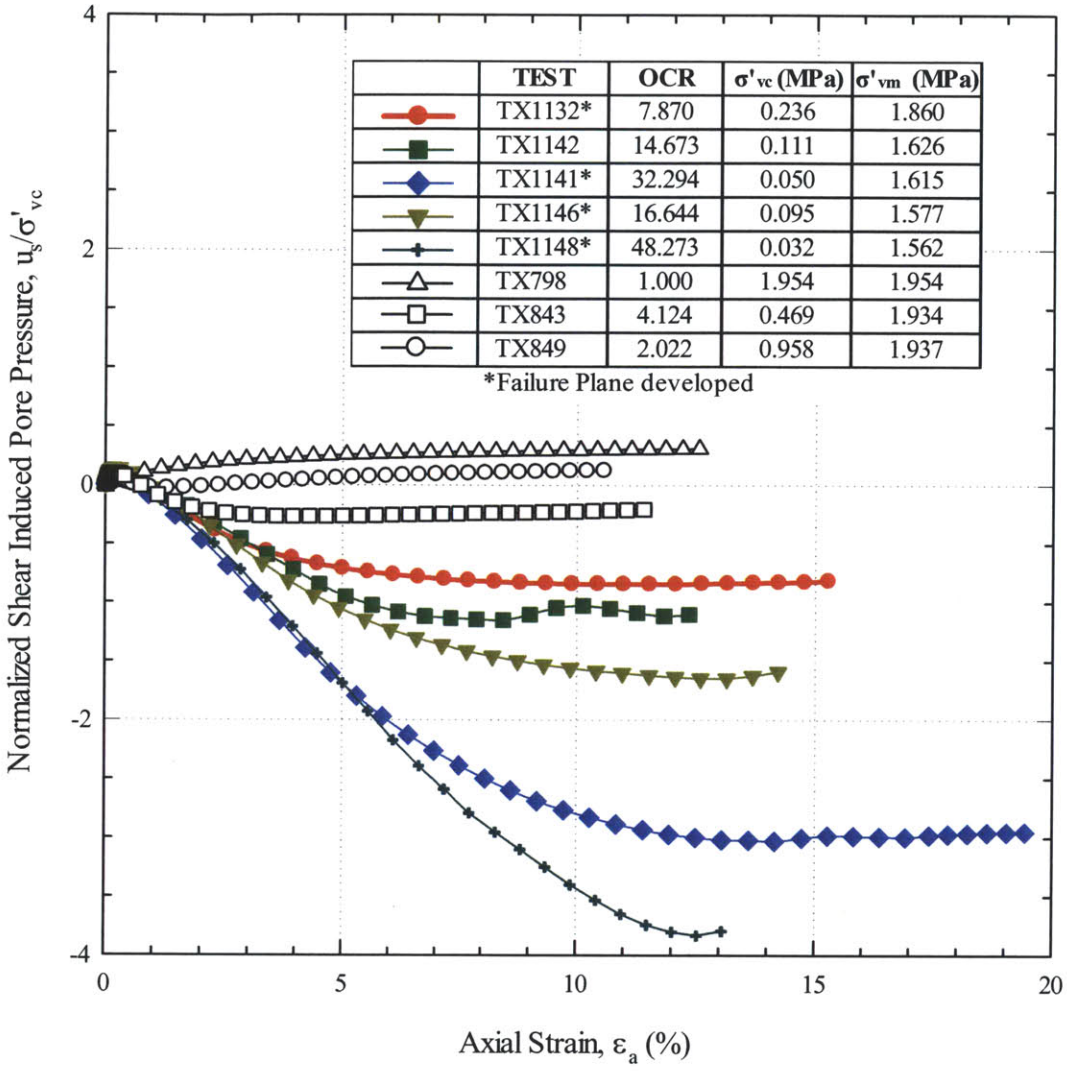

Figure 5-94 Normalized shear induced pore pressure versus strain for RBBC at different OCR

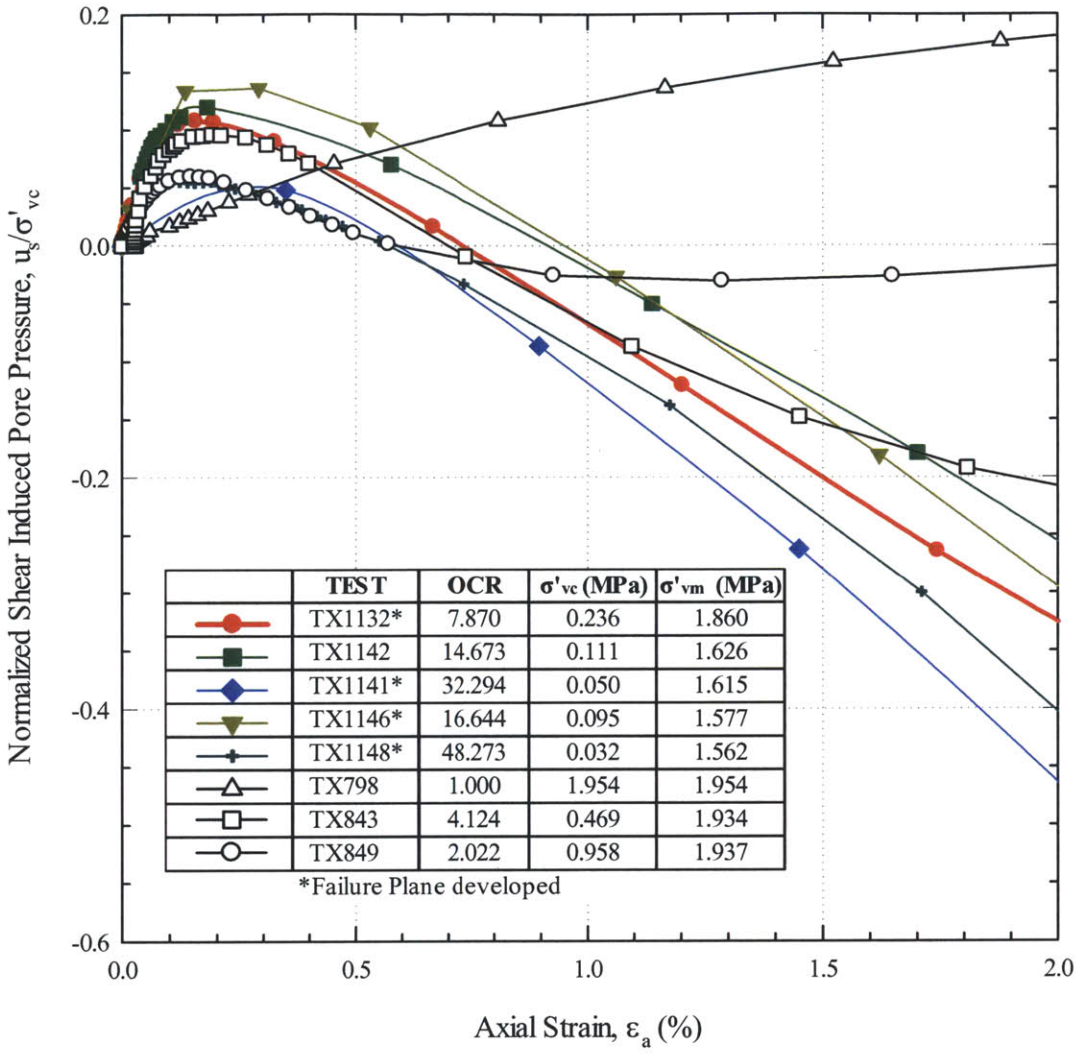

Figure 5-95 Normalized shear induced pore pressure versus strain (close up view) for RBBC at different OCR

6 CONCLUSIONS AND RECOMMENDATIONS

6.1 Overview

The main goal of this study consisted of understanding the behavior of overconsolidated clays. This objective has been achieved by reviewing studies by previous researchers from the 1930s to the present, and by analyzing the results of a triaxial compression testing program conducted by the author. This research comprised a comprehensive laboratory investigation of the mechanical behavior of soils in triaxial compression over a wide range of overconsolidation ratios (OCR = 5 - 62). The overconsolidation effects on undrained shear behavior have been investigated on Resedimented Boston Blue Clay (RBBC) and Intact Presumpscot Maine Clay (PMC).

The primary focus of the experimental program was to characterize the mechanical behavior of heavily overconsolidated Resedimented Boston Blue Clay. Over the past 40 years, an extensive knowledgebase on RBBC has been built by many researchers at the MIT Geotechnical Laboratory. The uniformity and reproducible behavior of this clay enabled the author to investigate the effect of overconsolidation over a wide range of intrinsic soil parameters and integrate these new test results with prior measurements on the same material.

The MIT Automated Stress Path Triaxial Apparatus was the main device used for this investigation. Since the OCR values were very high and consequently the computed stresses

resulted in small values, some minor changes to the constants in the test control algorithm were necessary to keep these small values constant during the aging (secondary compression) phases of the test.

The triaxial compression (CK_OUC) test results presented in this thesis comprise 16 tests and provide a comprehensive study of two mechanically overconsolidated materials. The experimental program consisted of ten triaxial tests performed on RBBC, and six tests conducted on intact PMC, at various overconsolidation ratios (OCR = 5 – 62).

Sections 6.2 and 6.3 summarize the results obtained from the one dimensional consolidation and undrained shearing in the triaxial compressions tests conducted. Finally, recommendations for further research are provided in section 6.4.

6.2 One-Dimensional Consolidation Behavior

All the triaxial tests were K_o-consolidated at a constant strain rate of 0.15%/hr and swelled to the target OCR, allowing 24 hours of aging after each phase. Swelling performed to a computed stress ratio rather than maintaining zero lateral strain.The compression behavior for RBBC reported by the author compares very well with previous results given by Abdulhadi (2009) and Casey (2011). Likewise, the results for PMC also lie in a very narrow band showing fine agreement for the various intact samples. These results are promising given that the author was able to compare the effects of overconsolidation.

As previously reported by researchers at MIT, the preconsolidation pressures defined by the compression curves are somewhat lower than those applied during the resedimentation process

on Boston Blue Clay. It has been concluded that this discrepancy is caused by friction between the soil sample and the sides of the consolidometer during resedimentation.

The lateral stress ratio (K_o) values reported in this thesis were obtained from recorded measurements in the triaxial apparatus. The overall trend of K_o during consolidation consisted of a decrease with loading until reaching the overconsolidation pressure and then plateaus at an average constant value of 0.56 for RBBC, and 0.48 for PMC. The lateral stress ratio for unloading was controlled to follow a linear stress path from the NC value to a hydrostatic stress state at the target OCR.

6.3 Undrained Shear Behavior

The triaxial compression tests investigated the effect of overconsolidation in two different materials. The shear stress-strain behavior demonstrated that the peak undrained strength decreases up to about 80% from a normally consolidated clay to a heavily overconsolidated clay for samples under similar stress levels. Furthermore, the normalized strength decreases, and the behavior is strongly dilative with high OCRs.

The strain at peak shear stress (ε_f) increased about 10% with increasing OCR. An interesting observation was that the maximum obliquity is reached significantly earlier than failure in all cases of OCR > 8, in contrast to NC and OC specimens up to OCR = 4.

The normalized undrained secant Young's modulus (E_u/σ'_{vc}) is related to OCR. As expected, the normalized stiffness of the soils increases with OCR. The RBBC results were

compared to Abdulhadi (2009) showing that OC soils had consistently larger normalized stiffness ratio than NC clay. However the actual value decreases with OCR.

The effective stress paths (ESPs) for all high OCR tests exhibit a similar behavior. The ESPs rise toward the failure envelope until reaching the peak stress at different locations. At all OCR the material first develops positive pore pressures and then dilates. The variation of the friction angle also showed a significant relationship with respect to OCR. The stress states at peak stress and maximum obliquity of heavily overconsolidated clays caused the failure envelope to be steeper in comparison to NC and lightly OC soils.

The high OCR values have a slight effect on the SHANSEP equation parameters. In general, the normalized strength increases with OCR but at a slightly lower rate. The parameter S increased, while the parameter m decreased when applying the regression equation for specimens under similar condition but at different OCR values. It was concluded that the application of SHANSEP equation to very high OCRs can be accurately used to model the undrained shear ratio.

6.4 Recommendations for further research

This research has emphasized the importance of understanding the particular behavior of overconsolidated clays and has established that high OCR follows a consistent extension of low OCR behavior. Medium stress tests were attempted in this research, but it is believed that the pressures were not high enough to cause a significant change in the microstructure of the material. Faster strain rates for shearing were also tried during this research; however, it was not found to strongly change the undrained behavior of the soil. It was concluded that the undrained shear ratio (USR) is more sensitive to stress levels than to a change in the strain rates.

Further research testing is required to provide a more comprehensive analysis of overconsolidated soils. Some of the topics for which the author suggests for future research are:

- Overconsolidated in-situ soils: triaxial testing should be extended in-situ overconsolidated soils. This may bring into the picture not just the stress changes but the time and temperature where these changes occurred.
- Cemented Samples: diagenetic processes cause cementation in natural soils. This process is triggered by physical and chemical changes in the soil. The occurrence of cementation may result in the appearance of a much more brittle behavior of the clays, having significant impact in the behavior of the clay.
- High Stress Levels above 10 MPa: Triaxial testing should be extended to higher stress levels at high OCR. This is an area of exploration for the brittle-ductile transition of soils.
- Other shearing modes: Triaxial testing should cover other shearing modes such as triaxial extension.
- Drained Shear Test: water migration within the sample may have a major impact in the development of cracks within the specimens. The shear induced pore pressures are believed to be related to the brittle behavior of this kind of material.

REFERENCES

Abdulhadi, N. O. (2009). *An Experimental Investigation into the Stress-Dependent Mechanical Behavior of Cohesive Soil with Application to Wellbore Instability.* Cambridge, MA: Massachusetts Institute of Technology.

Adams, A. L. (1991). *Laboratory Evaluation of the Constant Rate of Strain and Csonstant Head Techniques for Measuremen of the Hydraulic Conductivity of Fine Grained Soil.* Cambridge: Massachusetts Institute of Technology.

Ahmed, I. (1990). *Investigation of Normalized Behaviour of Resedimented Boston Blue Clay using Geonor Direct Simple Shear.* Cambridge: Massachusetts Institute of Technology.

Atkinson, J. H., Richardson, D., & Stallebrass, S. E. (1990). Effect of Recent Stress History on the Stiffness of. *Geotechnique, 40*(4), 531-540.

Banerjee, P. K., & Stipho, A. S. (1979). An elasto-plastic model for undrained shear behavior of heavily overconsolidated clays. *International Journal for Numerical and Analytical Methods in Geomechanics, 3*, 97-103.

Berman, D. R. (1993). Characterization of the Engineering Properties of Boston Blue Clay at the MIT Campus. *SM Thesis.* Cambridge, MA: Massachusetts Institute of Technology.

Binger, W. V. (1948). Analytical Studies of the Panama Canal Slides. *International Conference of Soil Mechanics and FE*, (pp. 54-59). Rotterdam.

Bishop, A. W., Kumapley, N. K., & El-Ruwayih, A. (1975). The Influence of Pore-Water Tension on the Strength of Clay. *Philosophical Transactions of the Royal Society of London, 278*, 511-554.

Bjerrum, L. (1967). Progressive failure in slopes of overconsolidated plastic clay and clay shales. *Journal of Soil Mechanics and Foundations Division, 93*, 3-49.

Bjerrum, L. (1973). Problems of Soil Mechanics and Construction on Soft Clays. *8th International Conference on Soil Mechanics and Foundation Engineering.* Moscow.

Brooker, E. W., & Ireland, H. O. (1965). Earth Pressure at test to Stress History. *Canadian Geotechnical Journal, 2*(1), 1-15.

Brooker, E. W., & Peck, R. B. (1993). Rational design treatment of slides in overconsolidated clays and clay shales. *Canadian Geotechnical Journal, 30*(3), 526.

Budhu, M. (2012). Design of shallow footings on heavily overconsolidated clays. *Canadian Geotechnical Journal, 49*, pp. 184-196.

Casey, B. (2011). *The Significance of Specimen End Restraint in High Pressure Triaxial Testing of Cohesive Soil.* Cambridge: Massachusetts Institute of Technology.

Cauble, D. F. (1996). *An Experimental Investigation of the Behavior of a Model Suction Caisson in a Cohesive Soil.* Cambridge: Massachusetts Institute of Technology.

Deere, D. U., & Miller, R. P. (1966). *Engineering Classification and Index Properties for Intact Rock.* Air Force Weapons Laboratory, Kirtland Air Force Base. New Mexico: US Air Force System Command.

Eslinger, E., & Pevear, D. (1988). *Clay minerals for petroleum geologists and engineers.* (Vol. Notes No. 22). Society of Economic Paleontologists and Mineralogists.

Fookes, P. G. (1965). Orientation of fissures in overconsolidated clay of the Siwalki System. *Geotechnique, 15*(2), 195-206.

Fookes, P. G., & Wilson, D. D. (1966). The Geometry of Discontinuities and Slope Failure in the Siwalki Clay. *Geotechnique, 15*(2), 305-320.

Gens , A. (1982). *Stress-strain and Strenght Characteristic of a Low Plasticity Clay.* Imperial College.

Germaine, J. T. (1982). *Development of the Directional Shear Cell for Measuring Cross-Anisotropic Clay Properties",.* Cambridge: Massachusetts Institute of Technology.

Germaine, J. T., & Germaine, A. V. (2009). *Geotechnical Laboratory Measurements for Engineers.* John Wiley & Sons.

Gouda, J. P. (1960). A study of shear failure in certain Tertiary Marine Sediments. *Proceedings ASCE Research Conference* (pp. 615-641). Boulder: ASCE.

Graton, L. C., & Fraser, H. J. (1935). Systematic packing of spheres—with particular relation to porosity and permeability. *Journal of Geology*(43), 709-785.

Gutierrez , M., Nygard, R., Hoeg, K., & Berre, T. (2008). Normalized Undrained Shear Strength of Clay Shale. *Engineering Geology, 99*, 31-39.

Henkel, D. J. (1955). Discussion on Earth Pressure on Stiff Fissured Clays. *Conference on the Correlation between calculated and observed stresses and displacements in structures*, (pp. 491-493).

Henkel, D. J. (1957). Investigation of two long-term failures in London Clay slopes at Wood Green and North-holt. *Proceedings 4th International Conference on Soil Mechanics and FM, 2*, pp. 315-320.

Henkel, D. J., & Skempton , A. W. (1955). A landslide at Jackfield, Shrosphire, in heavily overconsolidated clay. *Geotechnique, 5*(2), 131-137.

Horan, A. (2012, June). The Mechanical Behavior of Normally Consolidated Soils as a Function of Pore Fluid Salinity . *Master of Science Thesis.* Cambridge, MA, United States: Massachusetts Institute of Technology.

Horan, A. J. (2012). *The Mechanical Behavior of Normally Consolidated Soils as a Function of Pore Fluid Salinity.* Cambridge: Massachusetts Institute of Technology.

Hower, J., Eslinger, E. V., Hower, M. E., & Perry, E. A. (1976). Mechanism of burial metamorphism of argillaceous sediment: mineralogical and chemical evidence. *Geol. Society American Bulletin, 87*, 725-237.

Jennings, S., & Thompson, G. R. (1986). Diagenesis of Plio-Pleistocene sediments of the Colarado River delta, Southern California. *Journal of Sedimentary Petrology, 56*, 89-98.

Johsnton, I. W., & Novello, E. A. (1994). Soil Mechanics, Rock Mechanics and Soft Rock Technology. *Proceedings of Institution of Civil Engineering, 107*, pp. 3-9.

Kenney, T. C. (1964). Sea-Level Movements and the Geologic Histories of the Postglacial Marine Soils at Boston, Nicolet, Ottawa and Oslo,". *Géotechnique, 14*(3), 203-230.

Kontopoulus, N. S. (2012). The Effects of Sample Disturbance on Preconsolidation Pressure for. *ScD Thesis*. Cambridge, MA: Massachusetts Institute of Technology.

Koutsofas, D. C., & Ladd, C. C. (1985). Design Strengths for an Offshore Clay. *Journal of Geotechnical Engineering Division, 111*(3), 337-355.

Ladd, C. C. (1991). Stability Evaluation during Staged Construction. *Journal of Geotechnical Engineering, 117*(4), 540-615.

Ladd, C. C., & Foot, R. (1974). New Design Procedure for Stability of Soft Clays. *Journal of the Geotechnical Engineering Division, 100*(7), 763-786.

Ladd, C. C., & Varallyay, J. (1965). *The Influence of Stress System on the Behavior of Saturated Clays during Undrained Shear.* Soil Publication No. 177. Cambridge: Massachusetts Institute of Technology.

Lambe, T. W., & Whitman, R. V. (1969). *Soil Mechanics.* John Wiley and Sons.

Lundgard, P. D. (1992). Sandstone porosity loss—a "big picture" view of the importance of compaction. *Sandstone porosity loss—a "big picture" view of the importance of compaction.*(62), 250-260.

Lynch, F. L., Mack, L. E., & Land, L. S. (1997, May). Burial diagenesis of illite/smectite in shales and the origins of authigenic quartz and secondary porosity in sandstones. *Geochimica et Cosmochimica Acta, 61*(10), 1995-2006.

Marjanovic, J. (2012). *The Study of Shear and Longitudinal Velocity Measurements of Sands and Cohesive Soils.* Cambridge: Massachusetts Institute of Technology.

Moniz, S. R. (2009). *The Influence of Effective Consolidation Stress on the Normalized Extension Strenght Properties of Residemented Boston Blue Clay.* Cambridge: Massachusetts Institute of Technology.

Moregenstern, N. R., & Tchalenko, J. S. (1967). Microstructural Observation on shear zones from slips in natural clay. *Proceedings Geotechnical Conference*, (pp. 147-152). Oslo.

Pearson, N., & Gingras, M. (2006). An ichnological and sedimentological facies model for muddy point-bar deposits . *Journal of Sedimentary Research*, 771-782.

Peterson, R. F. (1954). Studies of Bearpaw Shale at a dam site in Sasketchewan. *Journal of Soil Mechanics and Foundation Division, 80*, 1-28.

Petley, D. N. (1999). Failure Envelopes of Mudrocks at High Confining Pressures. *Special Publications, 158*, 61-71.

Pollastro, R. M. (1993). Considerations and applications of the illite/smectite geothermometer in hydrocarbon-bearing rocks of miocene to mississippian age. *Clay and Clays Minerals, 41*(2), 119-133.

Reynolds, R. T. (1991). Geotechnical field techniques used in monitoring slopes stability at a landfield. *Proceedings of the 3rd International Symposium on Field Measurements in Geomechanics* (pp. 883-892). Oslo: A. A. Balkema.

Ringheim, A. S. (1964). Experiences with the Bearpaw shale at the South Saskatchewan River Dam. *8th Internationala Congress on Large Dams, 1*, pp. 529-550.

Roscoe, K. H., & Burland, J. B. (1968). On the Generalized Stress-Strain Behaviour of 'Wet' Clay. *Engineering Plasticity*, pp. 535-609.

Santagata, M. C. (1994). *"Investigation of Sample Disturbance in Soft Clays Using Triaxial Element Test.* Massachusetts Institute of Technology.

Santagata, M. C. (1998). Factors Affecting the Initial Stiffness and Stiffness Degradation of Cohesive. *ScD Thesis*. Cambridge, MA: Massachusetts Institute of Technology.

Schädlich, B., & Schweiger, H. F. (2011). A multilaminate soil model for highly overconsolidated clays. *15th European Conference of Soil Mechanics and Geotechnical Engineering.*

Schmidt, B. (1966). Discussion of "Earth Pressure at Rest Related to Stress History. *Canadian Geotechnical Journal, 3*(4), 239-242.

Schofield, A. N., & Wroth, C. P. (1968). *Critical State Soil Mechanics.* McGraw-Hill.

Seah, T. H. (1990). *Anisotropy of Resedimented Boston Blue Clay.* Cambridge: Massachusetts Institute of Technology.

Sheahan, T. C., & Germaine, J. T. (1992). Computer Automation of Conventional Triaxial. *Geotechnical Testing Journal, 15*(4), 311-322.

Sheahan, T. C., Germaine, J. T., & Ladd, C. C. (1990). Automated Triaxial Testing of Soft Clays: An Upgraded Commercial System. *ASTM, 13*(3), 153-163.

Sheahn, T. C. (1991). *An Experimental Study of the Time-Dependent Undrained Shear.* Cambridge: MIT.

Sinfield, J. V. (1994). *An Experimental Investigation of Sampling Disturbance Effects in Resedimented Boston Blue Clay.* Cambridge: Massachusetts Institute of Technology.

Singh, H. (1971). *The behavior of normally consolidated and heavily overconsolidated clays at low effective stress.* Civil Engineering. Cornell University.

Skempton , A. W. (1948). The rate of softening in still fissured clays with special reference to London Clay. *Proceedings 2nd International Conference of Soil Mechanics and FE, 2,* pp. 378-381.

Skempton, A. W. (1964). Long term stability of Clay Slopes. *Geotechnique, 14*(2), 77-102.

Smith, R. E., Jahangir, M. A., & Rinker, W. C. (2006). Selection of Design Strengths for Overconsolidated Clays and Clay Shales. *40th Symposium on Engineering Geology and Geotechnical Engineering.* Logan.

Steiger, R. P., & Lueng, P. K. (1991). Critical State Shale Mechanics. *Proceeding of 32nd US Symposium on Rock,* (pp. 293-302).

Terzagui, K. (1936). Stability of Slopes of Natural Clays. *International Conference of Soil Mechanics and FE, 1,* pp. 161-165. Cambridge.

Terzagui, K., & Peck, R. B. (1948). *Soil Mechanics in Engineering Practice.* John Wiley and Sons Inc.

Thomson, A. (1959). Pressure Solution and Porosity. *SEPM Spec. Publ. 7,* 92-110.

Turner, F. J. (1981). *Metamorphic Petrology.* New York: McGraw-Hill.

University of Canterbury. (n.d.). *University of Canterbury.* Retrieved September 2012, from GeoGlossary: http://www.outreach.canterbury.ac.nz/resources/geology/page2.shtml

Weaver, C. E. (1989). *Clays, muds, and shales* (Vol. 44). ELSEVIER.

Whittle, A. J., & Kavvadas, M. (1994). Formulation of the MIT-E3 Constitutive Model for Overconsolidated Clays. *Journal of the Geotechnical Engineering Division, 120,* 173-198.

Wilson, S. D., & Johnson, K. A. (1964). Slides in Overconsolidated Clays Along the Seattle Freeway. *Second Annual Engineering Geology and Soil Engineering Symposium* , (pp. 29-42).

Winkler, H. F. (1979). *Petrogenesis of metamorphic rocks.* New York: Springer-Verlag.

Yudhbir. (1969). *Engineering behavior of heavily overconsolidated clays and clay shales with special reference to long term stability.* Cornell University, Civil Engineering. Cornell University.

Zreik, D. A. (1994). *Behavior of Cohesive Soils and their Drained, Undrained, and Erosional.* Cambridge: Massachusetts Institute of Technology.

APPENDIX 1 PHASE RELATIONSHIPS

Test Number	TX1117	TX1121	TX1122	TX1125	TX1126	TX1130
INITIAL MEASUREMENTS	PMC	PMC	PMC	PMC	PMC	PMC
Wet soil and tare(g)	182.66	210.84	210.26	212.80	213.00	215.85
Tare (g)	49.80	58.52	58.43	58.51	58.50	58.49
Initial Wet Mass (g)	132.86	152.32	151.83	154.29	154.50	157.36
Initial Height (cm)	7.00	8.02	7.99	8.15	7.82	7.98
Area (cm2)	9.89	9.86	9.81	9.83	9.76	9.32
FINAL MEASUREMENTS						
Mass final specimen and tare (g)	136.69	155.82	156.35	144.46	139.24	147.94
Mass plate (g)	11.02	13.11	12.76	-	-	-
Mass wet section and tare (g)	125.67	142.71	143.59	144.46	139.24	147.94
Mass dry section and tare (g)	111.66	127.29	128.02	117.11	111.31	124.96
Mass oven tare (g)	11.02	13.11	12.76	-	-	-
Final water content (%)	24.87	24.99	24.58	23.35	25.09	18.39
Dry Mass (soil and salt) (g)	100.64	114.18	115.26	117.11	111.31	124.96
CONSTANTS						
Stress (ksc)	1.00	1.00	1.00	1.00	1.00	1.00
Salt Concentration (g/l)	16.00	16.00	16.00	16.00	16.00	16.00
Specific Gravity of grains	2.80	2.80	2.80	2.80	2.80	2.80
Temperature of initial specimen (C^{o})	24.00	24.00	24.00	24.00	24.00	24.00
Mass Density of water (g/cm3)(@TT)	1.00	1.00	1.00	1.00	1.00	1.00
Mass Density of water (g/cm3)(@20C)	1.00	1.00	1.00	1.00	1.00	1.00
Mass Density of salt (g/cm3)	3.36	3.36	3.36	3.36	3.36	3.36
Mass Density of salt water (g/cm3) (@TT)	1.01	1.01	1.01	1.01	1.01	1.01
INTERMEDIATES						
Final Mass of water (g)	25.03	28.53	28.33	27.35	27.93	22.98
Final Mass of salt (g)	0.40	0.46	0.46	0.44	0.45	0.37
Mass of soil grains (g)	100.24	113.72	114.80	116.67	110.86	124.59
Volume of grains (cc)	35.86	40.69	41.08	41.74	39.66	44.58
Height of solids (cm)	3.63	4.12	4.19	4.25	4.06	4.78
Initial Mass of salt (g)	0.52	0.61	0.59	0.60	0.69	0.52
RESULTS						
Initial Water Content (%)	**31.87**	**33.23**	**31.58**	**31.57**	**38.50**	**25.78**
Initial Void Ratio	**0.93**	**0.94**	**0.91**	**0.92**	**0.92**	**0.67**
Iniital Saturation (%)	**96.85**	**99.74**	**98.22**	**97.19**	**118.19**	**108.95**
Initial Wet Density (g/cm3)	**1.92**	**1.93**	**1.94**	**1.93**	**2.03**	**2.12**
Initial Dry Density (g/cm3)	**1.45**	**1.44**	**1.47**	**1.46**	**1.46**	**1.68**
Initial Porosity	**0.48**	**0.49**	**0.48**	**0.48**	**0.48**	**0.40**

Test Number	TX1130	TX1132	TX1134	TX1135	TX1138	TX1139
INITIAL MEASUREMENTS	PMC	RBBC	RBBC	PMC	RBBC	RBBC
Wet soil and tare(g)	215.85	212.40	200.53	214.52	192.84	182.15
Tare (g)	58.49	58.45	49.72	58.40	58.42	49.78
Initial Wet Mass (g)	157.36	153.95	150.81	156.12	134.42	132.37
Initial Height (cm)	7.98	8.02	8.09	8.00	7.91	7.92
Area (cm2)	9.32	9.98	9.99	9.83	8.99	9.03
FINAL MEASUREMENTS						
Mass final specimen and tare (g)	147.94	147.91	141.04	146.64	127.17	123.90
Mass plate (g)	-	-	-	-	-	-
Mass wet section and tare (g)	147.94	147.91	141.04	146.64	127.17	123.90
Mass dry section and tare (g)	124.96	115.57	109.14	120.55	94.07	95.14
Mass oven tare (g)	-	-	-	-	-	-
Final water content (%)	18.39	27.98	29.23	21.64	35.19	30.23
Dry Mass (soil and salt) (g)	124.96	115.57	109.14	120.55	94.07	95.14
CONSTANTS						
Stress (ksc)	1.00	1.00	1.00	1.00	1.00	1.00
Salt Concentration (g/l)	16.00	16.00	16.00	16.00	16.00	16.00
Specific Gravity of grains	2.80	2.80	2.80	2.80	2.80	2.80
Temperature of initial specimen (C°)	24.00	24.00	24.00	24.00	24.00	24.00
Mass Density of water (g/cm3)(@TT)	1.00	1.00	1.00	1.00	1.00	1.00
Mass Density of water (g/cm3)(@20C)	1.00	1.00	1.00	1.00	1.00	1.00
Mass Density of salt (g/cm3)	3.36	3.36	3.36	3.36	3.36	3.36
Mass Density of salt water (g/cm3) (@TT)	1.01	1.01	1.01	1.01	1.01	1.01
INTERMEDIATES						
Final Mass of water (g)	22.98	32.34	31.90	26.09	33.10	28.76
Final Mass of salt (g)	0.37	0.52	0.51	0.42	0.53	0.46
Mass of soil grains (g)	124.59	115.05	108.63	120.13	93.54	94.68
Volume of grains (cc)	44.58	41.16	38.86	42.98	33.47	33.87
Height of solids (cm)	4.78	4.13	3.89	4.37	3.72	3.75
Initial Mass of salt (g)	0.52	0.62	0.67	0.57	0.65	0.60
RESULTS						
Initial Water Content (%)	**25.78**	**33.10**	**37.98**	**29.35**	**42.72**	**38.94**
Initial Void Ratio	**0.67**	**0.94**	**1.08**	**0.83**	**1.12**	**1.11**
Iniital Saturation (%)	**108.95**	**99.26**	**99.64**	**100.10**	**107.70**	**99.34**
Initial Wet Density (g/cm3)	**2.12**	**1.92**	**1.87**	**1.99**	**1.89**	**1.85**
Initial Dry Density (g/cm3)	**1.68**	**1.44**	**1.35**	**1.53**	**1.32**	**1.33**
Initial Porosity	**0.40**	**0.49**	**0.52**	**0.45**	**0.53**	**0.53**

Test Number	TX1141	TX1146	TX1148	TX1149	TX1156
INITIAL MEASUREMENTS	RBBC	RBBC	RBBC	RBBC	RBBC
Wet soil and tare(g)	197.09	199.62	201.88	190.04	209.25
Tare (g)	54.76	54.65	58.41	58.40	58.44
Initial Wet Mass (g)	142.33	144.97	143.47	131.64	150.81
Initial Height (cm)	8.02	8.17	8.04	7.44	8.12
Area (cm2)	9.47	9.39	9.42	9.40	9.33
FINAL MEASUREMENTS					
Mass final specimen and tare (g)	135.30	137.00	136.41	125.13	147.52
Mass plate (g)	-	-	-	-	-
Mass wet section and tare (g)	135.30	137.00	136.41	125.13	147.52
Mass dry section and tare (g)	104.43	106.50	104.83	96.73	117.13
Mass oven tare (g)	-	-	-	-	-
Final water content (%)	29.56	28.64	30.12	29.36	25.95
Dry Mass (soil and salt) (g)	104.43	106.50	104.83	96.73	117.13
CONSTANTS					
Stress (ksc)	1.00	1.00	1.00	1.00	1.00
Salt Concentration (g/l)	16.00	16.00	16.00	16.00	16.00
Specific Gravity of grains	2.80	2.80	2.80	2.80	2.80
Temperature of initial specimen (C°)	24.00	24.00	24.00	24.00	24.00
Mass Density of water (g/cm3)(@TT)	1.00	1.00	1.00	1.00	1.00
Mass Density of water (g/cm3)(@20C)	1.00	1.00	1.00	1.00	1.00
Mass Density of salt (g/cm3)	3.36	3.36	3.36	3.36	3.36
Mass Density of salt water (g/cm3) (@TT)	1.01	1.01	1.01	1.01	1.01
INTERMEDIATES					
Final Mass of water (g)	30.87	30.50	31.58	28.40	30.39
Final Mass of salt (g)	0.50	0.49	0.51	0.46	0.49
Mass of soil grains (g)	103.93	106.01	104.32	96.27	116.64
Volume of grains (cc)	37.19	37.93	37.32	34.44	41.73
Height of solids (cm)	3.93	4.04	3.96	3.67	4.47
Initial Mass of salt (g)	0.61	0.62	0.62	0.56	0.54
RESULTS					
Initial Water Content (%)	**36.15**	**35.96**	**36.71**	**35.95**	**28.70**
Initial Void Ratio	**1.04**	**1.02**	**1.03**	**1.03**	**0.82**
Iniital Saturation (%)	**98.27**	**99.60**	**101.07**	**98.90**	**99.55**
Initial Wet Density (g/cm3)	**1.87**	**1.89**	**1.89**	**1.88**	**1.99**
Initial Dry Density (g/cm3)	**1.38**	**1.39**	**1.38**	**1.38**	**1.55**
Initial Porosity	**0.51**	**0.51**	**0.51**	**0.51**	**0.45**